Ring Opening of Decalin on Iridium- and Platinum-Containing Zeolite Catalysts of the FAU-, MTW- and MWW-Type

Von der Fakultät Chemie der Universität Stuttgart
zur Erlangung der Würde eines
Doktors der Naturwissenschaften (Dr. rer. nat.)
genehmigte Abhandlung

Vorgelegt von

Sandra Rabl

aus Attendorn

Hauptberichter:	Prof. Dr.-Ing. Jens Weitkamp
Mitberichter:	Prof. Dr. Thomas Schleid

Tag der mündlichen Prüfung: 07.02.2011

Institut für Technische Chemie
der Universität Stuttgart
2011

Die vorliegende Arbeit entstand in der Zeit von Oktober 2007 bis September 2010 am Institut für Technische Chemie der Universität Stuttgart.

Mein Dank gilt besonders Herrn Prof. Dr.-Ing. Jens Weitkamp für die Überlassung des hochinteressanten und facettenreichen Themas, sowie für die engagierte Betreuung meiner Arbeit.

Herrn Prof. Dr.-Ing. Elias Klemm danke ich für die guten Rahmenbedingungen am Institut für Technische Chemie.

Herrn Prof. Dr. Thomas Schleid danke ich für die Übernahme des Korreferats.

Ferner danke ich Herrn Dr. Vincenzo Calemma und Herrn Dr. Marco Ferrari von Eni S.p.A. für die gute Zusammenarbeit im Rahmen des Industrieprojekts.

Ein besonderer Dank gilt Dominic Santi und Andreas Haas, die zum einen im Rahmen ihrer Diplomarbeiten, aber vor allem auch später als Kollegen im Projekt eine große Unterstützung waren, immer mit Rat und Tat zur Seite standen und zusammen mit Tobias Holl und Frank Salzbauer ideale Diskussionspartner waren.

Dank gebührt ebenfalls Linda Kuhn, Manuel Weber, Jakob Belka, Nelli Pfaff, Andrea Inan und Corinne Hunger, die im Rahmen von Praktika und Diplomarbeiten einen großen Teil zum Gelingen dieser Arbeit beigetragen haben.

Frau Heike Fingerle danke ich für die zahlreichen Analysen und die viele Geduld gerade mit den lanthanhaltigen Proben. Frau Barbara Gehring und Frau Ines Kley danke ich für die vielen Analysen und REM-Aufnahmen. Ebenfalls bedanke ich mich für die MAS-NMR-Aufnahmen bei Herrn Prof. Dr. Michael Hunger und bei Frau Dr. Yvonne Traa für die Bereitstellung des Zeoliths MCM-22.

I Table of Contents

II Symbols, Indices and Abbreviations

Symbols

Symbol	Unit	Designation
A	- (or counts)	dimensionless peak area in the chromatogram
CN	-	cetane number
CMR	-	cracking mechanism ratio
d	m	diameter
f	-	compound-specific FID correction factor
F	-	relative fraction in ^{29}Si MAS NMR spectra
I	A	current intensity
k	-	number of aluminum atoms coordinated to a silicon atom
$LHSV$	h^{-1}	liquid hourly space velocity
m	kg	mass
$\dot{m}$	$kg \cdot s^{-1}$	mass flux
M	$kg \cdot mol^{-1}$	molar mass
MP	K	melting point
n	mol	molar amount
$\dot{n}$	$mol \cdot s^{-1}$	molar flux

p	Pa	pressure
pH	-	negative decimal logarithm of the oxonium ion concentration
S	-	selectivity
S^*	-	modified selectivity
SI	-	spaciousness index
t	s	time
T	K or °C	temperature
U	V	voltage
$\dot{V}$	$m^3 \cdot s^{-1}$	volumetric flow rate
$WHSV$	h^{-1}	weight hourly space velocity
X	-	conversion
Y	-	yield
δ	-	chemical shift
θ	°	angle
λ	m	wavelength
ν	-	stoichiometric factor

Indices

amorph.	amorphous
cat	catalyst
i	a reactant in the stoichiometric equation
j	a product or group of products in the stoichiometric equation
max.	maximum
r	reaction
ret	retention
RT	room temperature
spiro	spiro[4.5]decane
theo.	theoretical

Abbreviations

a.u.	arbitrary units
C	cracked products
C_8-	hydrocarbons with less than 9 carbon atoms (hydrocracked products)
C_9-	hydrocarbons with less than 10 carbon atoms (hydrocracked products)
C_{10}+	hydrocarbons with more than 9 carbon atoms
C_{11}+	hydrocarbons with more than 10 carbon atoms

DHP(s)	dehydrogenated product(s)
Eq(s).	equation(s)
Equil.	equilibrium
EU	Edinburgh University
FAU	faujasite
FCC	fluid catalytic cracking
FI	flow indicator
FID	flame ionization detector
FT	fourier transform
GC	gas chromatograph(y)
GC/MS	gas chromatography / mass spectrometry
HPDEC	high power decoupling
ICP-OES	inductively coupled plasma – optical emission spectrometer, spectrometry
IR	infrared spectroscopy
ITQ	Instituto de Tecnología Química Valencia
IUPAC	International Union of Pure and Applied Chemistry
IZA	International Zeolite Association
LCO	light cycle oil

LSX	low-silica X
M	metal
Ma.	Masse(n)
MAS	magic angle spinning
MCM	Mobil Composition of Matter
MTW	Mobil-twelve
MWW	Mobil-twenty-two
NMR	nuclear magnetic resonance
NNN(s)	next nearest neighbor(s)
NU	New (ICI)
NV	needle valve
OCA(s)	open-chain alkane(s)
OCD(s)	open-chain decane(s)
OCN(s)	open-chain nonane(s)
PI	pressure indicator
RE	rare earth
Ref.	reference
RO	ring opening
ROP(s)	ring opening product(s)

SAPO	silico-aluminophosphate
SEM	scanning electron microscope
SIMCA	soft independent modelling of class analogy
sk-Iso(s)	skeletal isomer(s)
TCD	thermal conductivity detector
TGA	thermogravimetric analyzer
USY	ultrastable Y zeolite
V	valve
vol.	volume
wt.	weight
XRD	X-ray diffractogram, diffractometer
Z^-	negatively charged zeolite framework
ZSM	Zeolite Socony Mobil

Abbreviations of Hydrocarbons

B-	butyl-
Bu	butane
c-Dec	cis-decalin
CPn	cyclopentane

De	decane
DE-	diethyl-
Dec	cis- and trans-decalin
DM-	dimethyl-
E-	ethyl
Hp	heptane
Hx	hexane
M-	methyl
Mn	methylnaphthalene
Nap	naphthalene
No	nonane
Oc	octane
P-	propyl-
Pr	propane
PHI	perhydroindan
TM-	trimethyl-
tr-Dec	trans-decalin
Ttr	tetralin

Nomenclature of the Catalysts

The charge-compensating cations in an aluminum-containing zeolite are separated from the zeolite type by a hyphen. The symbols of the cations are listed in the order of their equivalent fractions and separated from each other by a comma. The subscripts after the symbols stand for the mole fractions of the cations. The sum of the equivalent fractions is unity. The molar amounts of metal cations and the molar amount of aluminum are determined by ICP-OES. The molar amount of protons is calculated as the molar amount of aluminum minus the sum of equivalents of all metal cations. The symbol of a noble metal introduced into the zeolite appears in front of the charge-compensating cations from which it is separated by a diagonal slash. A number preceding the symbol of the noble metal denotes the mass fraction on the dry zeolite in percent. The molar ratio of silicon and aluminum in the zeolite is indicated after the zeolite type and a hyphen, if the molar ratio was varied. If the molar ratio of silicon and aluminum is not indicated, the unmodified zeolites were used: LSX (n_{Si} / n_{Al} = 1.01), X (n_{Si} / n_{Al} = 1.24), Y (n_{Si} / n_{Al} = 2.41) and MCM-22 (n_{Si} / n_{Al} = 21). Catalyst 1.2Ir/$Na_{0.77}$,$La_{0.06}$,$H_{0.05}$-Y, for example, is a Y-type zeolite with an n_{Si} / n_{Al} ratio of 2.41 and with 77 % Na^+ cations, 6 % La^{3+} cations and 5 % protons. 1.2 wt.-% iridium referenced to the dry zeolite were introduced into the pores.

Comments on the Title

The official IUPAC nomenclature of the hydrocarbon decalin is decahydronaphthalene or perhydronaphthalene. In this work the trivial and more commonly used name decalin was chosen. The designations FAU, MTW and MWW are framework type codes assigned by the Structure Commission of the International Zeolite Association (IZA). The designation FAU stands for the natural mineral **fau**jasite, whereas MTW and MWW are zeolites prepared by Mobil and thus called **M**obil-**tw**elve and **M**obil-t**w**enty-t**w**o.

1 Zusammenfassung

Raffinieriеströme, die reich an polycyclischen Aromaten sind, wie z. B. das light cycle oil (LCO) aus dem FCC-Verfahren, können nur in begrenzten Mengen zum Dieselkraftstoff zugemischt werden, da diese polycyclischen Aromaten zahlreiche negative Eigenschaften haben, zu denen unter anderem eine niedrige Cetanzahl und eine erhöhte Ruß- und Partikelemission gehören. Eine selektive Ringöffnung der Aromaten zu Alkanen mit der gleichen Kohlenstoffzahl würde die Eigenschaften dieser Raffinieriеströme und damit auch ihre Verwendbarkeit stark verbessern. Für eine solche Umsetzung müssen die Aromaten zunächst zu Naphthenen hydriert werden, wonach die Ringe selektiv zu öffnen sind. Die Hydrierung von Aromaten ist gut untersucht, aber die Öffnung der Ringe zu Alkanen ohne den gleichzeitigen Verlust von Kohlenstoffatomen gelingt bisher nicht zufriedenstellend.

Das Ziel dieser Arbeit war es, Schlüsselfaktoren zu identifizieren, die ein guter Katalysator haben muss, um eine hohe Ausbeute an offenkettigen Decanen bei der hydrierenden Umsetzung von cis-Decalin zu erreichen. Um das Ziel zu erreichen, wurden u. a. die Art des Edelmetalls, die Metallbeladung, die Konzentration und die Stärke der Brønsted-Säurezentren in Katalysatoren mit FAU-Struktur variiert.

Das erhaltene Produktgemisch von der hydrierenden Umsetzung von Decalin bestand aus mehr als 180 verschiedenen Kohlenwasserstoffen. Daher wurden die entstandenen Kohlenwasserstoffe zunächst hauptsächlich basierend auf der GC/MS-Analyse und den daraus erhaltenen molaren Massen in sechs Produktgruppen unterteilt: (i) Gerüstisomere von Decalin (sk-Isos) mit zwei naphthenischen Ringen und einer molaren Masse von 138 $g \cdot mol^{-1}$; (ii) Ringöffnungsprodukte (ROPs) mit nur noch einem naphthenischen Ring und einer molaren Masse von 140 $g \cdot mol^{-1}$; (iii) offenkettige Decane (OCDs) mit einer molaren Masse von 142 $g \cdot mol^{-1}$; (iv) dehydrierte C_{10}-Produkte (DHPs); (v) Kohlenwasserstoffe mit mehr als zehn Kohlenstoffatomen (C_{11}+) und (vi) Crackprodukte (C_9-). Für eine sichere Zuordnung der besonders gewünschten offenkettigen Decane wurde in einem anderen Experiment n-Decan an einem bifunktionellen Katalysator isomerisiert. Die erhaltenen iso-Decane wurden dann zusammen mit einer Flüssigprobe der Decalinumsetzung in den Gaschromatographen coinjiziert und zugeordnet.

Der Unterschied zwischen Iridium- und Platinkatalysatoren in der hydrierenden Umsetzung von cis-Decalin zeigte sich vor allem in den unterschiedlich gebildeten Primärprodukten bei niedrigen Umsätzen. An den Iridiumkatalysatoren wurden hauptsächlich Ringöffnungsprodukte gebildet, während Platinkatalysatoren erst das Decalinmolekül

isomerisieren. Lediglich Iridiumkatalysatoren mit einer hohen Konzentration oder Stärke an Brønsted-Säurezentren waren auch dazu in der Lage, eine hohe Selektivität an Gerüstisomeren von Decalin zu erreichen. Gute Ergebnisse bezüglich der Ausbeute von offenkettigen Decanen zeigten Na-Y-Katalysatoren mit einer Metallbeladung von etwa 3 Ma.-% Iridium bzw. Platin. Die maximale Ausbeute an OCDs an iridiumbeladenen Katalysatoren war 31 % und an platinbeladenen Na-Y-Katalysatoren 41 %.

Der Einfluss der Stärke der Brønsted-Säurezentren in Katalysatoren mit FAU-Struktur und einer Metallbeladung von 3 Ma.-% auf die Bildung von offenkettigen Decanen wurde auf zwei verschiedene Arten untersucht. Zum einen wurden die ladungskompensierenden Alkalikationen im Y-Zeolithen variiert, wobei die Stärke der Brønsted-Säurezentren in Li,H-Y-Zeolithen am stärksten ist und in der Reihe zu Cs,H-Y-Zeolithen abnimmt. Zum anderen wurde die Stärke der Säurezentren durch das n_{Si} / n_{Al} –Verhältnis im Zeolithen variiert. Schwächere Brønsted-Säurezentren als in Na,H-Y führten an iridiumbeladenen Katalysatoren zu deutlich geringeren Ausbeuten an OCDs. Eine leichte Erhöhung der Stärke dieser Zentren führte zu einer Verbesserung der Ausbeute von bis zu 39 %. Zu starke Brønsted-Säurezentren führten wiederum zu geringeren Ausbeuten an offenkettigen Decanen. An platinbeladenen Katalysatoren ließ sich keine Verbesserung der katalytischen Ergebnisse durch Variation der Säurestärke im Vergleich zum Na,H-Y-Katalysator erzielen. Schwächere Brønsted-Säurezentren als in Na,H-Y führten dagegen zu einem starken Verlust der Aktivität des Katalysators, und große Mengen an den dehydrierten Produkten Tetralin und Naphthalin traten auf.

In allen bisher erwähnten Katalysatoren befanden sich nur die Brønsted-Säurezentren, die durch die Reduktion des Edelmetallkations erzeugt wurden. Eine Erhöhung der Konzentration der Brønsted-Säurezentren durch das Eintauschen von Lanthanionen, die bei höheren Temperaturen über den Hirschler-Plank-Mechanismus Brønsted-Säurezentren bilden, erlaubte die Reduzierung der Metallbeladung mit Iridium auf 1 Ma.-% in X-Zeolithen ohne großen Verlust an der OCD-Ausbeute. Die maximale Ausbeute an OCDs an La-X- und La-Y-Zeolithen beladen mit 1 Ma.-% Iridium betrug 34 %. Die Variation der Konzentration der Brønsted-Säurezentren in platinbeladenen La-X- oder La-Y-Katalysatoren konnte zwar in einigen Fällen die Aktivität erhöhen, führte aber nur zu Ausbeuten von offenkettigen Decanen bis 30 %.

Der Versuch, durch Bildung einer Legierung aus Iridium und Platin in verschiedenen Stoffmengenverhältnissen verbesserte katalytische Eigenschaften zu erlangen, misslang. Die erhaltenen Ergebnisse suggerierten eher, dass sich keine Legierungen mit neuen

Eigenschaften gebildet hatten, sondern nur physikalische Mischungen der beiden monometallischen Katalysatoren vorlagen.

Alle erzielten Ergebnisse zeigten, dass sehr selektive Katalysatoren für die Ringöffnung von Decalin eine ausgewogene Balance zwischen der Metallfunktion und der Konzentration und Stärke der Brønsted-Säurezentren aufweisen müssen. Die Katalysatoren konnten aufgrund der Ergebnisse in drei Kategorien aufgeteilt werden: Katalysatoren an denen nur Hydrogenolyse am Metall ablief; bifunktionelle Katalysatoren, in denen das Metall die Dehydrier- / Hydrierkomponente darstellte und die Kohlenwasserstoffe an der sauren Funktion umgesetzt wurden sowie trifunktionelle Katalysatoren. An diesen trifunktionellen Katalysatoren überwog die Hydrogenolyse am Edelmetall, aber zusätzlich waren typische Anzeichen für bifunktionelle Katalyse wahrnehmbar. An fast allen Katalysatoren wurden offenkettige Decane gebildet, aber die höchsten Ausbeuten wurden an trifunktionellen Katalysatoren beobachtet.

Reine Hydrogenolyse an Platin führte zu wenig aktiven Katalysatoren. Hauptsächlich wurden die dehydrierten Produkte Tetralin und Naphthalin gebildet. Es konnten auch im geringeren Maße Gerüstisomere beobachtet werden. Nach der ersten Ringöffnung fand fast ausschließlich ein exocyclischer C-C-Bindungsbruch statt, der zu Crackprodukten führte, nicht aber zur Bildung von offenkettigen Decanen.

Reine Hydrogenolyse an Iridium ließ sich an dem Ausbleiben des Gerüstisomers Spiro[4.5]decan erkennen, zusätzlich zeigten diese Katalysatoren eine hängemattenförmige Verteilungskurve der Kohlenstoffanzahl der Crackprodukte. An diesen Katalysatoren fand keine Isomerisierung statt, sondern sehr selektiv die direkte Ringöffnung von Decalin in seine fünf Ringöffnungsprodukte (Butylcyclohexan, cis- / trans-1-Methyl-2-propylcyclohexan und cis- / trans-1,2-Diethylcyclohexan). Im nächsten Schritt konnten diese Ringöffnungsprodukte entweder einen endocyclischen C-C-Bindungsbruch eingehen und offenkettige Decane oder durch Methanabstraktion die drei direkten C_9-ROPs cis- / trans-1-Ethyl-2-methylcyclohexan und Propylcyclohexan bilden. Diese wiederum wurden sehr selektiv zu offenkettigen Nonanen umgesetzt.

An bifunktionellen Katalysatoren bestanden die gebildeten Crackprodukte fast ausschließlich aus iso-Butan und Methylcyclopentan. Die in diesen Fällen beobachtete M-förmige Verteilungskurve der Kohlenstoffanzahl der Hydrocrackprodukte mit zwei scharfen Maxima bei C_4 und C_6 ist auf die sogenannte „paring-reaction“ von C_{10}-Einringnaphthenen zurückzuführen. In diesen Naphthenen wurde eher die Seitenkette isomerisiert, bis eine

schnelle β-Spaltung des Typs A möglich war, als dass ein endocyclischer C-C-Bindungsbruch stattfand. Diese β-Spaltung des Typs A bildete ausschließlich die Hydrocrackprodukte iso-Butan und Methylcyclopentan. Da an diesen Katalysatoren aber auch offenkettige Decane mit einer Ausbeute von bis zu 12 % gebildet wurden, muss es einen noch unbekannten konkurrierenden Mechanismus geben, der an diesen Katalysatoren stattfand. Egal ob die Metallkomponente aus Platin oder Iridium bestand, unterschieden sich weder die Selektivitäten der einzelnen Produktgruppen noch die erhaltenen Signale im Gaschromatographen merklich voneinander. Dies war ein Hinweis darauf, dass die Rolle des Metalls in diesen Katalysatoren wirklich nur das Dehydrieren und Hydrieren der Kohlenwasserstoffe war.

An den trifunktionellen Katalysatoren überwog die Hydrogenolyse am Edelmetall, aber zusätzlich waren Anzeichen für die bifunktionelle Katalyse wahrnehmbar. Im Fall von iridiumbeladenen Katalysatoren stellte sich die Verteilungskurve der Anzahl der Kohlenstoffatome in den Hydrocrackprodukten als ein gutes Hilfsmittel heraus. Reine Hydrogenolyse an Iridium lieferte eine hängemattenförmige Verteilungskurve. Für Katalysatoren mit einer hohen Ausbeute an offenkettigen Decanen erhöhte sich die ursprüngliche Kurve im Bereich zwischen C_3 und C_7. Anhand der Verteilungskurve der Anzahl der Kohlenstoffatome in den Hydrocrackprodukten konnte man also erkennen, ob ein vermessener Katalysator eine höhere oder niedrigere Konzentration oder Stärke an Brønsted-Säurezentren braucht, um seine beste Leistung bezüglich der Bildung von offenkettigen Decanen zu erreichen. Dieses Hilfsmittel konnte leider nicht auf Katalysatorsysteme übertragen werden, die Platin enthalten. Die Verteilungskurven der Anzahl der Kohlenstoffatome in den Hydrocrackprodukten sahen sowohl für die Hydrogenolyse am Metall als auch für die trifunktionellen Katalysatoren ähnlich aus. Lediglich eine zu hohe Konzentration oder Stärke der Brønsted-Säurezentren konnte anhand dieser Verteilungen diagnostiziert werden, da sich dann eine Überlagerung mit der M-förmigen Verteilungskurve (scharfe Maxima bei C_4 and C_6), die an bifunktionellen Katalysatoren beobachtet wurde, ergab.

Edelmetallhaltige ZSM-12- und MCM-22-Katalysatoren wurden ebenfalls in der hydrierenden Umsetzung von Decalin getestet. Keiner dieser Katalysatoren konnte die Leistung der FAU-Katalysatoren steigern, da die Stärke der Brønsted-Säurezentren vermutlich zu hoch war. Effekte, die auf eine Formselektivität zurückzuführen wären, konnten ebenfalls nicht beobachtet werden. Die höchsten Ausbeuten an offenkettigen Decanen an ZSM-12- bzw. MCM-22-Katalysatoren waren 17 und 19 %.

Die monofunktionellen H-ZSM-12-Katalysatoren zeigten starke Desaktivierung, bildeten große Mengen an ungesättigten Kohlenwasserstoffen und Kohlenwasserstoffen mit mehr als zehn Kohlenstoffatomen und hatten eine hohe Tendenz zum Cracken. Offenkettige Decane wurden nur in Spuren gebildet. Auffälligkeiten ergaben sich allerdings bezüglich des Verhältnisses von cis- und trans-Decalin. Während alle metallhaltigen Katalysatoren in dieser Arbeit cis-Decalin fast vollständig zu trans-Decalin isomerisierten, wurde diese Isomerisierung an H-ZSM-12 nur in vernachlässigbarem Ausmaß beobachtet. Vergleiche mit anderen sauren Katalysatoren ließen vermuten, dass cis-Decalin zu sperrig für das Porensystem von ZSM-12 war.

2 Summary

The aim of this work was to identify key factors which a high-performance catalyst should have to achieve high yields of open-chain decanes in the hydroconversion of cis-decalin. In order to reach this goal, the kind of the noble metal, the metal loading and the concentration and strength of the Brønsted acid sites in catalysts of the FAU type were varied.

To cope with the more than 180 hydrocarbons in the product mixture of the hydroconversion of decalin, the products were classified mainly based on the GC/MS analyses and the determination of the molar mass in six product groups: (i) skeletal isomers of decalin (sk-Isos) with two naphthenic rings and a molar mass of 138 $g \cdot mol^{-1}$; (ii) ring opening products (ROPs) with one remaining naphthenic ring and a molar mass of 140 $g \cdot mol^{-1}$; (iii) open-chain decanes (OCDs) with a molar mass of 142 $g \cdot mol^{-1}$; (iv) dehydrogenated C_{10} products (DHPs); (v) hydrocarbons with more than 10 carbon atoms (C_{11}+) and (vi) hydrocracked products (C_9-). For a safe identification of the desired open-chain decanes, n-decane was isomerized in separate experiments, and the mixture of iso-decanes thereby generated was co-injected with the liquid products from decalin hydroconversion.

At low conversions on iridium-containing catalysts ring opening products of decalin were prevailing, whereas platinum-containing catalysts first isomerized decalin to skeletal isomers. With a pronounced concentration or strength of Brønsted acid sites also iridium-containing catalysts were able to isomerize significantly decalin to its skeletal isomers. The optimum metal loading for a high yield of open-chain decanes on Na-Y zeolites was for both metals around 3 wt.-%. Maximum yields of OCDs of 31 and 41 %, respectively, were obtained on the iridium- and platinum-containing Y catalysts.

The strength of Brønsted acid sites in FAU-type catalysts with 3 wt.-% of metal loading was influenced by using different alkali metals as charge-compensating cations in the zeolite or by varying the n_{Si} / n_{Al} ratio of the zeolite support between 1.0 and 5.5. On the iridium-containing catalysts the yield of open-chain decanes decreased significantly by using weaker Brønsted acid sites than in Na,H-Y. This was indeed the case by lowering the strength of Brønsted acid sites by using potassium, rubidium or cesium instead of sodium as charge-compensating cations or by using zeolites X and LSX with a lower n_{Si} / n_{Al} ratio than zeolite Y. Stronger Brønsted acid sites than in Na,H-Y could be obtained with n_{Si} / n_{Al} ratios above 2.4 or with lithium as charge-compensating cation. On catalyst Ir/Li,H-Y the yield of OCDs was lower than on Ir/Na,H-Y, but higher n_{Si} / n_{Al} ratios, obtained by the dealumination of Na-Y with $(NH_4)_2[SiF_6]$, led to higher yields of OCDs up to an n_{Si} / n_{Al} ratio of 4.1. The maximum yield

was 39 %. In contrast, on the platinum-containing Na,H-Y catalysts each variation of the Brønsted acid site strength lowered the yield of open-chain decanes. A lower strength of the Brønsted acid sites than in Pt/Na,H-Y led to a strong decrease in the activity of the catalyst and to large amounts of dehydrogenated products like tetralin and naphthalene.

In all above-mentioned catalysts only the Brønsted acid sites generated by the reduction of the noble metal were present. An enhancement of the concentration of Brønsted acid sites by introducing lanthanum ions which generated Brønsted acid sites *via* the Hirschler-Plank mechanism, allowed to reduce the iridium content to 1 wt.-% in La-X zeolites without significantly lowering the yield of OCDs. The maximum yield of open-chain decanes on Ir/La-X or Ir/La-Y catalysts was 34 %. The variation of the concentration of Brønsted acid sites in La-X or La-Y catalysts loaded with 1 wt.-% platinum did not lead to improved performances of the catalysts. The maximum yield of open-chain decanes on Pt/La-X or Pt/La-Y catalysts was 30 %.

An attempt was undertaken to form alloys of iridium and platinum with different molar ratios on Na,H-Y zeolites, but the obtained results suggested that only physical mixtures were generated leading to no significant improvement in contrast to the monometallic catalysts.

All results suggested that a balance between the metal content and the concentration and strength of Brønsted acid sites was important and necessary. The catalysts could be divided into three categories: catalysts on which only hydrogenolysis on the metal took place; bifunctional catalysts on which the metal had only a dehydrogenation / hydrogenation function and the acid sites are responsible for the conversion of decalin and trifunctional catalysts on which mainly hydrogenolysis on the metal took place but also hints of a superimposition of bifunctional catalysis were visible. On nearly all catalysts open-chain decanes were obtained, but the best catalysts belonged to the group of trifunctional catalysts.

Catalysts on which pure hydrogenolysis on platinum took place, had a very low activity. The main hydrocarbons were the dehydrogenated products tetralin and naphthalene. A few skeletal isomers were detected, and after ring opening mainly exocyclic C-C bond rupture of the ring opening products took place leading to hydrocracked products instead of the formation of open-chain decanes.

Pure hydrogenolysis on iridium was indicated by the absence of the skeletal isomer spiro[4.5]decane and a hammock-shaped carbon number distribution curve. In a first step

one ring of decalin was opened very selectively to the five direct ROPs butylcyclohexane, cis- and trans-1-methyl-2-propylcyclohexane and cis- and trans-1,2-diethylcyclohexane. In a further step these five ring opening products underwent either endocyclic C-C bond rupture and formed open-chain decanes or methane abstraction leading to the direct C_9-ROPs cis-/trans-1-ethyl-2-methylcyclohexane and propylcyclohexane. In a consecutive step these three direct C_9-ROPs formed very selectively open-chain nonanes.

On bifunctional catalysts very selectively iso-butane and methylcyclopentane as main hydrocracked products were formed. This effect of an M-shaped carbon number distribution was attributed to the paring reaction of C_{10} one-ring naphthenes. These naphthenes underwent several skeletal isomerizations in the alkyl side chain instead of endocyclic C-C bond rupture until precursors for the very rapid type A β-scissions originated leading to iso-butane and methylcyclopentane. In addition a competitive reaction seemed to occur, otherwise the formation of open-chain decanes with a yield around 10 % could not be explained. On bifunctional catalysts the results obtained with an iridium- or platinum-containing catalyst did not differ. The selectivities of the different product groups and the obtained signals in the gas chromatograms were nearly identical showing that the main role of the metal in these catalysts was the dehydrogenation and hydrogenation of the hydrocarbons.

The best trifunctional catalysts showed the prevailing mechanism of hydrogenolysis but also a clear contribution of bifunctional catalysis. In case of iridium-containing catalysts the carbon number distribution was a very good evidence for the identification of such catalysts. The hammock-shaped curve obtained from hydrogenolysis on iridium was then shifted between C_3 and C_7 to higher values. This carbon number distribution could also be used as a tool for the preparation of high-performance catalysts indicating whether a prepared catalyst needs a higher or lower concentration or strength of Brønsted acid sites to improve the ring opening performance. On platinum-containing catalysts no clear characteristics could be identified for the high-performance catalysts. The carbon number distributions are nearly identical on all catalysts except catalysts with a high strength or concentration of Brønsted acid sites, which was indicated by a significant superimposition of the M-shaped curve, with maxima at C_4 and C_6.

Iridium- and platinum-containing ZSM-12 and MCM-22 catalysts were also tested in the hydroconversion of decalin. With none of these catalysts the performances of the best FAU catalysts could be further improved. In all catalysts the strength of the Brønsted acid sites

was too high. The maximal obtained yields of OCDs were 17 and 19 %, respectively, on ZSM-12 and MCM-22 catalysts. No shape selectivity was observed.

Monofunctional acidic ZSM-12 catalysts suffered from strong deactivation, large amounts of unsaturated compounds, the formation of hydrocarbons with more than 10 carbon atoms and a high cracking activity. Negligible amounts of open-chain decanes were formed on these catalysts. The carbon number distribution of the cracked products gave hints for a contribution of the Haag-Dessau mechanism. A peculiarity occurred concerning the isomerization of cis- to trans-decalin. On all metal-containing catalysts cis-decalin was converted almost completely to trans-decalin whereas on H-ZSM-12 only small amounts of cis-decalin were isomerized. Comparison with other monofunctional acidic catalysts led to the assumption that cis-decalin could not enter the pores of H-ZSM-12.

3 Introduction and Objectives

The introduction of the Euro 5 standards [1] reduces the emissions of particulate matter of diesel vehicles from 25 to 5 mg km^{-1}. Comparative tests with normal diesel (DIN EN590) containing 25 % aromatics and diesel fuels with 0-5 % aromatics show that, upon reducing the aromatics content, the emission of particulate matter is reduced to 30 % [2]. Polycyclic aromatics have an even higher tendency for the formation of particulates than one-ring aromatics [3], and they bring about various additional undesirable properties, such as poor ignition characteristics and cetane numbers, an increased propensity for soot formation and unfavorable cold-flow properties. For these reasons, the content of polycyclic aromatics in diesel fuels is limited by legislation to 8 wt.-% [4]. Certain refinery streams, such as light cycle oil (LCO) from the FCC unit are rich in these undesired compounds and can be blended into diesel fuels only to a limited extent. A most attractive way for upgrading these refinery streams is the selective ring opening of polycyclic aromatics into alkanes, without degradation of the carbon number, as illustrated in Figure 3.1.

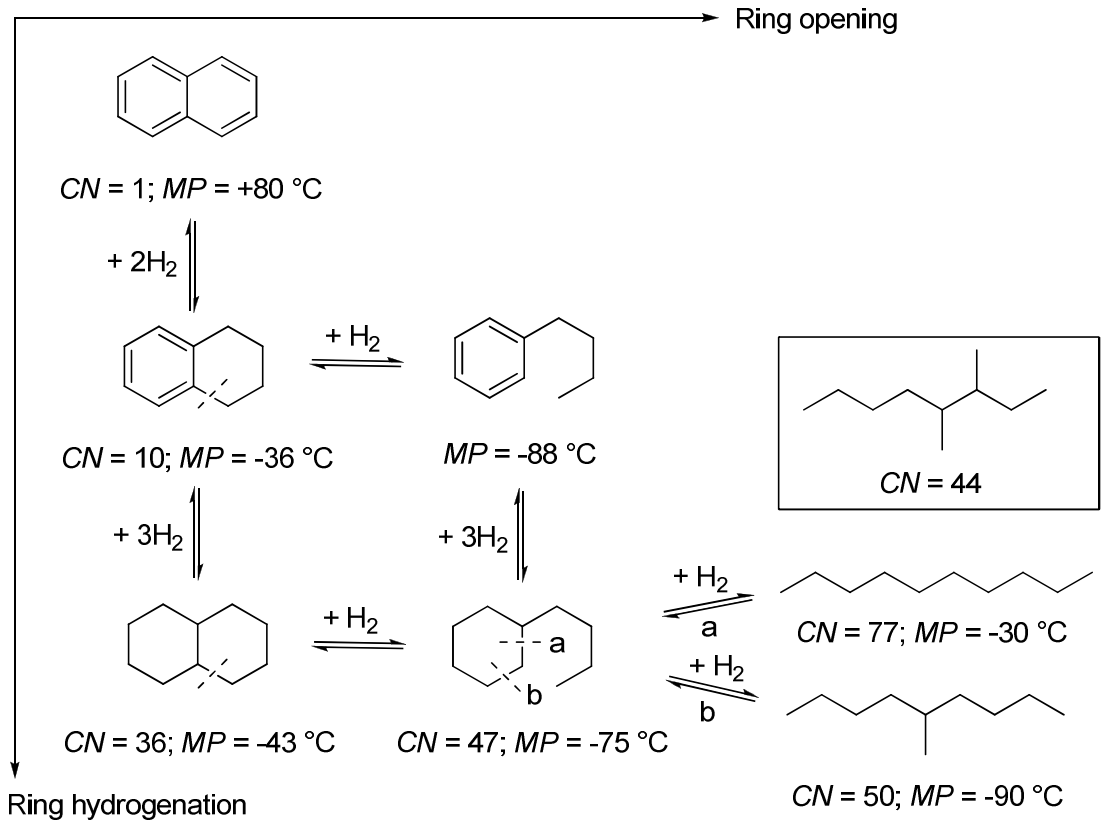

Figure 3.1: Idealized network for ring opening of a multi-ring aromatic hydrocarbon into alkanes, after Ref. [5]. Available cetane numbers (*CN*) and melting points (*MP*) of the components are also indicated.

The simplest polycyclic aromatic is naphthalene with a cetane number of 1. The ring opening is generally preceded by ring hydrogenation consuming large amounts of hydrogen (7 mol hydrogen per 1 mol of C_{10} alkanes formed from naphthalene). Upon ring hydrogenation and ring opening the cetane number increases. Very desirable compounds concerning the cetane number are open-chain alkanes with the same carbon number as the aromatic compound. n-Decane has the highest cetane number among the decane isomers, and with each branching the cetane number decreases. Nevertheless, mildly branched decanes are even more favored than n-decane because of the impact of branching on the cold flow properties. With each branching the melting point of the pure compound decreases by about 60 °C. A high contribution of aromatics in diesel fuel leads to a high cloud point because of the very high melting point of the pure aromatics. This can cause problems especially in the winter time.

The objective of this work was to maximize the yield of open-chain decanes in the ring opening of the model hydrocarbon decalin in a catalytic high-pressure flow-type apparatus under a hydrogen atmosphere. Different 12-membered ring zeolites were investigated as catalysts. The principal work is based on zeolites X and Y of the FAU type. The influence of the nature of the noble metal iridium or platinum, the metal loading, the concentration and the strength of Brønsted acid sites, varied by the n_{Si} / n_{Al} ratio of the zeolite and the kind of charge-compensating alkali cation, on the ring opening performance of decalin was examined. Key properties were determined which a catalyst should have to be a high-performance catalyst in the formation of open-chain decanes. In addition, mechanistic ideas are developed concerning important intermediates in the ring opening of decalin to iso-decanes.

Beside faujasites, zeolites ZSM-12 (MTW) and MCM-22 (MWW) were investigated as catalysts in the hydroconversion of decalin in order to search for possible shape-selectivity effects in the narrow pores of ZSM-12 or a reduced probability of readsorption of ring-opened products and thus further cracking by using only the pockets on the outer surface of MCM-22.

4 Literature Review

4.1 Zeolites and Acid Sites in Zeolites

Zeolites are microporous crystalline solids with well-defined structures. The elementary building units of zeolites are generally SiO_4 and AlO_4, less frequently other building units like PO_4 or TiO_4 are used. These tetrahedra are linked at their corners via a common oxygen atom and form a rich variety of different three-dimensional frameworks with channels and cages with diameters between 0.2 and 1 nm. The linkage of the tetrahedra is not entirely random, a restriction is described by Löwenstein´s rule [6]: The linkage of two tetrahedra with aluminum on tetrahedral positions is forbidden which results in $n_{Si} / n_{Al} \geq 1$ of the zeolite framework.

The Structure Commission of the International Zeolite Association (IZA) assigns to each framework type a Framework Type Code with three letters. A given framework type can consist of zeolites with different chemical compositions. In this work zeolites with framework types of FAU, MTW and MWW were used. Zeolite ZSM-12 is one member of the framework type MTW. This structure is illustrated in Figure 4.1. The corners of the structure represent the T-atoms (T = Si, Al, P, Ti, ...) whereas the lines connecting them represent T-O-T bonds. The structure of ZSM-12 consists of a 1-dimensional channel system with a 12-membered ring opening formed by 12 TO_4 tetrahedra. The pores are slightly elliptical with dimensions of 0.56 x 0.60 nm, which is very narrow for a 12-membered ring pore.

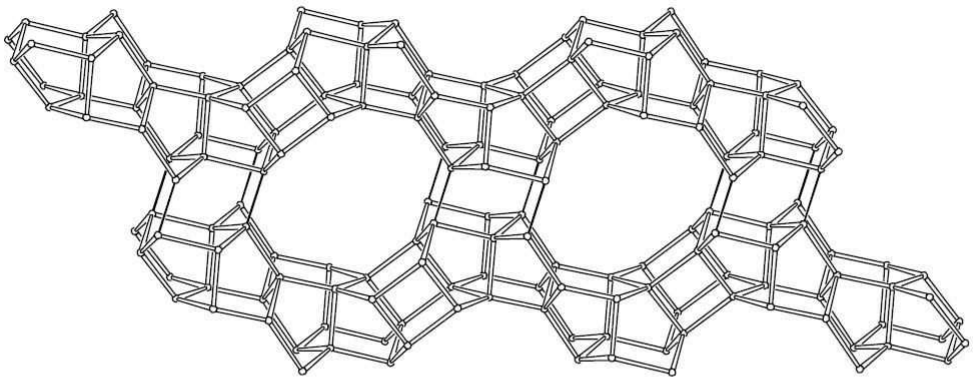

Figure 4.1: Structure of zeolite ZSM-12 (MTW) [7] viewed along [010].

The structure of the framework type MWW with its typical representative zeolite MCM-22 is illustrated in Figure 4.2. The framework topology is comprised of two non-intersecting 10-membered ring pore systems. One of the systems is defined by two-dimensional sinusoidal channels with a pore diameter of 0.40 x 0.55 nm, the other 10-membered ring system (A in Figure 4.2 right) has a pore diameter of 0.41 x 0.51 nm and gives access to large cages (C in

Figure 4.2 right) inside the channel. These cages, only accessible via the 10-membered rings, are defined by 12-membered rings and have an inner diameter of 0.71 nm and a height of 1.82 nm. The outer surface of MCM-22 is covered with 12-membered ring pockets (each pocket corresponds to a half of the large cage) with a depth of approximately 0.7 nm.

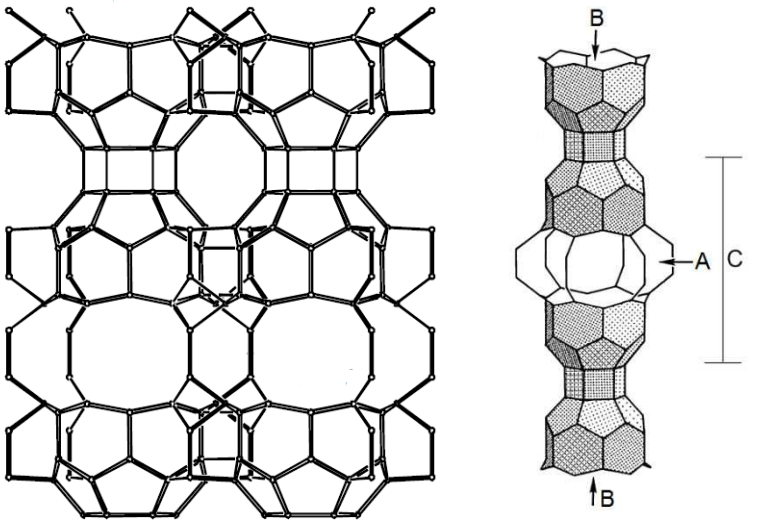

Figure 4.2: Structure of zeolite MCM-22 (MWW) viewed along [010] (left) [7] and a schematic illustration of two layers of MCM-22 showing the 10-membered ring apertures (A) to the large cage (C) and the surface pockets (B) (right) [8].

The mainly used framework type in this work is FAU named after the mineral faujasite. Faujasite possesses a three-dimensional, 12-membered ring channel system. In this structure 24 tetrahedra are linked together to a secondary building unit called sodalite cage (see Figure 4.3). These sodalite cages are connected via their hexagonal faces and form a large spherical cage, the supercage. This supercage is connected tetrahedrally with four neighboring cages through 12-membered ring windows. The 12-membered ring pores have a dimension of 0.74 x 0.74 nm, which is relatively spacious for a 12-membered ring zeolite. The supercages have a diameter of 1.3 nm.

Depending on the n_{Si} / n_{Al} ratio, the synthetic zeolites with faujasite structure are called LSX (low-silica X, $1 \leq n_{Si} / n_{Al} < 1.1$), X ($1.1 \leq n_{Si} / n_{Al} < 1.5$) and Y ($1.5 \leq n_{Si} / n_{Al} < 3$). Higher n_{Si} / n_{Al} ratios can be achieved via uneconomically high crystallization times or, more importantly, via chemical post-synthesis modification of the zeolite framework, *i. e.*, by dealumination. The principle is to remove framework aluminum in order to increase the n_{Si} / n_{Al} ratio. The removal of aluminum results in lattice defects, which can be diminished by incorporation of other elements like silicon. Industrially used methods are steaming of zeolites at high temperatures or leaching with mineral acids. Both techniques are cheap but result in lattice defects and generate mesopores. Leaching of aluminum-rich zeolites like faujasites with mineral acids diminishes the stability of the crystal structure and can result in

a collapse of the structure. Dealumination with silicon tetrachloride leads to a substitution of the aluminum in the framework by silicon from the dealumination agent without any substantial lattice damage. Great experience is necessary to find the exact conditions for partial dealumination of Y zeolites without essential damage to the lattice [9]. A much easier technique, although with a similar principle, is the dealumination with aqueous $(NH_4)_2[SiF_6]$ solution. Again, the aluminum of the lattice is substituted by the silicon of the dealumination agent. A limitation of the technique is that it is only applicable for partial dealumination. High dealumination degrees (> 50 %) lead to a collapse of the structure. The latter technique was applied in this work for partial dealumination of Y zeolites up to n_{Si} / n_{Al} ratios of 5.5.

Each AlO_4 tetrahedron in the zeolite generates a negative charge which must be compensated by cations. These commonly small and mobile cations sitting in the pores of the zeolite can be exchanged by other cations, which make zeolites to typical ion exchangers. Different positions for extra-framework cations exist in faujasite zeolites and are illustrated in Figure 4.3. Depending on the cations and the thermal pretreatment conditions different positions are preferred. In a commonly used Na-Y zeolite with an n_{Si} / n_{Al} ratio of 2.5, 54 Na^+ ions per unit cell occur [10]. 46 % of the cations are located in the small cages, thereof 7 at site I at the center of the hexagonal prism and 18 at site I´ displaced from a shared hexagonal face inside the sodalite cage. The remaining 29 Na^+ ions per unit cell are located in the supercages at position II slightly displaced from an unshared hexagonal face in the supercage. In Na-LSX zeolite with an n_{Si} / n_{Al} ratio of 1.0 also site III´ can be occupied by sodium cations [11]. Site IV at the center of the supercage, site V at the center of the 12-ring window and site U in the center of the sodalite cage are special cation positions found only in hydrated samples.

An important property of zeolites is their surface acidity. Both Brønsted acid sites and Lewis acid sites occur in zeolites. Brønsted acid sites are hydroxyl groups acting as proton donors, whereas the chemical nature of Lewis acid sites in zeolites is less clear. Kühl [12] proposed that the Lewis acid sites in zeolites are hexagonally coordinated $(AlO)^+$ species generated by the destruction of the zeolite framework. Brønsted acid sites in zeolites can be generated by four different methods represented by Eqs. (4.1) to (4.4) [13]. Z^- stands for the negatively charged zeolite framework in the vicinity of framework aluminum atoms.

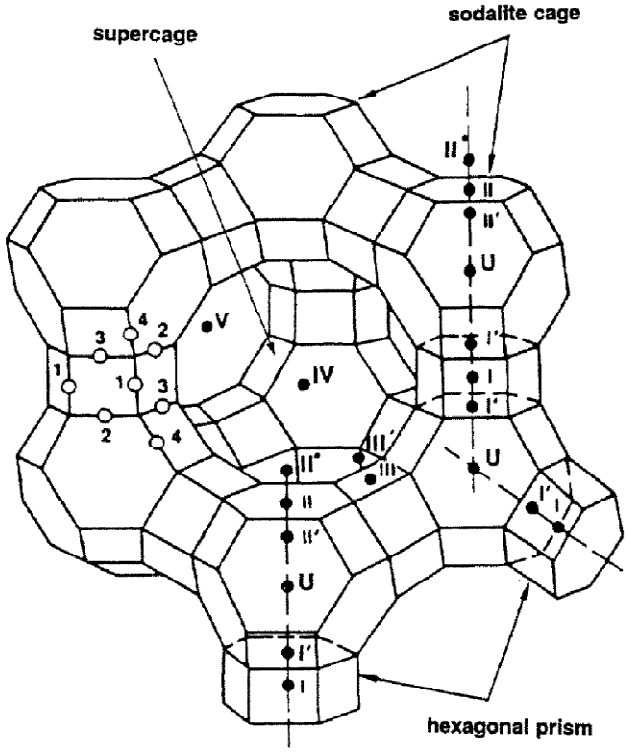

Figure 4.3: Structure of zeolite faujasite [14]. The projection is along [111]. The four crystallographically different oxygen framework atoms are marked by the numbers 1 to 4. The cation positions are marked by roman numerals.

The direct ion exchange with mineral acids (Eq. (4.1)) is a less favored method for the incorporation of Brønsted acid sites in zeolites. The exposure of zeolites to mineral acids can lead to the extraction of framework aluminum or, in case of zeolites with a low n_{Si} / n_{Al} ratio, to a collapse of the structure [15].

$$H^+ + Na^+Z^- \xrightarrow[-Na^+]{} H^+Z^- \qquad (4.1)$$

An often used method to generate Brønsted acid sites in zeolites is the aqueous ion exchange with ammonium salts followed by thermal decomposition of the ammonium ions in the zeolite (Eq. (4.2)). The concentration of the acid sites increases with the calcination temperature until all ammonium ions have been decomposed.

$$NH_4^+ + Na^+Z^- \xrightarrow[-Na^+]{} NH_4^+Z^- \xrightarrow[-NH_3]{\approx 300\text{-}400\ °C} H^+Z^- \qquad (4.2)$$

Ion exchanges with salts of multivalent cations like Mg^{2+} or La^{3+} followed by thermal dehydration generate Brønsted acid sites (Eq. (4.3)) in zeolites and in addition improve the thermal stability of hydrogen zeolites. The Hirschler-Plank mechanism shown in Eq. (4.3) assumes that, under the influence of the strong electrostatic field in the zeolite caused by the

multivalent cations, the remaining water molecules on the cation dissociate and give rise to a proton and a hydroxyl group.

$$[La(H_2O)_n]^{3+} + 3\,Na^+Z^- \xrightarrow[-\,3\,Na^+]{} [La(H_2O)_n]^{3+}(Z^-)_3 \xrightarrow[-(n-2)\,H_2O]{\approx 300\,^\circ C}$$

$$[La(OH)(H_2O)]^{2+}H^+(Z^-)_3 \longrightarrow [La(OH)_2]^+(H^+)_2(Z^-)_3 \qquad (4.3)$$

Ion exchange with aqueous solutions of noble metal salts is a frequently used method to incorporate a hydrogenation / dehydrogenation function into zeolites. During the reduction of the metal ion with hydrogen Brønsted acid sites are unavoidably formed (Eq. (4.4)).

$$[Pd(NH_3)_4]^{2+} + 2\,Na^+Z^- \xrightarrow[-\,2\,Na^+]{} [Pd(NH_3)_4]^{2+}(Z^-)_2 \xrightarrow[-4\,NH_3]{\approx 300\,^\circ C}$$

$$Pd^{2+}(Z^-)_2 \xrightarrow{+\,H_2} Pd^0(H^+)_2(Z^-)_2 \qquad (4.4)$$

The concentration or density of Brønsted acid sites in a zeolite is obviously related to the framework aluminum content expressed by the n_{Si} / n_{Al} ratio. The strength of the Brønsted acid sites depends on the zeolite structure and the n_{Si} / n_{Al} ratio. A high aluminum content in zeolites leads to a lower strength of Brønsted acid sites. This was explained in faujasites with the next nearest neighbors (NNNs) concept. Each framework aluminum atom is linked *via* oxygen atoms to four silicon atoms, which are connected with nine further T atoms (the NNNs) in the next coordination sphere. The lower the number of aluminum atoms within these NNNs the higher is the acid strength of the Brønsted acid sites in the zeolite [16]. In addition, it was observed in M,H-Y zeolites (M = Li, Na, K, Rb, Cs) that the strength of Brønsted acid sites decreases in the following order: Li,H-Y > Na,H-Y > K,H-Y > Rb,H-Y > Cs,H-Y [17 - 19]. This can be explained by the Sanderson concept [20] claiming that the electronegativity of solids and consequently their acid strength increases when an electronegative atom is added since the electronegativity decreases from lithium to cesium.

4.2 Generation of Brønsted Acid Sites in Zeolites by Addition of Rare Earth Metal Cations

4.2.1 Concentration and Strength of the Brønsted Acid Sites Generated by Rare Earth Metal Cations

In a conference discussion about the work of Pickert *et al.* [21], Plank reported about rare-earth (RE) exchanged zeolites. He observed that a strongly dehydrated (T = 650 °C) rare earth zeolite has very low activity for hexane cracking at 315 °C, whereas equilibration with water increases its activity several thousand times at the same temperature. He postulated an equilibrium as Hirschler [22] had assumed for alkaline earth cations:

$$RE^{3+} + H_2O \rightleftharpoons [RE(OH)]^{2+} + H^+ \qquad (4.5)$$

Ward [23] investigated rare-earth exchanged Y zeolites with 92 % exchange degree via IR spectroscopy. He observed that the concentration of Brønsted acid sites generated in RE-Y zeolites is intermediate between H-Y and Mg-Y, which is the alkaline earth zeolite with the highest concentration of Brønsted acid sites. Like in case of the alkaline earth cations these acid sites were generated by hydrolysis of the water attached to the cation.

$$[RE(H_2O)_2]^{3+} \rightleftharpoons [RE(OH)(H_2O)]^{2+} + H^+ \rightleftharpoons [RE(OH)_2]^{+} + 2\,H^+ \qquad (4.6)$$

If complete hydrolysis of water is assumed to occur (see Eq. (4.6)), zeolite RE-Y should have two-thirds of the concentration of acid sites of H-Y, whereas partial hydrolysis should give one-third of the concentration of acid sites of H-Y. The results obtained on the RE-Y zeolite indicate a complete hydrolysis of the cation. The hydroxyl groups attached to the rare earth ion give rise to an absorption band near 3522 cm^{-1}. This group is non-acidic with respect to a base of the strength of pyridine.

Moscou and Lakeman titrated rare-earth exchanged Y zeolites with $LiAlH_4$ [24]. They found that each rare earth ion in the zeolite produces one acidic hydroxyl group in the supercage, which is in contrast to the results obtained by Ward [23]. At temperatures above 200 °C the concentration of acidic OH groups in the supercages is decreasing because of dehydroxylation.

Similar observations were made by Lee and Rees [25]. At temperatures below 100 °C the effective lanthanum charge in the small cages is 3+ and decreases to 2+ at temperatures above 200 °C. This is due to the dissociation of one water molecule bonded to the lanthanum

ion and the concomitant formation of one hydroxyl group (see Eq. (4.6)) which reduces the effective charge on the lanthanum ion. At temperatures between 580 and 850 °C the effective charge increases again to 3+ caused by dehydroxylation of the zeolite [26]. The authors advanced a dehydroxylation mechanism which removes a hydroxyl group from the lanthanum ion and a proton from the framework and thus retains the zeolite structure (Figure 4.4). During calcination a release of aluminum and silicon is observed. The silicon released is probably present as an impurity. There is a linear relationship between the amount of aluminum removed from the framework and the total number of protons produced from the lanthanum hydrolysis. According to these results four protons are required to remove one aluminum atom from the framework.

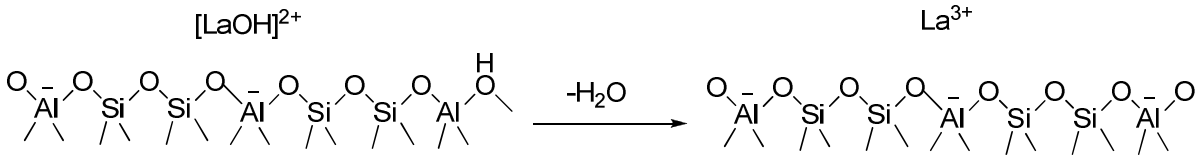

Figure 4.4: Dehydroxylation mechanism after Lee and Rees [26].

The dissociative adsorption of water at the multivalent lanthanum cations (see Eq. (4.6)) was found to be a reversible process in La,Na-X and La,Na-Y zeolites [27]. The maximum number of bridging OH groups occurs upon dehydration of these zeolites at 150 °C. A further raise of the dehydration temperature leads to a recombination of the hydroxyl groups to water (see Figure 4.4).

Eberly and Kimberlin [28] studied the Y, La, Ce, Pr, Sm, Eu, Gd, Dy, Er, Yb and Th forms of a Y zeolite on which pyridine was adsorbed by IR spectroscopy. The concentration of Brønsted acid sites increased with increasing ionic radius of the rare earth cations. The La, Eu and Yb forms showed a higher activity in the cumene cracking than the other rare earth Y zeolites.

Karge and Jozefowicz [29] investigated the differential heats of ammonia adsorption onto activated H-ZSM-5, H-Y, La,Na-Y and La,Na-X zeolites at an adsorption temperature of 152 °C. The differential heats of ammonia adsorption obtained for H-Y zeolite exhibit a plateau at 140 $kJ \cdot mol^{-1}$. The authors attributed this result to a homogeneous acid strength distribution of the Brønsted acid sites in the small cavities. In contrast, the Brønsted acid sites in the supercages seem to exhibit a broad distribution concerning their acid strength, but with a lower strength than the sites in the small cages. The absolute number of Brønsted acid sites in $La_{0.27},Na_{0.19}$-X is slightly higher than in $La_{0.24},Na_{0.28}$-Y (presumably due to the higher exchange degree) and lower than in H-Y. This was confirmed by IR spectroscopy with

pyridine as a probe molecule. As far as the strength of Brønsted acid sites is concerned, the sequence H-Y > La,Na-Y > La,Na-X was observed.

Huang *et al.* [27, 30] observed a slightly different sequence concerning the strength of Brønsted acid sites. They investigated the strength of the acid sites of H-Y, $La_{0.25}$,$Na_{0.25}$-Y and $La_{0.25}$,$Na_{0.25}$-X upon adsorption of deuterated acetonitrile by ^{1}H MAS NMR spectroscopy. The n_{Si} / n_{Al} ratios of all three zeolites were similar to those investigated by Karge and Jozefowicz [29]. However, at variance to their results obtained with IR spectroscopy, NMR spectroscopy indicated the following sequence: La,Na-Y > H-Y > La,Na-X. In case of La,Na-X zeolite, the strength of acid sites increased with increasing degree of lanthanum exchange. No effect of the degree of lanthanum exchange on the acid strength of bridging OH groups in zeolite La,Na-Y was found. During their ^{27}Al and ^{29}Si MAS NMR measurements the authors observed a local framework strain caused by lanthanum exchange and a polarizing effect of the multivalent cations. Hence they proposed that the inductive effect of the lanthanum ions causes a withdrawal of electrons from the O-H bonds of the Brønsted acid sites, thereby enhancing the acid strength of these groups.

4.2.2 Location of the Cations and Brønsted Acid Sites in Faujasite Zeolites Generated by Rare Earth Metal Cations

Hydrated La^{3+} ions have a diameter of 0.79 nm [25] and are therefore much too large to diffuse through six-membered rings (0.25 nm). Most or even all of the hydration shell must be stripped from the ion to enable lanthanum ions to migrate into the small cages of faujasite. Lee and Rees [25] observed a linear relationship between the number of lanthanum ions locked in the small cages and water molecules desorbed. They observed that lanthanum ion migration into the small cages starts at 60 °C, and the amount of lanthanum ions in the small cages reaches a constant level at temperatures above 300 °C.

This migration seems to start already during ion exchange at 80 °C. Zeolites X, Y and EMT were exchanged with $La(NO_3)_3$ solutions at 80 °C. Migration of some lanthanum cations to positions in the small cages takes place, but to what extent this occurs depends on the nature of the residual cations [31]. IR spectroscopy with pyridine and ^{1}H MAS NMR spectroscopy with deuterated pyridine as probe molecules showed that there is at least a 20 % higher concentration of Brønsted acid sites in the supercages in the sodium forms of the lanthanum-containing zeolites than in the respective potassium forms. The authors

concluded that the repulsive interactions of the large potassium cations presumably enhance the migration of lanthanum cations into the small cages.

The discussion about the location of the lanthanum ions in the small cages is controversial. In some papers it is claimed that lanthanum ions are located on sites I´ (see Figure 4.3) exclusively [14, 32]. In other publications it is proposed that these ions are mainly located on I sites [33]. A total of 14 lanthanum ions per unit cell can be located in the small cages on I´ and I positions [14, 33, 34]. The incorporation of rare earth cations into X and Y zeolites increases their thermal stability [35]. In general, zeolite Y exhibits a higher thermal stability than zeolite X.

The effect of drying RE-Y zeolites on the formation of acid sites was studied using techniques such as titration and reactions with $LiAlH_4$ in order to determine the location of water and acidic OH groups [24]. $LiAlH_4$ cannot enter the small cages and can therefore be used to probe the Brønsted acid sites in the supercages. During drying, migration of rare earth ions from the supercages to the small cages can be observed at 30 to 14 % weight loss after 1 h calcination at 1000 °C in comparison to the dry zeolite. Further drying results in the formation of acidic hydroxyl groups in the region between 14 and 10 % weight loss. These acidic OH groups can be titrated with $LiAlH_4$ and are therefore present in the supercages.

This observation has been supported by Karge and Jozefowicz [29]. H-Y zeolite exhibits a plateau in the differential heat of ammonia adsorption at 140 $kJ \cdot mol^{-1}$ (Section 4.2.1) which was attributed to Brønsted acid sites with a homogeneous strength located in the small cages. In case of $La_{0.24}$,$Na_{0.28}$-Y the isotherm does not exhibit such a plateau at 140 $kJ \cdot mol^{-1}$, indicating that the acidic OH groups do not exist in significant amounts in the small cavities of $La_{0.24}$,$Na_{0.28}$-Y. This points to the fact that the protons released via water dissociation at La^{3+} move into the supercages, whereas the OH groups attached to La^{3+} stay in the small cavities which is in accordance to the observations of Moscou and Lakeman [24].

4.2.3 Conclusions

The generation of Brønsted acid sites by rare earth cations is only well established for La^{3+} ions. The high charge results in the generation of up to two Brønsted acid sites per cation. But there is no agreement about whether one or two equivalents of Brønsted acid sites are generated by lanthanum ions. In general, there are more and stronger Brønsted acid sites generated by lanthanum ions in comparison to alkaline earth cations. It is again a matter of

debate if they are even stronger than the Brønsted acid sites in H-zeolites. The maximum concentration of Brønsted acid sites can be generated at temperatures around 150 °C. At higher temperatures dehydroxylation begins to take place. Upon thermal treatment of the ion-exchanged zeolites migration of the lanthanum ions into the small cages can be observed. The generated Brønsted acid sites seem to stay in the supercages.

In this work, X and Y zeolites with varying concentrations of lanthanum ions were used to investigate the influence of the concentration of Brønsted acid sites on the ring opening reaction. This goal could have been achieved as well by an exchange with ammonium ions and their subsequent thermal decomposition, but especially the acidic form of zeolite X is not stable. Lanthanum ions, in contrast, can stabilize the X zeolite and in addition can generate Brønsted acid sites.

4.3 Ring Opening of Multi-Ring Aromatics, Naphthenoaromatics and Multi-Ring Naphthenes

4.3.1 Mechanisms of Ring Opening

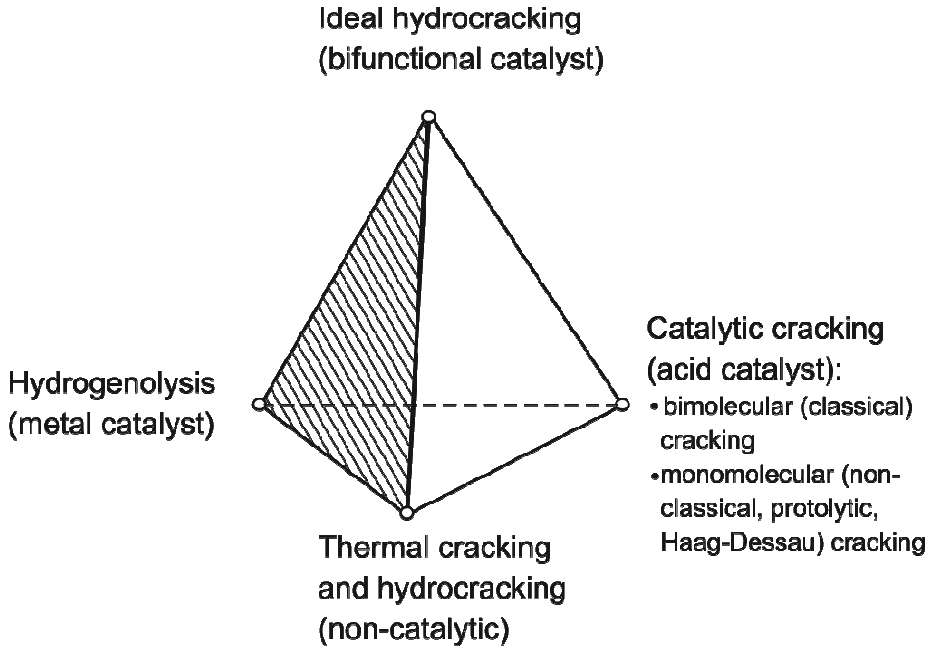

Figure 4.5: Pure mechanisms of hydrocracking and cracking [5].

Ring opening or, more precisely, hydrodecyclization is a special case of hydrocracking in which the carbon-carbon bond to be broken forms part of a naphthenic ring. In principle there exist four pure mechanisms for the C-C bond rupture, namely thermal hydrocracking,

hydrogenolysis, catalytic cracking and hydrocracking on bifunctional catalysts (see Figure 4.5). In many cases a superimposition of more than one mechanism is taking place. Here, some aspects of the four fundamental mechanisms will be presented.

4.3.1.1 Thermal Hydrocracking

Above temperatures of 500 °C C-C bond rupture can occur without use of a catalyst. This mechanism proceeds via radicals. At hydrogen partial pressures about 50 bar the hydrogen can be incorporated into the cracked products whereby less olefinic species are produced [36]. Nevertheless, thermal hydrocracking produces large amounts of light hydrocarbons, especially methane, which makes this kind of cracking unattractive.

4.3.1.2 Hydrogenolysis on Metal Catalysts

This class of catalytic reactions involves the rupture of carbon-carbon bonds via interaction with hydrogen. This interaction takes place while both species are adsorbed on a metal surface. Typical catalysts for this kind of reactions are noble metals on non-acidic supports. The hydrogenolysis activity of the metals depends mostly on the nature of noble metal and the metal dispersion. Both for ethane hydrogenolysis and for n-heptane hydrogenolysis the trends in the hydrogenolysis activities are the same at 205 °C: The reaction rates decrease from Ru over Rh, Ir to Pt and Pd [37].

In addition to hydrogenolysis, isomerization of hydrocarbons can occur, while they are adsorbed on a noble metal. This is particularly true for platinum, and to a lesser extent for rhodium, iridium, palladium and ruthenium [38]. Two principal mechanisms, by which skeletal isomerization on metals can occur, are generally distinguished, namely the bond shift mechanism and the C_5 cyclic mechanism. The bond shift mechanism is the only possible one for alkanes with less than six carbon atoms. Generally, there are two different pathways proposed as bond shift mechanism with a number of minor variations (Figure 4.6). The first one involves a cyclopropane intermediate (Figure 4.6a) which is formed from an α,γ-diadsorbed species on two metal sites. Subsequently, the bond shift occurs by breaking of a C-C bond which is different from the one formed before. The second mechanism (Figure 4.6b) involves an α,γ-diadsorbed species on a single metal atom in such a manner that a metallacyclobutane results. In a next step a metal-carbene complex and an alkene are formed which allows the alkenes to rotate and reassemble to another metallacyclobutane species which then desorbs from the metal site and forms an isomer of the reactant.

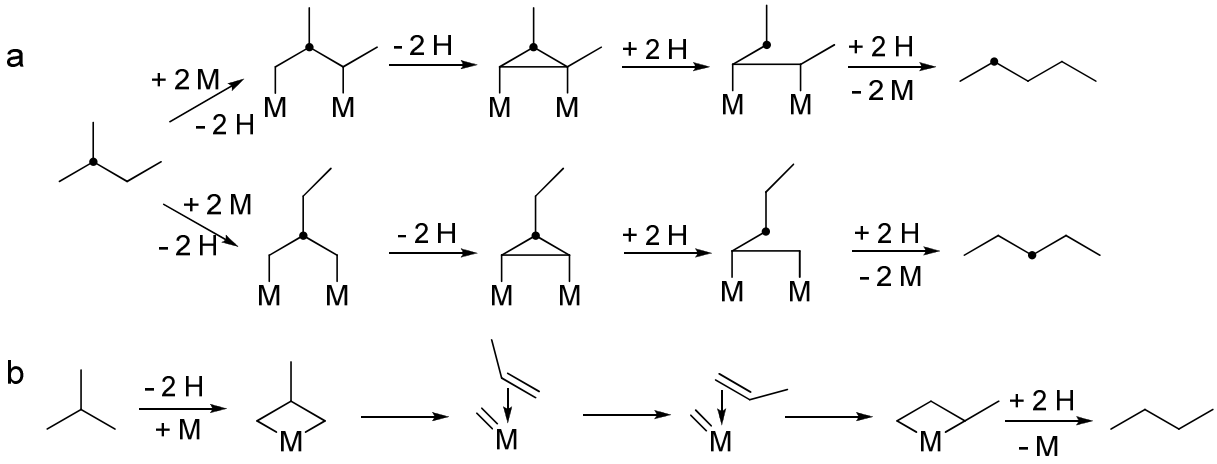

Figure 4.6: The bond shift mechanisms via a) a cyclopropane and b) a metallacyclic intermediate [38]. The 2-methylpentane was labeled with ^{13}C.

As the name says, in the C_5 cyclic mechanism (Figure 4.7) a cyclopentane intermediate adsorbed on the metal is first formed from an alkane via 1,5-dehydrocyclization. Subsequently, an interconversion between isomeric adsorbed cyclopentyl intermediates occurs which allows the ring to be ruptured at different positions from where it was closed.

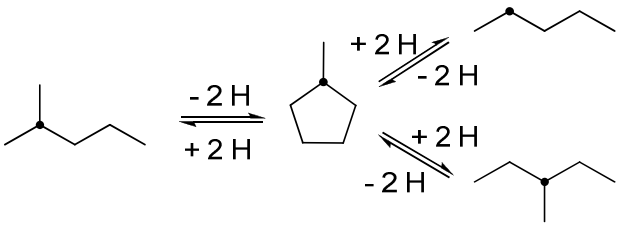

Figure 4.7: Isomerization of ^{13}C-containing 2-methylpentane via the C_5 cyclic mechanism [38].

Investigations on the ring opening of one-ring naphthenes such as methylcyclopentane show very different ring-opening selectivities depending on the dispersion and nature of the metal. In Figure 4.8, the selectivities of the ring opening of methylcyclopentane obtained on Pt/Al_2O_3 catalysts with different dispersion are shown. These results were compared with the predicted selectivities for a statistical breaking of the endocyclic carbon-carbon bonds (non-selective) and the selective rupture of endocyclic bonds between two secondary carbon atoms (selective). The results show that there exist at least two hydrogenolysis mechanisms, namely the non-selective and the selective ring opening mechanism. Non-selective ring opening of the endocyclic carbon-carbon bonds is also called the multiplet mechanism, and it involves a flat adsorption of the cyclopentane ring on the metal. This mechanism occurs on highly dispersed platinum particles. On poorly dispersed platinum particles as well as on ruthenium, rhodium and iridium (independent of the dispersion), selective ring opening takes

place. In this mechanism, which is also called the dicarbene mechanism, the cyclopentane ring seems to be adsorbed perpendicularly to the metal surface via two adjacent secondary carbon atoms.

Competing with the last-mentioned mechanism seems to be a third mechanism which can open the ring partially selectively between secondary-tertiary or tertiary-tertiary C-C bonds. The mechanism should be analogous to the metallacyclobutane bond shift mechanism (Figure 4.6b) [39].

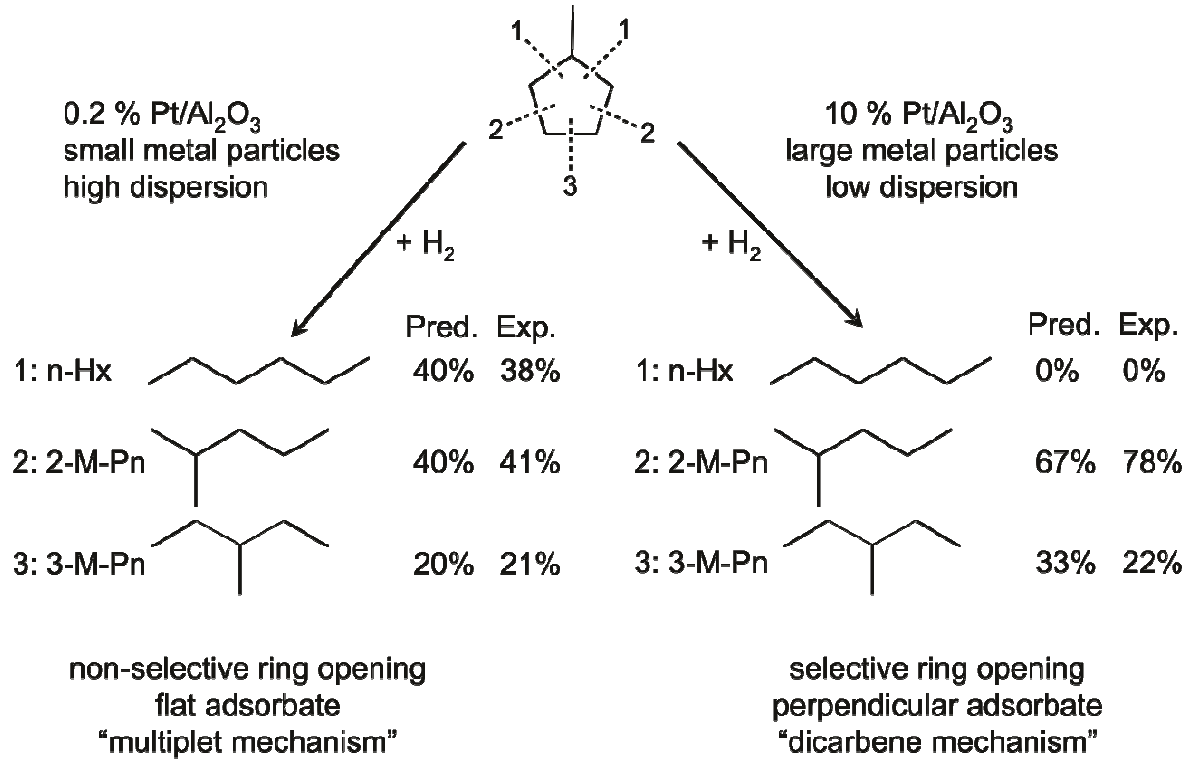

Figure 4.8: Non-selective and selective ring opening of methylcyclopentane on Pt/Al_2O_3 catalysts of high and low metal dispersion [5, 40].

4.3.1.3 Catalytic Cracking on Acidic Catalysts

Catalytic cracking can be observed on monofunctional acidic catalysts. Two principal mechanisms can be distinguished: Bimolecular or classical cracking and monomolecular or Haag-Dessau cracking.

Bimolecular Cracking

In Figure 4.9 the mechanism of bimolecular cracking of n-alkanes is shown for the model hydrocarbon n-hexane. The catalytic cycle starts with the formation of a carbenium ion by protonation of either n-hexane followed by abstraction of dihydrogen or n-hexene that might be present as an impurity. Now the carbenium ions can undergo type A or B rearrangements. A type A rearrangement, in which the number of branchings of the carbenium ion remains constant, is faster than a type B rearrangement in which the number of branchings increases or decreases. The secondary hexyl cation in Figure 4.9 undergoes a type B skeletal rearrangement into a branched hexyl cation (step I). This 2-methylpentyl-(2) cation is in equilibrium via intramolecular hydride shifts (step II) with the 4-methylpentyl-(2) cation which can show a classical β-scission (step III). β-Scission means that the carbon-carbon bond in β-position relative to the positively charged carbon atom is cleaved. β-Scission is the faster the more highly branched the precursors are (Figure 4.10), hence the rates of β-scissions strongly decrease from type A to type D. Type A β-scissions starting from a tertiary carbenium ion and leading to a smaller tertiary carbenium ion and a branched alkene is the fastest type of β-scissons [41].

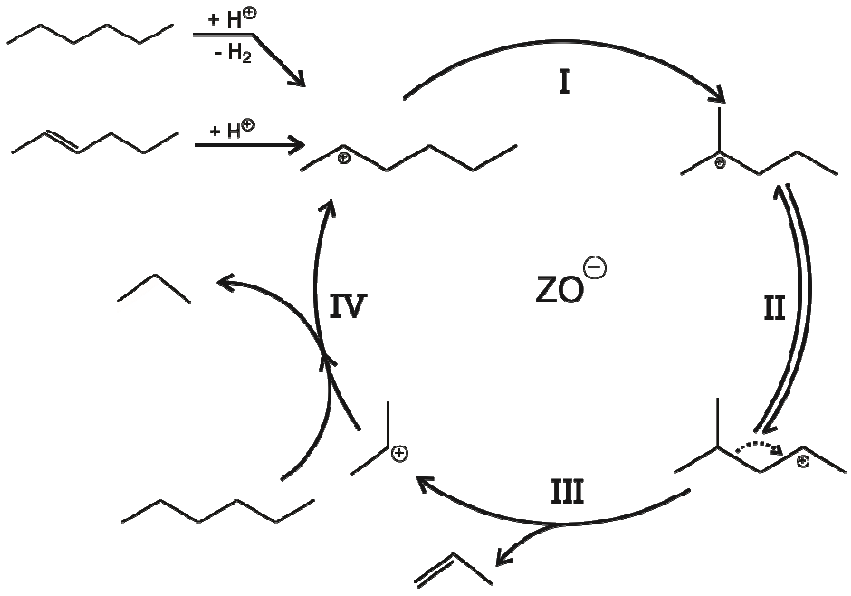

Figure 4.9: Bimolecular (or classical) mechanism of cracking of an n-alkane on a zeolite with Brønsted acid sites [42]. ZO^- stands for an anionic framework oxygen of the zeolite.

The 4-methylpentyl-(2) cation in Figure 4.9 (step III) undergoes a β-scission of type C and forms propene and the propyl-(2) cation. The rate controlling step in this mechanism is the

intermolecular hydride shift between a new reactant molecule and the propyl-(2) cation (step IV). This step, which closes the cycle, is bimolecular which gives this mechanism the name “bimolecular cracking”. This type of reaction cannot lead to the formation of methane and ethane due to the instability of primary carbenium ions (type D) but to large amounts of alkenes.

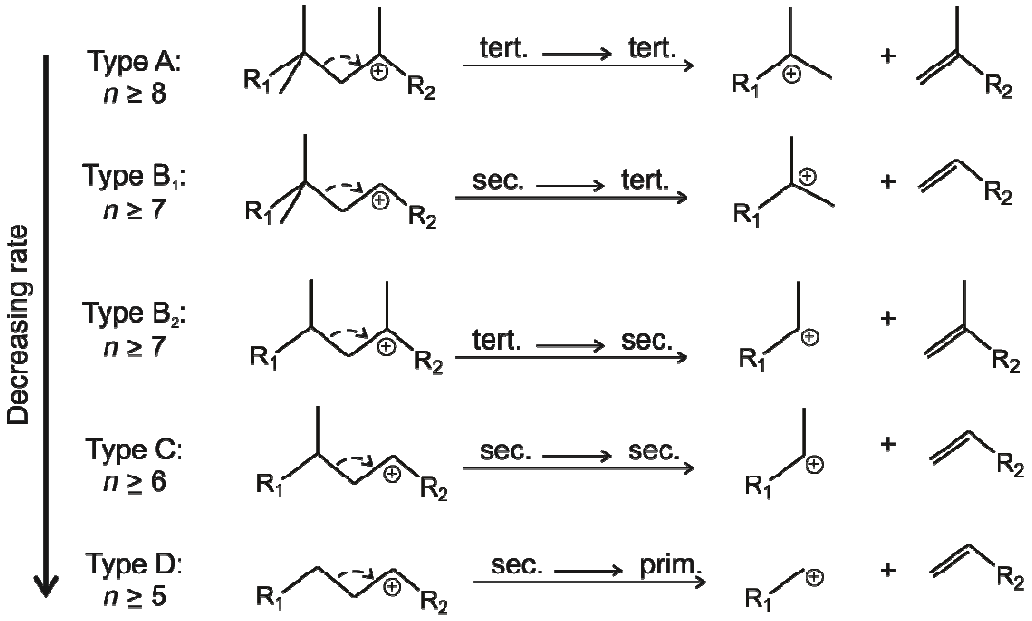

Figure 4.10: Classification of β-scissions of alkylcarbenium ions; *n* is the number of carbon atoms of alkylcarbenium ions that can undergo the respective type of β-scission [41, 42].

Monomolecular Cracking

Haag and Dessau observed that a second principal mechanism can be operative on monofunctional acidic catalysts, called Haag-Dessau or monomolecular cracking [43]. In this mechanism (Figure 4.11) the alkane is first protonated to a carbonium ion (step I) with a three-center-two-electron bond in the transition state which directly collapses into a smaller alkane or dihydrogen and a carbenium ion (step II). The carbenium ion is desorbed as an alkene and leaves a proton behind, which closes the cycle (step III). In contrast to the bimolecular cracking, with Haag-Dessau cracking methane and ethane can be formed.

The bimolecular and the monomolecular mechanisms compete with each other. Factors that favor the monomolecular mechanism are high reaction temperatures (around 530 °C) and low partial pressures of hydrocarbons. In addition, narrow pores of a zeolite catalyst can allow the monomolecular reaction while restricting the bimolecular reaction (the

intermolecular hydride transfer, step IV, Figure 4.9) of classical cracking because of the steric limitations in the pores.

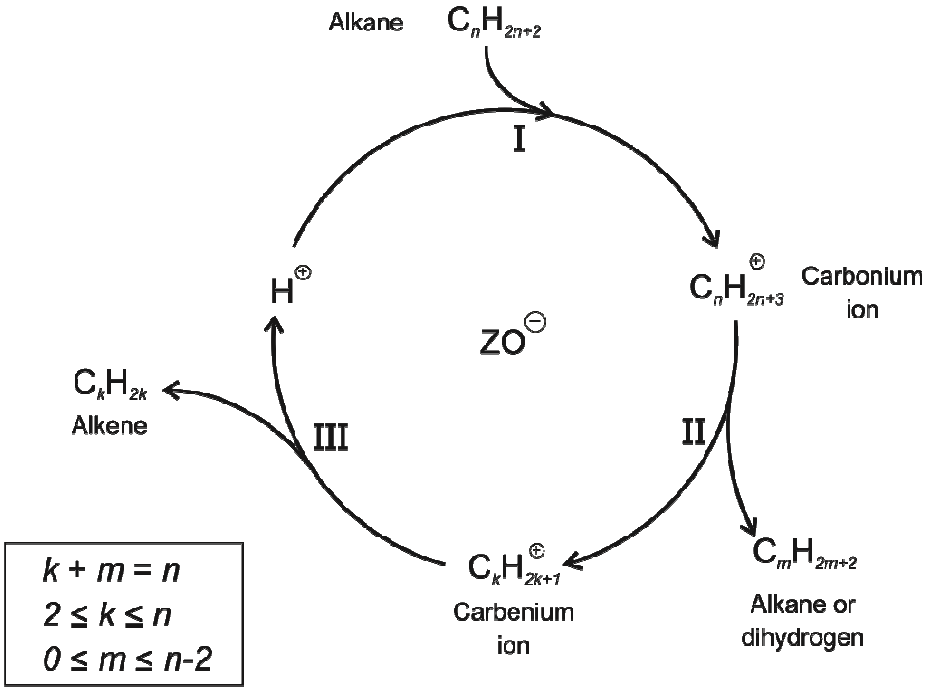

Figure 4.11: Monomolecular or Haag-Dessau cracking of an alkane on a zeolite with Brønsted acid sites [42]. ZO^- stands for an anionic framework oxygen of the zeolite.

Wielers *et al.* [44] introduced a ratio that allows to quantify the relative contributions of monomolecular and bimolecular cracking. This ratio was called the cracking mechanism ratio (*CMR*), and is defined as the selectivity ratio of products typically formed by monomolecular (methane, ethane, ethene) and bimolecular cracking (iso-butane):

$$CMR = \frac{S_{\text{methane}} + S_{\text{ethane}} + S_{\text{ethene}}}{S_{\text{iso-butane}}} \qquad (4.7)$$

A high value for the *CMR* (*CMR* > 1) reflects a significant contribution of monomolecular cracking, while a low value (0 < *CMR* < 1) is indicative of the bimolecular mechanism prevailing.

Under certain reaction conditions, dihydrogen can be activated on acidic zeolites and can be partially incorporated into the products of hydrocracking leading to large amounts of n-alkanes instead of alkenes [45].

4.3.1.4 Hydrocracking on Bifunctional Catalysts

On bifunctional catalysts metal and Brønsted acid sites are present. For the hydrocracking of n-alkanes it is widely accepted that the alkane is first dehydrogenated on the metal to a mixture of the corresponding n-alkenes in their equilibrium ratio. These n-alkenes diffuse through the zeolite pores until they are adsorbed on a Brønsted acid site. On this site the adsorbed hydrocarbon can undergo skeletal rearrangements and β-scissions exactly as described for the bimolecular cracking on monofunctional acidic catalysts (Section 4.3.1.3). On bifunctional catalysts the step of β-scissions is rate- and selectivity-controlling. The formed products are desorbed from the Brønsted acid sites as alkenes and diffuse to the metal sites where they are hydrogenated to alkanes. The additional metal sites in bifunctional catalysts, in contrast to the monofunctional acidic catalysts, bring about a complete saturation of the hydrocracked products, *i. e.* no alkenes are usually obtained.

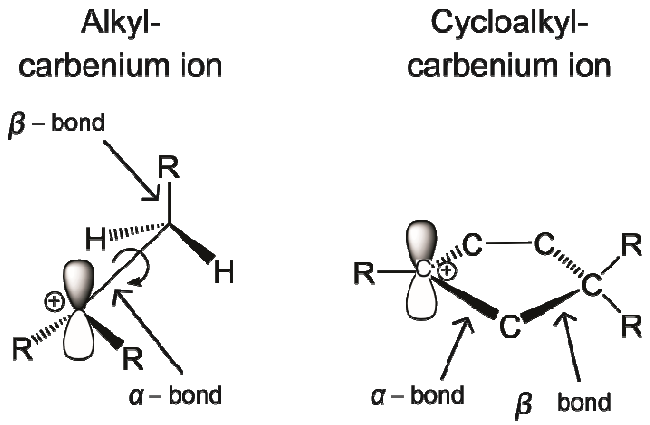

Figure 4.12: Possible role of orbital orientation for the easiness of β-scission in alkylcarbenium ions and cycloalkylcarbenium ions [5].

In cyclic hydrocarbons the β-scission of carbon-carbon bonds which are part of a naphthenic ring is very slow. A possible explanation is that in an alkylcarbenium ion there is a free rotation around the α-bond. Hence, a conformation exists where the vacant p-orbital and the β-bond to be broken are ideally coplanar, and this results in a maximal orbital overlap in the transition state of β-scission. By contrast, in the cycloalkylcarbenium ion the β-bond is perpendicular to the vacant p-orbital. The α-bond is fixed in the ring and cannot rotate to get a better overlap of the orbitals. Hence, β-scission is unfavorable for naphthenic carbocations [5]. Instead, C_{10} naphthenes undergo a series of type A and type B skeletal isomerizations until they reach one of the three carbenium ions shown in Figure 4.13. Type A β-scission is the fastest type of β-scission and results in all three cases in methylcyclopentane and iso-butane. Indeed, these products were predominantly observed independent of the nature of the C_{10} naphthene used as reactant (n-butyl-, sec-butyl-, iso-butyl-, tert-butyl-, 1,2-diethyl- or

1,2,4,5-tetramethylcyclohexane [46]). Hydrocracking of cyclic C_{10} hydrocarbons on bifunctional catalysts into methylcyclopentane and iso-butane is known as the “paring reaction” [47].

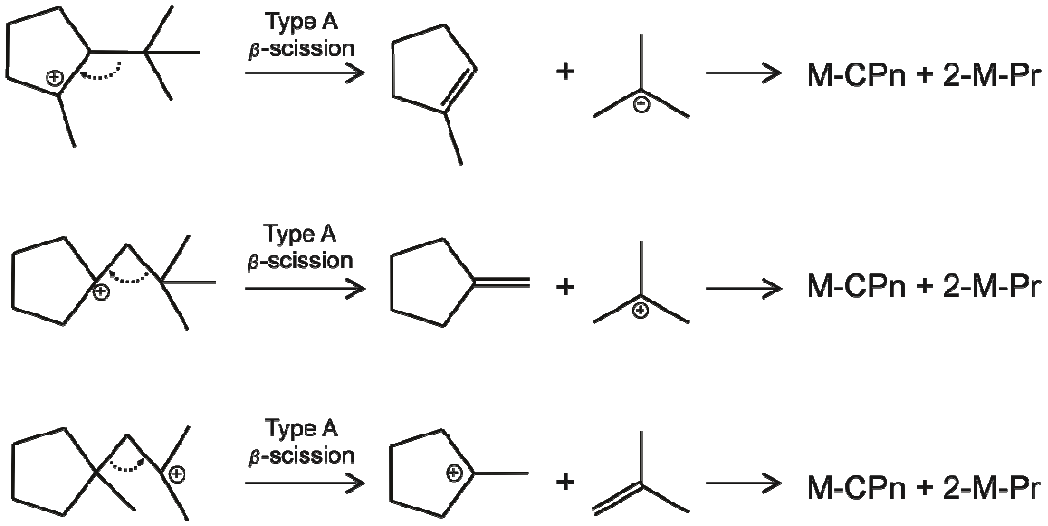

Figure 4.13: The three possible C_{10} cycloalkylcarbenium ions that can undergo exocyclic type A β-scission [5]. M-CPn, methylcyclopentane; 2-M-Pr, 2-methylpropane (iso-butane).

This paring reaction is only selective on zeolites with large pores. The three precursor cycloalkylcarbenium ions are relatively bulky and too large to be accommodated in 10-membered-ring zeolites. In these zeolites hydrocracking proceeds via type B β-scissions because this type requires less bulky carbenium ions. On 10-membered-ring zeolites n-butane rather than iso-butane is mostly formed. The significant differences in the composition of the C_4-fractions were used in a new index for characterizing the pore width of 12-membered-ring zeolites, the Spaciousness Index (*SI*) [48]. This Spaciousness Index is defined as the yield of iso-butane divided by the yield of n-butane in the hydrocracking of butylcyclohexane on bifunctional catalysts. The value increases with increasing space inside the pore system. In Figure 4.14, the Spaciousness Indices of the three zeolites used in this work are shown in comparison to various other zeolites. Zeolite ZSM-12 has a very narrow pore system for a 12-membered-ring zeolite (*SI* = 3), whereas the faujasites (zeolite X and Y) have very large pores (*SI* = 20). The 12-membered-ring pockets of zeolite MCM-22 have medium-sized pores (*SI* = 7). By contrast, all 10-membered-ring zeolites have essentially the same Spaciousness Index around 1.

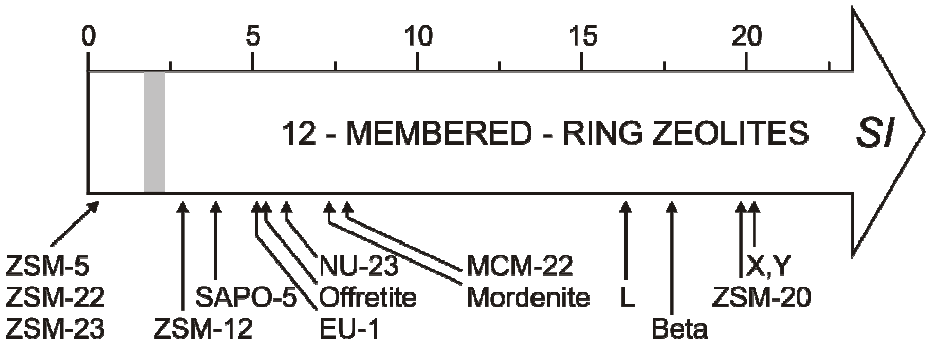

Figure 4.14: The Spaciousness Index of various zeolites, after Ref. [49]. The numbers above the arrow denote the numerical value of *SI*.

4.3.2 Ring Opening on Bifunctional or Acidic Catalysts

Kubička *et al*. [50] investigated the activity of zeolites H-Beta with two different n_{Si} / n_{Al} ratios of 25 and 75, H-Y, H-mordenite and H-MCM-41 in the ring opening of decalin in the presence of hydrogen in the temperature range of 200-300 °C at a total pressure of 2 MPa. For all catalysts, except H-mordenite, the initial activity increased with increasing concentration of Brønsted acid sites. The latter was determined by quantitative FT-IR spectroscopy with pyridine as a probe molecule. All catalysts suffered from fast deactivation. The results showed that the rate of deactivation is influenced by the pore structure of the zeolite and the amount of Brønsted acid sites. For the same structure the deactivation rate increased with increasing amount of acid sites in the zeolite. Comparing catalysts of approximately the same concentration of Brønsted acid sites, like dealuminated H-Y (n_{Si} / n_{Al} = 12) and H-Beta-25, it was found that H-Y deactivated more rapidly. The difference was explained by the presence of large cavities in H-Y zeolite, which enable the formation of large organic molecules blocking the pores. H-mordenite had the highest concentration of Brønsted acid sites. Nevertheless, it showed the lowest activity among the zeolite catalysts investigated. The authors explained this finding with a rapid blockage of the 12-membered ring pores by coke or adsorbed hydrocarbon molecules at the pore entrance, resulting in its very fast deactivation. In the complete temperature range studied almost no conversion was observed over mesoporous H-MCM-41, due to the extremely low concentration of Brønsted acid sites. Comparing the catalysts with respect to their ring opening activities H-Beta showed the best performance (Figure 4.15). H-Beta-25 gave the highest yield of ring opening products (ROPs), but it also produced more undesired hydrocarbons, such as cracked products, dehydrogenated products and hydrocarbons with more than 10 carbon atoms, than H-Beta-75. The maximum yields of ROPs attained on various acidic zeolites are shown in Figure 4.15 and listed in Table 4.1. The values given in Table 4.1 were taken from Figure 4.15. In

reference [50] no absolute values for the yields of ring opening products on the different catalysts were mentioned. The only information given was that the maximum yield of ring opening products achieved was 8 % over the proton-form zeolites. This value did, however, not agree with Figure 4.15 in reference [50].

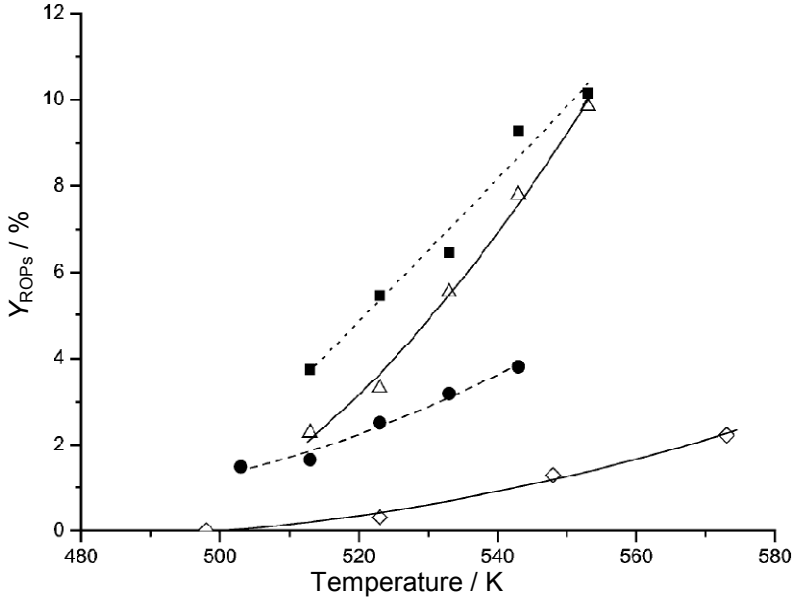

Figure 4.15: Temperature dependency of ROP yield after 360 min time-on-stream over zeolites H-Beta-25 (■), H-Beta-75 (Δ), H-Y (●) and H-mordenite (◊) [50].

In another paper, the same group [51] compared the results obtained on the monofunctional acidic zeolites H-Beta, H-Y and H-mordenite with those measured on their bifunctional counterparts containing 2 wt.-% platinum in the hydroconversion of decalin in the temperature range of 200-270 °C and a total pressure of 2 MPa. They found that impregnation of the acidic zeolites with hexachloroplatinic acid does not increase the concentration of Brønsted acid sites. Nevertheless, the bifunctional catalysts showed a substantially increased initial activity in comparison with the monofunctional zeolites. Therefore, the enhanced initial reaction rate can be attributed to the presence of platinum which seems to facilitate the formation of reaction intermediates and their subsequent transformation into products. The initial activity of the catalysts impregnated with platinum decreased in the same order as observed with the monofunctional zeolites: 2.0Pt/H-Beta > 2.0Pt/H-Y > 2.0Pt/H-mordenite. Hydroconversion of decalin at different hydrogen pressures and replacement of hydrogen by argon led the authors to the conclusion that ring opening of decalin is a zero-order reaction with respect to hydrogen. However, the catalysts tend to deactivate faster in the absence of hydrogen. Over Pt/H-zeolites less cracking was observed at comparable conversions than on the H-zeolites, which was interpreted in terms of a lower strength of the Brønsted acid sites upon platinum impregnation, as measured by quantitative FT-IR spectroscopy with pyridine as probe molecule. Monofunctional acidic zeolites were

able to open one ring of decalin [50]. With the assumption that Brønsted acid sites are the only active sites in these zeolites it could be expected that the decreased strength of Brønsted acid sites will lead to a suppression of ROP formation. But at comparable conversions, proton-form and platinum-containing zeolites yield the same amount of ROPs. Therefore, other active sites in addition to Brønsted acid sites could be responsible for ROP formation. The formation of dehydrogenated products and products with more than 10 carbon atoms as well as deactivation are suppressed by the presence of platinum. A maximum yield of ROPs amounting to 30.2 % was observed on 2.0Pt/H-Beta at 250 °C.

Table 4.1: Maximum yields of ring opening products ($Y_{ROPs,\ max.}$) obtained from bicyclic C_{10} hydrocarbons on acidic catalysts.

Feed	**Catalyst**	***T* / °C**	**p_{H_2} / MPa**	**$Y_{ROPs,\ max.}$ / %**	**Ref.**
Decalins	H-Beta-25	280	2	10	[50]
Decalins	H-Beta-75	280	2	9.5	[50]
Decalins	H-Y	270	2	4	[50]
Decalins	H-mordenite	300	2	2	[50]
Decalins	H-Y	260	2	19.1	[52]

Santikunaporn *et al*. [52] tested three H-Y zeolites with different concentrations of Brønsted acid sites (H-Y1 < H-Y2 < H-Y3) in the hydroconversion of a mixture of decalin isomers at 260 °C, 2 MPa, $\dot{n}_{H_2} / \dot{n}_{Dec}$ = 65 and compared the results with those obtained on a platinum-containing H-Y zeolite. Among the three H-Y zeolite catalysts the sample with the lowest concentration of acid sites showed the best performance concerning the formation of ROPs with a yield of 9.4 % and a selectivity of 86.2 %. Upon increasing the concentration of acid sites, the conversion of decalin increased, but the yield of cracked products increased as well, and catalyst deactivation became much more severe. The catalyst with the highest concentration of Brønsted acid sites gave a maximum yield of ROPs amounting to 19.1 %, but with a poor selectivity of 46.8 %. Incorporation of platinum into the zeolite with the highest concentration of Brønsted acid sites reduced the number of acid sites. This led to a lower yield of cracked products and a lower decalin conversion, whereas the fast deactivation did no longer occur. On 1.0Pt/H-Y the maximum yield of ROPs at 260 °C was 11.8 %.

In the same study [52] these catalysts were tested in the hydroconversion of tetralin at 325 °C, 2 MPa and an $\dot{n}_{H_2} / \dot{n}_{Ttr}$ ratio of 60. At variance to the experiments with a mixture of decalin isomers as feed, the incorporation of platinum led to a large increase in the conversion of 93 % in comparison with the H-Y catalyst (24 %). This can be explained by the conclusion of Arribas and Martínez [53]. The initiation step for the hydrocracking of

naphthalene on Pt/H-Y is the sequential hydrogenation of naphthalene to tetralin and the two stereoisomers of decalin on the metal. The maximum yield of ROPs from tetralin on 1.0Pt/H-Y is 15.0 %. Nearly 95 % of the ring opening products are alkylcyclocompounds, whereas on monofunctional acidic H-Y catalysts mainly alkylbenzenes are formed. A series of experiments were made in order to discern the role of the individual functions of the catalyst. Tetralin was converted over physical mixtures of H-Y and Pt/SiO_2 and over separated beds of both solids in alternating order. From the results of these experiments the authors concluded that the metal is responsible for the hydrogenation of aromatics and the isomerization of cis-decalin to trans-decalin, whereas the acid sites are responsible for the ring opening which is easier for decalin than tetralin.

Kubička *et al*. [54] proposed the reaction scheme shown in Figure 4.16 for the transformation of decalin (Dec) on Pt-modified zeolite Beta. For the sake of simplicity only surface reactions, but no adsorption/desorption steps are shown. The reaction scheme starts with the dehydrogenation of decalin on the metal. The resulting olefin moves to a Brønsted acid site where it rearranges into a skeletal isomer (sk-Isos). At this level, two reactions are possible, *viz*. hydrogenation into a saturated skeletal isomer of decalin or ring opening into a dienic C_{10}-hydrocarbon with a single ring (ROPs). Here again, two types of reaction compete with each other, namely hydrogenation to monocyclic C_{10}-hydrocarbons and the formation of cracked products with less than 10 carbon atoms (C). In its essence, the scheme is nothing else than an application of the classical hydrocracking mechanism to the conversion of decalin. According to Kubička *et al*. [54], the scheme also holds for the reactions of decalin on acidic catalysts lacking a metal component, however, the presence of a metal is envisaged to enhance the reaction rates and to improve the selectivity by eliminating undesired side reactions, such as hydrogen transfer or protolytic cracking. Based on the mechanism presented in Figure 4.16, Kubička *et al*. [54] established a kinetic model which turned out to adequately describe experimental rate data measured with decalin as feed hydrocarbon and 2.0Pt/H-Beta [51] as catalyst.

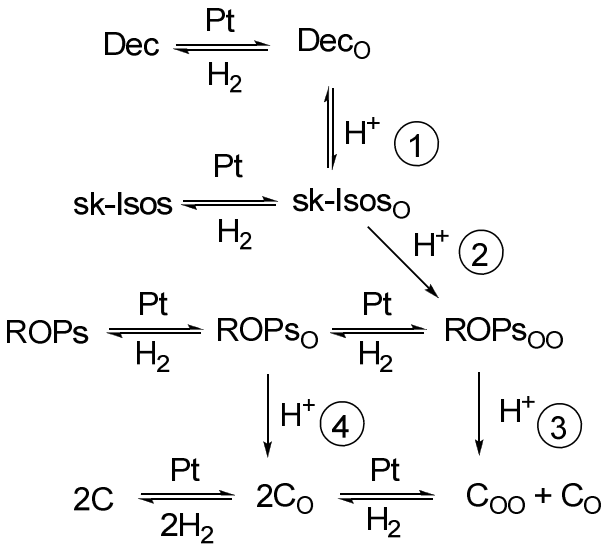

Figure 4.16: Reaction scheme of decalin transformations on Pt-modified zeolite Beta. The indices O and OO denote an olefin and a diene, respectively. The circled numbers stand for reaction types, *viz*. skeletal isomerization (1), ring opening (2) and cracking (3, 4). After Ref. [54].

In another study, Kubička *et al*. [55] analyzed in detail by GC/MS the hydrocarbons formed by skeletal isomerization of decalin. SIMCA (soft independent modeling of class analogy) models were developed for the classification of C_{10}-bicycloalkanes. Kubička *et al*. [55] defined 14 classes of C_{10}-bicycloalkanes based on the size of the naphthenic rings and the configuration of the rings. The mass spectra available in the literature were transformed by means of mathematical transformations into a set of parameters. These parameters were calculated for three to six components of each class to have calibration sets. Nine of the hypothetical classes of C_{10}-bicycloalkanes contained too few members to be modeled, *i. e*. spiro[4.5]decane or bicyclo[5.3.0]decane. In the 14 classes only methyl groups as side chains were considered. The individual products were classified into methyl-bicyclo[4.3.0]nonanes, dimethyl-bicyclo[3.3.0]octanes, dimethyl-bicyclo[3.2.1]octanes, dimethyl-bicyclo[2.2.2]octanes and trimethyl-bicyclo[2.2.1]heptanes. The best model was used for real GC/MS data of products of decalin transformation. More than 90 % of all products could be assigned to one of the five suggested classes. Based on their experimental findings, the scheme shown in Figure 4.17 was proposed for skeletal isomerization of decalin.

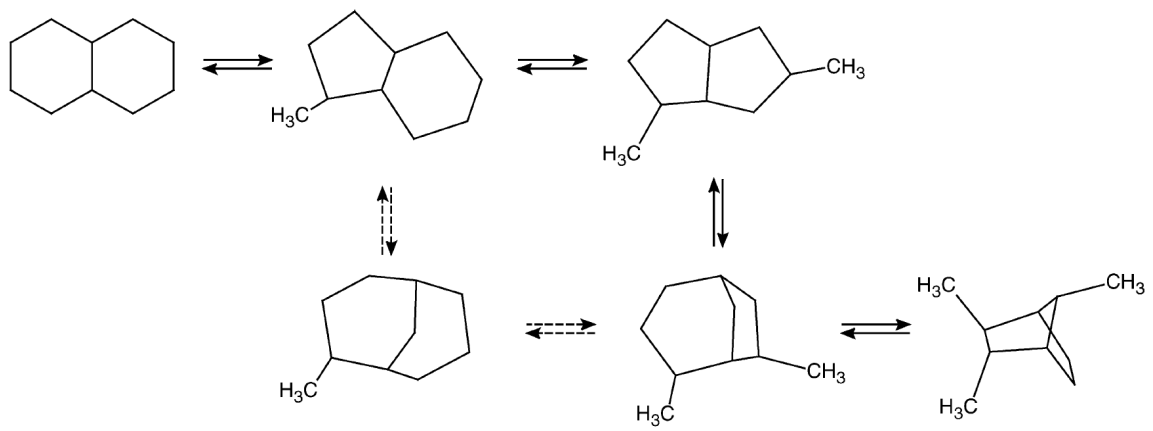

Figure 4.17: Proposed reaction scheme for decalin isomerization based on GC/MS analysis of the reaction products [55]. The pathway with the dashed arrows could not be proven due to the lack of spectral MS data.

Arribas *et al*. [56] investigated the influence of the proximity between the metal and acid sites and of the n_{Pt} / n_{H^+} ratio in Pt/USY catalysts on the ring opening of tetralin at 275 °C, 3 MPa, $\dot{n}_{H_2} / \dot{n}_{Ttr}$ = 10 and *WHSV* = 2.5 h^{-1}. For studying the influence of the distance between both types of sites in the bifunctional catalyst they used different bed configurations as shown in Figure 4.18. The largest distance was created by using a bed of platinum on a non-acidic carrier, *viz*. 1.0Pt/Al_2O_3, as the top layer, followed by a separating layer from quartz wool. Next was a layer of the acid catalyst USY zeolite (Figure 4.18, left). A much smaller average distance was achieved by physically mixing 1.0Pt/Al_2O_3 and USY zeolite with particle sizes of 0.25-0.42 mm (Figure 4.18, center). Finally, the catalyst with the lowest distance between both types of sites was USY zeolite impregnated with 1.0 wt.-% of platinum (Figure 4.18, right).

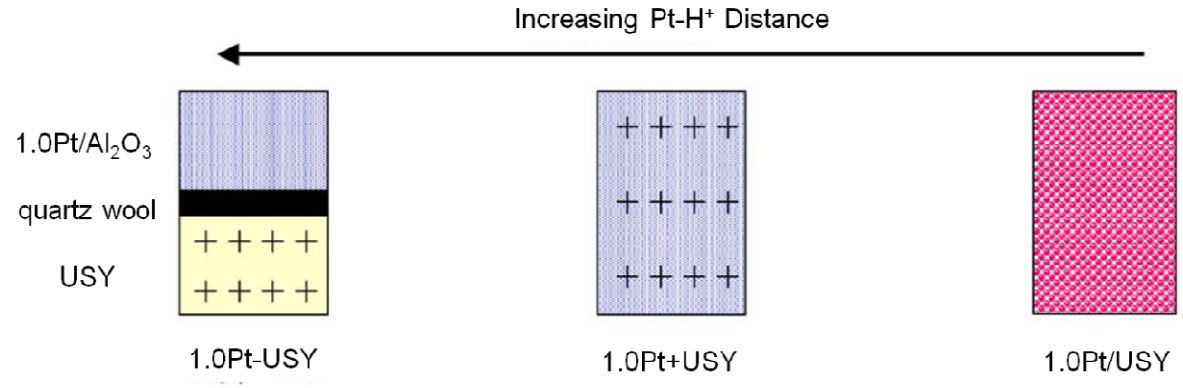

Figure 4.18: Schematic representation of the different bed configurations used by Arribas *et al*. for studying the influence of the proximity between metallic and acid sites [56].

The catalytic experiments showed that the yield of sk-Isos and ROPs increases with decreasing distance between the metal and acid sites. The yield of ROPs for the best catalyst 1.0Pt/USY was 16.0 %. Concerning the influence of the n_{Pt} / n_{H^+} ratio on the ring opening, several Pt/USY catalysts were prepared with different loadings of platinum varying between 0.25 and 4 wt.-%. With increasing platinum loading, a continuous decrease of the decalins yield was observed at tetralin conversions > 99 % (except for 0.25Pt/USY on which the conversion was 94.8 %). With increasing platinum content the yield of ROPs also increased and reached a value of 21.2 % for 4.0Pt/USY. Above 2 wt.-% Pt the increase in the ROPs yield slowed down due to an ever more extensive formation of cracked and dealkylation products. Impregnation of 1 wt.-% iridium onto the bifunctional 1.0Pt/USY catalyst did not lead to an increase in the yield of ROPs with respect to the monometallic 2.0Pt/USY. The monometallic catalyst 1.0Ir/USY showed hardly any ring-opening activity under the reaction conditions used.

ITQ-21 is a zeolite with a very spacious pore system consisting of large cavities with six 12-membered-ring windows. Arribas *et al*. [57] advanced the hypothesis that relatively bulky hydrocarbons like the products from tetralin conversion can even more freely egress from the cavities of ITQ-21 than from those of faujasites where the large cavities have only four windows. Based on this hypothesis, these authors believed that ITQ-21 could be a particularly attractive ring opening catalyst. They used 1.0Pt/H-ITQ-21 in the hydroconversion of tetralin at a total pressure of 3 MPa, $\dot{n}_{H_2} / \dot{n}_{Ttr}$ = 10, *WHSV* = 2.5 h^{-1} and *T* = 250 to 325 °C and compared the results with those obtained with 1.0Pt/USY and 1.0Pt/H-Beta. In-line with their expectations, the yield of ROPs was highest on 1.0Pt/H-ITQ-21 at 300 °C, but the maximum yield even on this catalyst was 20.1 %. Attempts to improve this yield by lowering the concentration of Brønsted acid sites by steaming of the zeolite were unsuccessful.

0.5Pt/USY catalysts with different concentrations of Brønsted acid sites were also tested by Ma *et al*. [58] in the hydroconversion of tetralin at 250 °C, a total pressure of 4 MPa, $\dot{n}_{H_2} / \dot{n}_{Ttr}$ = 12 and *LHSV* = 2.0 h^{-1}. In their materials, the concentration of Brønsted acid sites was lowered, starting from a parent USY zeolite, by impregnation with KNO_3. While the parent 0.5Pt/USY catalyst was very active and gave a yield of cracked products as high as 98 %, this yield rapidly decreased upon loading the catalyst with increasing amounts of potassium. The yield of ROPs passed through a remarkably high maximum of 45.6 % for 0.5Pt/1.2K-USY.

The ring opening of tetralin and 1-methylnaphthalene was investigated on bifunctional 1.0Pt/Beta catalysts by Arribas *et al*. [59]. Different n_{Si} / n_{Al} ratios and crystal sizes were used. Similar trends were found for both aromatic reactants. The temperature at which the maximum yield of ring opening products was observed depended on the properties of the Beta zeolite. The temperatures of the maxima increased with decreasing concentration of Brønsted acid sites indicating a lower cracking and dealkylation activity of the catalysts with a lower amount of Brønsted acid sites. Further, the yield of ROPs increased upon decreasing the concentration of Brønsted acid sites and decreasing the size of the crystallites. The latter effect as well as the better performance of steamed Pt/Beta were explained by a faster diffusion of ROPs from the zeolite voids to the gas phase, thus decreasing the probability of these products to undergo secondary reactions. With both feeds the best performance with respect to the maximum yield of ROPs was observed on the steamed 1.0Pt/H-Beta zeolite with 10 % for 1-methylnaphthalene as feed and 26 % for tetralin.

In a further study with the same feeds and conditions but different medium-pore and large-pore 1.0Pt/zeolites Arribas *et al*. [60] investigated the influence of the zeolite structure on the ring opening activity. The results listed in Table 2 clearly show that the formation of ring opening products is favored on large-pore zeolites and in particular on the three-dimensional 12-membered ring Beta and USY zeolites. Molecular docking simulation with butylcyclohexane and diethylcyclohexane as representative molecules for ROPs supported the existence of diffusional limitations in the 10-membered ring zeolites which lead to very low yields of ROPs. In addition the low yield of ROPs on 1.0Pt/H-mordenite was explained by the accumulation of carbonaceous deposits which were also believed to be responsible for the observed deactivation. These deposits hinder the diffusion of ROPs through the one-dimensional pores of mordenite. Under the reaction conditions applied the maximum yield of ring opening products was found for 1.0Pt/H-Beta (22 %) followed by 1.0Pt/USY (16 %). The 1.0Pt/USY catalyst generated less cracked products (6 %) compared with 1.0Pt/H-Beta (30 %). With the larger feed 1-methylnaphthalene, 1.0Pt/USY generated a higher yield of ROPs (15 %) in comparison to 1.0Pt/H-Beta (8 %) [12]. Decreasing the concentration of framework aluminum and increasing that of extra-framework aluminum in 1.0Pt/USY led to an increase in the yield of ROPs by *ca*. 17 % using 1-methylnaphthalene as feed at 300 °C, 4 MPa, $\dot{n}_{H_2} / \dot{n}_{1\text{-MN}}$ = 30 and *WHSV* = 0.44 h^{-1} [53].

With a dealuminated bimetallic 2.0Pd,0.5Pt/H-Y zeolite catalyst the effect of sulfur compounds on the hydrogenation of tetralin was investigated [61]. At 280 °C, a total pressure of 4 MPa, an $\dot{n}_{H_2} / \dot{n}_{Ttr}$ ratio of 14.7 and a *WHSV* of 16 h^{-1} a yield of 21.3 % ROPs was achieved.

Mouli *et al*. [62] tested bimetallic catalysts made from Ir (0-1.5 wt.-%) and Pt (0-1.5 wt.-%) on H-Zr-MCM-41 in the hydroconversion of decalin in a temperature range of 300-400 °C, a total pressure of 5 MPa and an *LHSV* of 1.5 h^{-1}. The ring opening yield and selectivity increased as the iridium loading was varied from 0 to 1.5 wt.-%. The optimum ring opening yield was observed with a combination of 1.5 wt.-% iridium and 0.75 wt.-% of platinum loading. Unfortunately, 1.5Ir/H-Zr-MCM-41 was not included in the catalysts employed which would have allowed to directly study the effect of the absence and presence of platinum. The authors just stated that the maximum ring opening yield and selectivity from decalin at 350 °C were 16 % and 26 %, respectively, on H-Zr-MCM-41 with 1.5 wt.-% Ir and 0.75 wt.-% Pt. In Figure 4.19 the ring opening yields are plotted against the metal loadings. From Figure 4.19 it looks as if the highest yield of ROPs at 350 °C was only 4.19 wt.-%. and the maximum yield of ROPs was achieved for 1.5Ir,0.75Pt/H-Zr-MCM-41 at 400 °C with 14 %. There seems to be a discrepancy between the written text and the given figures. In addition, the data of the selectivity of ROPs and the conversion are also plotted against the metal loading. Taking the conversion and yield with one catalyst it should be possible to calculate the selectivity of ROPs, but in this case the calculated values do not coincide with the values in the figures. Furthermore, the decalin feed was diluted with n-heptane and n-dodecane. There is no indication in the paper by Mouli *et al*. [62] as to whether or not n-heptane and n-dodecane are reacting under the conditions applied. The published results must hence be considered with care.

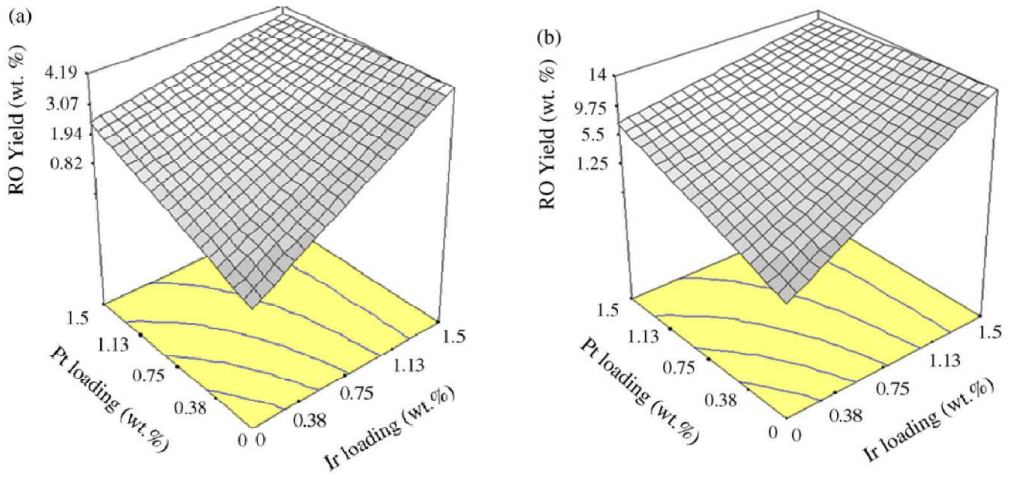

Figure 4.19: Hydroconversion of decalin on Pt,Ir/H-Zr-MCM-41. Influence of different Ir and Pt loadings on the yield of ring opening products. (a) T = 350 °C and (b) T = 400 °C. p_{total}= 5 MPa; *LHSV* = 1.5 h^{-1} [62].

Some investigations were done concerning the influence of the incorporation method of the metal on the ring opening of decalin. Platinum or ruthenium were incorporated into H-MCM-41 by *in situ* synthesis, ion exchange and impregnation [63, 64]. Iridium was

incorporated into zeolite H-Beta by impregnation and atomic layer deposition [65]. The atomic layer deposition is a gas-phase material depositing technique based on reactions between the metal precursor and reactive groups of the support leading to a monolayer of the metal on the support. The catalytic properties of these catalysts were investigated using the ring opening of decalin as a test reaction. The results of all three studies have to be taken with care because the metal contents of the compared catalysts differ strongly. Nevertheless, all studies have in common that the impregnated samples provide the lowest yield of ROPs.

Similar to the introduction of metals into acid zeolites, the incorporation of Mo_2C was found to reduce the amount and strength of Brønsted acid sites, which in turn mitigated the carbon deposition and concomitant catalyst deactivation [66, 67]. Bulk Mo_2C and Mo_2C catalysts supported on H-Y zeolite with different n_{Si} / n_{Al} ratios and different Mo_2C loadings were investigated as catalysts for the vapor-phase hydrogenation and selective ring opening of naphthalene at temperatures of 280–340 °C at a total pressure of 3 MPa and $\dot{n}_{H_2} / \dot{n}_{Nap}$ = 30. The highest yield of ROPs amounted to 39 %, it was observed on 5.0 wt.-% Mo_2C supported on H-Y with n_{Si} / n_{Al} = 15, but catalyst deactivation was severe. Included in the above value for the yield of ROPs is the yield of sk-Isos.

In addition to Mo_2C supported on acidic zeolites, also NiMoS [68, 69] and NiMoC [70] catalysts supported on acidic supports were investigated in the ring opening of tetralin. On the NiMoS catalysts higher amounts of aromatic compounds in comparison to noble-metal-containing bifunctional catalysts were obtained, especially with increasing concentration of Brønsted acid sites of the support. The highest yield of ROPs on NiMoS catalysts was achieved when supported on zeolite H-Y with 30.5 % at 310 °C and a total pressure of 4.0 MPa [68]. NiMoC supported on H-Y provided a ROPs yield of 33.7 % at 240 °C and a total pressure of 5.0 MPa [70].

An overview on the widely scattering yield data of ring opening products from bicyclic C_{10}-hydrocarbons is given in Table 4.2.

Table 4.2: Maximum yields of ring opening products ($Y_{ROPs,\ max.}$) obtained from bicyclic C_{10} hydrocarbons on bifunctional catalysts.

Feed	Catalyst	T / °C	p_{H_2} / MPa	$Y_{ROPs,\ max.}$ / %	Ref.
Decalins	2.0Pt/H-Beta	250	2.0	30.2	[51]
Decalins	2.0Pt/H-Y	250	2.0	27.2	[51]
Decalins	2.0Pt/H-mordenite	270	2.0	8.8	[51]
Tetralin	1.0Pt/H-Y	325	2.0	15.0	[52]
Tetralin	4.0Pt/USY	275	3.0	21.2	[56]
Tetralin	1.0Pt/H-ITQ-21	300	3.0	20.1	[57]
Tetralin	1.0Pt/USY	275	3.0	16.1	[57]
Tetralin	1.0Pt/H-Beta	300	3.0	14.5	[57]
Tetralin	0.5Pt/1.2K-USY	250	4.0	45.6	[58]
Tetralin	1.0Pt/H-Beta	300	3.0	26	[59]
Tetralin	1.0Pt/H-ZSM-5	300	3.0	0.9	[60]
Tetralin	1.0Pt/H-MCM-22	300	3.0	4.6	[60]
Tetralin	1.0Pt/H-mordenite	275	3.0	6.8	[60]
Tetralin	1.0Pt/H-Beta	250	3.0	22.4	[60]
Tetralin	1.0Pt/USY	275	3.0	16.1	[60]
Tetralin	2.0Pd,0.5Pt/H-Y	280	4.0	21.3	[61]
Decalins	1.5Ir,0.75Pt/H-Zr-MCM-41	400	5.0	14	[62]
Naphthalene	5.0Mo_2C/H-Y	300	3.0	39[a]	[66]
Tetralin	NiMoS/H-Y	310	4.0	30.5	[68]
Decalins	NiMoC/H-Y	240	5.0	33.7	[70]
Decalins	1.5Ir,0.75Pt/H-Y	220	5.0	31.7[b]	[70]

[a] yield of sk-Isos and ROPs

[b] in addition open-chain decanes with a yield of 4 % were found

In none of the above-reviewed papers from the recent literature yields or selectivities of the particularly desired open-chain decanes (OCDs) were given. Mouli *et al.* [62] qualitatively reported that they observed 3,5-dimethyloctane as a product of the ring opening of decalin, but they gave no quantitative yield or selectivity data for this product. Likewise, Contreras *et al.* [71] reported about some small quantities of decane among the ring opening products of tetralin on a Pt/MFI-SBA-15 hybrid catalyst. Up to now only one paper reported about selectivities and yields of OCDs [70]. The authors investigated the ring opening of decalin on Pt,Ir/H-Y and Pt,Ir/H-Beta catalysts at 5.0 MPa total pressure. A selectivity of open-chain

decanes of 5 % and a yield of 4 % were observed at 220 °C on 1.5Ir,0.75Pt/H-Y with an n_{Si} / n_{Al} ratio of 13.5.

The scarcity of information concerning the formation of OCDs in the ring opening of polycyclic hydrocarbons is surprising. With all the above-mentioned catalysts ring opening yields of up to 46 % are achieved, and there are publications reporting on ring opening of butylcyclohexane and pentylcyclopentane on bifunctional catalysts with yields of OCDs of up to 47 % [72 - 75]. Unfortunately, the promising Ir/ECR-32 catalyst, which turned out to be so effective in the hydrodecyclization of C_{10} one-ring naphthenes, was not tested in the hydroconversion of decalin. ECR-32 is a dealuminated mesoporous faujasite. Not exactly the same catalyst but a broad variety of similar faujasite materials were tested in the hydroconversion of bicyclic C_{10} hydrocarbons (see Table 4.2), and in the reports about these numerous studies a formation of open-chain decanes was even not mentioned. This could be a hint that the ring opening of bicyclic C_{10} hydrocarbons is much more complicated than that of one-ring alkylnaphthenes or that there are general problems with the peak identification of open-chain decanes.

Except for reference [70] no open-chain decanes were obtained in the hydroconversion of bicyclic hydrocarbons. It is an open question whether in the products generated on the catalysts mentioned in Tables 4.1 and 4.2, open-chain decanes were really absent, or whether the analytical procedures employed in these studies were inadequate for an efficient separation of the OCDs from the skeletal isomers of decalin and its ring opening products and an unambiguous identification of individual OCDs. It cannot be ruled out that some undetected OCDs were in fact present in the products made from bicyclic C_{10}-hydrocarbons on the catalysts listed in Tables 4.1 and 4.2 and that catalysts enabling high yields of ROPs are likewise capable of producing OCDs. On this basis, the following general conclusions can be drawn:

Monofunctional acidic zeolites are not ideal catalysts for hydrodecyclization of multi-ring naphthenes and aromatics. These catalysts tend to deactivate rapidly and to form alkylbenzenes which have lower cetane numbers than the saturated alkylnaphthenes. In addition, the yield of ROPs on acidic zeolites is not very high, rather the very undesired formation of hydrocracked products with less than ten carbon atoms is favored even at moderate conversions. Investigations with different catalyst bed configurations [56] showed that the metal and acid sites should be in a close proximity to each other, preferentially inside the zeolite pores. The n_{metal} / n_{H^+} ratio has a strong influence on the ring opening yield [56] and has to be optimized to achieve good yields of ROPs. In addition to the n_{metal} / n_{H^+} ratio

also the concentration of Brønsted acid sites has to be optimized, and a concentration, which is lower than in most traditional bifunctional catalysts, seems to be favorable [59]. Large-pore zeolites like Beta or Y with a three-dimensional pore system seem to be favorable for the formation of ring opening products. In the catalyst 0.5Pt/1.2K-USY, all these positive features seem to be combined, and it showed the best performance so far in the ring opening of multi-ring naphthenes and aromatics. There is, however, room for further investigations and an optimization of the properties of the metal and acid component of large-pore zeolites. In particular, the influence of other metals than platinum and the effect of the strength of the Brønsted acid sites is largely unexplored.

4.3.3 Ring Opening on Metal Catalysts

The number of publications concerning the ring opening of bicyclic hydrocarbons on metal catalysts without Brønsted acid sites is very limited. There are a few reports on the ring opening of tetralin on bimetallic cobalt- and ruthenium-containing mesoporous silica [76] or of naphthalene on bimetallic platinum- and palladium-containing mesoporous aluminosilicates [77, 78], but these are of limited value, mostly due to the analytical procedures that were inadequate in view of the complex product patterns formed.

The hydroconversion of indan at atmospheric pressure and at 4.0 MPa was investigated on metal catalysts supported on boehmite, γ-Al_2O_3 and CeO_2 [79 - 81]. The metal component consisted of platinum, iridium, or mixed platinum and iridium. At atmospheric pressure and a temperature of 325 °C in a first step the saturated five-membered ring of indan was opened to 2-ethyltoluene and n-propylbenzene (Figure 4.20). Consecutive cracking reactions led to o-xylene and toluene as main hydrocracked products. At atmospheric pressure strong deactivation was observed, especially on catalysts with a high platinum content. At a high hydrogen pressure of 4.0 MPa, the deactivation of the catalysts was significantly reduced. The first reaction step on 1.5Ir,0.5Pt/boehmite was the almost complete hydrogenation of indan to perhydroindan with a yield of 95 % at 300 °C (Figure 4.20). At higher temperatures again the five-membered ring was opened, and the ring opening products 1-ethyl-2-methylcylohexane and n-propylcyclohexane were formed with a yield of 33 %. At the same time very large yields of hydrocracked products and of the dehydrogenated products indan and indene were observed.

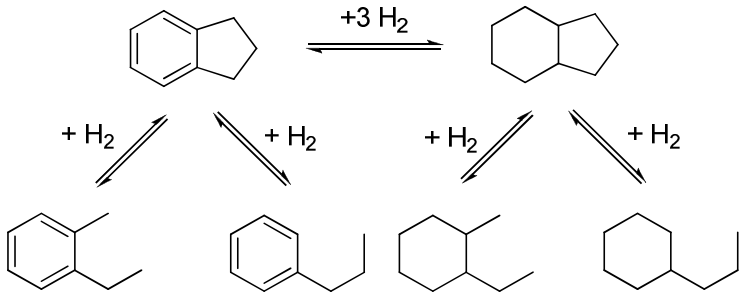

Figure 4.20: Reaction pathways of indan on Pt-Ir-based monofunctional metal catalysts, after Ref. [79].

Indan conversion at atmospheric pressure on 1.9Ir,0.1Pt/CeO_2 gave a ring opening yield of 45.6 %. The same catalyst was used in the hydroconversion of tetralin at 4.0 MPa [80]. Like in the case of indan (Figure 4.20), tetralin was hydrogenated in a first step to cis- and trans-decalin with a yield around 98 %. This high yield of the two decalin isomers persists over a wide temperature range from *ca*. 160 to 300 °C. At even higher temperatures ring opening products are formed, together with the dehydrogenated product naphthalene and very large yields of hydrocracked products. The maximum yield of ROPs obtained on the catalyst 1.9Ir,0.1Pt/CeO_2, the catalyst which was quite successful in the ring opening of indan, was only 6 %.

Table 4.3: Ring opening of bicyclic naphthenes on 0.9Ir/Al_2O_3 at 3.5 MPa total pressure, after Ref. [82].

Feed	T / °C	$LHSV$ / h^{-1}	X / %	S_{ROPs} / %	S_{OCAs} / %
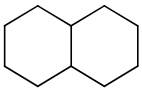 Decalin	275	1.6	4.4	91	traces
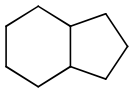 Perhydroindan	275	1.6	68	82	traces
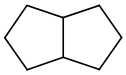 Bicyclo[3.3.0]octane	225	1.6	81	74	26
	225	0.8	99	17	83

Similar observations were made by McVicker *et al.* [82]. They investigated the ring opening of bicyclo[3.3.0]octane, perhydroindan and decalin on 0.9Ir/Al_2O_3. While bicyclo[3.3.0]octane, a hydrocarbon with two five-membered rings, shows a very high conversion at 225 °C with good selectivities of open-chain alkanes (OCA) with the same carbon number as the feed

(here: open-chain octanes) between 26 and 83 %, decalin, a hydrocarbon with two six-membered rings, gives hardly any conversion even at 50 °C higher temperatures and only traces of open-chain decanes (Table 4.3). The authors explain these drastic differences on the basis of the ring opening rates of five-membered and six-membered rings. In Figure 4.21, the ring opening of methylcyclohexane is illustrated. Nonbranching ring contraction to ethylcyclopentane is the preferred path because this five-membered ring with only one substituent has the highest ring opening rate. Moreover, less branched open-chain heptanes are obtained, which are preferred in terms of cetane number improvement. Branching isomerization of methylcyclohexane to dimethylcyclopentanes is undesirable since subsequent ring opening would be retarded and the obtained open-chain heptanes would be highly branched. Direct ring opening of methylcyclohexane is the least favored path, as the ring cleavage rate is very low.

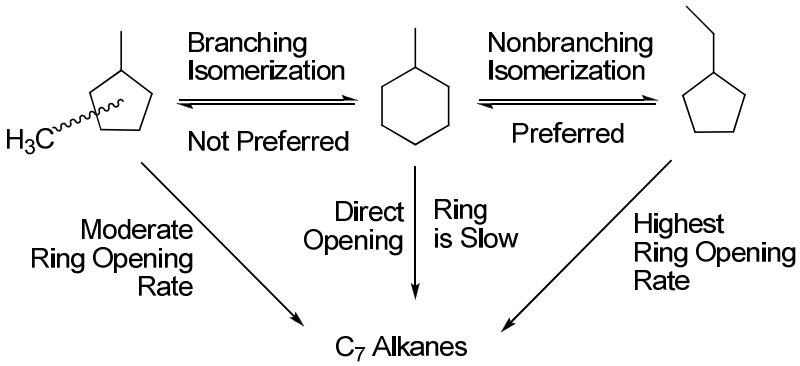

Figure 4.21: Different ring opening rates of five-and six-membered rings [82].

Starting from decalin, a potential route could be to use a metal catalyst combined with a balanced acid function which would isomerize the six-membered ring to a five-membered ring prior to ring opening. This concept has been successfully proven for the ring opening of methylcyclohexane. By adding an isomerization catalyst (Pt/USY) to the ring opening catalyst Ir/Al_2O_3 a significant increase in the ring opening yield of methylcyclohexane could be obtained [82]. In the same way the ring opening yield of butylcyclohexane was enhanced by addition of the same isomerization catalyst to Ir/Al_2O_3. A proper balance between the metal and the acid sites is very important, and even more important than in case of methylcyclohexane, because when adding too much of Pt/USY to Ir/Al_2O_3, the ring opening yield drops because highly branched cyclopentanes are obtained which are less reactive and, in addition, undesired hydrocracking to products with less than seven carbons atoms takes place.

Hydrogenolysis over metals can be used to convert five-membered ring naphthenes into open-chain alkanes with the same carbon number as the feed. The ring opening rates of six-membered rings are very slow, thus until now only traces of open-chain decanes from the

ring opening of decalin were obtained on metal catalysts [82]. A potential strategy could be a metal catalyst with a very mild isomerization function added, in order to convert the six-membered rings in decalin to five-membered rings. This strategy was successful in the ring opening of methylcyclohexane and butylcyclohexane but until now not investigated in the ring opening of decalin.

5 Experimental Section

The chemicals used in this work are listed in Table 5.1 and were used without prior purification.

Table 5.1: Overview of the used chemicals.

Chemical	**Producer, Purity / Composition**
Aluminum nitrate nonahydrate	Merck, > 98.5 wt.-%
Ammonium acetate	Aldrich, > 98 wt.-%
Ammonium hexafluorosilicate	Ventron, > 99 wt.-%
Ammonium nitrate	Merck, > 99 wt.-%
Cesium chloride	Sigma, > 99 wt.-%
Chromosorb	Merck, particle size: 0.25-0.60 mm, P/AW
cis-Decalin	Merck, 97.4 wt.-%
Hydrofluoric acid	Merck, 40 wt.-%
Hydrogen 5.0	Westfalen AG, 99.999 vol.-%
Lanthanum nitrate hexahydrate	Merck, > 99 wt.-%
Lithium chloride	Sigma Aldrich, > 99 wt.-%
Ludox HS-40	Sigma Aldrich, 40 wt.-% SiO_2 in H_2O
Methyltriethylammonium bromide	Fluka, > 99 wt.-%
Pentaamminechloroiridium(III) chloride	Aldrich, 50.07 wt.-% Ir
Perhydroindan	kindly provided by Eni S.p.A., 96.7 wt.-%
Potassium chloride	Riedel-de Haën, > 99.5 wt.-%
Potassium hydroxide	unknown, DAB
Rubidium chloride	Aldrich, > 99 wt.-%
Sulfuric acid	unknown, 96 %
Sodium aluminum oxide	Riedel-de Haën, 54 wt.-% Al_2O_3, 41 wt.-% Na_2O, 5 wt.-% H_2O
Sodium hydroxide	Merck, > 99 wt.-%
Sodium nitrate	Merck, > 99 wt.-%
Sodium silicate solution	Merck, 8 wt.-% Na_2O, 27 wt.-% SiO_2, 65 wt.-% H_2O
Spectromelt A 20	Merck, > 99 wt.-% $LiBO_2$
Tetraammineplatinum(II) chloride hydrate	ChemPur, 55.63 wt.-% Pt
Tetraethylammonium bromide	Merck-Schuchardt, > 99 wt.-%
Zeolite X	Strem Chemicals, lot No. 14 247S
Zeolite Y	Strem Chemicals, lot No. 148 960

5.1 Preparation of the Catalysts

5.1.1 Preparation of the Starting Materials

Zeolites X (n_{Si} / n_{Al} = 1.21) and Y (n_{Si} / n_{Al} = 2.41) were purchased from Strem Chemicals with lot Nos. 14 247S and 148 960, respectively. Zeolite MCM-22 with an n_{Si} / n_{Al} = 21 was synthesized in the group of Privatdozentin Dr. Yvonne Traa. The other two zeolites used in this work, zeolites LSX and ZSM-12, were prepared by hydrothermal syntheses.

5.1.1.1 Zeolite LSX

9.4 g sodium aluminum oxide were dissolved in 17 g demineralized water. Subsequently, 11.2 g sodium hydroxide in 20 g demineralized water and 8.4 g potassium hydroxide in 20 g demineralized water were added under vigorous stirring. After 5 min 21.4 g sodium silicate solution in 15 g demineralized water were added. Approximately after 2 min gelling could be observed. The gelled mixture was then aged for 48 h at 45 °C in a sealed plastic jar. The crystallization was carried out for 2 h at 100 °C. The mixture was filtered, washed with 3 dm^3 demineralized water and dried for at least 12 h at 80 °C in an oven. In order to remove the potassium ions, the zeolite sample was stirred two times for 4 h at 80 °C in 25 cm^3 of a 1 mol dm^{-3} aqueous solution of $NaNO_3$ per 1 g of dry zeolite sample. Each time after 4 h the sample was filtered and washed with demineralized water until no nitrate ions could be detected any more and dried for at least 12 h at 80 °C in an air oven. The n_{Si} / n_{Al} ratio of the synthesis gel was 0.97, and the n_{Si} / n_{Al} ratio of the solid sample determined by ICP-OES amounted to 1.01.

5.1.1.2 Zeolite ZSM-12

All syntheses were carried out in stainless steel autoclaves with Teflon inlets with a capacity of 150 cm^3. After each synthesis the resulting gel was filtered, washed with 2 dm^3 demineralized water and dried for at least 12 h at 80 °C in an oven. The template was removed by heating under a synthetic air flow rate of 58 $dm^3 \cdot h^{-1}$ from room temperature to 200 °C with a heating rate of 1 $K \cdot min^{-1}$ and holding at 200 °C for 3 h and then heating from 200 °C to 540 °C with a heating rate of 1 $K \cdot min^{-1}$ and hold at the final temperature for 7 h.

Na-ZSM-12-24 [83]:

80.96 g sodium silicate solution were mixed with 80 g demineralized water and stirred for 10 min. 30.64 g methyltriethylammonium bromide and 100 g demineralized water were stirred for 10 min and added. Subsequently, a solution of 4.77 g $Al(NO_3)_3 \cdot 9H_2O$ in 30 g demineralized water was added. Afterwards, 4.77 g H_2SO_4 were added under vigorous stirring. After 5 min the gel was transferred into a Teflon-lined stainless steel autoclave, and crystallization was carried out at 160 °C for 90 h. The n_{Si} / n_{Al} ratio of the synthesis gel was 28.6, and the n_{Si} / n_{Al} ratio of the solid sample determined by ICP-OES amounted to 24.3.

Na-ZSM-12-39 [84]:

8.81 g tetraethylammonium bromide were mixed with 25 g demineralized water and 0.90 g sodium hydroxide. 0.68 g sodium aluminum oxide were then added, and the mixture was stirred for 10 min. A mixture of 50.02 g Ludox HS-40 and 20 g demineralized water was added, and the resulting mixture was stirred for additional 20 min. The gel was then transferred into a Teflon-lined stainless steel autoclave, and crystallization was carried out at 160 °C for 112 h. The n_{Si} / n_{Al} ratio of the synthesis gel was 45.4, and the n_{Si} / n_{Al} ratio of the solid sample determined by ICP-OES amounted to 39.0.

Na-ZSM-12-42 [84]:

8.83 g tetraethylammonium bromide were mixed with 25 g demineralized water and 0.89 g sodium hydroxide. 0.69 g sodium aluminum oxide were then added, and the mixture was stirred for 10 min. A mixture of 50.22 g Ludox HS-40 and 20 g demineralized water was added, and the resulting mixture was stirred for additional 20 min. The gel was then transferred into a Teflon-lined stainless steel autoclave, and crystallization was carried out at 160 °C for 117 h. The n_{Si} / n_{Al} ratio of the synthesis gel was 46.0, and the n_{Si} / n_{Al} ratio of the solid sample determined by ICP-OES amounted to 42.1.

Na-ZSM-12-125 [84]:

8.61 g tetraethylammonium bromide were mixed with 25 g demineralized water and 0.69 g sodium hydroxide. 0.20 g sodium aluminum oxide were then added, and the mixture was stirred for 10 min. A mixture of 50.01 g Ludox HS-40 and 20 g demineralized water was added, and the resulting mixture was stirred for additional 15 min. The gel was then

transferred into a Teflon-lined stainless steel autoclave, and crystallization was carried out at 160 °C for 120 h. The n_{Si} / n_{Al} ratio of the synthesis gel was 161, and the n_{Si} / n_{Al} ratio of the solid sample determined by ICP-OES amounted to 125.

5.1.2 Modification of the Zeolites

Each zeolite used in this work was stirred two times for 4 h at 80 °C in 40 cm^3 of a 1 $mol \cdot dm^{-3}$ aqueous solution of $NaNO_3$ per 1 g of dry zeolite sample. Each time after 4 h the samples were filtrated and washed with demineralized water until no nitrate ions could be detected any more and dried for at least 12 h at 80 °C in an air oven. This procedure was done to ensure that each exchangeable cation is a sodium cation in order to start from a well-defined zeolite composition for each modification step.

5.1.2.1 Ion Exchange with Ammonium, Alkali and Lanthanum Ions

Ion Exchange with Ammonium Ions

For a nearly fully exchange of the zeolites Na-ZSM-12-24, Na-ZSM-12-125 and Na-Y, the samples were stirred two times for 4 h at 80 °C in 40 cm^3 of a 1 $mol \cdot dm^{-3}$ aqueous solution of NH_4NO_3 per gram of dry zeolite. Each time after 4 h the samples were filtered and washed with demineralized water until no nitrate ions could be detected any more and dried for at least 12 h at 80 °C in an air oven. The resulting zeolites NH_4-ZSM-12-24 and NH_4-ZSM-12-125 had an exchange degree of 98 and 99 %, respectively. An exchange degree of ammonium ions of 83 % was obtained in the $(NH_4)_{0.83}$,$Na_{0.17}$-Y zeolite. This zeolite was used for the dealumination step described in Section 5.1.2.2.

Zeolite Na-ZSM-12-42 was partially exchanged with ammonium ions. The zeolite was suspended in 20 cm^3 of a 0.02 $mol \cdot dm^{-3}$ aqueous ammonium nitrate solution per gram of dry zeolite. The ion exchange was carried out for 4 h at 80 °C under stirring. The resulting zeolite was filtered, washed with demineralized water and dried for at least 12 h at 80 °C in an air oven. The resulting zeolite $Na_{0.53}$,$(NH_4)_{0.47}$-ZSM-12-42 has an exchange degree of 47 %.

A bifunctional Pt/H,Na-Y catalyst was used for the isomerization of n-decane. For its preparation, Na-Y was partially exchanged with ammonium ions. The zeolite was suspended in 5 cm^3 of a 0.08 $mol \cdot dm^{-3}$ aqueous ammonium nitrate solution per gram of dry zeolite. The

ion exchange was carried out for 4 h at 80 °C under stirring. The resulting zeolite was filtered, washed with demineralized water and dried for at least 12 h at 80 °C in an air oven. The resulting zeolite $(NH_4)_{0.60}$,$Na_{0.40}$-Y has an exchange degree of 60 %.

Ion Exchange with Alkali Ions

$Li_{0.74}$,$Na_{0.21}$,$H_{0.05}$-Y:

Zeolite Na-Y was slurried under stirring in 33 cm^3 of a 1 $mol \cdot dm^{-3}$ aqueous solution of LiCl per gram of dry Na-Y. The suspension was stirred for 4 h at 80 °C. Upon filtration, the zeolite was washed with demineralized water and dried at 80 °C for 12 h in an air oven. This procedure was repeated four times. The final n_{Li} / n_{Al} ratio as determined by ICP-OES amounted to 0.74 and the n_{Na} / n_{Al} ratio to 0.21.

$K_{0.95}$,$H_{0.05}$-Y:

Zeolite Na-Y was slurried under stirring in 33 cm^3 of a 1 $mol \cdot dm^{-3}$ aqueous solution of KCl per gram of dry Na-Y. The suspension was stirred for 4 h at 80 °C. Upon filtration, the zeolite was washed with demineralized water and dried at 80 °C for 12 h in an air oven. This procedure was repeated three times. The final n_K / n_{Al} ratio as determined by ICP-OES amounted to 0.95. No sodium ions were detectable.

$Rb_{0.83}$,$Na_{0.17}$-Y:

Zeolite Na-Y was slurried under stirring in 42 cm^3 of a 0.1 $mol \cdot dm^{-3}$ aqueous solution of RbCl per gram of dry Na-Y. The suspension was stirred for 4 h at 80 °C. Upon filtration, the zeolite was washed with demineralized water and dried at 80 °C for 12 h in an air oven. The sample was calcined in air by heating from room temperature to 120 °C with a heating rate of 0.5 $K \cdot min^{-1}$ and held at this temperature for 2 h in an oven under a synthetic air flow rate of 58 $dm^3 \cdot h^{-1}$. Subsequently the sample was heated to 200 °C with the above-mentioned heating rate and held at this temperature for 2 h. Afterwards, the sample was heated to 450 °C with the same heating rate, and the end temperature was held for 2 h. The calcination is necessary to achieve a higher exchange degree of rubidium by migration of the bulky Rb^+ ions into the small cages at elevated temperature, as in the case of Cs,Na-Y (see below).

The procedure of ion exchange and the following calcination was repeated three times. The final n_{Rb} / n_{Al} ratio as determined by ICP-OES amounted to 0.85 and the n_{Na} / n_{Al} ratio to 0.17.

In this case, slightly more cations than aluminum ions were detected. The determination of rubidium seems to be less sensitive than that of sodium, therefore the amount of rubidium was reduced so that the sum of rubidium and sodium ions is equal to the amount of aluminum ions.

$Cs_{0.86}Na_{0.14}$-Y:

Zeolite Na-Y was slurried under stirring in 42 cm^3 of a 0.1 $mol \cdot dm^{-3}$ aqueous solution of CsCl per gram of dry Na-Y. The suspension was stirred for 4 h at 80 °C. Upon filtration, the zeolite was washed with demineralized water and dried at 80 °C for 12 h in an air oven. The sample was calcined in air by heating from room temperature to 120 °C with a heating rate of 0.5 $K \cdot min^{-1}$ and held at this temperature for 2 h in an oven under a synthetic air flow rate of 58 $dm^3 \cdot h^{-1}$. Subsequently, the sample was heated to 200 °C with the above-mentioned heating rate and held at this temperature for 2 h. Afterwards, the sample was heated to 450 °C with the same heating rate, and the end temperature was held for 2 h. The calcination is necessary to achieve a higher exchange degree of cesium ions by migration of the bulky Cs^+ ions into the small cages at elevated temperature [85].

The procedure of ion exchange and the following calcination was repeated three times. The final n_{Na} / n_{Al} ratio as determined by ICP-OES amounted to 0.14. The concentration of cesium could not be determined by ICP-OES measurements. Therefore, the assumption were made that all other missing cations are cesium cations and no other cations like protons are present. An n_{Cs} / n_{Al} ratio of 0.86 then results.

Ion Exchange with Lanthanum Ions

The zeolites Na-X or Na-Y were slurried under stirring in approximately 20 cm^3 of an aqueous solution ($pH \approx 6$) of $La(NO_3)_3$ per gram of dry zeolite. The ion exchange with lanthanum ions is quantitative up to an exchange degree of 72 %. The concentration of the lanthanum nitrate solution was varied between 0.016 and 0.076 mol l^{-1}. The suspension was stirred for 3 h at 80 °C. Upon filtration, the zeolites were washed with demineralized water and dried at 80 °C for 12 h in an air oven. The samples were calcined in air by heating from room temperature to 120 °C with a heating rate of 0.5 $K \cdot min^{-1}$ and held at this temperature for 2 h in an oven under a simultaneous synthetic air flow rate of 14.5 $dm^3 \cdot h^{-1}$ and a nitrogen flow rate of 14.5 $dm^3 \cdot h^{-1}$. Subsequently, the sample was heated to 200 °C with the above-mentioned heating rate and held at this temperature for 2 h. Thereafter, the sample was

heated to 450 °C with the same heating rate, and the end temperature was held for 2 h. During calcination a lanthanum cation migration from the supercages into the sodalite cages and hexagonal prisms took place [14].

La,Na-Y zeolites with exchange degrees of 18, 33 and 45 % and La,Na-X zeolites with exchange degrees of 39, 51, 66 and 90 % were prepared. For the exchange degree of 90 % on zeolite X, the above-mentioned procedure of ion exchange and calcination was repeated a second time.

5.1.2.2 Dealumination of Zeolite Y

For the dealumination with $(NH_4)_2[SiF_6]$ an ammonium-exchanged Y zeolite is required. It is believed that the process proceeds in two steps: (1) removal of aluminum from the framework and (2) the insertion of Si atoms into the lattice vacancies left by aluminum release. This technique is only applicable to zeolites the charge-compensating cations of which form soluble fluoroaluminate and hexafluorosilicate salts. This is indeed the case with protons or ammonium ions.

15.2 g of the dry $(NH_4)_{0.83}Na_{0.17}$-Y zeolite were suspended in 160 cm^3 of a 10 $mol \cdot dm^{-3}$ aqueous ammonium acetate solution used as a buffer. The suspension was heated to 75 °C. $(NH_4)_2[SiF_6]$ was added dropwise within 50 min as an 1 $mol \cdot dm^{-3}$ aqueous solution. Afterwards, the slurry was heated to 90 °C and held for 3 h. The exact amounts of ammonium hexafluorosilicate used are listed in Table 5.2. The dealumination is not quantitative. The theoretical ratio $(n_{Si} / n_{Al})_{theo.}$ is every time higher than the real one determined by ICP-OES. It could be that the ammonium hexafluorosilicate did not react quantitatively or that the second step, namely the insertion of Si atoms into the lattice vacancies, was not completed.

Table 5.2: Overview of the molar amount of $(NH_4)_2[SiF_6]$ used and the resulting n_{Si} / n_{Al} ratio in the zeolite.

$m_{(NH_4)_2[SiF_6]}$ / g	$n_{(NH_4)_2[SiF_6]}$ / mmol	$(n_{Si} / n_{Al})_{theo.}$	$(n_{Si} / n_{Al})_{real}$
3.61	20.34	3.90	3.44
5.16	28.95	4.95	4.11
7.50	42.10	6.49	5.49

The dealuminated zeolite was filtered off and washed with 1 dm^3 of demineralized boiling water. For a complete removal of the ammonium hexafluorosilicate and -aluminate the zeolite was heated five times to 95 °C for 1 h in 1 dm^3 demineralized water and filtered off in a hot stage. Finally, the zeolite was back-exchanged two times in a typical procedure (see Section 5.1.2) with sodium nitrate in order to get the sodium form of the dealuminated zeolite. Then the zeolites were calcined in air by heating from room temperature to 400 °C with a heating rate of 0.5 $K \cdot min^{-1}$ and held at the end temperature for 2 h in an oven under a synthetic air flow rate of 58 $dm^3 \cdot h^{-1}$. This was done to ensure that there are no small amounts of $(NH_4)_2[SiF_6]$ left, which can form HF during heating and destroy the zeolite.

5.1.2.3 Incorporation of the Noble Metal

The zeolite sample was suspended in 12-15 g demineralized water per gram of dry zeolite sample. An aqueous solution of $[Pt(NH_3)_4]Cl_2$ or $[Ir(NH_3)_5Cl]Cl_2$ in 50 g demineralized water was slowly added by means of a dropping funnel within 20 min under vigorous stirring. For the exchange with the platinum complex the amount of complex was calculated under the assumption that all platinum was loaded onto the zeolite sample. In case of iridium an excess of 20 % was used in comparison to the calculated amount. The used zeolite samples and the resulting catalysts are listed in Table 5.3. In cases where the ratio $n_{cations} / n_{Al}$ determined by ICP-OES is smaller than 1, protons were added in the sample designation to reach a value of 1. In general, modifications of the n_{Si} / n_{Al} ratio of the zeolites are indicated in the designation after a hyphen with the new n_{Si} / n_{Al} ratio, otherwise LSX has an n_{Si} / n_{Al} ratio of 1.01, X of 1.21, Y of 2.41 and MCM-22 of 21.

Zeolite Na-MCM-22 was planned to be loaded with 3 wt.-% of iridium, and an excess of 20 % was used as usually. ICP-OES measurements after the first ion exchange indicated, however, 0.77 wt.-% iridium only. A second exchange was done with iridium which was expected to lead to 2.2 wt.-% metal loading. This time the suspension was stirred for 95 h at 80 °C. Nevertheless, an iridium loading of only 1.4 wt.-% was achieved.

Table 5.3: Zeolite samples used for the ion exchange with iridium or platinum and designations of the resulting catalysts.

Zeolite sample	**Catalyst designation after loading with**	
	$[Ir(NH_3)_5Cl]Cl_2$	**$[Pt(NH_3)_4]Cl_2$**
Na-LSX	3.0Ir/$Na_{0.90}$,$H_{0.10}$-LSX	2.9Pt/$Na_{0.89}$,$H_{0.11}$-LSX
Na-X	2.5Ir/$Na_{0.91}$,$H_{0.09}$-X	2.8Pt/$Na_{0.86}$,$H_{0.14}$-X
Na-X	0.94Ir/$Na_{0.90}$,$H_{0.10}$-X	0.96Pt/$Na_{0.88}$,$H_{0.12}$-X
$Na_{0.54}$,$La_{0.13}$,$H_{0.07}$-X	1.1Ir/$Na_{0.52}$,$La_{0.13}$,$H_{0.09}$-X	1.1Pt/$Na_{0.52}$,$La_{0.13}$,$H_{0.09}$-X
$Na_{0.43}$,$La_{0.17}$,$H_{0.06}$-X	0.94Ir/$Na_{0.41}$,$La_{0.16}$,$H_{0.11}$-X	0.99Pt/$Na_{0.43}$,$La_{0.17}$,$H_{0.06}$-X
$Na_{0.28}$,$La_{0.22}$,$H_{0.06}$-X	0.99Ir/$Na_{0.26}$,$La_{0.22}$,$H_{0.08}$-X	0.87Pt/$Na_{0.26}$,$La_{0.22}$,$H_{0.08}$-X
$La_{0.30}$,$H_{0.06}$,$Na_{0.04}$-X	0.85Ir/$La_{0.30}$,$H_{0.06}$,$Na_{0.04}$-X	1.0Pt/$La_{0.30}$,$H_{0.06}$,$Na_{0.04}$-X
Na-Y	3.8Ir/$Na_{0.89}$,$H_{0.11}$-Y	4.2Pt/$Na_{0.87}$,$H_{0.13}$-Y
Na-Y	3.1Ir/$Na_{0.90}$,$H_{0.10}$-Y	4.0Pt/$Na_{0.88}$,$H_{0.12}$-Y
Na-Y	2.9Ir/$Na_{0.90}$,$H_{0.10}$-Y	3.7Pt/$Na_{0.86}$,$H_{0.14}$-Y
Na-Y	2.4Ir/$Na_{0.93}$,$H_{0.07}$-Y	3.0Pt/$Na_{0.88}$,$H_{0.12}$-Y
Na-Y	1.9Ir/$Na_{0.92}$,$H_{0.08}$-Y	2.7Pt/$Na_{0.88}$,$H_{0.12}$-Y
Na-Y	1.0Ir/$Na_{0.93}$,$H_{0.07}$-Y	2.0Pt/$Na_{0.91}$,$H_{0.09}$-Y
Na-Y		1.7Pt/$Na_{0.91}$,$H_{0.09}$-Y
Na-Y		0.94Pt/$Na_{0.94}$,$H_{0.06}$-Y
Na-Y-3.44	3.3Ir/$Na_{0.88}$,$H_{0.12}$-Y-3.44	3.0Pt/$Na_{0.89}$,$H_{0.11}$-Y-3.44
Na-Y-4.11	3.3Ir/$Na_{0.90}$,$H_{0.10}$-Y-4.11	2.9Pt/$Na_{0.87}$,$H_{0.13}$-Y-4.11
Na-Y-5.49	3.1Ir/$Na_{0.77}$,$H_{0.23}$-Y-5.49	2.9Pt/$Na_{0.75}$,$H_{0.25}$-Y-5.49
$(NH_4)_{0.60}$,$Na_{0.40}$-Y		0.49Pt/$H_{0.55}$,$Na_{0.45}$-Y
$Li_{0.74}$,$Na_{0.21}$,$H_{0.05}$-Y	3.0Ir/$Li_{0.68}$,$Na_{0.21}$,$H_{0.11}$-Y	3.0Pt/$Li_{0.58}$,$Na_{0.25}$,$H_{0.17}$-Y
$K_{0.95}$,$H_{0.05}$-Y	2.7Ir/$K_{0.88}$,$H_{0.12}$-Y	2.9Pt/$K_{0.90}$,$H_{0.10}$-Y
$Rb_{0.83}$,$Na_{0.17}$-Y	2.6Ir/$Rb_{0.70}$,$Na_{0.15}$,$H_{0.15}$-Y	2.9Pt/$Rb_{0.68}$,$Na_{0.15}$,$H_{0.17}$-Y
$Cs_{0.86}$,$Na_{0.14}$-Y	2.6Ir/$Cs_{0.71}$,$Na_{0.16}$,$H_{0.13}$-Y	3.1Pt/$Cs_{0.71}$,$Na_{0.16}$,$H_{0.13}$-Y
$Na_{0.78}$,$La_{0.06}$,$H_{0.04}$-Y	1.2Ir/$Na_{0.77}$,$La_{0.06}$,$H_{0.05}$-Y	0.95Pt/$Na_{0.76}$,$La_{0.07}$,$H_{0.03}$-Y
$Na_{0.64}$,$La_{0.11}$,$H_{0.03}$-Y	1.2Ir/$Na_{0.63}$,$La_{0.11}$,$H_{0.04}$-Y	1.2Pt/$Na_{0.62}$,$La_{0.11}$,$H_{0.05}$-Y
$Na_{0.49}$,$La_{0.15}$,$H_{0.06}$-Y	1.1Ir/$Na_{0.50}$,$La_{0.15}$,$H_{0.05}$-Y	0.97Pt/$Na_{0.50}$,$La_{0.16}$,$H_{0.02}$-Y
Na-ZSM-12-39	1.7Ir/$H_{0.65}$,$Na_{0.35}$-ZSM-12-39	2.9Pt/$H_{0.95}$,$Na_{0.05}$-ZSM-12-39
Na,NH_4-ZSM-12-42	0.94Ir/$H_{0.76}$,$Na_{0.24}$-ZSM-12-42	1.3Pt/$H_{0.76}$,$Na_{0.24}$-ZSM-12-42
Na-MCM-22	1.4Ir/$H_{0.54}$,$Na_{0.46}$-MCM-22	2.9Pt/$H_{0.76}$,$Na_{0.24}$-MCM-22

For the preparation of the bimetallic catalysts, Na-Y zeolite was suspended in 25-30 g demineralized water per gram of dry zeolite. An aqueous solution of $[Pt(NH_3)_4]Cl_2$ in 25 g demineralized water and of $[Ir(NH_3)_5Cl]Cl_2$ in 25 g demineralized water were mixed and

slowly added by means of a dropping funnel within 20 min under vigorous stirring. Like in the monometallic case an excess of 20 % for the iridium salt and for platinum the exact theoretical amount were used. The suspension was stirred for 4 h at 80 °C. The solid was then filtered off, washed with demineralized water and dried for at least 12 h at 80 °C in an air oven. Three bimetallic Y zeolites with a total metal content of 3 wt.-% and n_{Ir} / (n_{Ir} + n_{Pt}) ratios of 0.76, 0.50 and 0.25 were prepared (Table 5.4).

Table 5.4: Catalyst designation of the three bimetallic Y zeolites with different n_{Ir} / (n_{Ir} + n_{Pt}) ratios.

Catalyst designation	n_{Ir} / (n_{Ir} + n_{Pt})
2.3Ir,0.73Pt/$Na_{0.90}$,$H_{0.10}$-Y	0.76
1.5Ir,1.5Pt/$Na_{0.95}$,$H_{0.05}$-Y	0.50
0.76Ir,2.3Pt/$Na_{0.89}$,$H_{0.11}$-Y	0.25

5.1.3 Decomposition of the Complex

After ion exchange, all metal-containing samples were calcined in air by heating from room temperature to 300 °C with a heating rate of 0.5 $K \cdot min^{-1}$ and held at the end temperature for 2 h in an oven under a synthetic air flow rate of 58 $dm^3 \cdot h^{-1}$. This step is necessary to destroy the $[Pt(NH_3)_4]^{2+}$ and $[Ir(NH_3)_5Cl]^{2+}$ complexes. If it is omitted, highly mobile amino hydrides are formed during the subsequent reduction of the metal in hydrogen (Section 5.1.5). These mobil species would migrate out of the zeolite pores and form large metal clusters with a low dispersion on the external surface [86].

The zeolites H-ZSM-12-24 and H-ZSM-12-125 were formed by calcination of NH_4-ZSM-12-24 and NH_4-ZSM-12-125 by heating first from room temperature to 200 °C with a heating rate of 1 $K \cdot min^{-1}$ and held at 200 °C for 3 h and then from 200 °C to 540 °C with the same heating rate and held at the end temperature for 7 h under a synthetic air flow with a rate of 58 $dm^3 \cdot h^{-1}$.

5.1.4 Forming of the Catalyst Powder

For the catalytic experiments the catalyst powders would have been inappropriate, mainly as they would have caused a too high pressure drop in the fixed-bed reactor. Larger particles were formed by pressing the powders without a binder at 127 MPa for 15 min, and the

tablets thereby formed were crushed. The size fraction of 0.20 mm < d_{cat} < 0.32 mm was used in the catalytic experiments.

5.1.5 Reduction of the Noble Metal

The noble metal on the catalysts were reduced in the catalytic flow-type apparatus under a hydrogen pressure of 5.2 MPa and a hydrogen flow of 130 $cm^3 \cdot min^{-1}$ while heating the sample from room temperature to 380 °C with a rate of 2 $K \cdot min^{-1}$ and holding at 380 °C for 2 h. During this reduction step two Brønsted acid sites per divalent noble metal cation were generated (see Section 4.1, Eq. (4.4)).

5.2 Characterization of the Starting Materials and Catalysts

5.2.1 X-Ray Diffraction

After each synthesis and modification step, it was ascertained by powder X-ray diffractometry (XRD) that the zeolite was phase-pure and had retained its structure. A Bruker D8 Advance diffractometer with CuKα radiation (λ = 0.154 nm) was used. A voltage of U = 35 kV and a current intensity of I = 40 mA were applied. The diffractograms were collected between 2θ values of 3 and 50° with a step width of 0.02° and a step time of 1.5 s.

5.2.2 Chemical and Thermogravimetric Analysis

A Varian optical emission spectrometer with an inductively coupled plasma (ICP-OES) Vista-MPX CCD was used for chemical analysis of the zeolites. Silicon, aluminum, lithium, sodium, potassium, rubidium, lanthanum, iridium and platinum were determined by ICP-OES. For that purpose, *ca*. 100 mg of the zeolite sample were dissolved in 3 cm^3 of diluted hydrofluoric acid (10 wt.-% HF in doubly distilled water) and 6 cm^3 of nitrohydrochloric acid. This mixture was filled up to 250 cm^3 with doubly distilled water and was then analyzed. To determine the metal content of iridium and platinum, the zeolite samples after ion exchange with the iridium or platinum salt prior to the calcination were used because after oxidation of the metal during the calcination process the zeolite sample cannot be completely dissolved with the above-mentioned procedure.

To determine the lanthanum content of the X and Y zeolites, *ca.* 60 mg of the samples were mixed with approximately 350 mg lithium metaborate and heated up to 920 °C in a platinum crucible and held at this temperature for 15 min in order to get the lanthanum species dissolved. After cooling to room temperature, the clear melt was dissolved in hydrofluoric and nitrohydrochloric acid and analyzed as described above. To determine the platinum and iridium content of lanthanum-containing samples, *ca.* 60 mg of the sample were suspended in diluted hydrofluoric acid and nitrohydrochloric acid and heated to 180 °C for 1 h in a microwave oven.

The metal content of all samples is defined as the mass of the metal per dry mass of the catalyst. To detect the mass of the dry catalyst, it was first stored in a desiccator over a saturated aqueous solution of calcium nitrate for at least 24 h. The precise water content of the resulting samples was then measured by means of a Setaram Thermogravimetric Analyzer (TGA) Setsys TG-16/18. In the TGA experiment, the sample was heated in a nitrogen flow from room temperature to 600 °C with a heating rate of 20 K min^{-1}.

5.2.3 MAS NMR Spectroscopy

A Bruker MSL 400 spectrometer was used for measuring the ^{1}H, ^{27}Al and ^{29}Si MAS NMR spectra. Prior to the ^{1}H MAS NMR experiments, the zeolite samples were dehydrated under vacuum ($p < 10^{-2}$ mPa) at 450 °C for 12 h.

^{1}H MAS NMR spectra of the dehydrated zeolites were measured in a rotor with a diameter of 4 mm at a resonance frequency of 400.1 MHz with a sample spinning rate of 10 kHz with 160 accumulations. The spectra were recorded using a pulse length of 2.1 µs and a repetition time of 10 s. A Na,H-Y zeolite with a proton exchange degree of 35 % was used as external standard.

^{27}Al MAS NMR spectra were measured on the hydrated zeolites (stored over saturated aqueous sodium chloride solution at room temperature) in a rotor with a diameter of 4 mm at a resonance frequency of 104.3 MHz and 800-4800 accumulations. The spinning rate was 9 kHz. The spectra were recorded against aluminum nitrate using a pulse length of 0.61 µs and a repetition time of 0.5 s.

The ^{29}Si HPDEC MAS NMR spectra were measured on the hydrated zeolites (stored over saturated aqueous sodium chloride solution at room temperature) in a rotor with a diameter

of 7 mm at a resonance frequency of 79.5 MHz and 250-500 accumulations. The spinning rate was 4 kHz. The spectra were recorded against tetramethylsilane using a pulse length of 5 µs and a repetition time of 10 s. The program WINFIT from Bruker was used to simulate and integrate the signals.

In contrast to ICP-OES measurements where only the n_{Si} / n_{Al} ratio of the whole solid can be determined, ^{29}Si MAS NMR measurements enable one to determine the n_{Si} / n_{Al} ratio of the zeolite lattice by means of Eq. (5.1) [87]. In the ^{29}Si MAS NMR spectra different signals were obtained for different surroundings of a silicon atom. A spectrum of a faujasite zeolite can consist of up to five different signals, depending on how many aluminium atoms are coordinated to a silicon atom. In Eq. (5.1), k is the number of aluminum atoms coordinated to a silicon atom and F is the relative fraction of the different signals.

$$n_{Si} / n_{Al} = \frac{\sum_{k=0}^{4} F_{Si\,(k\ Al)}}{\sum_{k=0}^{4} 0.25 \cdot k \cdot F_{Si\,(k\ Al)}} \qquad (5.1)$$

5.2.4 H_2 Chemisorption

For the determination of the noble-metal dispersion the amount of irreversibly adsorbed hydrogen was measured in a Quantachrome Autosorb-1-C instrument. For hydrogen chemisorption by static volumetry an adsorption stoichiometry of n_H / $n_{noble\ metal}$ = 1 was assumed. After the reduction treatment with the same temperature program as used in the reactor of the catalytic flow-type apparatus (Section 5.1.5), two isotherms were measured at T = 40 °C. The first isotherm is considered to be a combination of physi- and chemisorption, and the second isotherm, measured after evacuating the sample, is interpreted as physisorption only. The difference of these two isotherms originating from irreversibly and strongly adsorbed molecules is applied for calculating the noble-metal dispersion.

5.2.5 Scanning Electron Microscopy

To determine the morphology and the size of the crystals a scanning electron microscope (SEM) Cam Scan 44 was used. The samples were coated with an ultrathin coating of gold by a sputter coating equipment K550 of Emitech. An excitation voltage of 5 kV was used to achieve a high resolution.

5.2.6 CHN Analysis

The carbon content of the catalysts H-ZSM-12-24 and H-ZSM-12-125 after their use in the hydroconversion of cis-decalin was measured by quantitative high-temperature decomposition of *ca*. 20 mg of the material at 950 °C in an elemental analyzer Elementar Vario EL. The resulting carbon dioxide, water and nitrogen contents were detected with a TCD. The carbon content is given in mass on the mass of the dry catalyst.

5.3 Procedures of the Catalytic Experiments

5.3.1 Hydroconversion of cis-Decalin and Perhydroindan

5.3.1.1 Experimental Set-Up of the High-Pressure Flow-Type Apparatus

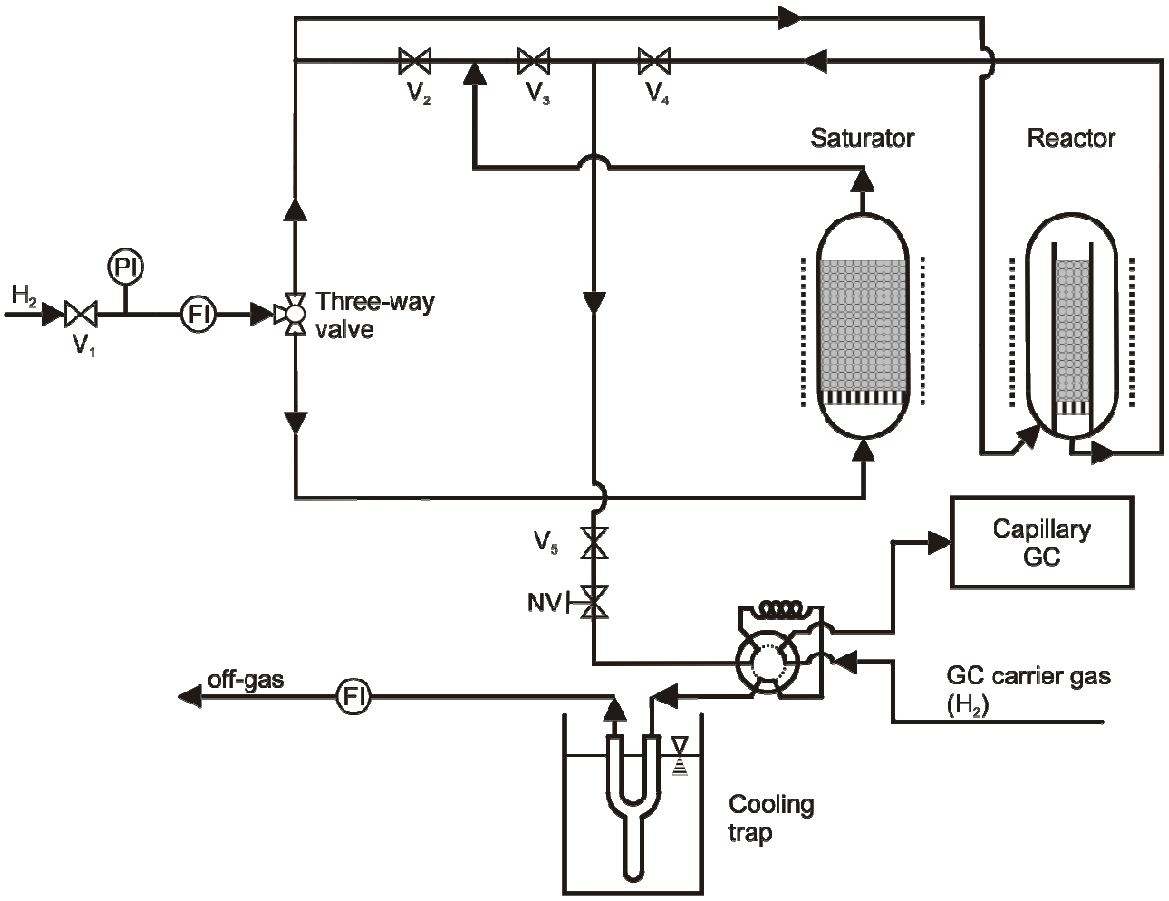

Figure 5.1: Scheme of the high-pressure flow-type apparatus used for the catalytic hydroconversion of cis-decalin (FI: flow indicator; GC: gas chromatograph; NV: needle valve; PI: pressure indicator; V: shut-off valve) [88].

All experiments for the catalytic hydroconversion of cis-decalin were conducted in a high-pressure flow-type apparatus which is schematically shown in Figure 5.1. The main parts of this apparatus were a saturator for generating the desired hydrogen/cis-decalin feed mixtures, a fixed-bed reactor and a heated sampling valve connected with a capillary gas chromatograph. All parts downstream of the saturator were kept at a sufficiently high temperature, such as to avoid condensation of hydrocarbon vapors. The saturator and the reactor were heated electrically and kept at constant temperature by temperature controllers. Valves V_2 to V_5 and the needle valve were mounted inside aluminum blocks to ensure a nearly homogeneous temperature.

Hydrogen was taken from a pressurized cylinder, and the pressure was reduced to the desired value of 5.2 MPa. By means of a three-way valve, the hydrogen flow could be routed either to the saturator or to the reactor. The saturator contained a fixed-bed of an inert solid (chromosorb P/AW, 0.25–0.60 mm) impregnated with liquid cis-decalin. On its way through the saturator the hydrogen gas is loaded with the vapor of cis-decalin. A thermocouple (not shown in Figure 5.1) was mounted axially in the fixed-bed to measure the temperature in the saturator. A more detailed description of the functionality of this kind of saturators may be found in Ref. [89]. After leaving the saturator the hydrogen/cis-decalin stream either flowed through valves V_3 and V_5 to the needle valve, where the gas was expanded before it passed through a heated 6-port-2-position gas sampling valve connected to a capillary gas chromatograph (see Section 5.4.1) or through valve V_2 to the reactor. A detailed drawing of the fixed-bed reactor is shown in Figure 5.2.

The feed gas entered the reactor at the bottom and was preheated to the reaction temperature while flowing upwards through an annulus. At the top, the flow direction was changed, and the feed mixture passed the catalyst bed downwards. Both the saturator and the reactor were fabricated from stainless steel and designed for a maximum temperature and pressure of 400 °C and 11.5 MPa, respectively. The product gas flowed through valves V_4 and V_5, the needle valve and through the heated 6-port-2-position gas sampling valve to the capillary gas chromatograph where the gas was analyzed. The exit gas from this sampling valve was routed to a cooling trap held at -10 °C. In the cooling trap, storable liquid product samples were gained. These samples were used for qualitative product identification only. All quantitative evaluations were based on analyses of gaseous samples inserted into the capillary gas chromatograph by actuating the 6-port valve.

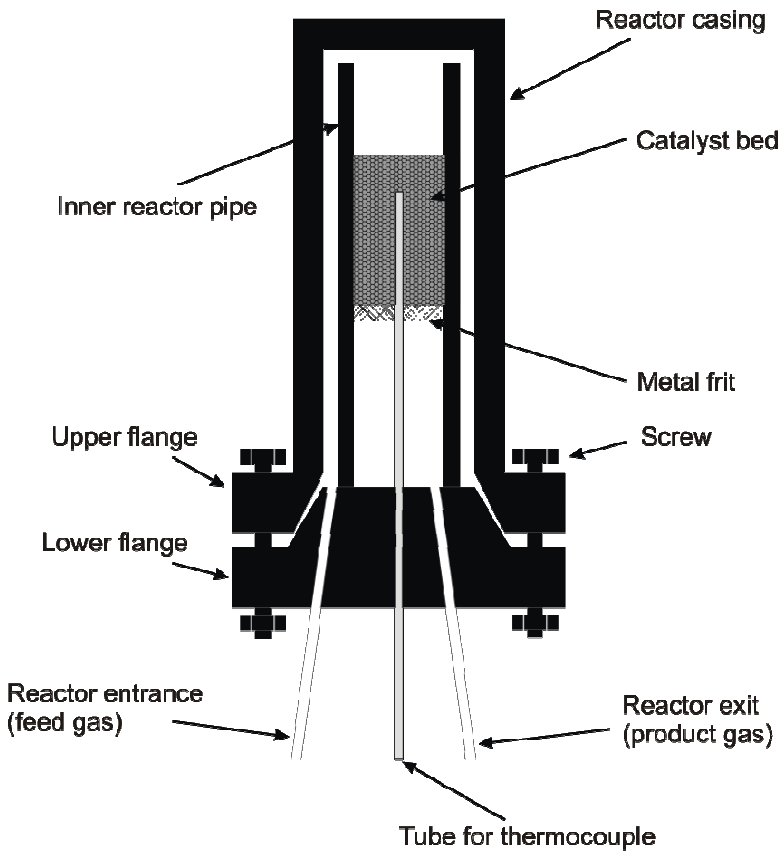

Figure 5.2: Detailed drawing of the fixed-bed reactor.

The apparatus shown in Figure 5.1 was used for various purposes:

(i) Reduction of the noble metal on the catalyst (Section 5.1.5): Three-way valve open in the direction towards the reactor; valves V_2 and V_3 closed, valves V_4 and V_5 open.

(ii) Calibrating the saturator temperature for the desired $n_{H_2}/n_{c\text{-}Dec}$ ratio: Three-way valve open in the direction towards the saturator; valves V_2 and V_4 closed, valves V_3 and V_5 open.

(iii) Catalytic conversion of gaseous hydrogen/cis-Decalin mixtures: Three-way valve open in the direction towards the saturator; valve V_3 closed, valves V_2, V_4 and V_5 open.

The hydroconversion of perhydroindan was performed in another, similarly constructed high-pressure flow-type apparatus. The functionality of all parts was identical but the architecture, especially of the fixed-bed reactor, differed slightly.

5.3.1.2 Conditions in the Catalytic Experiments with cis-Decalin

In all experiments with cis-decalin (purity 97.4 wt.-%; impurities: trans-decalin 0.9 wt.-%; 1.7 wt.-% other impurities, mainly skeletal isomers of decalin and hydrocarbons with more than 10 carbon atoms) the mass of dry catalyst was varied between 0.20 and 0.30 g corresponding to a bulk volume of 0.4 cm^3. The reaction temperature was varied between 200 and 380 °C. The total pressure was 5.2 MPa, while the cis-decalin partial pressure at the reactor entrance was 25 kPa corresponding to a saturator temperature of 135 °C. The *LHSV* assumed values between 0.3 and 0.4 h^{-1}. At each reaction temperature at least two on-line samples of the product were introduced into the capillary gas chromatography for analysis, one after 45 min time-on-stream and the other directly after the first analysis was finished, usually after 205 min time-on-stream. In case of experiments with a monofunctional acidic catalyst the second analysis was started after 275 min. For the evaluation of the experiments, usually the results of the second analysis were chosen.

5.3.1.3 Conditions in the Catalytic Experiments with Perhydroindan

In the experiments with perhydroindan (purity 96.7 wt.-%; cis-isomer 67.4 wt.-%; trans-isomer 29.3 wt.-%; impurities 3.3 wt.-%, mainly hydrocarbons with more than 9 carbon atoms and ring opening products) as feed hydrocarbon the mass of dry catalyst varied between 0.19 and 0.23 g corresponding to a bulk volume of 0.4 cm^3. The reaction temperature was varied between 209 and 371 °C. The total pressure was 5.2 MPa throughout, while the perhydroindan partial pressure at the reactor entrance was 31 kPa corresponding to a saturator temperature of 116 °C. An *LHSV* of 0.4 h^{-1} was applied. At each reaction temperature at least two gaseous on-line samples of the products were analyzed by capillary gas chromatography, normally one after 45 min time-on-stream and the other directly after the first analysis was finished, *i. e.* usually after 205 min time-on-stream. For the evaluation of the experiments, usually the results of the second analysis were chosen.

5.3.2 Isomerization of n-Decane

n-Decane was isomerized on the bifunctional catalyst 0.49Pt/$H_{0.55}$,$Na_{0.45}$-Y. These experiments were done at ambient pressure in a flow-type apparatus from glass, equipped again with a saturator and a fixed-bed reactor. 0.42 g of dry catalyst were used. For metal reduction, the catalyst was heated in a hydrogen flow of 98 $cm^3 \cdot min^{-1}$ from room temperature to 350 °C with a heating rate of 10 $K \cdot min^{-1}$. For the catalytic experiments, the reactor temperature, the total gas flow rate, the decane partial pressure and the hydrogen partial

pressure were 262 °C, 130 $cm^3 \cdot min^{-1}$, 0.9 kPa and 100 kPa, respectively (the saturator temperature amounted to 50 °C). The isomerization product was collected in a cooling trap at 0 °C.

5.4 Product Analysis by Capillary Gas Chromatography

5.4.1 On-line Gas Chromatography

Quantitative evaluation of the catalytic experiments was based on the GC analyses of the gaseous product samples introduced into the on-line capillary gas chromatograph via a gas sampling valve. For the analysis of the products of the cis-decalin hydroconversion an Agilent 7890 A instrument and a PC with an Agilent Chemstation software was used. Details of the analytical conditions are listed in Table 5.5.

Table 5.5: Conditions of the on-line analyses of the products of the cis-decalin hydroconversion by capillary gas chromatography.

Column	Petrocol DH 150
Stationary phase	Dimethyl polysiloxane
Length	150 m
Internal diameter	0.25 mm
Film thickness	1.0 µm
Temperature program	10 min at 35 °C; heating with 1 $K \cdot min^{-1}$ to 100 °C; heating with 0.5 $K \cdot min^{-1}$ to 140 °C; hold for 1 min
Carrier gas	Hydrogen
Pressure at column entrance	193 kPa
Flow through column	1.5 $cm^3 \cdot min^{-1}$
Injection	via gas sampling loop
Volume of sampling loop	250 µl
Split ratio	5 : 1
Injector temperature	250 °C
Detector	Flame ionization detector (FID)
Temperature	250 °C
$\dot{V}_{H_2}$ to FID	35 $cm^3 \cdot min^{-1}$
$\dot{V}_{air}$ to FID	350 $cm^3 \cdot min^{-1}$

Decalin hydroconversion on the monofunctional acidic catalysts also gave products with more than ten carbon atoms. For the analysis of these products, the temperature program of the GC was extended. After the standard program listed in Table 5.5 an additional temperature ramp of 1 $K \cdot min^{-1}$ to 200 °C and holding for 10 min were added.

For the analysis of the products of the perhydroindan hydroconversion a Hewlett-Packard HP 6890N instrument and a PC with an Agilent Chemstation software were used. The analytical conditions were similar to those listed in Table 5.5, except for $\dot{V}_{H_2}$ to the FID and $\dot{V}_{air}$ to the FID which were 40 $cm^3 \cdot min^{-1}$ 450 $cm^3 \cdot min^{-1}$, respectively.

5.4.2 Off-line Gas Chromatography / Mass Spectrometry

For ancillary off-line analyses of the liquid product samples collected in the cooling trap, a third gas chromatograph (Agilent 6890 N) coupled with a mass spectrometer (Agilent 5876 B inert XL MSD) was used. These analyses were aimed at qualitative peak assignment only. Listed in Table 5.6 are the conditions of the GC/MS analyses.

For analyzing the liquid samples of the decalin conversion on monofunctional acidic catalysts the temperature program was again modified. The end temperature of 180 °C was held for 240 min instead of 1 min in the standard program.

Table 5.6: Conditions of the ancillary analyses by capillary gas chromatography / mass spectrometry.

Column	Petrocol DH 150
Stationary phase	Dimethyl polysiloxane
Length	150 m
Internal diameter	0.25 mm
Film thickness	1.0 µm
Temperature program	10 min at 35 °C; heating with 1 $K \cdot min^{-1}$ to 100 °C; heating with 0.5 $K \cdot min^{-1}$ to 180 °C; hold for 1 min
Carrier gas	Helium
Pressure at column entrance	177 kPa
Flow through column	1.5 $cm^3 \cdot min^{-1}$
Injection	liquid, via syringe
Injected volume	0.1 µl
Split ratio	5 : 1
Injector temperature	250 °C
Detector	Flame ionization detector (FID)
Temperature	250 °C
$\dot{V}_{H_2}$ to FID	35 $cm^3 \cdot min^{-1}$
$\dot{V}_{air}$ to FID	450 $cm^3 \cdot min^{-1}$
Mass spectrometer	
Acceleration voltage	70 eV
Temperature of ion source	230 °C
Temperature of quadrupole analyzer	150 °C

5.5 Evaluation of the Catalytic Experiments

5.5.1 Terminology of the Reactions and Products

The hydroconversion of multi-ring naphthenes is a very complex reaction. Therefore it is useful to classify the possible reactions into different classes. During the hydroconversion of cis-decalin six different kinds of reactions can occur, which are summarized in Table 5.7. The designations of the different products and product groups used in this work are also listed. Trans-decalin was formed in a very fast reaction, but this stereoisomer of the feed was

treated as unconverted decalin. Whenever the mixture of cis- and trans-decalin is meant, the short designation Dec will be used.

Table 5.7: Reactions occurring in the catalytic conversion of cis-decalin (c-Dec) with hydrogen.

Reaction	**Products**	**Formula**	**Short Designation**
Isomerization	Isomers	$C_{10}H_{18}$	
	a) trans-decalin		tr-Dec
	b) skeletal isomers		sk-Isos
Ring opening	Ring opening products	$C_{10}H_{20}$	ROPs
	a) alkylcyclopentanes		
	b) alkylcyclohexanes		
Double ring opening	Open-chain decanes	$C_{10}H_{22}$	OCDs
Dehydrogenation	Dehydrogenated products		DHPs
	a) tetralin	$C_{10}H_{12}$	Ttr
	b) naphthalene	$C_{10}H_{8}$	Nap
Formation of higher hydrocarbons	Hydrocarbons with more than 10 carbon atoms		C_{11}+
Hydrocracking	Hydrocarbons with less than 10 carbon atoms		C_{9}-

For comparative purposes some catalysts were tested in the hydroconversion of perhydroindan. Analogous to the designation in the hydroconversion of cis-decalin, the reactions in the hydroconversion of perhydroindan were classified into six different classes which are listed in Table 5.8 along with the corresponding product groups.

Table 5.8: Reactions occurring in the catalytic conversion of perhydroindan (PHI) with hydrogen.

Reaction	**Products**	**Formula**	**Short Designation**
Isomerization	Skeletal isomers	C_9H_{16}	sk-Isos
Ring opening	Ring opening products	C_9H_{18}	ROPs
	a) alkylcyclopentanes		5-ring ROPs
	b) alkylcyclohexanes		6-ring ROPs
Double ring opening	Open-chain nonanes	C_9H_{20}	OCNs
Dehydrogenation	Dehydrogenated products		DHPs
	a) indan	C_9H_{10}	
	b) indene	C_9H_8	
Formation of higher hydrocarbons	Hydrocarbons with more than 9 carbon atoms		C_{10}+
Hydrocracking	Hydrocarbons with less than 9 carbon atoms		C_8-

5.5.2 Assignment of the GC Signals

Assignment of the peaks in a chromatogram was mainly based on GC/MS analyses of the liquid products in the cooling trap. Even though it was not in all cases possible to assign to each signal a specific hydrocarbon, it was possible to identify the molar mass of the compound. With this molar mass the products could be assigned to one of the different product classes mentioned in Tables 5.7 and 5.8.

In addition, pure hydrocarbons were co-injected with the liquid product samples from the catalytic experiments, whenever such hydrocarbons were commercially available. Furthermore, for a safe assignment of the peaks of OCDs, n-decane was isomerized in separate experiments on a Pt/H,Na-Y zeolite (see Section 5.3.2), and the mixture of iso-decanes thereby generated was co-injected with the liquid products from decalin hydroconversion. The analogous procedure was done with n-nonane to ensure the correct assignment of the peaks of OCNs formed in the hydroconversion of perhydroindan.

In the Appendix 12.1 the current peak assignment is given.

5.5.3 Conversion, Yields and Selectivities

The general definitions of the conversion $X_{c\text{-}Dec}$, the yield of products Y_j and the selectivity of products S_j in a continuously operated flow-type reactor are given in Eqs. (5.2) to (5.4).

$$X_{c-Dec} = \frac{(\dot{n}_{c-Dec})_{in} - (\dot{n}_{c-Dec})_{out}}{(\dot{n}_{c-Dec})_{in}} \tag{5.2}$$

$$Y_j = \frac{(\dot{n}_j)_{out} - (\dot{n}_j)_{in}}{(\dot{n}_{c\text{-}Dec})_{in}} \cdot \frac{|\nu_{c\text{-}Dec}|}{\nu_j} \tag{5.3}$$

$$S_j = \frac{(\dot{n}_j)_{out} - (\dot{n}_j)_{in}}{(\dot{n}_{c\text{-}Dec})_{in} - (\dot{n}_{c\text{-}Dec})_{out}} \cdot \frac{|\nu_{c\text{-}Dec}|}{\nu_j} \tag{5.4}$$

While $(\dot{n}_{c-Dec})_{out}$ can be directly calculated from the area of the cis-decalin peak $A_{c\text{-}Dec}$ in the chromatogram (see Appendix 12.2.2.2), there are three options for evaluating $(\dot{n}_{c-Dec})_{in}$ which are presented in Appendix 12.2.2.3. One method is to analyze several times the hydrogen/decalin mixture generated in the saturator, without going through the reactor, with the GC and taking the arithmetic mean of the cis-decalin peak area for calculating $(\dot{n}_{c-Dec})_{in}$. Another simplified method is to assume that the sum of the masses of all product hydrocarbons j is not too different from the mass of cis-decalin converted. Since not too much hydrocracking to C_9- occurs this method is relatively accurate. For the evaluation of the catalytic data in this work method 3 was used, which takes care of the compound-specific FID correction factors *f* and the stoichiometric factors of all products formed. The assumptions of all three methods and the calculations of the conversion, the yields and the selectivities for all three methods are described in detail for the conversion of cis-decalin in Appendix 12.2.2.3.

In all catalytic experiments with cis-decalin, trans-decalin which forms rapidly from cis-decalin was not considered as a product, *i. e.*, cis- and trans-decalin were lumped and treated as reactants designated by Dec. The final equations used for the calculations of X_{Dec}, Y_j and S_j with method 3 are given in Eqs. (5.5) to (5.7).

$$X_{Dec} = \frac{\sum_j \frac{|\nu_{Dec}|}{\nu_j} \cdot \frac{M_{Dec}}{M_j} \cdot f_j \cdot A_j}{f_{Dec} \cdot A_{Dec} + \sum_j \frac{|\nu_{Dec}|}{\nu_j} \cdot \frac{M_{Dec}}{M_j} \cdot f_j \cdot A_j} \tag{5.5}$$

$$Y_j = \frac{f_j \cdot A_j}{\sum_j \frac{|\nu_{Dec}|}{\nu_j} \cdot \frac{M_{Dec}}{M_j} \cdot f_j \cdot A_j + f_{Dec} \cdot A_{Dec}} \cdot \frac{|\nu_{Dec}|}{\nu_j} \cdot \frac{M_{Dec}}{M_j} \tag{5.6}$$

$$S_j = \frac{f_j \cdot A_j}{\sum_j \frac{|\nu_{Dec}|}{\nu_j} \cdot \frac{M_{Dec}}{M_j} \cdot f_j \cdot A_j} \cdot \frac{|\nu_{Dec}|}{\nu_j} \cdot \frac{M_{Dec}}{M_j} \tag{5.7}$$

Particularly desired products in the hydroconversion of decalin are the ROPs and OCDs. Conversely, the hydrocracked products (C_9-) are particularly undesired. Nevertheless, in this work much emphasis on their detailed analysis was placed hoping that their nature and quantitative distribution could furnish valuable mechanistic information. For a quantitative discussion, the modified hydrocracking selectivity will be used which is defined as the molar amount of hydrocarbons with j carbon atoms formed (j = 1 to 9) divided by the molar amount of decalin converted into hydrocracked products (Eq. (5.8)).

$$S_j^* = \frac{(\dot{n}_j)_{out}}{(\dot{n}_{Dec})_{converted\ to\ C_{9-}}} = \frac{f_j \cdot A_j}{\sum_j \frac{|\nu_{Dec}|}{\nu_j} \cdot \frac{M_{Dec}}{M_j} \cdot f_j \cdot A_j} \cdot \frac{M_{Dec}}{M_j} \tag{5.8}$$

5.5.4 Liquid Hourly Space Velocity

The liquid hourly space velocity (*LHSV)* is the ratio of the hourly volume of liquid decalin at room temperature and 1 bar to the bulk volume of the catalyst bed (see Eq. (5.9)). In all catalytic experiments with cis-decalin and perhydroindan only the reaction temperature was varied, while the *LHSV* was kept constant around 0.4 h^{-1}. The bulk volume of catalyst in all experiments was 0.4 cm^3. The volume of the liquid decalin can be calculated from the hourly mass flux and the density of liquid cis-decalin. The hourly mass flux was determined for each experiment. The hydrogen/cis-decalin mixture generated in the saturator was condensed in the cooling trap, and the mass of the liquid collected during one hour was determined at constant hydrogen flow and saturator temperature. This value was around 0.14 $g \cdot h^{-1}$.

$$LHSV = \frac{\dot{V}_{Dec,\ liquid,\ RT}}{V_{bulk,\ cat}} \tag{5.9}$$

6 Characterization of the Catalyst Precursors and Catalysts

The strength and concentration of Brønsted acid sites of the catalysts are important factors in the hydrocracking of hydrocarbons. In this work mostly catalysts with a low concentration of Brønsted acid sites were deliberately used. In most cases just the Brønsted acid sites co-generated during the reduction of the noble metals iridium or platinum were present. This low concentration was unfortunately below the detection limit of IR spectroscopy with pyridine as a probe molecule. Other characterization methods were considered, but they could not be implemented with the desired reliability up till the end of this work. Therefore, the changes in the strength and concentration of Brønsted acid sites occurring upon chemically modifying the catalysts are mainly based on the knowledge of the current literature. Based on the next nearest neighbor (NNN) theory (see Section 4.1) the strength of Brønsted acid sites should increase from LSX over X to Y, and it should be even higher in dealuminated Y zeolites. An increase in the strength of Brønsted acid sites in Na,H-Y zeolites upon a more severe dealumination was confirmed by Beaumont and Barthomeuf [90]. The concentration of Brønsted acid sites in La,Na-X and La,Na-Y zeolites depends on the degree of lanthanum exchange, and the strength is higher in La,Na-Y than in La,Na-X (see Section 4.2.1). In addition, the nature of the charge-compensating cations has an influence on the strength of the Brønsted acid sites which decreases, under otherwise equal properties, in the following order: Li,H-Y > Na,H-Y > K,H-Y > Rb,H-Y > Cs,H-Y (see Section 4.1).

6.1 Zeolite Na-LSX

The n_{Si} / n_{Al} ratio of the as-synthesized LSX zeolite as determined by ICP-OES amounted to 1.01. The n_{Si} / n_{Al} ratio of the LSX lattice determined by ^{29}Si MAS NMR (see Section 5.2.3) is in agreement with the one obtained by ICP-OES. 97 % of the cation sites are occupied by sodium atoms, the occupancy of the remaining 3 % could not be identified. A powder X-ray diffractogram of the Na-LSX zeolite is depicted in Figure 6.1a. It reveals that the material is phase-pure and possesses a high degree of crystallinity. No reflexes of the most likely impurity, *i. e.* zeolite A, are visible. In Figure 6.1b the enlarged diffractograms of the zeolites LSX, X and Y are shown at $2\theta \approx 6°$. It is clearly seen that, with increasing n_{Si} / n_{Al} ratio, the peak is shifted to higher 2θ values. This effect is due to a decreasing lattice constant from zeolite LSX to zeolite Y. The Al-O bond length is higher than that of Si-O. With increasing n_{Si} / n_{Al} ratio the amount of Al-O bonds is lower and so the lattice constant decreases, resulting in the observed shift of 2θ. At higher 2θ values the shift between the signal of LSX, X and Y is increasing.

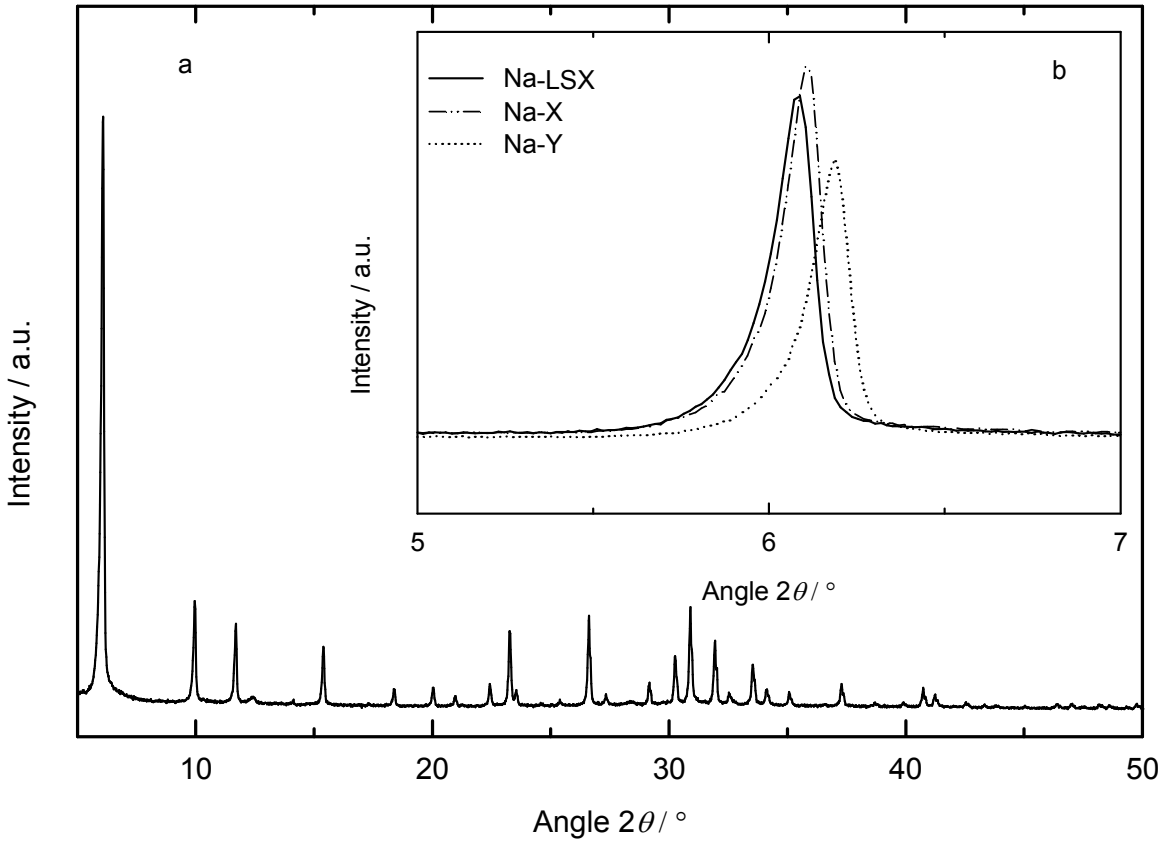

Figure 6.1: X-ray diffractograms of a) zeolite Na-LSX and b) of Na-LSX, Na-X and Na-Y at around 2θ = 6°.

The ^{27}Al MAS NMR spectrum of Na-LSX (Figure 6.2) possesses a signal at *ca*. 60 ppm which originates from tetrahedrally coordinated aluminum [87]. There is no signal at 0 ppm, which would have originated from octahedrally coordinated extra-framework aluminum [87]. These extra-framework aluminum species would indicate lattice defects of the zeolite, hence not all aluminum atoms detected by ICP-OES would be incorporated in the zeolite lattice.

In Figure 6.3 the SEM image of zeolite Na-LSX is shown. The sample possesses spherical crystals typical for LSX [91] with average diameters between 2 and 3 µm. No impurities are visible.

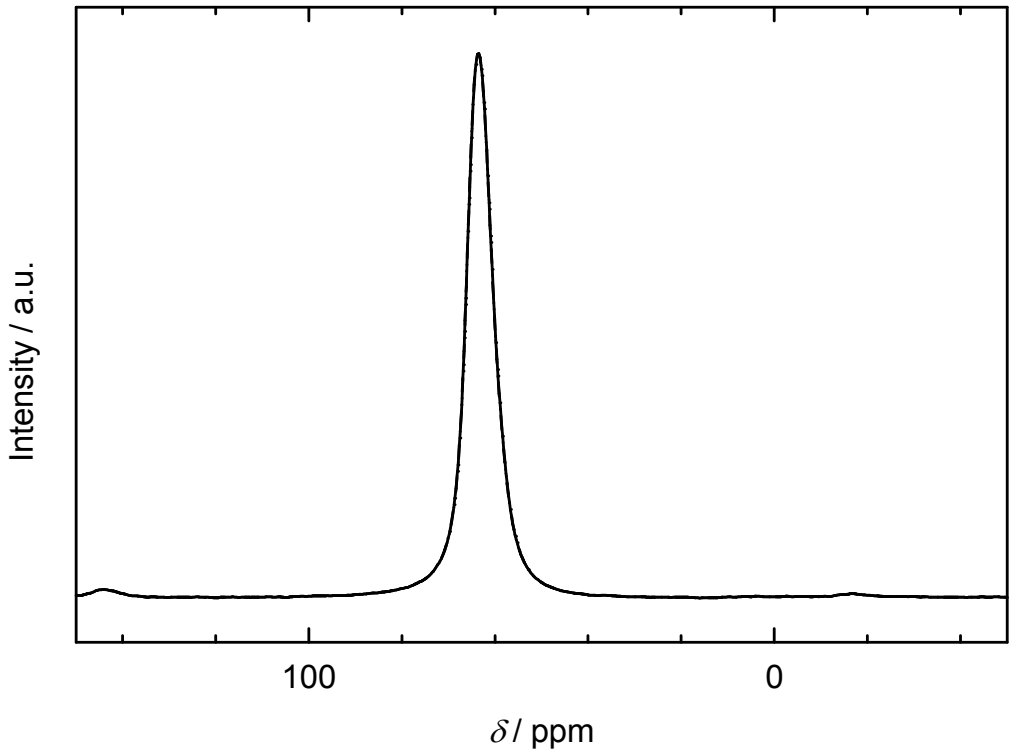

Figure 6.2: ^{27}Al MAS NMR spectrum of Na-LSX. The signal at 60 ppm originates from tetrahedrally coordinated aluminum.

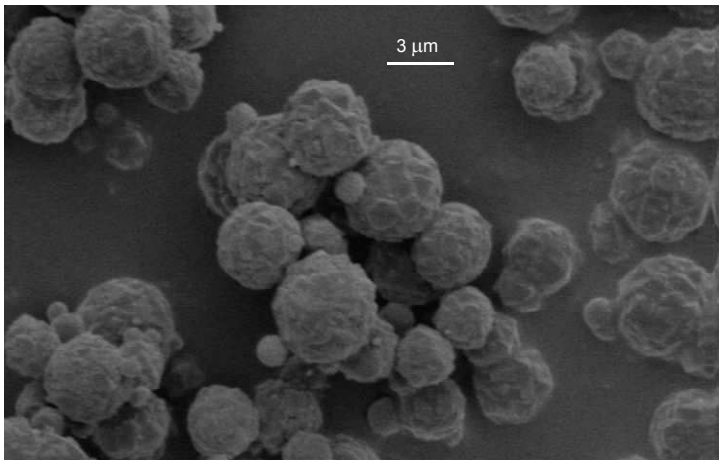

Figure 6.3: SEM image of zeolite Na-LSX.

The very high aluminum content of Na-LSX renders the zeolite sensitive towards acids. During the reduction of the noble metals Pt^{2+} and Ir^{2+}, two Brønsted acid sites per noble metal ion are formed. To ensure that the obtained catalytic data with decalin are not generated by amorphous SiO_2 and Al_2O_3, X-ray diffractograms were measured after the catalytic experiments. With both metal-containing catalysts the typical reflexes of zeolite LSX still exist, but their intensities are lower than those obtained on the as-synthesized Na-LSX zeolite. This difference could originate from lattice defects caused by the generation of

Brønsted acid sites during the reduction of the metal. Experiments with $[Pt(NH_3)_4]$,NH_4-Y zeolites calcined at 350 °C showed that, after the hydration of Pt/H-Y in humid air, the zeolite lattice, depending on the degree of ammonium exchange, is partially or nearly fully destroyed, whereas if the zeolite is stored in a water free surrounding, the structure remains intact [92]. The decrease in the intensities of the reflexes after the hydroconversion of decalin was observed on all metal-containing faujasite catalysts, but it was more pronounced on the catalysts with a low n_{Si} / n_{Al} ratio.

6.2 X Zeolites

6.2.1 Zeolite Na-X

All X zeolites used in this work were based on zeolite Na-X purchased from Strem Chemicals, lot No. 14 247S. The n_{Si} / n_{Al} ratio as determined by ICP-OES and ^{29}Si MAS NMR amounted to 1.21. 92 % of the cation sites are occupied by sodium atoms, the remaining 8 % could not be identified. The powder X-ray diffractogram of the Na-X zeolite (see Section 6.2.2, Figure 6.5) is similar to the one of Na-LSX but shifted to higher 2θ values as shown in Figure 6.1. The material is phase-pure and possesses a high degree of crystallinity.

The ^{27}Al MAS NMR spectrum of Na-X (not shown) consists of a signal at *ca*. 60 ppm which originates from tetrahedrally coordinated aluminum. No signal at 0 ppm, which would have originated from octahedrally coordinated aluminum, was detected.

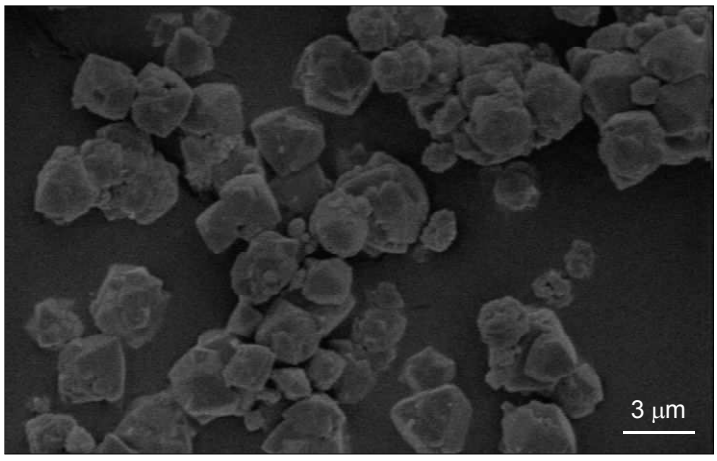

Figure 6.4: SEM image of zeolite Na-X.

Figure 6.4 shows the SEM image of Na-X. The zeolite consists of octahedral crystals with a diameter of 2-3 µm. All results show that the Na-X zeolite purchased from Strem Chemicals is pure and possesses a high crystallinity.

6.2.2 La-X Zeolites

The Na-X zeolite was ion-exchanged with an aqueous solution of lanthanum nitrate. The ion exchange is quantitative up to an exchange degree of 72 %. A higher exchange degree is only possible after calcination and an additional ion exchange. A powder X-ray diffractogram of $Na_{0.43}La_{0.17}H_{0.06}$-X zeolite before and after calcination as a representative of the La-X zeolites is depicted in Figure 6.5 in comparison to the diffractogram of Na-X.

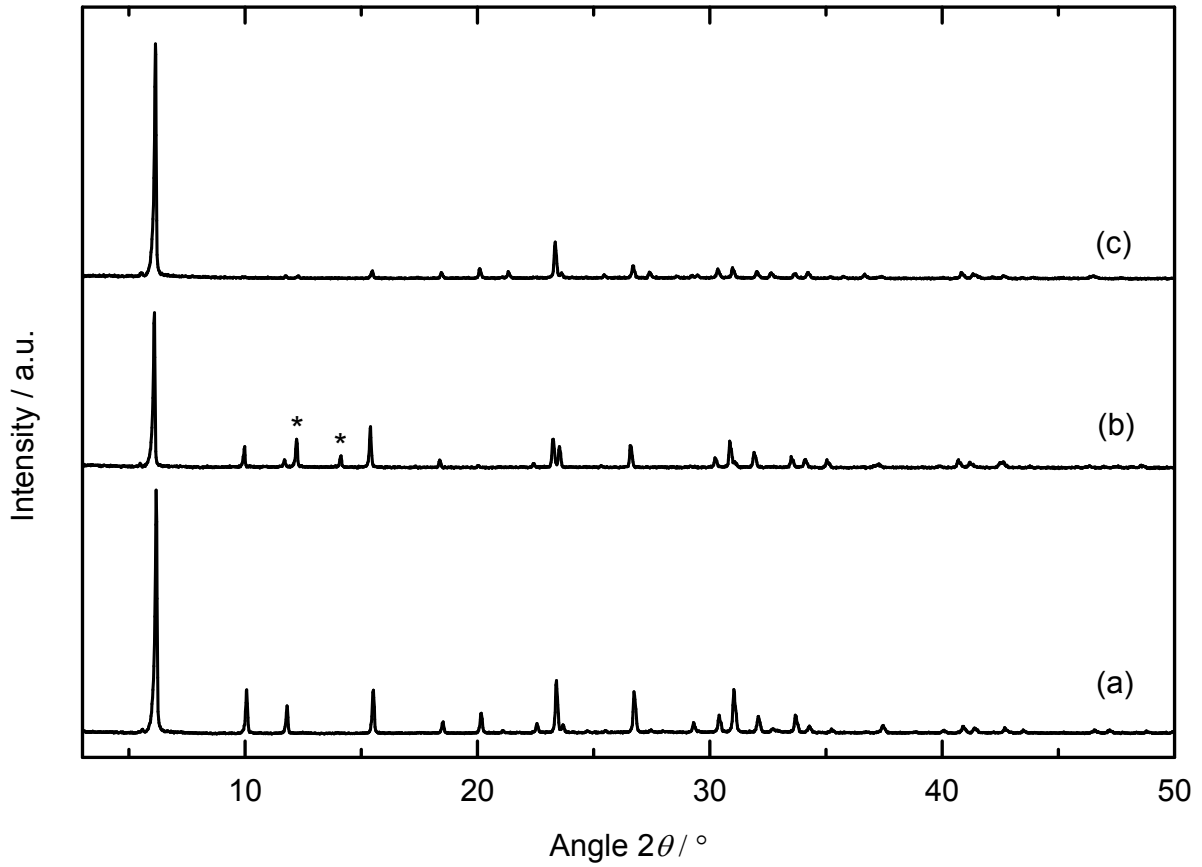

Figure 6.5: X-ray diffractogram of zeolite Na-X (a), $Na_{0.43}La_{0.17}H_{0.06}$-X (b) before and (c) after calcination. Asterisks denote newly generated peaks after the ion exchange with lanthanum.

After ion exchange with lanthanum the intensities of all reflexes decrease, and two additional reflexes at 12.2° and 14.1° emerge, presumably caused by the lanthanum ions. After

calcination and hence migration of the lanthanum ions into the smaller cages, a general decrease in the intensity of the peaks, except for that at 6.1° which increased instead, could be observed, as reported for La,Na-Y zeolite [93]. These tendencies are even stronger with a higher exchange degree in $La_{0.30},H_{0.06},Na_{0.04}$-X (not shown).

In all lanthanum zeolites 6-7 % of all cations are protons. They result from the fact that not all cation positions in Na-X could be exchanged with sodium (Section 6.2.1). By heating of the zeolite samples Brønsted acid sites are generated via the Hirschler-Plank mechanism. The concentration of Brønsted acid sites depends on the temperature [27]. The concentration cannot be determined by ICP-OES.

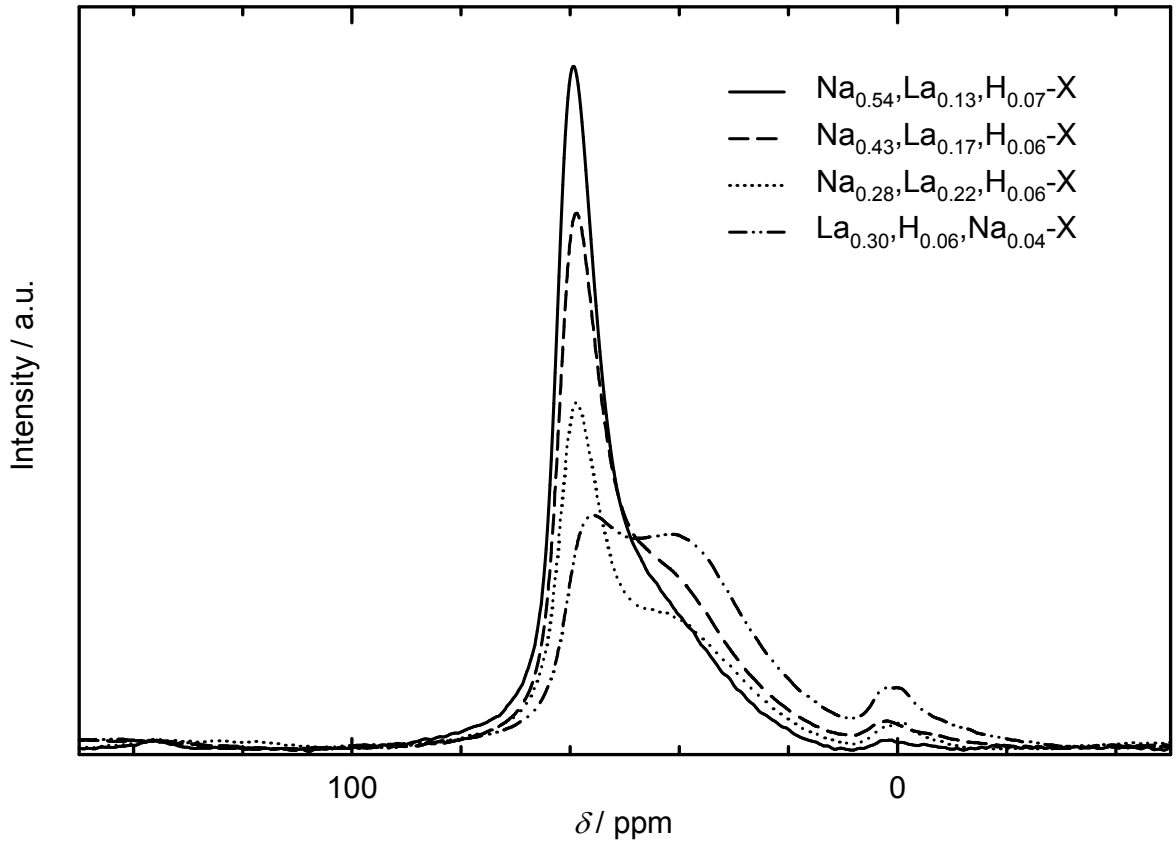

Figure 6.6: ^{27}Al MAS NMR spectra of La,Na-X with different exchange degrees. The signals at δ = 0 ppm and 60 ppm originate, respectively, from octahedrally and tetrahedrally coordinated aluminum. The signal at δ = 40 ppm is due to framework aluminum atoms in the vicinity of lanthanum cations.

The ^{27}Al MAS NMR spectra of the La,Na-X samples are shown in Figure 6.6. The spectra show small damages of the zeolite structures indicated by the signal at δ = 0 ppm which increases with increasing lanthanum exchange degree. The lanthanum ions stabilize the H-Y

zeolite but cannot completely avoid some lattice damages due to the generation of Brønsted acid sites. In addition to the signal at δ = 60 ppm which originates from tetrahedrally coordinated aluminum a broad signal at *ca*. 40 ppm is observed. This signal is due to framework aluminum atoms in the vicinity of lanthanum cations. In case of $Na_{0.43}$,$La_{0.17}$,$H_{0.06}$-X the intensity of the signal at 40 ppm is approximately 30 % of the intensity of the signal at 60 ppm. In case of $La_{0.30}$,$H_{0.06}$,$Na_{0.04}$-X both intensities are nearly equal. The intensity of the signal at 40 ppm in comparison to the intensity of the signal at 60 ppm increases with increasing lanthanum exchange degree which is in line with other observations on La,Na-X zeolites [27].

6.3 Y Zeolites

6.3.1 Zeolite Na-Y

All Y Zeolites prepared in this work are based on zeolite Na-Y purchased from Strem Chemicals, lot No. 148 960. The n_{Si} / n_{Al} ratio as determined by ICP-OES amounted to 2.41. 96 % of the cation sites are occupied by sodium atoms, the remaining 4 % could not be identified. The powder X-ray diffractogram of the Na-Y zeolite (Section 6.3.4, Figure 6.11) is similar to the diffractograms of Na-LSX and Na-X but shifted to higher 2θ values as shown in Figure 6.1. The material has no crystalline impurities and possesses a high degree of crystallinity.

The ^{27}Al MAS NMR spectrum of Na-Y (not shown) consists of one signal at *ca*. 60 ppm which originates from tetrahedrally coordinated aluminum. No signal at 0 ppm was detected. In Figure 6.7 the SEM image of zeolite Na-Y is shown. The sample consists of crystals with a diameter between 0.5 and 1.5 µm.

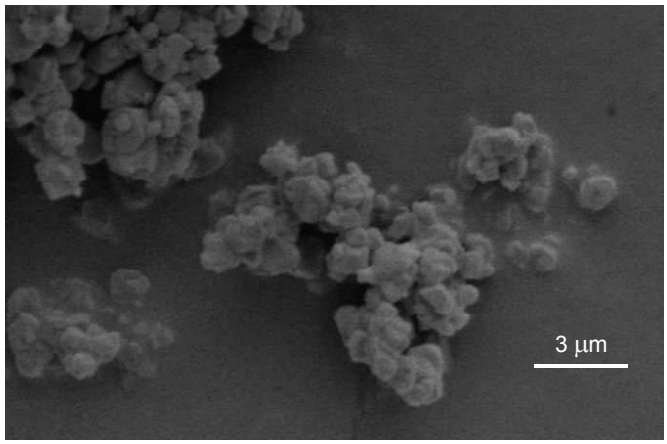

Figure 6.7: SEM image of zeolite Na-Y.

6.3.2 M-Y Zeolites (M = Li, K, Rb, Cs)

Zeolite Na-Y was ion-exchanged with an aqueous solution of the respective alkali metal salt. The ion exchange is quantitative for potassium. With lithium an exchange degree of only 74 % was reached after five ion exchange steps which perhaps reflects its low selectivity [94]. With rubidium and cesium an exchange degree of 83 and 86 % was reached, respectively. This was only possible with calcination steps after each ion exchange [85].

The powder XRDs of the four zeolites are shown in Figure 6.8. The intensities of the peaks decrease from lithium (a) to cesium (d). This could be caused by a lower crystallinity of the materials, a disorder in the lattice or a higher scattering factor, especially in case of rubidium and cesium. The diffractogram of Li,Na,H-Y is completely equal to the one of Na-Y. The diffractograms of the other three zeolites show the characteristic peaks of Na-Y but with some small additional peaks like the one at 12.4°.

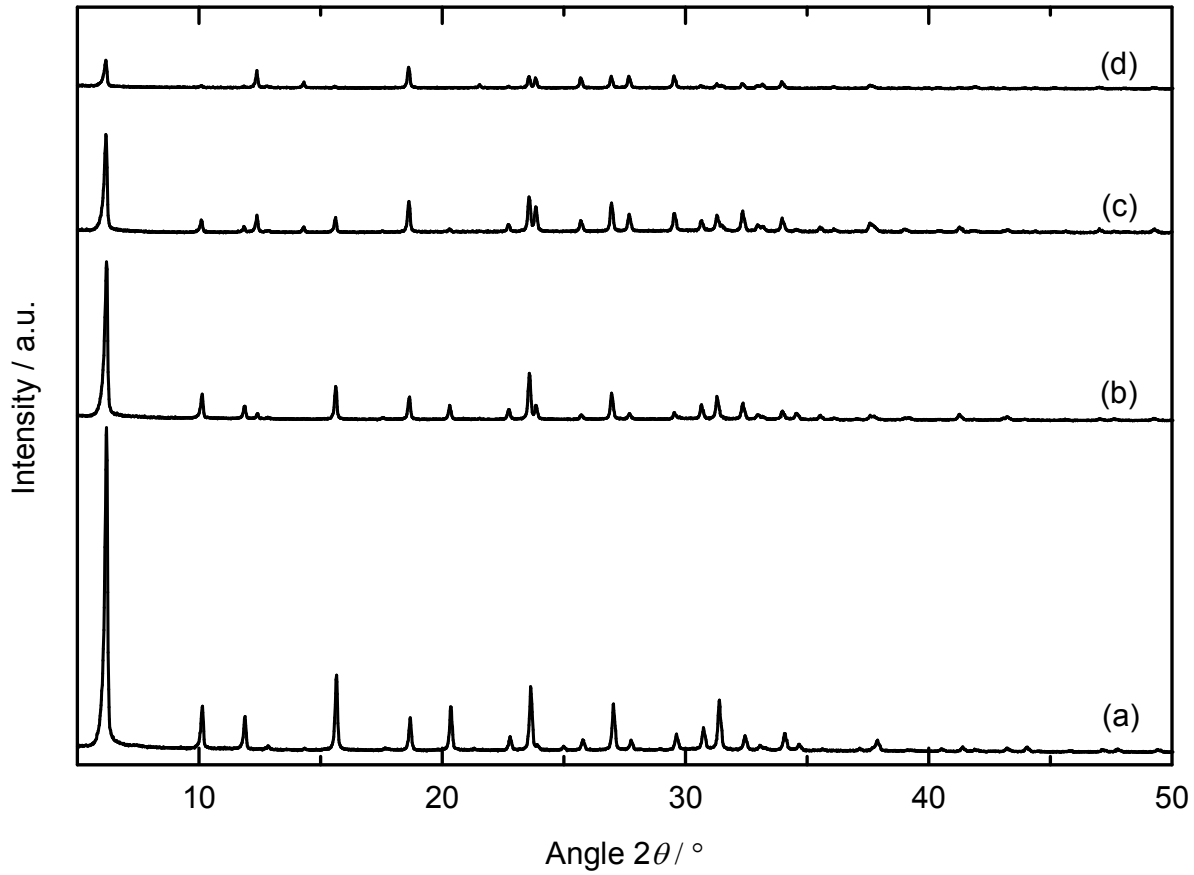

Figure 6.8 X-ray diffractogram of (a) $Li_{0.74}Na_{0.21}H_{0.05}$-Y, (b) $K_{0.95}H_{0.05}$-Y, (c) $Rb_{0.83}Na_{0.17}$-Y and (d) $Cs_{0.86}Na_{0.14}$-Y.

The ^{27}Al MAS NMR spectra of the four zeolites possess only one peak at *ca*. 60 ppm which is caused by tetrahedrally coordinated aluminum in the framework of the zeolite. No signals of extra-framework aluminum could be observed. As expected, the ion exchange with the different alkali ions caused no damage in the zeolite lattice.

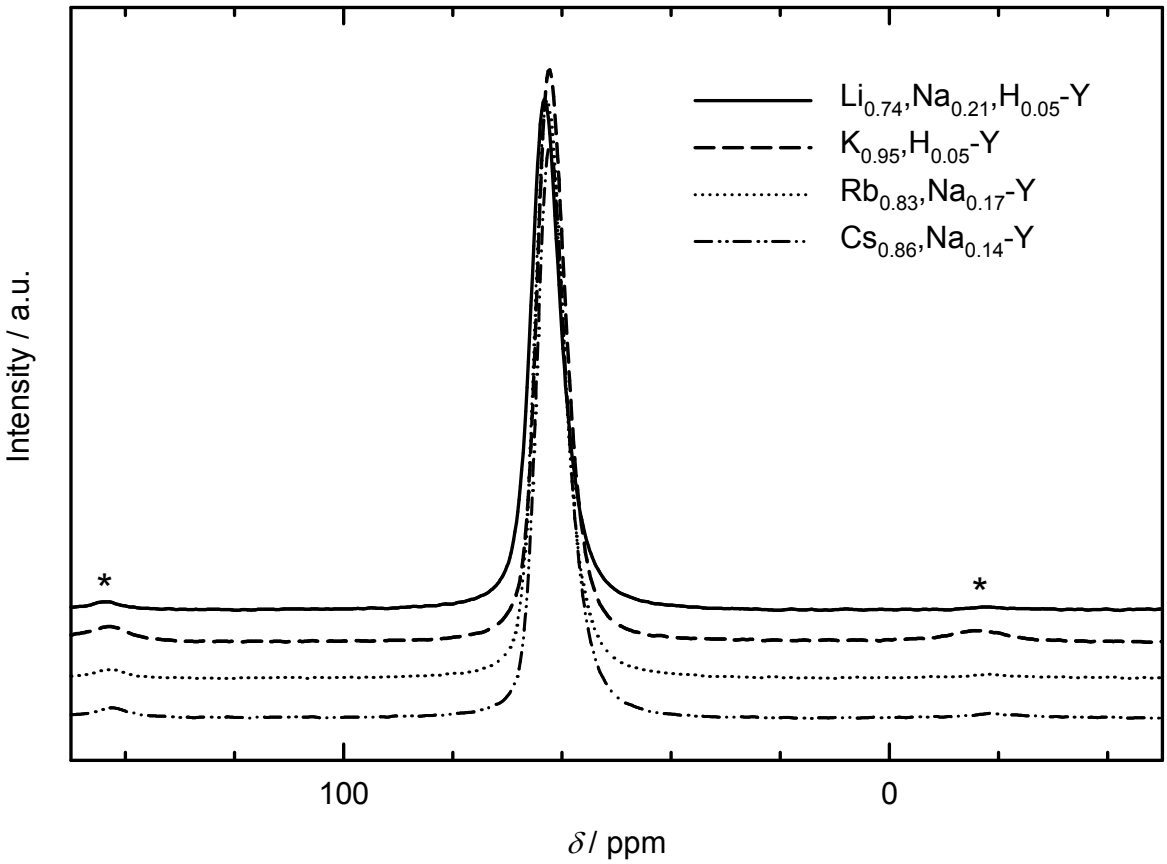

Figure 6.9: ^{27}Al MAS NMR spectrum of the alkali-Y zeolites. The signals at 60 ppm originate from tetrahedrally coordinated aluminum. Asterisks denote spinning side bands.

The zeolites show some peculiarities concerning their water content. They were stored in a desiccator over a saturated aqueous solution of calcium nitrate for at least 24 h before the precise water content was measured (see Section 5.2.2). The water content of the zeolites decreases from the smallest alkali cation Li^+ to the biggest Cs^+. $Li_{0.74}$,$Na_{0.21}$,$H_{0.05}$-Y has a water content of 27.1%, Na-Y of 24.8 %, $K_{0.95}$,$H_{0.05}$-Y of 21.4 %, $Rb_{0.83}$,$Na_{0.17}$-Y of 18.1 % and $Cs_{0.86}$,$Na_{0.14}$-Y of 15.4 %. The decreasing water content correlates with the increasing cation radius. The water level can be largely attributed to the diminished available space caused by large cations [94].

6.3.3 La-Y Zeolites

The Na-Y zeolite was ion-exchanged with an aqueous solution of lanthanum nitrate. The ion exchange is quantitative in all three cases. The X-ray diffractograms of the three Na,La-Y samples (not shown) show the same reflexes like Na-Y (see Section 6.3.4, Figure 6.11). As observed on La-X zeolites (see Section 6.2.2) the intensities of all reflexes decrease after ion exchange with lanthanum. After calcination and hence migration of the lanthanum ions into the small cages, a general decrease in the intensity of the peaks, except for that at 6.1° which increased instead, could be observed, as reported in the literature [93]. No additional signals at 12.2° and 14.1° after ion exchange as in the case of Na,La-X zeolites were observed.

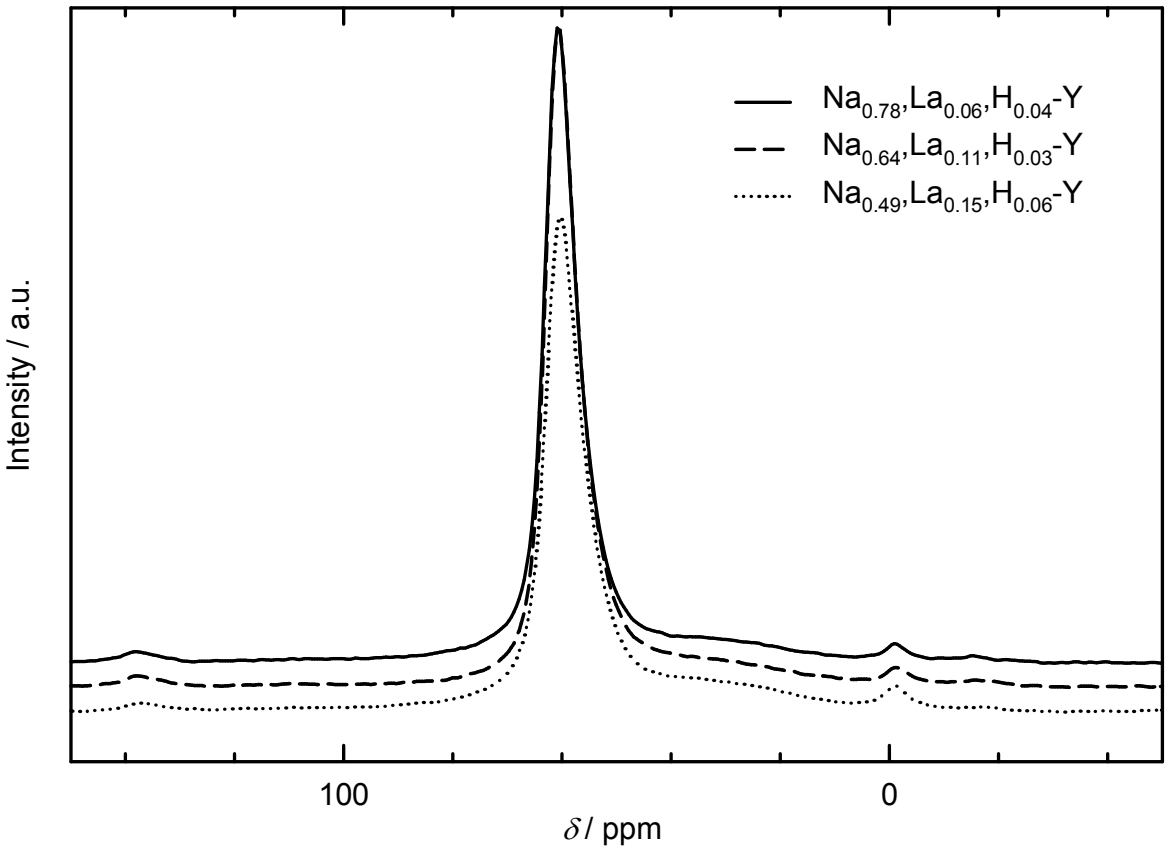

Figure 6.10: ^{27}Al MAS NMR spectra of Na,La-Y with different exchange degrees. The signals at δ = 0 ppm and 60 ppm originate, respectively, from octahedrally and tetrahedrally coordinated aluminum. The extremely weak signal at δ = 40 ppm is due to framework aluminum atoms in the vicinity of lanthanum cations.

The ^{27}Al MAS NMR spectra of all Na,La-Y samples are shown in Figure 6.10. The spectra show very small damages of the zeolite structures indicated by the signal at δ = 0 ppm. In

addition to the signal at δ = 60 ppm which originates from tetrahedrally coordinated aluminum a very weak and broad signal at *ca*. 40 ppm is observed which nearly disappears in the baseline. This signal is due to framework aluminum atoms in the vicinity of lanthanum cations. In contrast to the Na,La-X samples this signal at 40 ppm has a very low intensity which is in accordance with the literature [27], but no explanation for the weaker signal in Na,La-Y zeolites was given in this reference.

The amount of Brønsted acid sites generated by the Hirschler-Plank mechanism depends on the temperature [27] and cannot be quantified by ICP-OES. Hence, more Brønsted acid sites are present in the zeolites than indicated in their formulae.

6.3.4 Dealuminated Y Zeolites

The dealuminated Y zeolites were prepared by ion exchange with an ammonium salt and then by dealumination with different amounts of $(NH_4)_2[SiF_6]$. After this treatment the zeolite was filtered and washed with boiling water. Powder X-ray diffractograms of the Na-Y zeolite and the resulting zeolite after one washing treatment are depicted in Figure 6.11a and b. The material possesses a high degree of crystallinity, but five new signals in comparison to zeolite Na-Y (Figure 6.11a) can be observed, marked with an asterisk. These signals are due to remaining $(NH_4)_2[SiF_6]$. Traces of this compound can be responsible for a loss in crystallinity after thermal treatment due to the formation of HF. Four to five washing processes are reported to be needed to eliminate this compound [95]. The powder X-ray diffractogram of the product obtained after five washing steps is depicted in Figure 6.11c. Indeed, no reflexes of $(NH_4)_2[SiF_6]$ could be observed any more. To ensure that no undetectable amounts of $(NH_4)_2[SiF_6]$ were left which could damage the zeolite, the samples were heated up to 400 °C before all other characterization techniques were applied.

Again, as in the case of LSX, X and Y (see Section 6.1, Figure 6.1), the reflexes shift to higher 2θ values with increasing n_{Si} / n_{Al} ratio. In Figure 6.12 the shift of the signal around 2θ = 6° is shown. Between the faujasites with n_{Si} / n_{Al} of 4.11 and 5.49 no shift can be observed presumably due to the lower change of the aluminum content.

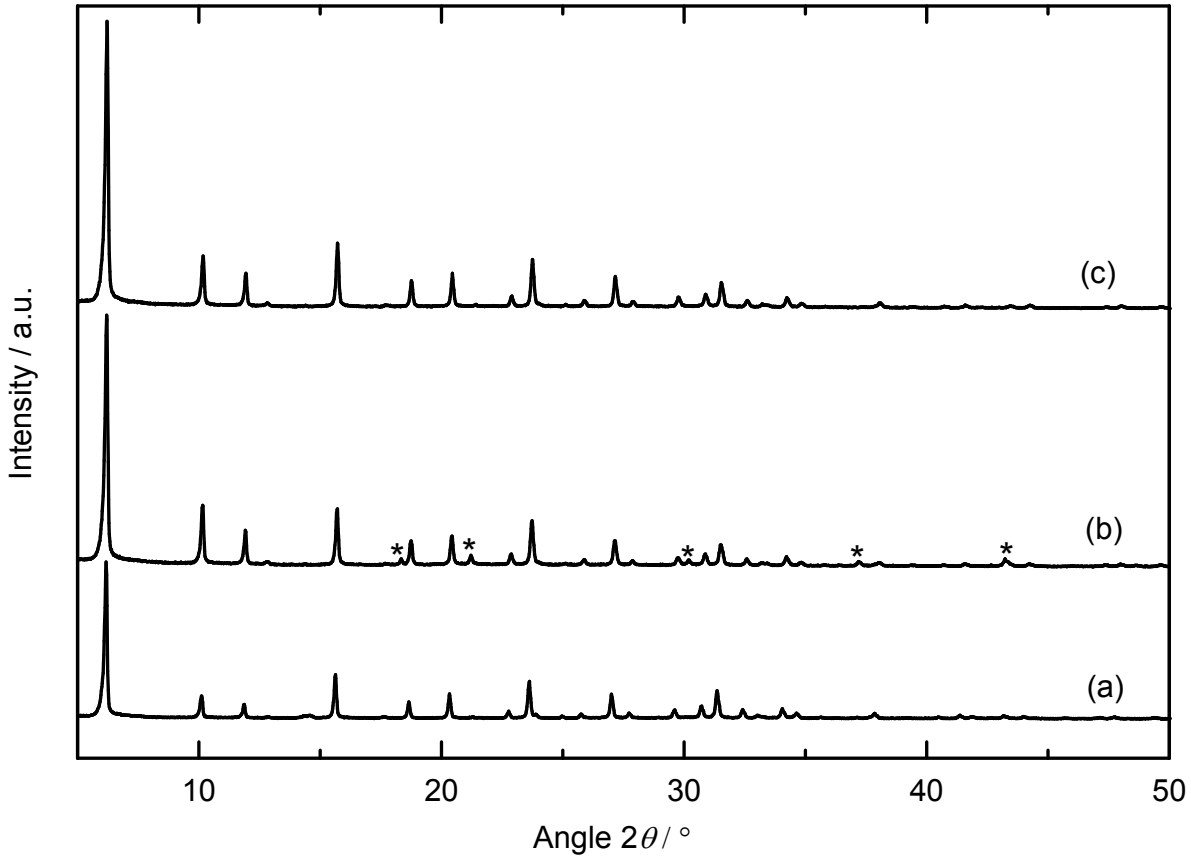

Figure 6.11: X-ray diffractograms of (a) Na-Y and NH_4-Y-4.11 (b) after dealumination and one washing step and (c) after dealumination and five washing steps. The asterisks indicate the signals of $(NH_4)_2[SiF_6]$.

The ^{27}Al MAS NMR spectra of the zeolites (not shown) consist only of signals at *ca*. 60 ppm which originate from tetrahedrally coordinated aluminum. No signals at 0 ppm, which would have originated from octahedrally coordinated aluminum, were detected.

The n_{Si} / n_{Al} ratios of the zeolites calculated from the ^{29}Si MAS NMR spectra (see Section 5.2.3) are listed in Table 6.1. They are in good agreement with the absolute values determined by ICP-OES. Amorphous silica species could be observed. Therefore the calculated ratios $(n_{Si} / n_{Al})_{ICP\text{-}OES}$ and $(n_{Si} / n_{Al})_{NMR}$ are not the real n_{Si} / n_{Al} ratio of the zeolite framework $(n_{Si} / n_{Al})_{framework}$. This value can be calculated by excluding the amount of amorphous silica. All values are listed in Table 6.1. With a higher degree of dealumination the fraction of amorphous silica is increasing. Hence, the structure of all dealuminated zeolite samples was damaged to some extent during dealumination.

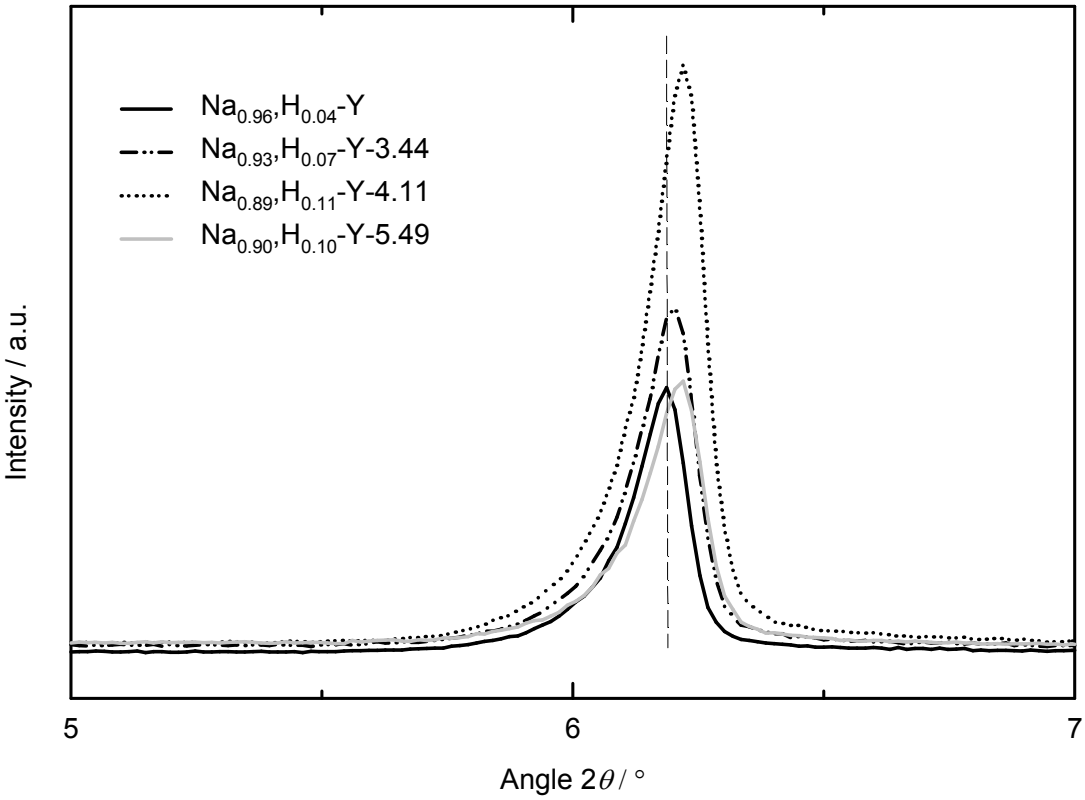

Figure 6.12: X-ray diffractograms of faujasite zeolites with different n_{Si} / n_{Al} ratios at around 2θ = 6°.

Table 6.1: Comparison of the n_{Si} / n_{Al} ratios of the zeolite samples obtained by ICP-OES and n_{Si} / n_{Al} ratios in the framework of the zeolites obtained by ^{29}Si MAS NMR of the dealuminated faujasite samples.

Zeolite	$(n_{Si} / n_{Al})_{ICP-OES}$	$(n_{Si} / n_{Al})_{NMR}$	$(n_{Si} / n_{Al})_{framework}$	$n_{SiO_2,\ amorph.}$ / $n_{SiO_2,\ total}$ / %
$Na_{0.93},H_{0.07}$-Y-3.44	3.44	3.41	3.36	5.3
$Na_{0.89},H_{0.11}$-Y-4.11	4.11	4.03	3.64	9.9
$Na_{0.90},H_{0.10}$-Y-5.49	5.49	5.53	4.25	23.2

6.4 ZSM-12 Zeolites

Powder X-ray diffractograms of the four ZSM-12 samples are depicted in Figure 6.13. It reveals that the materials are phase-pure. In comparison to the simulated patterns of calcined ZSM-12 [96], the samples do not exhibit all reflexes, and these are not all completely resolved, but the measured diffractograms do show all reflexes of high intensities and are in agreement with diffractograms in the literature [83, 97].

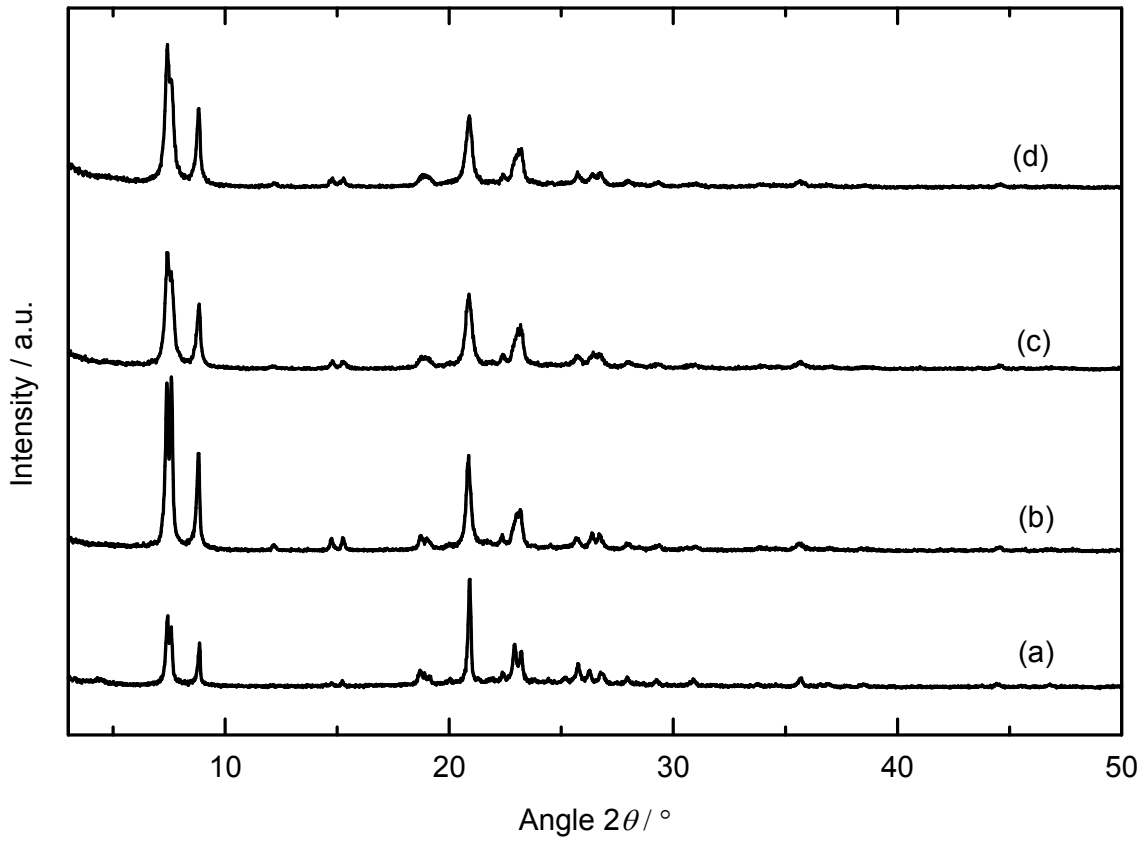

Figure 6.13: X-ray diffractograms of zeolites a) Na-ZSM-12-24, b) Na-ZSM-12-125, c) Na-ZSM-12-39 and d) Na-ZSM-12-42 after removal of the template.

Figure 6.14 shows the SEM images of the four ZSM-12 zeolites. Na-ZSM-12-24 (Figure 6.14a) consists of crystals with an average length of *ca*. 3 µm and a diameter of 1.5 µm. Some small crystals or impurities can be observed like in the SEM images of Ernst *et al*. [83]. Na-ZSM-12-125 (Figure 6.14b) consists of cube-shaped crystals of *ca*. 1 µm as reported by Yoo *et al*. [84]. The crystals of Na-ZSM-12-39 and Na-ZSM-12-42 are also cube-shaped but have crystal sizes of *ca*. 0.5 µm.

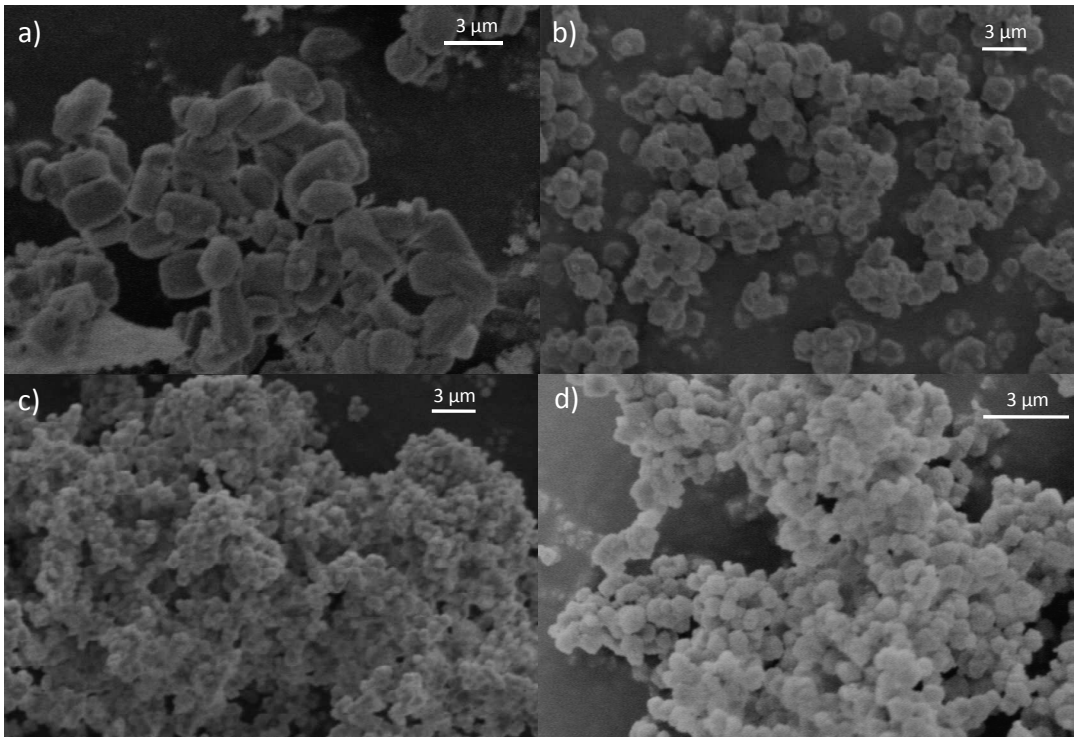

Figure 6.14: SEM images of a) Na-ZSM-12-24, b) Na-ZSM-12-125, c) Na-ZSM-12-39 (and d) Na-ZSM-12-42 after removal of the template.

The first step after the synthesis and removal of the template of the ZSM-12 samples is a two-fold ion exchange with an excess of sodium ions. Unlike in Na-Y, not all cation positions can be filled with sodium ions. The assumption was made that the number of cation positions in the zeolite equals the number of aluminum atoms. Results obtained from ICP-OES showed that in Na-ZSM-12-24 only 74.4 % of the cation positions were filled with sodium ions. With increasing n_{Si} / n_{Al} ratio of Na-ZSM-12 a higher percentage of cation positions can be filled with sodium ions. In Na-ZSM-12-39 81.2 %, in Na-ZSM-12-42 79.6 % and in Na-ZSM-12-125 85.5 % of the cation positions were occupied by sodium ions. In an attempt to find out which kind of cations occupies the other cation positions NMR studies were undertaken. ^{27}Al MAS NMR investigations (Figure 6.15) show that Na-ZSM-12-24 and Na-ZSM-12-125 have no signals at *ca*. 0 ppm. This indicates that, in these samples, no perfectly octahedrally coordinated aluminum is present. Therefore, Al^{3+} cations cannot be invoked as filling the 20 % gap of the cation balance. Figure 6.15 also indicates that preparation of the acidic form of Na-ZSM-12-24 partly damages the zeolite framework. In case of the zeolite with the lower amount of aluminum, *i. e.* Na-ZSM-12-125, and hence a lower amount of Brønsted acid sites in the acidic form, no damage of the framework can be detected.

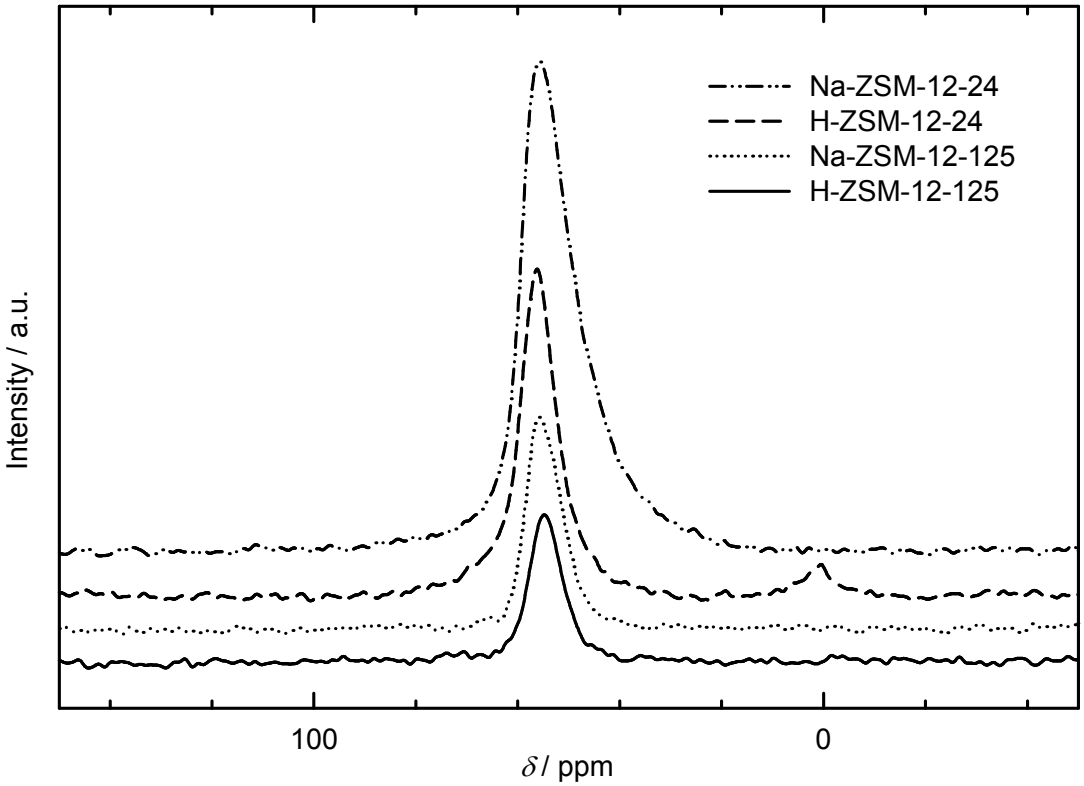

Figure 6.15: ^{27}Al MAS NMR spectra of catalysts H-ZSM-12-24, H-ZSM-12-125 and their starting materials. The signals at δ = 0 ppm and δ = 60 ppm originate, respectively, from octahedrally and tetrahedrally coordinated aluminum.

^{1}H MAS NMR measurements were also done (not shown). Unfortunately, the interpretation of these ^{1}H spectra is at the moment not possible for zeolite ZSM-12, because no literature is available about the chemical shifts of AlOH, SiOH and SiOHAl (Brønsted acid sites) groups in this zeolite. Without further investigations, it is difficult to decide about the number of signals and the chemical shifts at which these signals appear. Therefore, the question as to which kind of cations is filling the gap of the missing 20 % cannot be answered. Either protons or aluminum cations, which are not completely octahedrally coordinated and thus not visible in the ^{27}Al MAS NMR spectra, can be considered. Answering this question would require further NMR investigations with advanced techniques. For the sample designation it was assumed, like in case of the faujasite zeolites, that the missing cations are protons.

6.5 Zeolite MCM-22

Zeolite MCM-22 with an n_{Si} / n_{Al} ratio of 21, as determined by ICP-OES, was prepared in the group of Privatdozentin Dr. Yvonne Traa. 72 % of the cation sites can be exchanged with sodium ions, the remaining 28 % are assumed to be protons incorporated during the

synthesis. The powder X-ray diffractogram of Na-MCM-22 is depicted in Figure 6.16. Peak positions and relative intensities agree reasonably well with those given the literature [98] and show that the material is phase-pure. The relatively broad peaks could be the result of structural disorder.

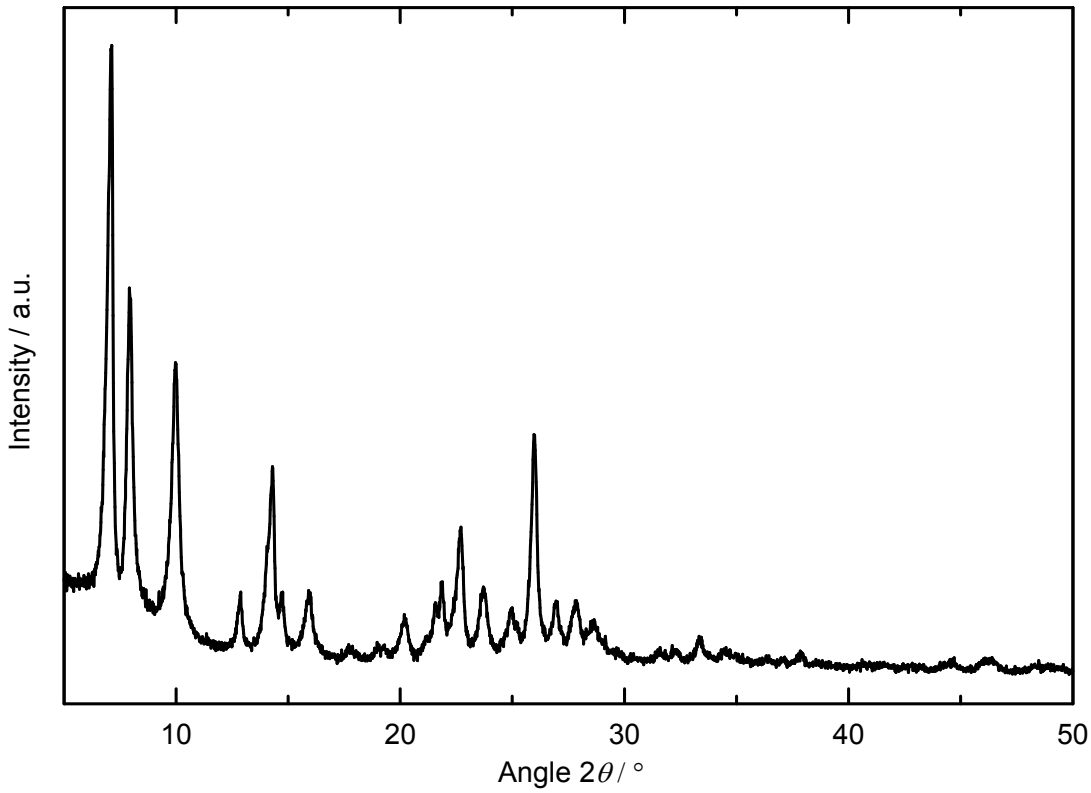

Figure 6.16: X-ray diffractogram of Na-MCM-22.

The ^{27}Al MAS NMR spectrum of Na-MCM-22 (Figure 6.17) possesses no signal of octahedrally coordinated extra-framework aluminum at 0 ppm. Between 50 and 60 ppm one signal is visible with at least one shoulder. These signals originate from nonequivalent tetrahedrally coordinated framework aluminum [99].

In Figure 6.18, SEM images of zeolite Na-MCM-22 are shown. The zeolite appears in form of very thin, interpenetrating platelets forming spherical particles of 8 to 10 µm which is in line with Ref. [100].

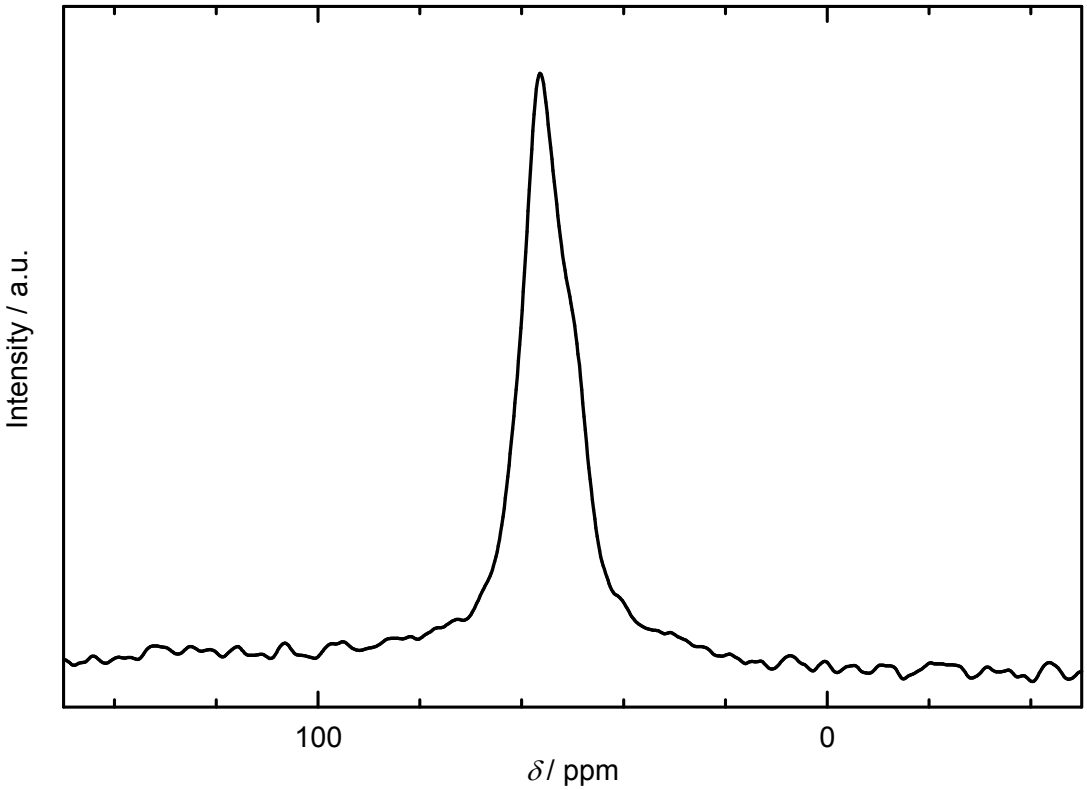

Figure 6.17: ^{27}Al MAS NMR spectrum of Na-MCM-22. The signals between 50 and 60 ppm originate from cyrstallographically nonequivalent tetrahedrally coordinated aluminum.

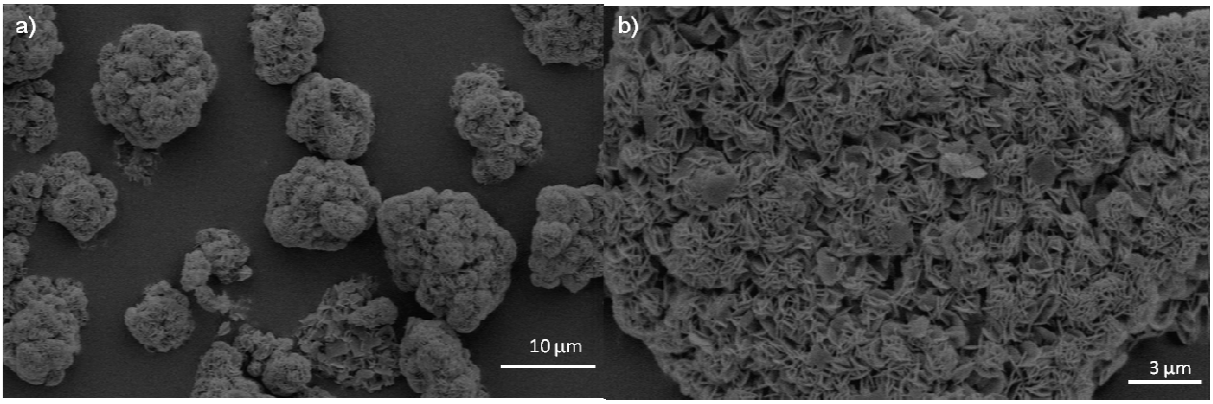

Figure 6.18: SEM images of zeolite Na-MCM-22.

6.6 Metal Dispersion of the Catalysts

The metal dispersions of some catalysts ordered by catalyst groups which were compared to each other in the hydroconversion of decalin are listed in Table 6.2. All catalysts were calcined and reduced under nearly the same conditions (see Sections 5.1.3 and 5.1.5).

Table 6.2: Metal dispersions of various catalysts.

Catalyst	Metal Dispersion	Catalyst	Metal Dispersion
4.2Pt/$Na_{0.87}$,$H_{0.13}$-Y	0.57	3.8Ir/$Na_{0.89}$,$H_{0.11}$-Y	1.17
4.0Pt/$Na_{0.88}$,$H_{0.12}$-Y	0.57	3.1Ir/$Na_{0.90}$,$H_{0.10}$-Y	1.25
3.7Pt/$Na_{0.86}$,$H_{0.14}$-Y	0.62	2.9Ir/$Na_{0.90}$,$H_{0.10}$-Y	1.13
3.0Pt/$Na_{0.88}$,$H_{0.12}$-Y	0.73	2.4Ir/$Na_{0.93}$,$H_{0.07}$-Y	0.94
2.7Pt/$Na_{0.88}$,$H_{0.12}$-Y	0.51	1.9Ir/$Na_{0.92}$,$H_{0.08}$-Y	0.65
2.0Pt/$Na_{0.91}$,$H_{0.09}$-Y	0.70	1.0Ir/$Na_{0.93}$,$H_{0.07}$-Y	0.90
1.7Pt/$Na_{0.91}$,$H_{0.09}$-Y	0.42		
0.94Pt/$Na_{0.94}$,$H_{0.06}$-Y	0.51	3.0Ir/$Li_{0.68}$,$Na_{0.21}$,$H_{0.11}$-Y	0.75
		2.7Ir/$K_{0.88}$,$H_{0.12}$-Y	1.06
3.0Pt/$Li_{0.58}$,$Na_{0.25}$,$H_{0.17}$-Y	0.59	2.6Ir/$Rb_{0.70}$,$Na_{0.15}$,$H_{0.15}$-Y	1.31
2.9Pt/$K_{0.90}$,$H_{0.10}$-Y	0.52	2.6Ir/$Cs_{0.71}$,$Na_{0.16}$,$H_{0.13}$-Y	0.92
2.9Pt/$Rb_{0.68}$,$Na_{0.15}$,$H_{0.17}$-Y	0.52		
3.1Pt/$Cs_{0.71}$,$Na_{0.16}$,$H_{0.13}$-Y	0.58	3.0Ir/$Na_{0.90}$,$H_{0.10}$-LSX	1.73
		2.5Ir/$Na_{0.91}$,$H_{0.09}$-X	1.45
2.9Pt/$Na_{0.89}$,$H_{0.11}$-LSX	0.39	3.3Ir/$Na_{0.88}$,$H_{0.12}$-Y-3.44	1.05
2.8Pt/$Na_{0.86}$,$H_{0.14}$-X	0.36	3.3Ir/$Na_{0.90}$,$H_{0.10}$-Y-4.11	1.23
3.0Pt/$Na_{0.89}$,$H_{0.11}$-Y-3.44	0.49	3.1Ir/$Na_{0.77}$,$H_{0.23}$-Y-5.49	1.03
2.9Pt/$Na_{0.87}$,$H_{0.13}$-Y-4.11	0.56		
2.9Pt/$Na_{0.75}$,$H_{0.25}$-Y-5.49	0.56	0.94Ir/$Na_{0.90}$,$H_{0.10}$-X	1.42
		1.1Ir/$Na_{0.52}$,$La_{0.13}$,$H_{0.09}$-X	1.57
0.96Pt/$Na_{0.88}$,$H_{0.12}$-X	0.37	0.94Ir/$Na_{0.41}$,$La_{0.16}$,$H_{0.11}$-X	1.40
1.1Pt/$Na_{0.52}$,$La_{0.13}$,$H_{0.09}$-X	0.26	0.99Ir/$Na_{0.26}$,$La_{0.22}$,$H_{0.08}$-X	1.58
0.99Pt/$Na_{0.43}$,$La_{0.17}$,$H_{0.06}$-X	0.47	0.85Ir/$La_{0.30}$,$H_{0.06}$,$Na_{0.04}$-X	0.76
0.87Pt/$Na_{0.26}$,$La_{0.22}$,$H_{0.08}$-X	0.36		
1.0Pt/$La_{0.30}$,$H_{0.06}$,$Na_{0.04}$-X	0.43		

Nevertheless, there are in some cases large variations between the metal dispersions which can be effected by the support or by unintended changes in the conditions of the calcination and reduction. The mean metal dispersion of the platinum-containing catalysts is between 0.50 and 0.60. In case of the X zeolites the dispersion is lower. The improvement of the metal dispersion was not a subject of this work, but this could lead to a reduction of the total metal content required. The metal dispersion of the iridium-containing catalysts is in most cases above 1. For the hydrogen adsorption experiments a stoichiometry of n_H / n_{Ir} = 1 was assumed. Presumably, there is a deviation from this stoichiometry, and more than one hydrogen atom is adsorbed on a single iridium atom.

The metal dispersion within a group is nearly comparable with some exceptions like 1.9Ir/$Na_{0.92}$,$H_{0.08}$-Y or 0.85Ir/$La_{0.30}$,$H_{0.06}$,$Na_{0.04}$-X. Table 6.2 was given for completeness and will not be discussed in detail, but the results could be used if some peculiarities are obtained in the hydroconversion of decalin with some very high- or low-dispersed catalysts.

7 Preliminary Investigations

7.1 Co-Injection of n-Alkane Isomers

To make the assignment of open-chain decanes much safer, n-decane was isomerized at 262 °C (see Section 5.3.2). The resulting mixture of open-chain decane isomers was analyzed by GC/MS. In addition, the assignment of product peaks from the isomerization of long-chain n-alkanes was to a large extent adopted from prior work of the group [101, 102]. The mixture of these decane isomers and a liquid product sample of the hydroconversion of decalin on a catalyst producing large amounts of open-chain decanes were co-injected into the capillary gas chromatograph. The relevant section of the gas chromatogram of the co-injection is depicted in Figure 7.1.

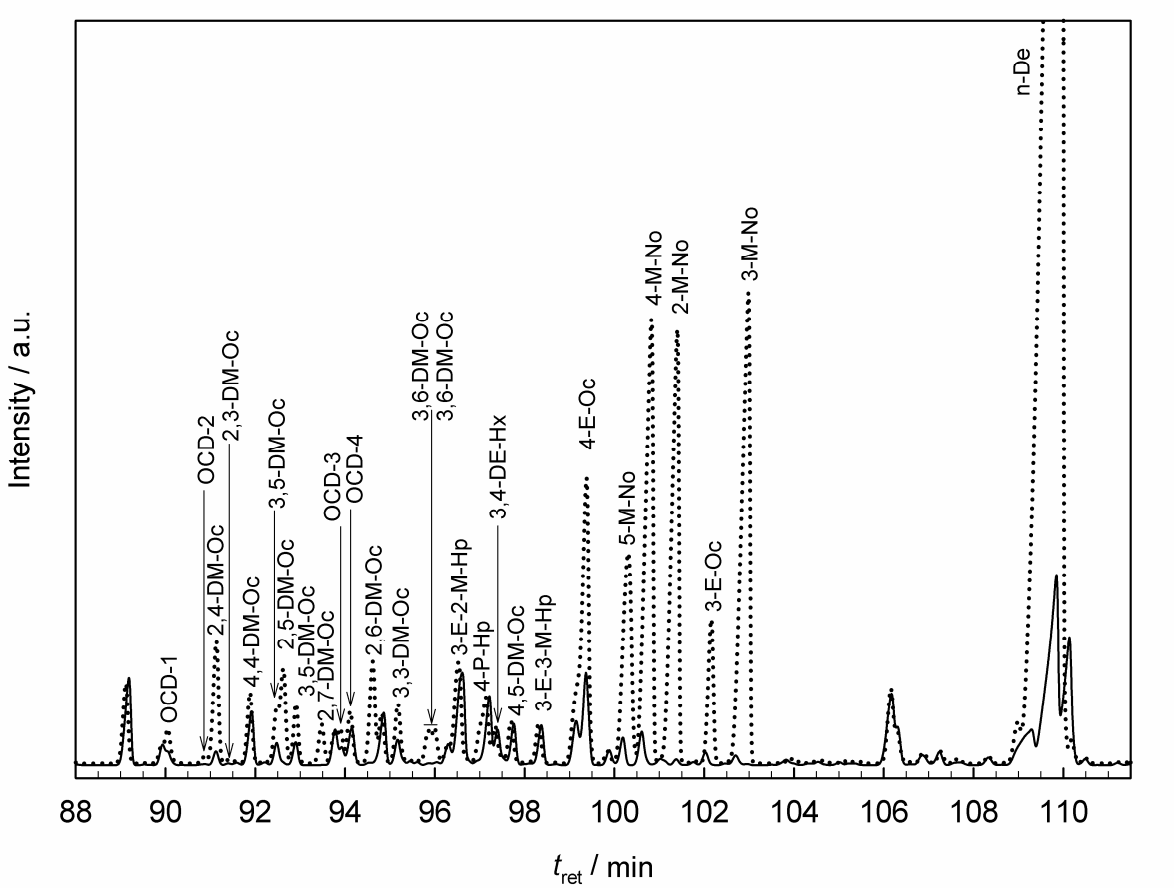

Figure 7.1: Extraction of the gas chromatogram of the product of decalin hydroconversion at 290 °C on 2.9Ir/$Na_{0.90}$,$H_{0.10}$-Y (solid line) and the same sample co-injected with the product of n-decane isomerization (dotted line).

A comparison of the gas chromatograms obtained by the co-injection and the pure product of decalin hydroconversion reveals that there are a lot of peaks mainly between 90 and 103 min which are identical and that the areas of these peaks increase upon co-injection. Other

peaks like in the area between 105 and 108 min are not affected by the co-injection at all and are hence definitively not components of the isomerization of n-decane at 262 °C. These facts are strong evidence for the formation of open-chain decanes in the hydroconversion of decalin. Of course, not every theoretically possible isomer of n-decane is generated under the isomerization conditions of n-decane and hence included in the isomer mixture obtained. Moreover, not every signal is well resolved in the gas chromatogram, and some peak overlap of open-chain decanes with isomers of or ring opening products from decalin cannot be excluded. This would generate erroneous selectivity results. Nevertheless, this method can be used to identify the main open-chain decanes.

In conclusion, the procedure of admixing a sample of open-chain decanes with a known composition to a product of decalin hydroconversion was employed in this work for the first time. It is considered to allow for a qualitatively safe identification of open-chain decanes. In quantitative terms, the accuracy of their analysis has its limits, due to some peak overlap with other hydrocarbons. Since the gas-chromatographic analyses form the basis for calculating the selectivities and yields of open-chain decanes, these reported values have a limited accuracy either.

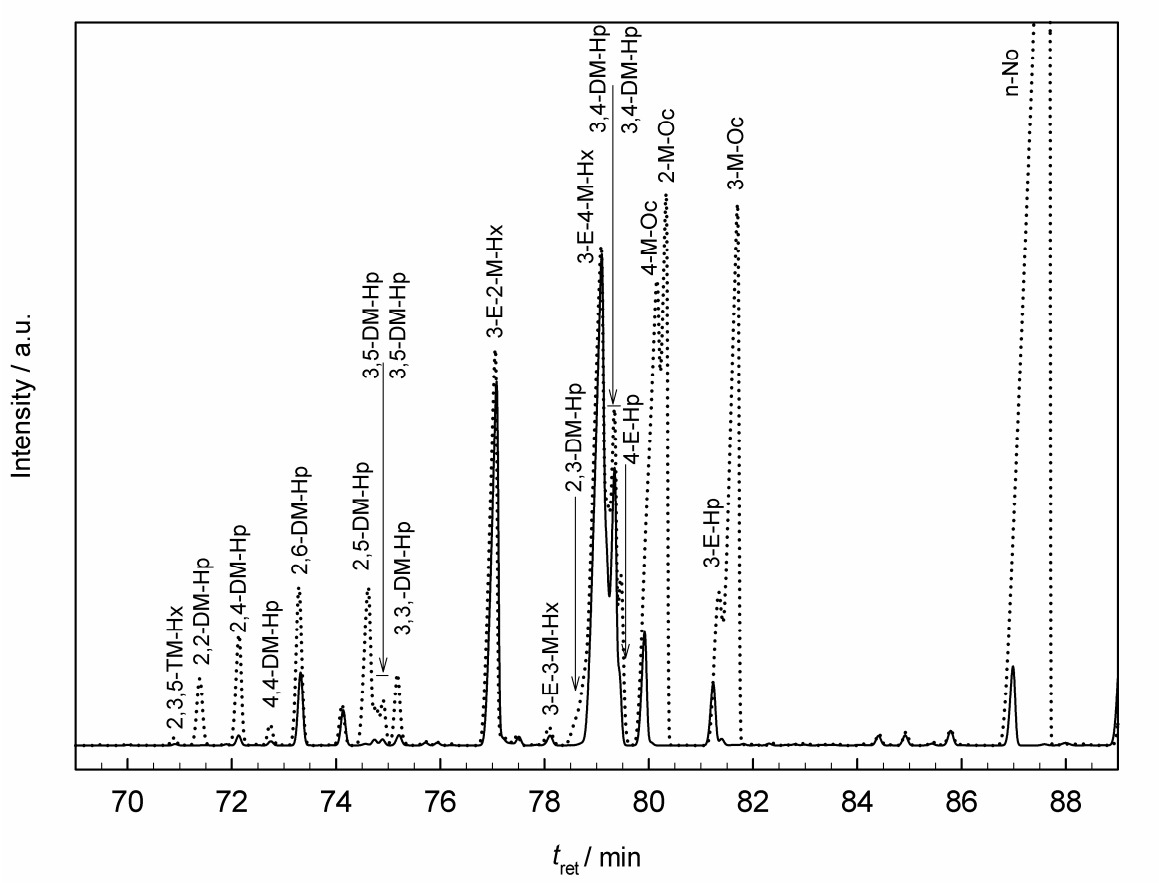

Figure 7.2: Extraction of the gas chromatogram of the product of decalin hydroconversion at 309 °C on 2.6Ir/$Rb_{0.70}$,$Na_{0.15}$,$H_{0.15}$-Y (solid line) and the same sample co-injected with the product of n-nonane isomerization (dotted line).

On some catalysts also large amounts of open-chain nonanes were obtained. The co-injection method was applied for their safe identification as well: A liquid mixture of iso-nonanes with known composition [101] was generated by isomerization of n-nonane on a 0.5Pd/Na,H-Y zeolite catalyst [103]. This mixture was co-injected into a capillary gas chromatograph with a liquid product sample obtained in the hydroconversion of decalin on a catalyst producing large amounts of open-chain nonanes. The relevant section of the gas chromatogram of the co-injection is depicted in Figure 7.2.

In much the same way as in the co-injection of iso-decanes, there are peaks mainly between 84 and 86 min which are not affected by the co-injection and other peaks mainly between 72 and 82 min which increase upon co-injection. Those peaks which increase upon co-injection are products which also appear in the isomerization of n-nonane and were assigned to open-chain nonanes. As mentioned-above, there definitively exist more open-chain nonanes in the product from decalin hydroconversion than generated in the isomerization of n-nonane.

7.2 Blank Tests

To ensure that there are no contributions of thermal hydrocracking or reactions catalyzed by the substances of the catalytic equipment, blank tests were done. The conditions were chosen as in the typical catalytic experiments of decalin hydroconversion (see Section 5.3.1.2). In one experiment the reactor was empty, and in another one it was filled with pelletized Aerosil (SiO_2) with a bulk volume of 0.4 cm^3 to reach the same conditions as in the real experiments. The results obtained in both experiments are listed in Table 7.1.

The commercially available cis-decalin (Merck) consisted of 97.4 wt.-% cis-decalin and 0.9 wt.-% trans-decalin. Another 1.7 wt.-% were impurities like sk-Isos and C_{11}+. This would have resulted according to the definition of conversion (Section 5.5.3) in an apparent conversion X_{Dec} of 1.7 %. Without a catalyst in the reactor the conversion of decalin at 371 °C was 6.0 %. The selectivities of hydrocracked products and ring opening products were negligible, and no open-chain decanes were formed. Decalin was mainly converted to tetralin and naphthalene. The obtained values fitted well with the calculated values from the thermodynamic equilibrium between cis-decalin, trans-decalin, tetralin and naphthalene [92]. The remaining products were skeletal isomers of decalin, which were still observed in the cis-decalin from Merck.

Table 7.1: Conversion and selectivities obtained in two blank tests.

Catalyst	T / °C	X_{Dec} / %	S_{C_9-} / %	S_{OCDs} / %	S_{ROPs} / %	$S_{sk\text{-}Isos}$ / %	S_{Ttr} / %	S_{Nap} / %	$S_{C_{11}+}$ / %
-	371	6.0	3.6	-	1.9	18.9	72.1	3.5	-
SiO_2	368	15.8	0.4	-	0.5	19.6	75.8	3.7	-

Catalytic tests with Aerosil (SiO_2) at 368 °C gave a conversion of 16 %. Thus the conversion increased but the selectivities were nearly the same. An explanation for the higher conversion could be hydroconversion of decalin on the very weak acid sites in Aerosil, but in this case one would expect not only a higher conversion but also a change in the product selectivities, particularly a higher selectivity of skeletal isomers.

Blank tests showed that there are no contributions of thermal hydrocracking up to temperatures of 370 °C. Mainly the thermodynamic equilibrium between decalin, tetralin and naphthalene is established. There are no contributions to the formation of the desired product groups, *i. e.* ring opening products or open-chain decanes.

8 Ring Opening of Decalin on Faujasite (FAU) Catalysts

8.1 Influence of the Metal Loadings

8.1.1 Iridium-Containing Y Catalysts

Na-Y zeolites loaded with five different amounts of iridium were prepared to identify on the one hand the role of iridium and on the other hand the influence of the metal loading on the hydroconversion of decalin. The metal content was varied between 1.0 and 3.8 wt.-%. In all cases only the Brønsted acid sites generated during the reduction of iridium were present. Hence, the n_{Ir} / n_{H+} ratio was constant in all five catalysts but the total amount of Brønsted acid sites was higher the higher the metal loading was.

In Figure 8.1 the conversion of decalin at different temperatures is illustrated for the five investigated catalysts. Over the whole temperature range the activity of the catalysts increases with increasing iridium content which is explainable by the increasing amount of active sites.

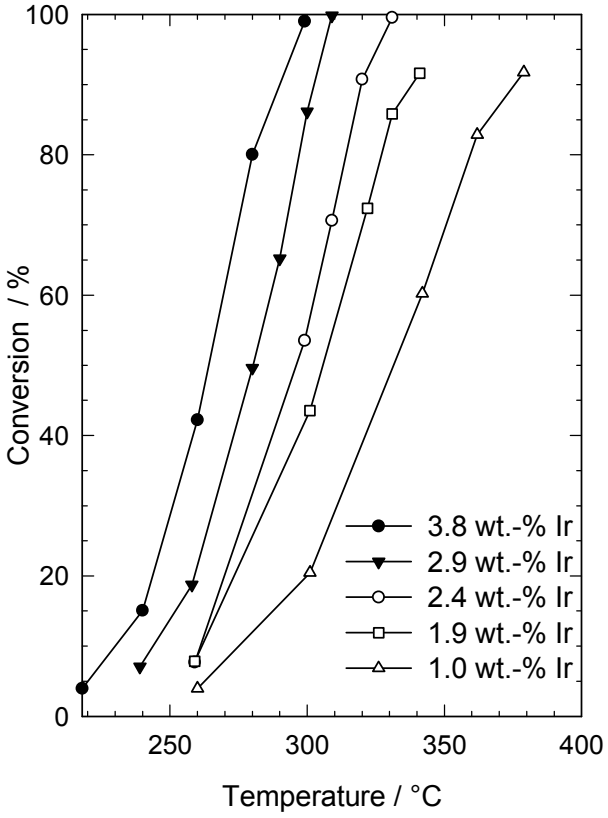

Figure 8.1: Dependence of the decalin conversion on the reaction temperature for Ir/Na,H-Y zeolites with different iridium loadings.

The different selectivities of products obtained in the hydroconversion of decalin are exemplarily shown for three catalysts in Figure 8.2. In the same way as the iridium content influences the activity of the catalyst, it also influences the nature of primary products observed at low conversion. The main products obtained on 2.9Ir/$Na_{0.90}$,$H_{0.10}$-Y are ring opening products (ROPs) of decalin with a selectivity of around 75 %. With a lower iridium loading, namely 1.9 wt.-%, the selectivity of ring opening products decreases, instead the selectivity of skeletal isomers of decalin (sk-Isos) increases. On 1.0Ir/$Na_{0.93}$,$H_{0.07}$-Y the main products at low conversion are skeletal isomers of decalin with a selectivity of 65 % and only 26 % of ring opening products. At higher temperatures the selectivities of the primary products decrease and products from consecutive reactions like open-chain decanes (OCDs) and hydrocracked products are formed. The best results concerning the yield of open-chain decanes obtained on all iridium-containing Y catalysts are listed in Table 8.1. In addition, the yields of open-chain nonanes (OCNs) and of the hydrocracked products are given. The hydrocracked products are very undesired since they reduce the yield of the diesel fraction, hence a minimal Y_{C_9-} is desired. The open-chain nonanes are also hydrocracked products, and in case of decalin as a feed they would not belong any longer to the diesel fraction. Nevertheless, in case of diesel as real feed open-chain alkanes with one carbon atom less than the feed would still belong to the boiling range of diesel and would improve the cetane number. These products are less favored than open-chain alkanes with the same carbon number but are still relatively valuable products.

Table 8.1: Maximum yields of open-chain decanes obtained on iridium-containing Y catalysts.

Catalyst	T_r / °C	X_{Dec} / %	S_{OCDs} / %	$Y_{OCDs, max.}$ / %	Y_{OCNs} / %	Y_{C_9-} / %
3.8Ir/$Na_{0.89}$,$H_{0.11}$-Y	280	80.0	27.2	21.8	10.1	34.7
3.1Ir/$Na_{0.90}$,$H_{0.10}$-Y	300	97.6	31.3	30.5	14.3	46.7
2.9Ir/$Na_{0.90}$,$H_{0.10}$-Y	300	86.2	35.7	30.7	7.2	24.6
2.4Ir/$Na_{0.93}$,$H_{0.07}$-Y	320	90.7	32.9	29.8	8.7	30.9
1.9Ir/$Na_{0.92}$,$H_{0.08}$-Y	341	91.6	33.6	30.8	8.7	31.2
1.0Ir/$Na_{0.93}$,$H_{0.07}$-Y	379	91.8	23.8	21.9	4.3	27.5

The maximum yield of open-chain decanes is obtained on catalyst 2.9Ir/$Na_{0.90}$,$H_{0.10}$-Y with a yield of 31 % at 300 °C and even 7 % open-chain nonanes. This catalyst was completely reproduced from the preparation to the catalytic experiments. The resulting catalyst 3.1Ir/$Na_{0.90}$,$H_{0.10}$-Y shows a similar behavior, and the good results are essentially

reproducible. At variance to the former catalyst, catalyst 3.1Ir/$Na_{0.90}$,$H_{0.10}$-Y has a higher tendency to form hydrocracked products.

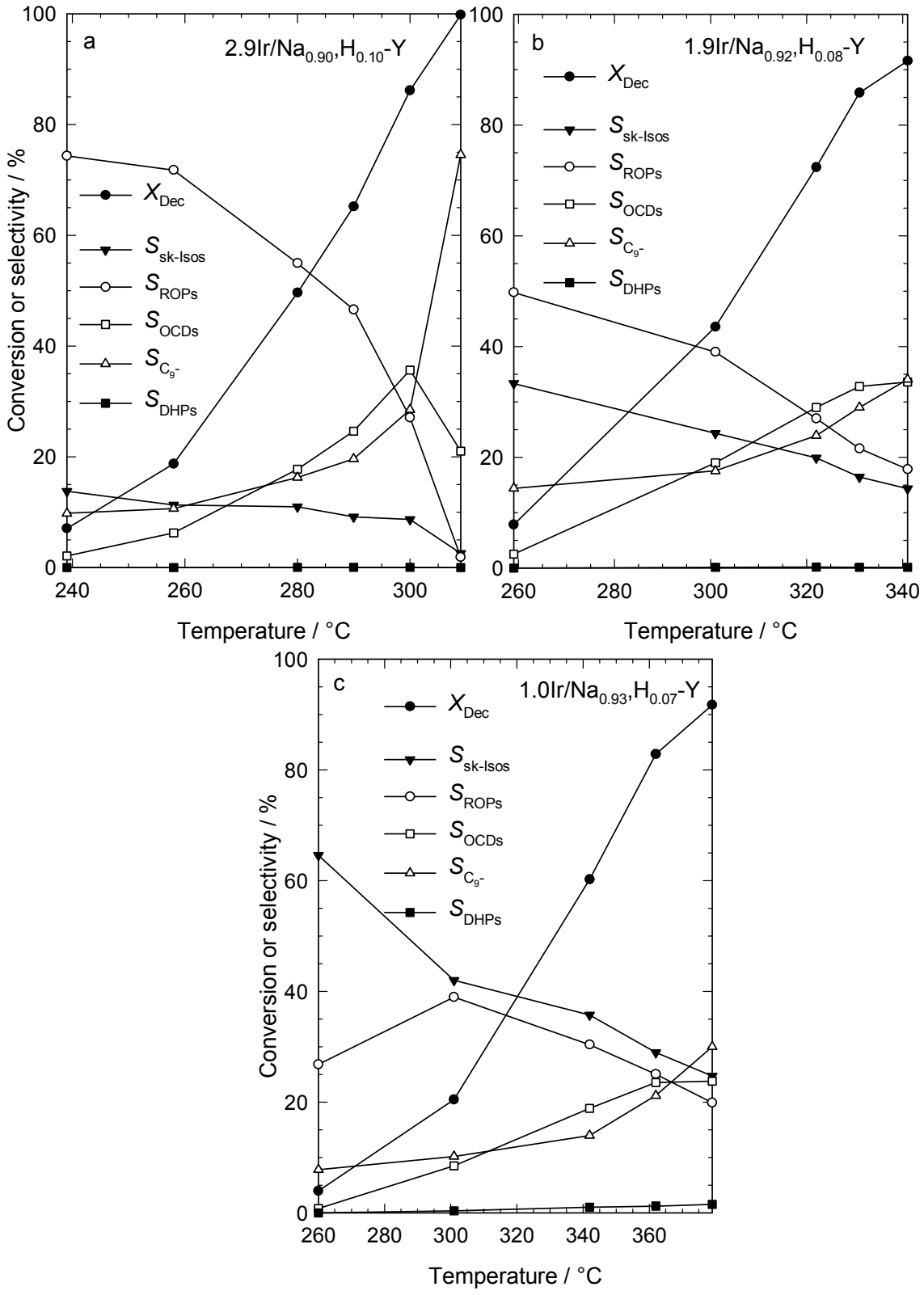

Figure 8.2: Conversion of decalin and selectivities of different groups of products in dependence of the reaction temperature for Ir/Na,H-Y zeolite catalysts with different iridium loadings.

In Figure 8.3, the maximal selectivities and yields of open-chain decanes with the different iridium loadings are illustrated. As mentioned above, the best performance is shown by an Ir/Na,H-Y catalyst with 2.9 wt.-% iridium, but there seems to be a relatively broad plateau between 1.9 and 2.9 wt.-% iridium loading in which all catalysts show a very good performance concerning the formation of open-chain decanes.

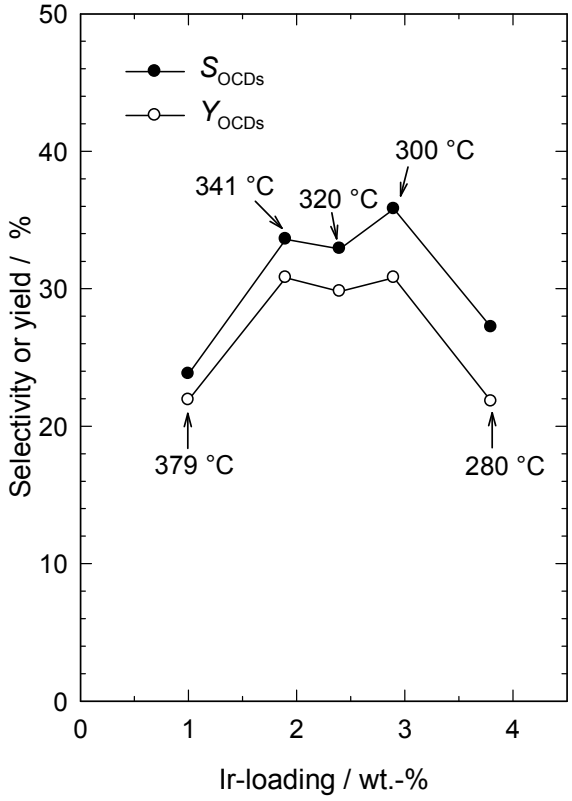

Figure 8.3: Maximal selectivities and yields of open-chain decanes (OCDs) on Ir/Na,H-Y zeolites with different iridium loadings.

The carbon number distributions of the hydrocracked products obtained at conditions of the maximal yields of OCDs are depicted in Figure 8.4. All distribution curves are nearly symmetrical around C_5. The curves resemble a hammock with a strongly preferred formation of methane and C_9 fragments and very little C_4, C_5 and C_6. All curves have a $\sum S_j^*$ below 220 % indicating an almost pure primary hydrocracking which is also indicated by the symmetry of the curves. These curves differ strongly from distribution curves given in the literature obtained on ideal bifunctional catalysts with C_{10} hydrocarbons [47, 104]. On ideal bifunctional catalysts, C_{10} naphthenic structures undergo the paring reaction (see Section 4.3.1.4) leading to an M-shaped curve due to the formation of much iso-butane (i-Bu) and methylcyclopentane (M-CPn). In contrast, C_{10} paraffins form bell-shaped curves with a maximum at C_5, slightly lower amounts of C_4 and C_6 and small amounts of C_3 and C_7 [105].

With carbocation chemistry the distribution curves in Figure 8.4 cannot be explained since methane, the predominating C_9- product, cannot be formed via carbocations. These distribution curves can only be interpreted in terms of a mechanism that furnishes C_9-hydrocarbons via hydrogenolysis on the metal iridium. Upon decreasing the total metal loading there seems to be a superimposition of a carbocationic mechanism indicated by the ratio $n_{M\text{-}CPn}$ / $n_{i\text{-}Bu}$. While no iso-butane or methylcyclopentane are formed on the Y catalyst with 3.8 wt.-% Ir, the ratio increases with lower metal loading from 0.04, 0.11, 0.16 to 0.43 on the catalyst with 1.0 wt.-% iridium.

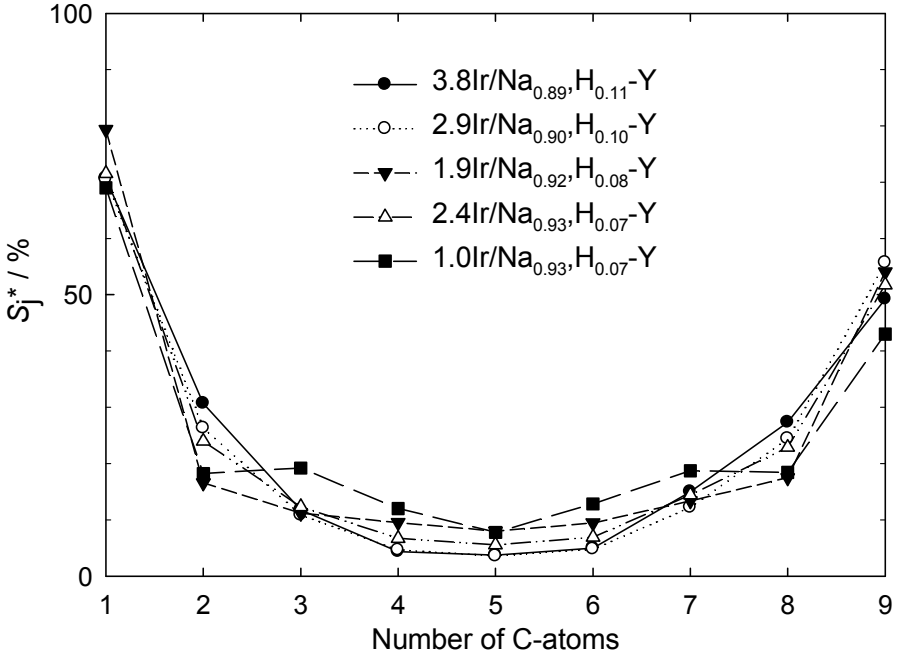

Figure 8.4: Modified hydrocracking selectivities S_j^* on the iridium-containing Y catalysts:

3.8Ir/$Na_{0.89}$,$H_{0.11}$-Y: T_r = 280 °C; X_{Dec} = 80 %; $Y_{C_{9-}}$ = 33 %; $\sum S_j^*$ = 222 %.

2.9Ir/$Na_{0.90}$,$H_{0.10}$-Y: T_r = 300 °C; X_{Dec} = 86 %; $Y_{C_{9-}}$ = 24 %; $\sum S_j^*$ = 217 %.

2.4Ir/$Na_{0.93}$,$H_{0.07}$-Y: T_r = 320 °C; X_{Dec} = 91 %; $Y_{C_{9-}}$ = 30 %; $\sum S_j^*$ = 218 %.

1.9Ir/$Na_{0.92}$,$H_{0.08}$-Y: T_r = 341 °C; X_{Dec} = 92 %; $Y_{C_{9-}}$ = 31 %; $\sum S_j^*$ = 219 %.

1.0Ir/$Na_{0.93}$,$H_{0.07}$-Y: T_r = 379 °C; X_{Dec} = 92 %; $Y_{C_{9-}}$ = 28 %; $\sum S_j^*$ = 219 %.

All in all, the iridium-containing catalysts with a high metal loading seem to behave as pure hydrogenolysis catalysts. These catalysts are not able to isomerize the decalin molecule, thus leading to high selectivities of ring opening products. By reducing the iridium content, more and more isomerization can be observed leading to higher selectivities of skeletal isomers and a higher $n_{M\text{-}CPn}$ / $n_{i\text{-}Bu}$ ratio in the hydrocracked products. Since the n_{Ir} / n_{H^+} ratio in all catalysts is the same, the observations can perhaps be explained by a faster reaction of the decalin molecules on metal sites than Brønsted acid sites. On catalyst 3.8Ir/$Na_{0.89}$,$H_{0.11}$-Y

the amount of active sites is much larger than on catalyst 1.0Ir/$Na_{0.93}$,$H_{0.07}$-Y, thus on the former catalyst the decalin molecules are preferentially adsorbed on the metal sites and react there, whereas on the latter catalyst more decalin molecules adsorb on the Brønsted acid sites because of the lower number of metal sites.

On all catalysts only negligible deactivation is observed up to 60 h time-on-stream. Hydrocarbons with more than ten carbon atoms are not formed at any time. In order to get more information about the number of branchings in the product group of open-chain decanes, the OCDs are subdivided into non-branched decane (n-C_{10}), monobranched decanes with a methyl group (M-C_9) or an ethyl group (E-C_8) and multibranched decanes (xM,yE-$C_{10-(x+2y)}$). The theoretically possible isomer 4-propylheptane was not observed. Figure 8.5 presents the selectivities of the differently branched decanes on the representative catalysts 3.8Ir/$Na_{0.89}$,$H_{0.11}$-Y and 1.0Ir/$Na_{0.93}$,$H_{0.07}$-Y at conditions where maximal OCD yields were obtained. On the catalyst with the high iridium loading the multibranched decanes are strongly prevailing (Figure 8.5a) whereas by lowering the metal loading more methylnonanes are formed (Figure 8.5b) which are more favorable concerning the enhancement of the cetane number.

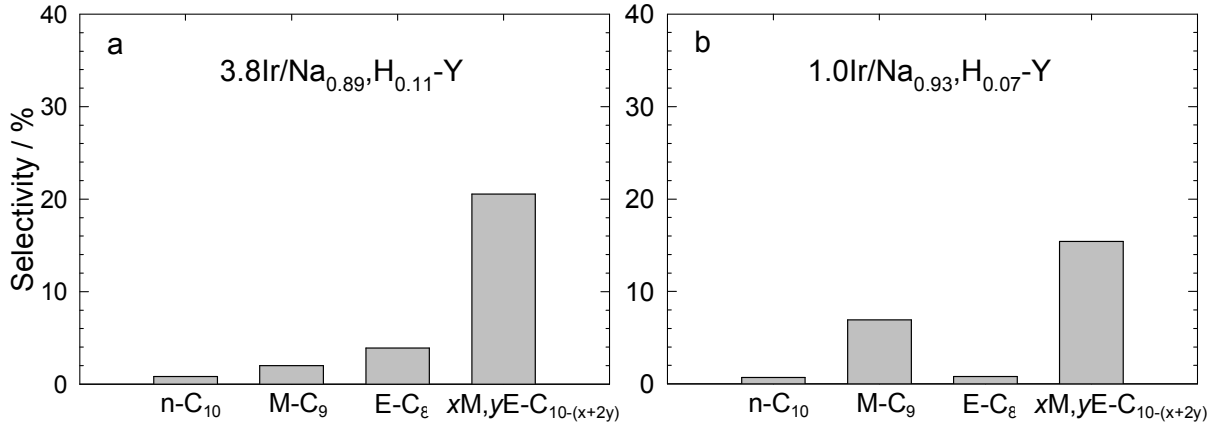

Figure 8.5: Breakdown of the selectivities of OCDs into differently branched decanes:
3.8Ir/$Na_{0.89}$,$H_{0.11}$-Y: T_r = 280 °C; X_{Dec} = 80 %; Y_{OCDs} = 22 %; S_{OCDs} = 27 %.
1.0Ir/$Na_{0.93}$,$H_{0.07}$-Y: T_r = 379 °C; X_{Dec} = 92 %; Y_{OCDs} = 22 %; S_{OCDs} = 24 %.

8.1.2 Platinum-Containing Y Catalysts

In order to investigate the role of platinum as a metal and the influence of the metal loading on the hydroconversion of decalin, Na-Y zeolite was loaded with different amounts of platinum. The metal content was varied between 0.94 and 4.2 wt.-%. In all cases only the Brønsted acid sites generated during the reduction of platinum are present. Hence, as in case of Ir/Na,H-Y catalysts (Section 8.1.1), the n_{Pt} / n_{H^+} ratio was constant in all seven catalysts but the total amount of Brønsted acid sites was higher the higher the metal loading was.

The conversion of decalin at different temperatures is exemplarily illustrated for four catalysts in Figure 8.6. As in case of iridium, over the whole temperature range the activity of the catalysts increases with increasing platinum content. As mentioned above, this can be explained by the increasing amount of active sites. In comparison to the Ir/Na,H-Y catalysts, the Pt/Na,H-Y catalysts with comparable metal loadings need higher temperatures than their iridium-containing counterparts.

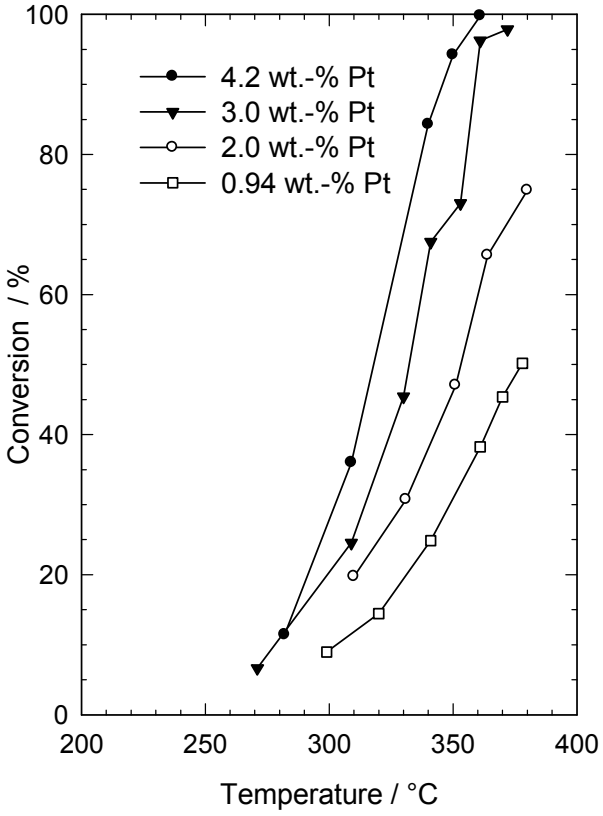

Figure 8.6: Dependence of the decalin conversion on the reaction temperature for Pt/Na,H-Y zeolites with different platinum loadings.

The different selectivities of products obtained in the hydroconversion of decalin on the Pt/Na,H-Y catalysts are exemplarily shown for the catalysts 3.7Pt/$Na_{0.86}$,$H_{0.14}$-Y and 1.7Pt/$Na_{0.91}$,$H_{0.09}$-Y in Figure 8.7. On all Pt/Na,H-Y catalysts, in contrast to the Ir/Na,H-Y catalysts, the prevailing products at low conversions are skeletal isomers of decalin with selectivities above 90 %. Skeletal isomerization of decalin can occur either on the Brønsted acid sites generated by the reduction of platinum or on the metal since platinum is known to be able to isomerize hydrocarbons (see Section 4.3.1.2). At slightly higher temperatures the selectivity of the consecutive products, *viz*. ROPs, increases up to 30 % and at even higher temperatures large amounts of open-chain decanes and hydrocracked products are formed on 3.7Pt/$Na_{0.86}$,$H_{0.14}$-Y. By lowering the metal loading a lower selectivity of ring opening products is observed. Similarly, lower selectivities of open-chain decanes and hydrocracked products are obtained. Catalyst 0.94Pt/$Na_{0.94}$,$H_{0.06}$-Y (not shown) has the lowest activity among all Pt/Na-Y catalysts and forms the dehydrogenated products tetralin and naphthalene with selectivities of up to 15 %. Calculations of the thermodynamic equilibrium show that at 380 °C nearly the equilibrium value of tetralin and naphthalene is reached [92]. The catalysts with metal loadings between 3.7 and 1.7 wt.-% platinum show an intermediate behavior of the two catalysts shown in Figure 8.7. The highest yields of OCDs obtained on the platinum-containing Y catalysts are listed in Table 8.2.

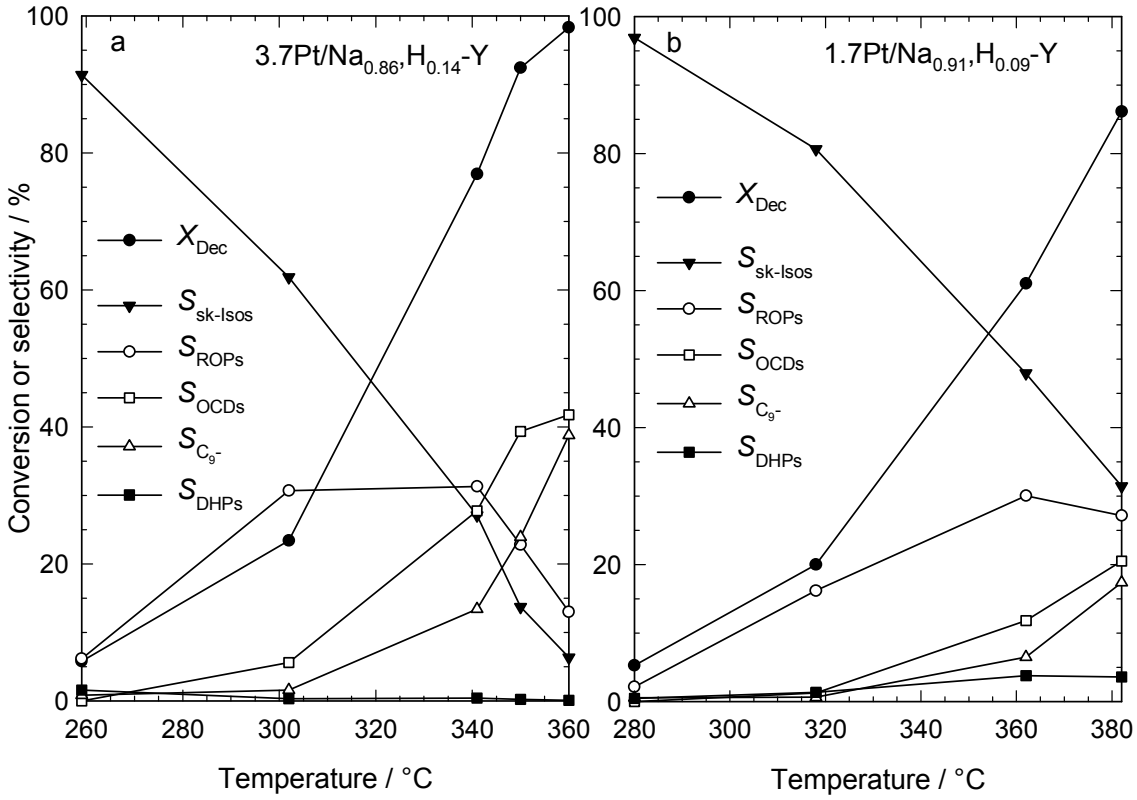

Figure 8.7: Conversion of decalin and selectivities of different groups of products in dependence of the reaction temperature for two Pt/Na,H-Y zeolite catalysts with different platinum loadings.

The maximum yield of open-chain decanes is obtained on catalyst 3.7Pt/$Na_{0.86}$,$H_{0.14}$-Y with a yield of 41 % at 360 °C. Starting from Na-Y this catalyst was reproduced resulting in 4.0Pt/$Na_{0.88}$,$H_{0.12}$-Y. The catalytic test with the latter catalyst (Table 8.2) is in very good agreement with the former one, proving that the results are reproducible. The yields of open-chain decanes on the best Pt/Na,H-Y catalysts are much higher than on the Ir/Na,H-Y catalysts. Together with the open-chain nonanes a yield of 47 % was achieved on 3.7Pt/$Na_{0.86}$,$H_{0.14}$-Y.

Table 8.2: Maximum yields of open-chain decanes obtained on platinum-containing Y catalysts.

Catalyst	T_r / °C	X_{Dec} / %	S_{OCDs} / %	$Y_{OCDs, max.}$ / %	Y_{OCNs} / %	Y_{C_9-} / %
4.2Pt/$Na_{0.87}$,$H_{0.13}$-Y	350	94.2	41.6	39.2	3.5	28.4
4.0Pt/$Na_{0.88}$,$H_{0.12}$-Y	359	98.6	40.7	40.1	5.8	42.1
3.7Pt/$Na_{0.86}$,$H_{0.14}$-Y	360	98.3	41.8	41.1	5.6	38.1
3.0Pt/$Na_{0.88}$,$H_{0.12}$-Y	361	96.3	40.7	39.1	3.9	32.8
2.7Pt/$Na_{0.88}$,$H_{0.12}$-Y	373	98.8	37.4	36.9	5.7	44.4
2.0Pt/$Na_{0.91}$,$H_{0.09}$-Y	380	74.9	13.9	10.4	0.4	8.2
1.7Pt/$Na_{0.91}$,$H_{0.09}$-Y	382	86.1	20.5	17.7	0.8	15.0

In Figure 8.8, the influence of the platinum loading on the selectivity and yield of open-chain decanes is illustrated. With increasing metal content, the selectivity and the yield of OCDs are increasing. One exception is catalyst 2.0Pt/$Na_{0.91}$,$H_{0.09}$-Y which generates a lower yield and selectivity than the catalyst with 1.7 wt.-% platinum. Catalyst 2.0Pt/$Na_{0.91}$,$H_{0.09}$-Y shows also some peculiarities concerning the metal dispersion. This catalyst has a metal dispersion of 0.70 while catalysts 2.7Pt/$Na_{0.88}$,$H_{0.12}$-Y and 1.7Pt/$Na_{0.91}$,$H_{0.09}$-Y have a metal dispersion of 0.51 and 0.42, respectively (Section 6.6, Table 6.2). Possibly, platinum particles with a lower dispersion show a better performance in the hydroconversion of decalin than highly dispersed ones, but this was not further investigated in this work. The optimal value of the platinum content seems to be between 2.7 and 4.1 wt.-%.

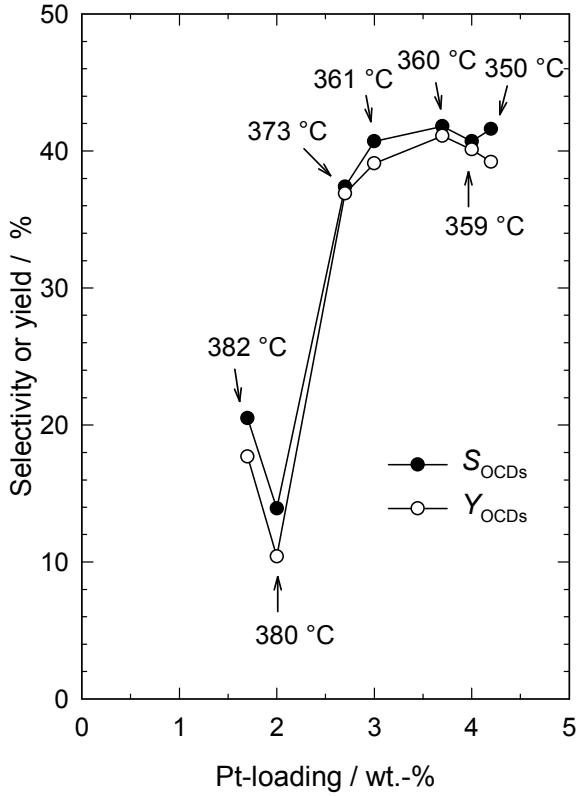

Figure 8.8: Maximal selectivities and yields of open-chain decanes (OCDs) on Pt/Na,H-Y zeolites with different platinum loadings.

The carbon number distributions of the hydrocracked products of all catalysts of this series are depicted in Figure 8.9. Except for the distribution curve of 0.94Pt/$Na_{0.94}$,$H_{0.06}$-Y, all curves are nearly equal, and they look completely different compared to the hammock-shaped curves obtained on the Ir/Na,H-Y catalysts. All possible carbon numbers appear in comparable molar amounts, except for C_2, C_5 and C_8 which are formed in relatively low amounts. From the fact that C_1 and C_9 are formed in relatively large amounts, it can be concluded with a high degree of certainty that hydrogenolysis on the metal is playing a major, if not the exclusive role in generating the hydrocracked products. A closer look at the nature of the C_4 and C_6 hydrocarbons reveals that the $n_{M\text{-}CPn}$ / $n_{i\text{-}Bu}$ ratio is constant around 0.30 between 4.2 and 2.7 wt.-% platinum, at lower metal loadings (2.0 to 1.7 wt.-%) this ratio increases to 0.70 and reaches 1.18 on the catalyst with the lowest metal content. Bearing in mind that exactly these two hydrocarbons are formed in the acid-catalyzed paring reaction of C_{10} naphthenes, one is led to interpret Figure 8.9 as being indicative of a mixed mechanism of carbon-carbon bond cleavage being operative: hydrogenolysis appears to be the predominating hydrocracking mechanism, but some elements of acid catalysis might be superimposed. On catalyst 0.94Pt/$Na_{0.94}$,$H_{0.06}$-Y severe secondary hydrocracking can be observed leading to large amounts of methane and much less C_9, which is also indicated by $\sum S_j^* = 264$ %.

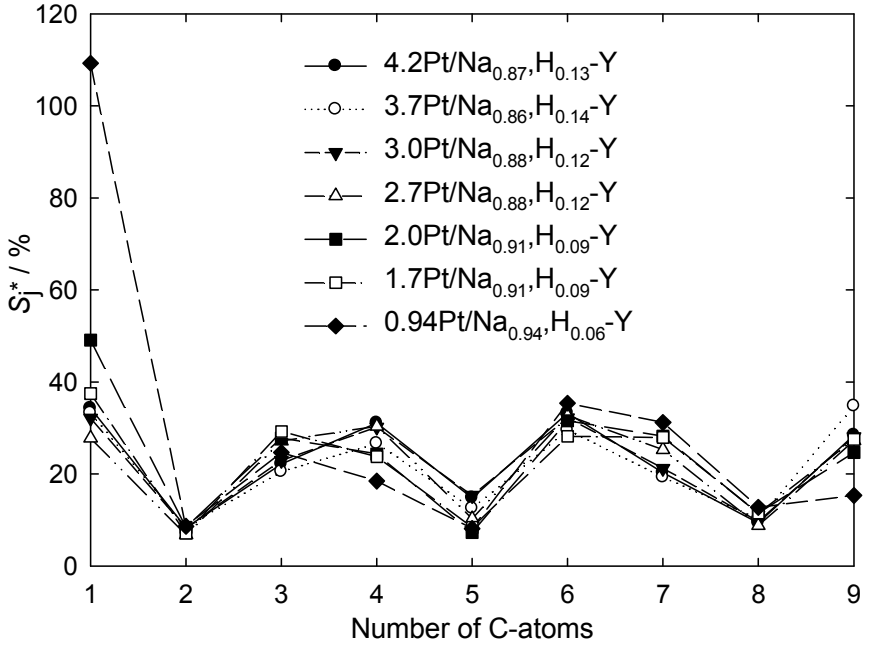

Figure 8.9: Modified hydrocracking selectivities S_j^* on the platinum-containing Y catalysts:

$4.2Pt/Na_{0.87},H_{0.13}$-Y: T_r = 350 °C; X_{Dec} = 94 %; $Y_{C_{g^-}}$ = 28 %; $\sum S_j^*$ = 202 %.

$3.7Pt/Na_{0.86},H_{0.14}$-Y: T_r = 350 °C; X_{Dec} = 92 %; $Y_{C_{g^-}}$ = 22 %; $\sum S_j^*$ = 196 %.

$3.0Pt/Na_{0.88},H_{0.12}$-Y: T_r = 361 °C; X_{Dec} = 96 %; $Y_{C_{g^-}}$ = 33 %; $\sum S_j^*$ = 200 %.

$2.7Pt/Na_{0.88},H_{0.12}$-Y: T_r = 369 °C; X_{Dec} = 90 %; $Y_{C_{g^-}}$ = 19 %; $\sum S_j^*$ = 196 %.

$2.0Pt/Na_{0.91},H_{0.09}$-Y: T_r = 380 °C; X_{Dec} = 75 %; $Y_{C_{g^-}}$ = 8 %; $\sum S_j^*$ = 214 %.

$1.7Pt/Na_{0.91},H_{0.09}$-Y: T_r = 382 °C; X_{Dec} = 86 %; $Y_{C_{g^-}}$ = 15 %; $\sum S_j^*$ = 202 %.

$0.94Pt/Na_{0.94},H_{0.06}$-Y: T_r = 378 °C; X_{Dec} =50 %; $Y_{C_{g^-}}$ = 2 %; $\sum S_j^*$ = 264 %.

The deactivation on all catalysts is negligible up to 60 h time-on-stream. Hydrocarbons with more than ten carbon atoms are not observed at any time. In Figure 8.10 the selectivities of the differently branched decane isomers for the two catalysts $3.7Pt/Na_{0.86},H_{0.14}$-Y and $1.7Pt/Na_{0.91},H_{0.09}$-Y are depicted. On all Pt/Na,H-Y zeolites nearly the same distribution of OCDs is obtained. In contrast to the Ir/Na,H-Y catalysts, much more methylnonanes are formed. In all cases the sum of the selectivities of n-decane, the methylnonanes and the ethyloctanes is at least equal to or even higher than that of the multibranched decanes which is much more favorable in view of an enhancement of the cetane number.

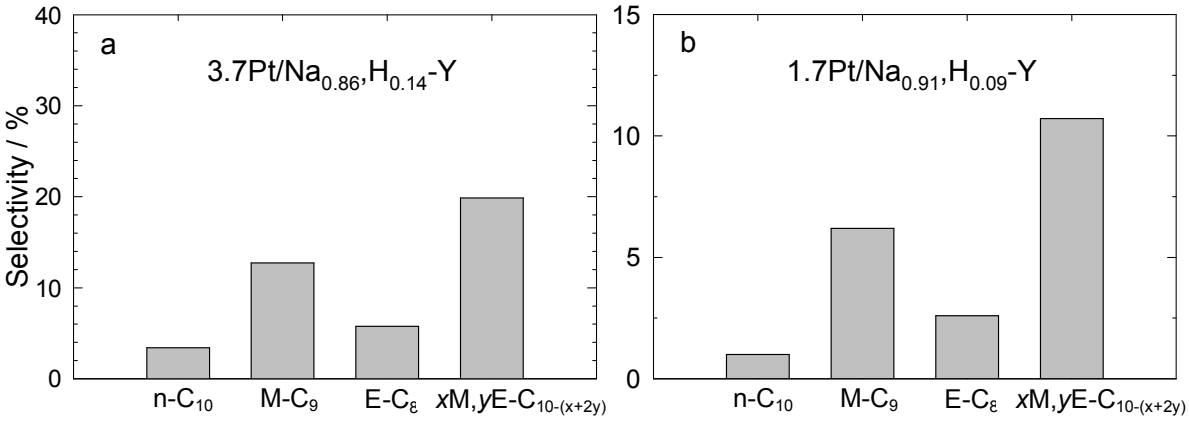

Figure 8.10: Breakdown of the selectivities of OCDs into differently branched decanes:
3.7Pt/$Na_{0.86}$,$H_{0.14}$-Y: T_r = 360 °C; X_{Dec} = 98 %; Y_{OCDs} = 41 %; S_{OCDs} = 42 %.
1.7Pt/$Na_{0.91}$,$H_{0.09}$-Y: T_r = 382 °C; X_{Dec} = 86 %; Y_{OCDs} = 18 %; S_{OCDs} = 20 %.

8.1.3 Comparative Studies with Perhydroindan

McVicker *et al.* [82] reported that five-membered rings are much faster to open than six-membered rings. With bicyclo[3.3.0]octane, a hydrocarbon with two five-membered rings, they achieved a high selectivity of open-chain octanes while with perhydroindan and decalin only traces of open-chain nonanes and open-chain decanes, respectively, were formed. The authors suggested that the catalysts need an isomerization function to isomerize the six-membered rings into five-membered rings before the latter can be opened (see Section 4.3.3). The question arose, as to what happens on the best Ir/Na,H-Y and Pt/Na,H-Y catalysts with a hydrocarbon containing a five- and a six-membered ring. Which ring will be opened? Is the ring opening of the five-membered ring really faster and can higher selectivities of open-chain nonanes be achieved than the selectivities of open-chain decanes with decalin?

The catalytic results of the hydroconversion of perhydroindan on the two catalysts 2.9Ir/$Na_{0.90}$,$H_{0.10}$-Y and 3.7Pt/$Na_{0.86}$,$H_{0.14}$-Y are shown in Figure 8.11.

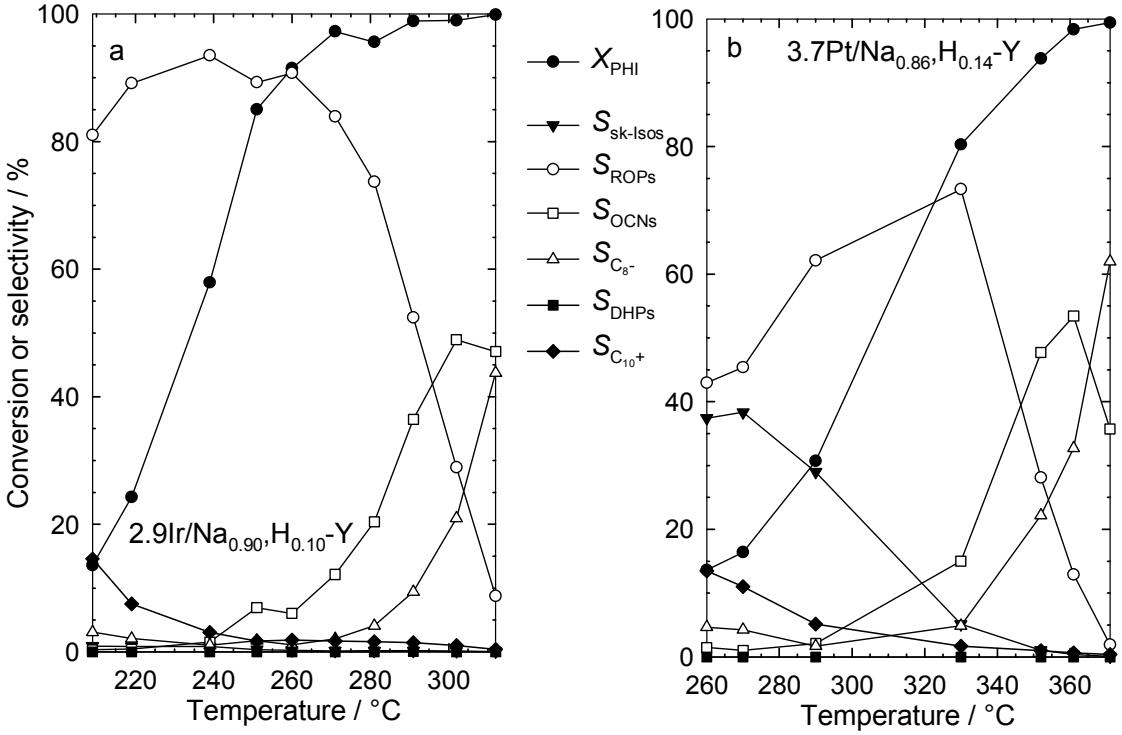

Figure 8.11: Conversion of perhydroindan and selectivities of the different groups of products in dependence of the reaction temperature.

As in case of decalin, on catalyst 2.9Ir/$Na_{0.90}$,$H_{0.10}$-Y no skeletal isomers of perhydroindan are formed. Up to 91 % conversion the ring opening products are prevailing with small amounts of open-chain nonanes. The selectivity of ROPs around 90 % keeps constant in a range of around 40 °C, indicating that this ring opening is very fast and the consecutive steps need much higher temperatures. At even higher conversions the selectivity of ROPs is decreasing and mainly the selectivity of OCNs is increasing. The selectivity of OCNs passes through a maximum of S_{OCNs} = 49 % at 302 °C with a yield of 48 %. The relatively high selectivity of C_{10}+ at low conversion originates from feed impurities, see Section 5.3.1.3.

At low conversion on catalyst 3.7Pt/$Na_{0.86}$,$H_{0.14}$-Y (Figure 8.11b) nearly the same selectivities of skeletal isomers and ring opening products can be observed. At higher conversions the selectivity of skeletal isomers decreases and S_{ROPs} increases up to 80 % conversion. At even higher conversions the selectivity of ROPs sharply decreases, and OCNs are formed. The selectivity of OCNs passes through a maximum of S_{OCNs} = 53 % at 361 °C with a yield of 53 %. Again the relatively high selectivity of C_{10}+ at low conversion originates from feed impurities.

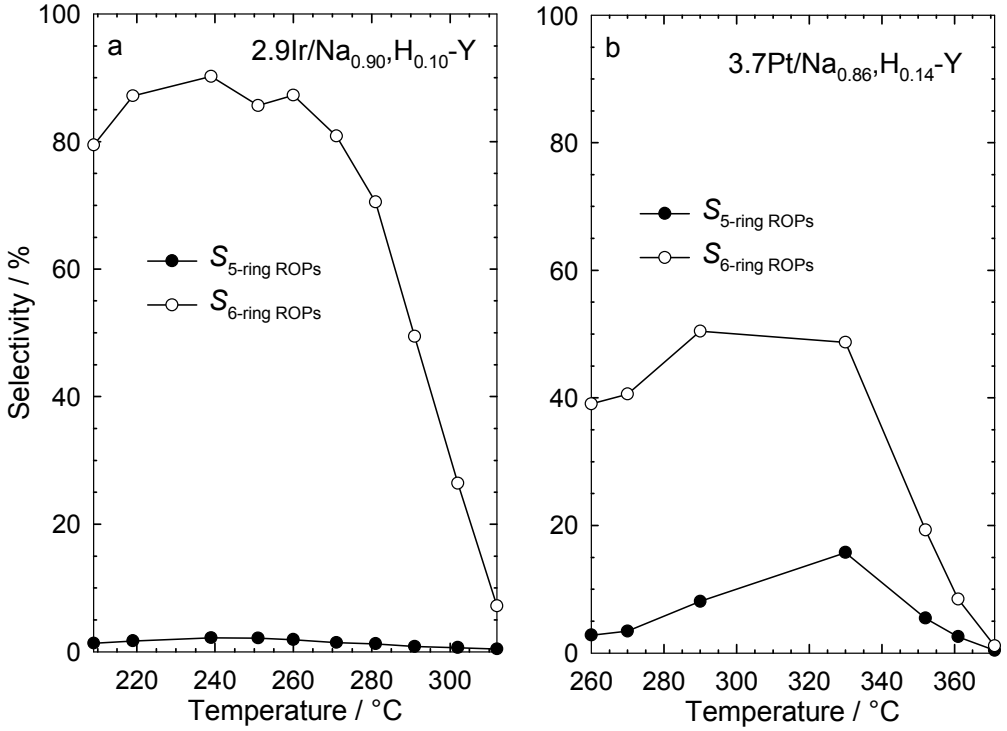

Figure 8.12: Selectivities of 5- and 6-ring ROPs in the hydroconversion of perhydroindan in dependence of the reaction temperature.

In Figure 8.12 the selectivities of ring opening products containing a 5-membered ring (5-ring ROPs) or a 6-membered ring (6-ring ROPs) are plotted. On catalyst 2.9Ir/$Na_{0.90}$,$H_{0.10}$-Y (Figure 8.12a) 6-ring ROPs are almost exclusively formed. This catalyst opens selectively the 5-membered ring in perhydroindan and forms 1-ethyl-2-methylcyclohexane with $S_{1\text{-E-2-M-CHx}}$ = 89 % at 239 °C.

Catalyst 3.7Pt/$Na_{0.86}$,$H_{0.14}$-Y is less selective and tends to form skeletal isomers (Figure 8.11b) which lead to 5-ring ROPs (Figure 8.12b). At 260 °C almost all ROPs contain 6-membered rings. These products can only have arisen from the ring opening of the 5-membered ring in perhydroindan. At higher temperatures the selectivity of 6-ring ROPs shows a plateau, and the selectivity of 5-ring ROPs increases. Simultaneously the selectivity of skeletal isomers (Figure 8.11b) decreases. This fact could indicate that at low temperatures, first the 5-membered ring of perhydroindan is opened. After the isomerization of perhydroindan to skeletal isomers which consist all of two condensed 5-membered rings it is possible to open these 5-membered rings and form 5-ring ROPs and consecutively OCNs. This supports the assumption that 5-membered rings are faster to open than 6-membered rings. On the platinum-containing catalysts the formation of 1-ethyl-2-methylcyclohexane prevails at 290 °C ($S_{1\text{-E-2-M-CHx}}$ = 25 %) but also a high selectivity of propylcyclohexane is detected ($S_{\text{P-CHx}}$ = 20 %).

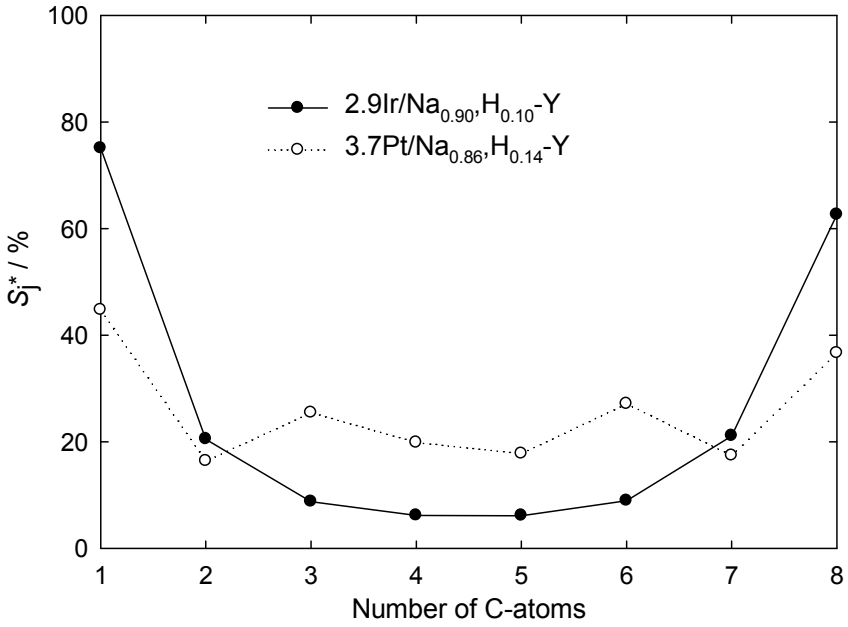

Figure 8.13: Modified hydrocracking selectivities S_j^* in the hydroconversion of perhydroindan on the best Ir/Na,H-Y and Pt/Na,H-Y catalysts:

2.9Ir/$Na_{0.90}$,$H_{0.10}$-Y: T_r = 302 °C; X_{PHI} = 99 %; Y_{C_8-} = 21 %; ΣS_j^* = 209 %.

3.7Pt/$Na_{0.86}$,$H_{0.14}$-Y: T_r = 361 °C; X_{PHI} = 98 %; Y_{C_8-} = 32 %; ΣS_j^* = 205 %.

The modified hydrocracking selectivities on both catalysts are presented in Figure 8.13. Catalyst 2.9Ir/$Na_{0.90}$,$H_{0.10}$-Y shows the hammock-shaped curve which points to carbon-carbon bond cleavage by hydrogenolysis. In contrast, on catalyst 3.7Pt/$Na_{0.86}$,$H_{0.14}$-Y nearly equal amounts of all carbon numbers, except C_1 and C_8, are formed. The distributions of the hydrocracked products on these catalysts, especially on the iridium-containing Y zeolite, are similar to the curves obtained with decalin as a feed.

The breakdown of the selectivities of the open-chain nonanes into differently branched nonanes is presented in Figure 8.14. The iridium-containing catalyst (Figure 8.14a) produces mainly multibranched nonanes like in case of the decane isomers. The nonane isomers on 3.7Pt/$Na_{0.86}$,$H_{0.14}$-Y (Figure 8.14b) consist of relatively large amounts of n-nonane and mono-branched isomers. The total selectivity of OCNs is 53 %. Only one third of these are multibranched isomers which is even better than the results obtained in the hydroconversion of decalin.

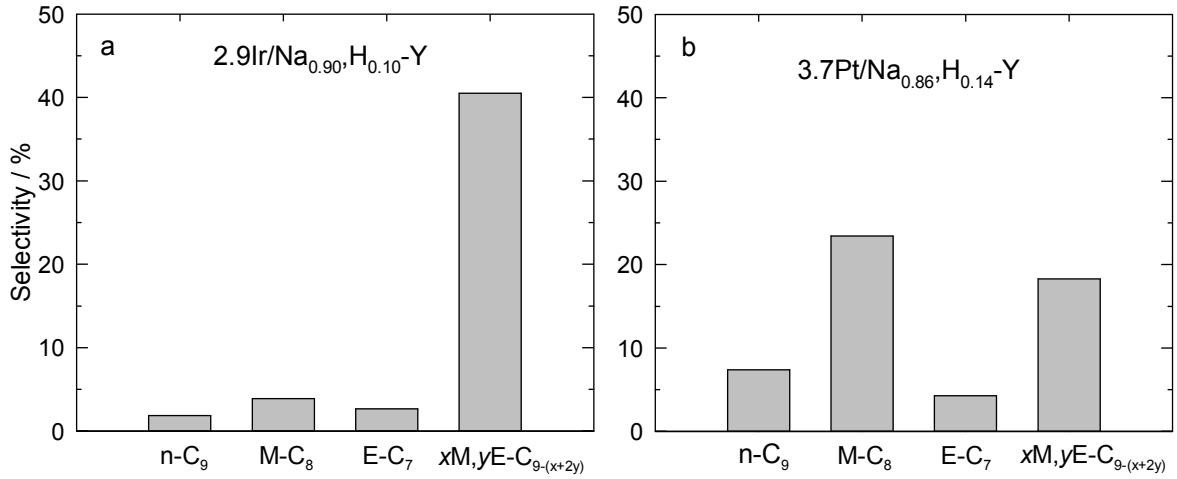

Figure 8.14: Breakdown of the selectivities of OCNs into differently branched nonanes:
2.9Ir/$Na_{0.90}$,$H_{0.10}$-Y: T_r = 302 °C; X_{PHI} = 99 %; Y_{OCNs} = 48 %; S_{OCNs} = 49 %.
3.7Pt/$Na_{0.86}$,$H_{0.14}$-Y: T_r = 361 °C; X_{PHI} = 98 %; Y_{OCNs} = 53 %; S_{OCNs} = 53 %.

The results show that the five-membered ring in perhydroindan on the iridium catalyst is opened very selectively, and much higher temperatures are needed to open also the remaining six-membered ring. On the platinum-containing catalyst also mainly the five-membered ring is opened. In addition, the catalyst can isomerize the six-membered ring into a five-membered ring. On both catalysts much higher selectivities of open-chain nonanes are observed than open-chain decanes from decalin. Again on the platinum-containing catalyst higher selectivities of OCNs are obtained and less multibranched nonanes are formed which have a high impact on the cetane number.

8.2 Influence of the Nature of Alkali Metal Cations

In former studies (Section 8.1) the charge-compensating cations of all catalysts were sodium ions. Since the different electronegativities of the alkali metal cations influence the strength of Brønsted acid sites in the order: Li,H-Y > Na,H-Y > K,H-Y > Rb,H-Y > Cs,H-Y [17-19], investigations were done to ascertain the best charge-compensating cation for the formation of OCDs from decalin. Therefore, iridium- (Section 8.2.1) and platinum-containing (Section 8.2.2) Y catalysts were prepared with 3 wt.-% metal loading which turned out to be an ideal metal content for both kind of metals (Section 8.1).

8.2.1 Iridium-Containing Alkali-Y Catalysts

In Figure 8.15 the results obtained in the hydroconversion of cis-decalin on catalysts 3.0Ir/$Li_{0.68}$,$Na_{0.21}$,$H_{0.11}$-Y (Figure 8.15a) and 2.7Ir/$K_{0.88}$,$H_{0.12}$-Y (Figure 8.15b) are depicted. The performances of catalysts 2.6Ir/$Rb_{0.70}$,$Na_{0.15}$,$H_{0.15}$-Y and 2.6Ir/$Cs_{0.71}$,$Na_{0.16}$,$H_{0.13}$-Y are not shown because they resemble those of catalyst 2.7Ir/$K_{0.88}$,$H_{0.12}$-Y. The varying strength of the Brønsted acid sites has only a minor influence on the activity of the catalysts which will be discussed together with the results of the platinum-containing catalysts in Section 8.2.2. On the potassium-, rubidium- and cesium-containing catalysts almost exclusively ring opening products are found, the selectivity of skeletal isomers is negligible and even less than on the sodium-containing catalyst (Section 8.1.1, Figure 8.2). At higher conversions the selectivities of ROPs decrease, and the formation of hydrocracked products becomes prevailing. The selectivity of open-chain decanes is much lower than on the Ir/Na,H-Y catalyst. The highest yield of OCDs among these three catalysts is observed on catalyst 2.6Ir/$Rb_{0.70}$,$Na_{0.15}$,$H_{0.15}$-Y with 11.1 % at 97.0 % conversion (Table 8.3) which is much less than the yield of 30.7 % obtained on catalyst 2.9Ir/$Na_{0.90}$,$H_{0.10}$-Y.

Table 8.3: Maximum yields of open-chain decanes obtained on the iridium-containing alkali-Y catalysts.

Catalyst	T_r / °C	X_{Dec} / %	S_{OCDs} / %	$Y_{OCDs,\ max.}$ / %	Y_{OCNs} / %	Y_{C_9-} / %
3.0Ir/$Li_{0.68}$,$Na_{0.21}$,$H_{0.11}$-Y	299	82.1	32.6	26.8	5.8	28.9
2.9Ir/$Na_{0.90}$,$H_{0.10}$-Y	300	86.2	35.7	30.7	7.2	24.6
2.7Ir/$K_{0.88}$,$H_{0.12}$-Y	309	89.4	11.7	10.5	15.5	44.4
2.6Ir/$Rb_{0.70}$,$Na_{0.15}$,$H_{0.15}$-Y	309	97.0	11.4	11.1	24.0	60.6
2.6Ir/$Cs_{0.71}$,$Na_{0.16}$,$H_{0.13}$-Y	319	85.1	8.0	6.8	18.1	53.6

In contrast, at low conversion on catalyst 3.0Ir/$Li_{0.68}$,$Na_{0.21}$,$H_{0.11}$-Y (Figure 8.15a) only slightly more ring opening products than skeletal isomers are formed. The lithium-containing catalyst shows a higher isomerization tendency than the Ir/Na,H-Y catalyst. At higher conversions the selectivities of ROPs and sk-Isos decrease. The selectivities of OCDs pass through a maximum at 290 °C with X_{Dec} = 72 % and S_{OCDs} = 34 %. The maximum yield of open-chain decanes is only slightly lower than the one observed on 2.9Ir/$Na_{0.90}$,$H_{0.10}$-Y (Table 8.3). A variation of the charge-compensating cation could not improve the good performance of 2.9Ir/$Na_{0.90}$,$H_{0.10}$-Y. The lithium form shows a good performance, too, but it could not enhance the yield of open-chain decanes. The incorporation of K, Rb or Cs, leading to a lower strength of Brønsted acid sites, brings about a strong decrease of the yield of OCDs.

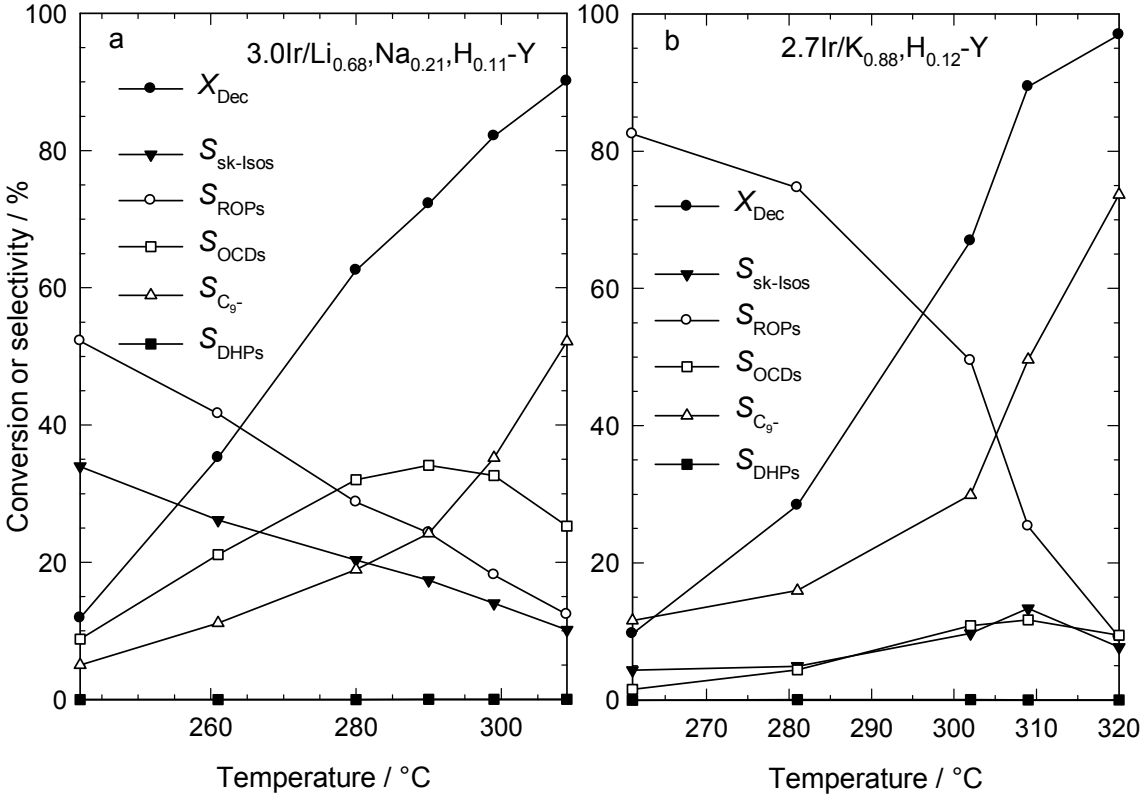

Figure 8.15: Conversion of decalin and selectivities of different groups of products in dependence of the reaction temperature for two iridium-containing zeolite Y catalysts with different alkali cations.

Some peculiarities can be observed on the potassium-, rubidium- and cesium-containing catalysts. Usually, the first product formed from cis- and trans-decalin is a skeletal isomer directly next to trans-decalin in the gas chromatogram (Figure 8.16), which is assigned by GC/MS to spiro[4.5]decane. This assignment, however, is not safe, since the GC/MS proposes the spiro compound also for two other signals in the chromatogram. This signal is observed on the lithium and sodium form as well as on all catalysts from Section 8.1. With the potassium-, rubidium- and cesium- containing catalysts this product is not formed at all at any temperature. The chromatograms obtained at low conversion consist mainly of the primary ring opening products of decalin, namely cis- and trans-1,2-diethylcyclcohexane, cis- and trans-1-methyl-2-propylcyclohexane and butylcyclohexane. At higher conversion significant amounts of open-chain nonanes are formed with maximal yields of up to 24 %. The appearance or the absence of the spiro[4.5]decane signal and the possible mechanisms involved on this kind of catalysts will be discussed in Section 8.6.

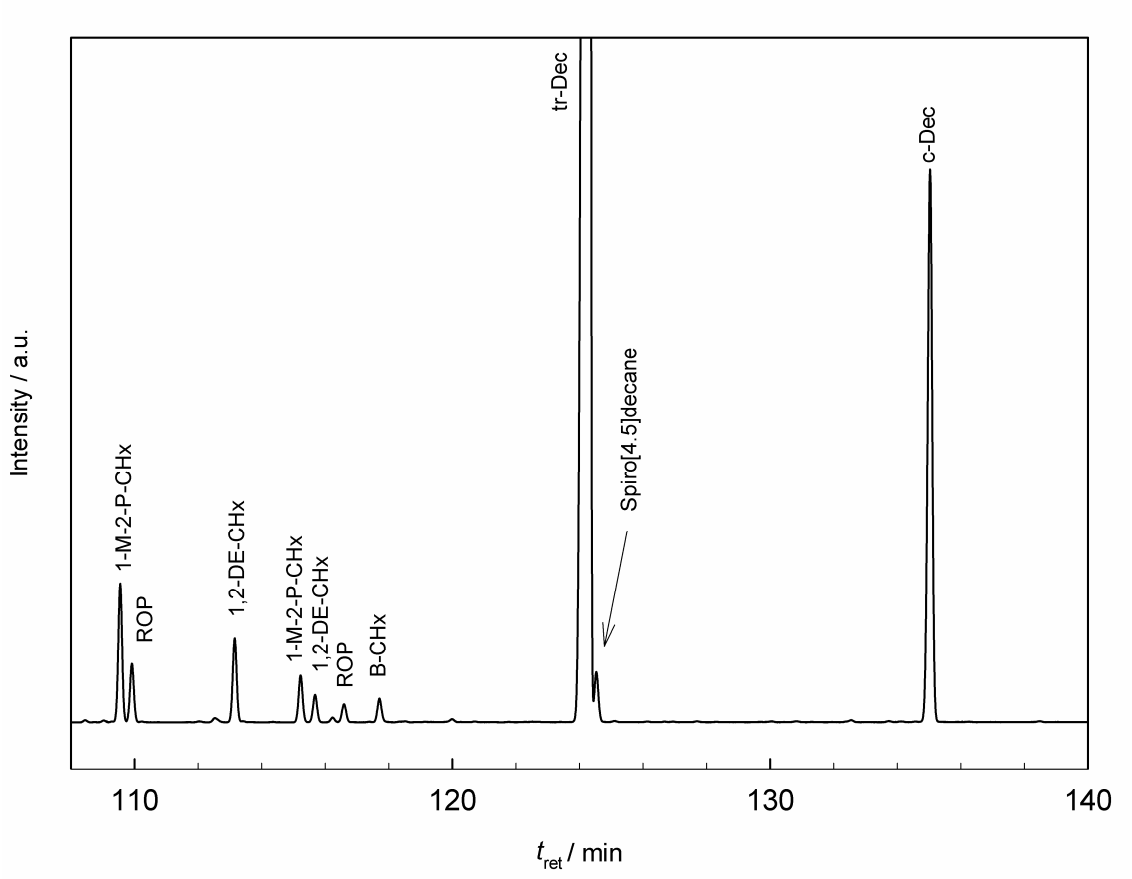

Figure 8.16: Extraction of the gas chromatogram of the product of cis-decalin hydroconversion on 2.9Ir/$Na_{0.90}$,$H_{0.10}$-Y at T_r = 239 °C and X_{Dec} = 7.1 %.

In Figure 8.17, the carbon number distributions of the hydrocracked products on the iridium-containing alkali-Y catalysts are given. Except for the distribution for the lithium-exchanged zeolite Y all curves are hammock-shaped which clearly points to carbon-carbon bond cleavage by hydrogenolysis as observed on the Ir/Na,H-Y catalysts with a high metal content (Section 8.1.1). The curve of 3.0Ir/$Li_{0.68}$,$Na_{0.21}$,$H_{0.11}$-Y shows an almost equal distribution of all carbon numbers between C_2 and C_8 with a strong contribution of hydrogenolysis leading to C_1 and C_9. Moreover, one could receive the impression that the fraction of C_4 and C_6 is slightly favored which could be a hint for a minor contribution of bifunctional catalysis. A closer look at the molar amount of iso-butane and methylcyclopentane shows, however, that in the whole temperature range the molar amount of iso-butane is at least ten times as high as that of methylcyclopentane.

The distributions of the selectivities of the decane isomers resemble that of 3.8Ir/$Na_{0.89}$,$H_{0.11}$-Y given in Figure 8.5 (Section 8.1.1). No deactivation was observed within 40 h on the potassium-, rubidium- and cesium-containing catalysts. In contrast, very mild deactivation occurred on catalyst 3.0Ir/$Li_{0.68}$,$Na_{0.21}$,$H_{0.11}$-Y.

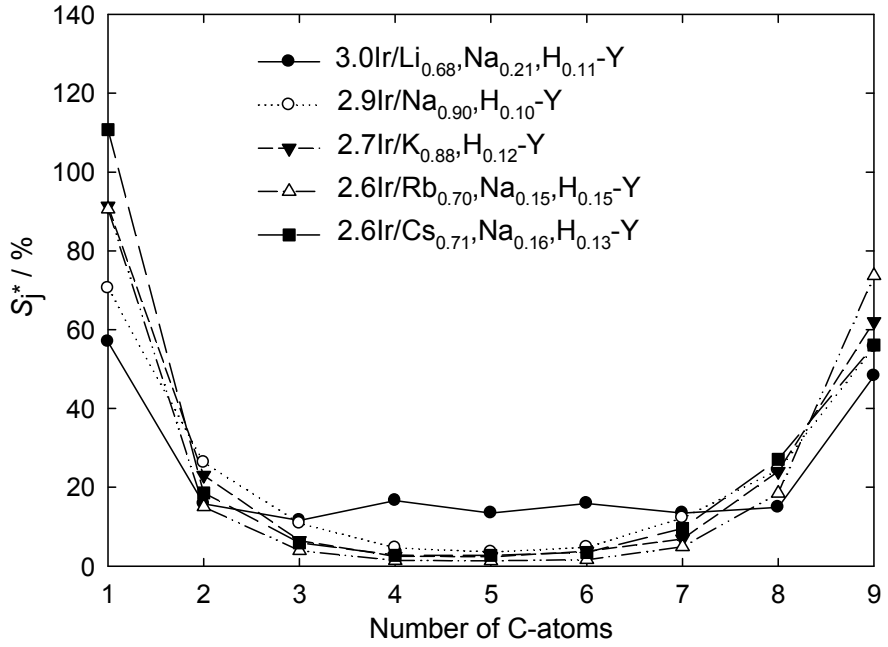

Figure 8.17: Modified hydrocracking selectivities S_j* on the iridium-containing alkali-Y catalysts:

3.0Ir/$Li_{0.68}$,$Na_{0.21}$,$H_{0.11}$-Y: T_r = 290 °C; X_{Dec} = 72 %; $Y_{C_{9-}}$ = 18 %; $\sum S_j^*$ = 207 %.

2.9Ir/$Na_{0.90}$,$H_{0.10}$-Y: T_r = 300 °C; X_{Dec} = 86 %; $Y_{C_{9-}}$ = 24 %; $\sum S_j^*$ = 217 %.

2.7Ir/$K_{0.88}$,$H_{0.12}$-Y: T_r = 309 °C; X_{Dec} = 89 %; $Y_{C_{9-}}$ = 42 %; $\sum S_j^*$ = 229 %.

2.6Ir/$Rb_{0.70}$,$Na_{0.15}$,$H_{0.15}$-Y: T_r = 299 °C; X_{Dec} = 86 %; $Y_{C_{9-}}$ = 33 %; $\sum S_j^*$ = 219 %.

2.6Ir/$Cs_{0.71}$,$Na_{0.16}$,$H_{0.13}$-Y: T_r = 319 °C; X_{Dec} = 85 %; $Y_{C_{9-}}$ = 51 %; $\sum S_j^*$ = 243 %.

8.2.2 Platinum-Containing Alkali-Y Catalysts

The conversion of decalin on all platinum-containing alkali-Y catalysts in comparison to the iridium-containing counterparts is depicted in Figure 8.18. The activity of the platinum-containing catalysts (Figure 8.18b) decreases in the same order as the strength of Brønsted acid sites does, namely Pt/Li,Na,H-Y > Pt/Na,H-Y > Pt/K,H-Y > Pt/Rb,Na,H-Y > Pt/Cs,Na,H-Y. The difference in the activities of the lithium, sodium and potassium catalysts is large, whereas the activities of the potassium, rubidium and cesium catalysts are similar. In comparison to the platinum-containing catalysts, the activity of the iridium-containing catalysts is less influenced by the strength of Brønsted acid sites. All platinum-containing catalysts have nearly the same metal loading of 3 wt.-%, and the metal dispersions are comparable. Since the concentrations of Brønsted acid sites generated during the reduction of the noble metal are also the same in all five catalysts, the change in the activity of the

catalysts is probably due to the change in the strength of Brønsted acid sites. With a lower strength also the activity drops. The greater change in the activity of the platinum-containing catalysts denotes that the Brønsted acid sites have a higher influence in the hydroconversion of decalin than in the catalyst loaded with iridium which is presumably due to the higher hydrogenolysis activity of iridium in comparison to platinum. Since the strength of Brønsted acid sites has nearly no influence on the activity of the potassium-, rubidium- and cesium-containing Pt/Y zeolites, these catalysts seem to be pure hydrogenolysis ones.

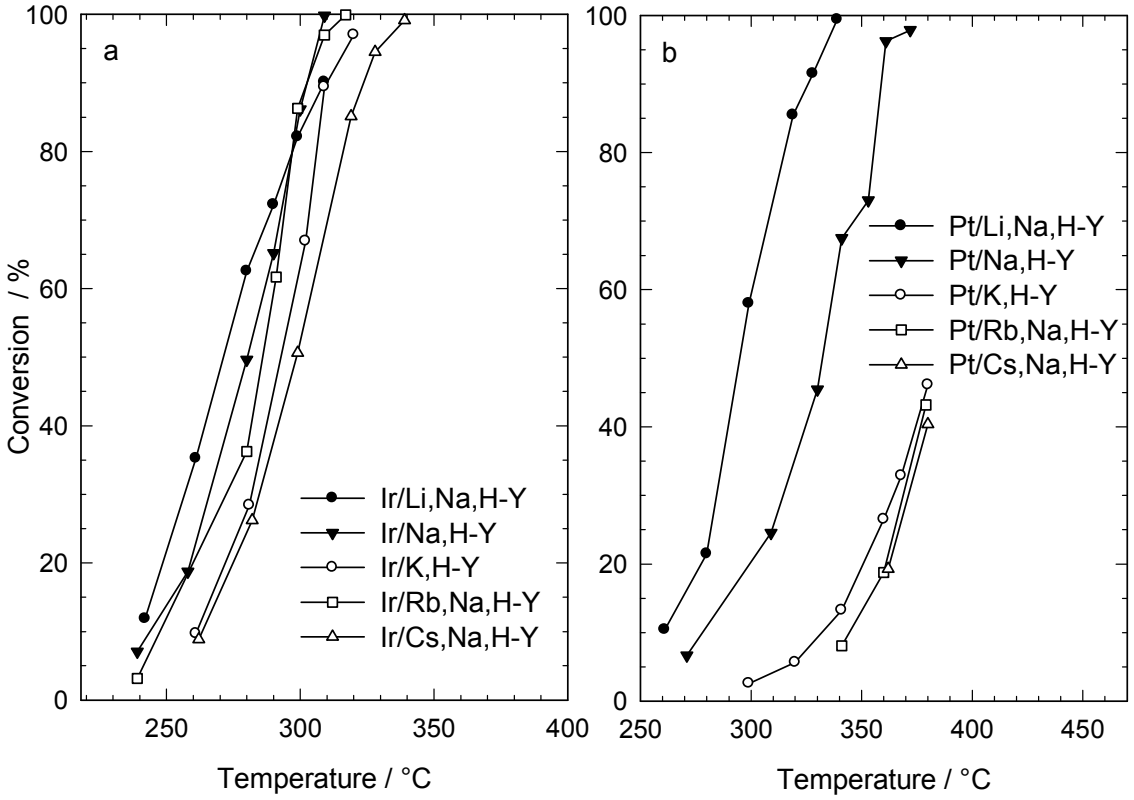

Figure 8.18: Dependence of the decalin conversion on the reaction temperature for the iridium- and platinum-containing zeolite Y catalysts with different alkali cations.

In Figure 8.19, the selectivities obtained in the hydroconversion of cis-decalin on the alkaline-exchanged Pt/Y catalysts are depicted. With decreasing activity the selectivities of the dehydrogenated products tetralin and naphthalene are increasing. On 3.1Pt/$Cs_{0.71}$,$Na_{0.16}$,$H_{0.13}$-Y the products consist to 60 % of tetralin and naphthalene. The amount of tetralin is consistent with the thermodynamic equilibrium, but the amount of naphthalene is too high. The activity of the catalysts 2.9Pt/$K_{0.90}$,$H_{0.10}$-Y, 2.9Pt/$Rb_{0.68}$,$Na_{0.15}$,$H_{0.17}$-Y and 3.1Pt/$Cs_{0.71}$,$Na_{0.16}$,$H_{0.13}$-Y is so low that only a conversion of approximately 40 % is reached at the maximal possible temperature of 380 °C. Only traces of OCDs are obtained on these three catalysts.

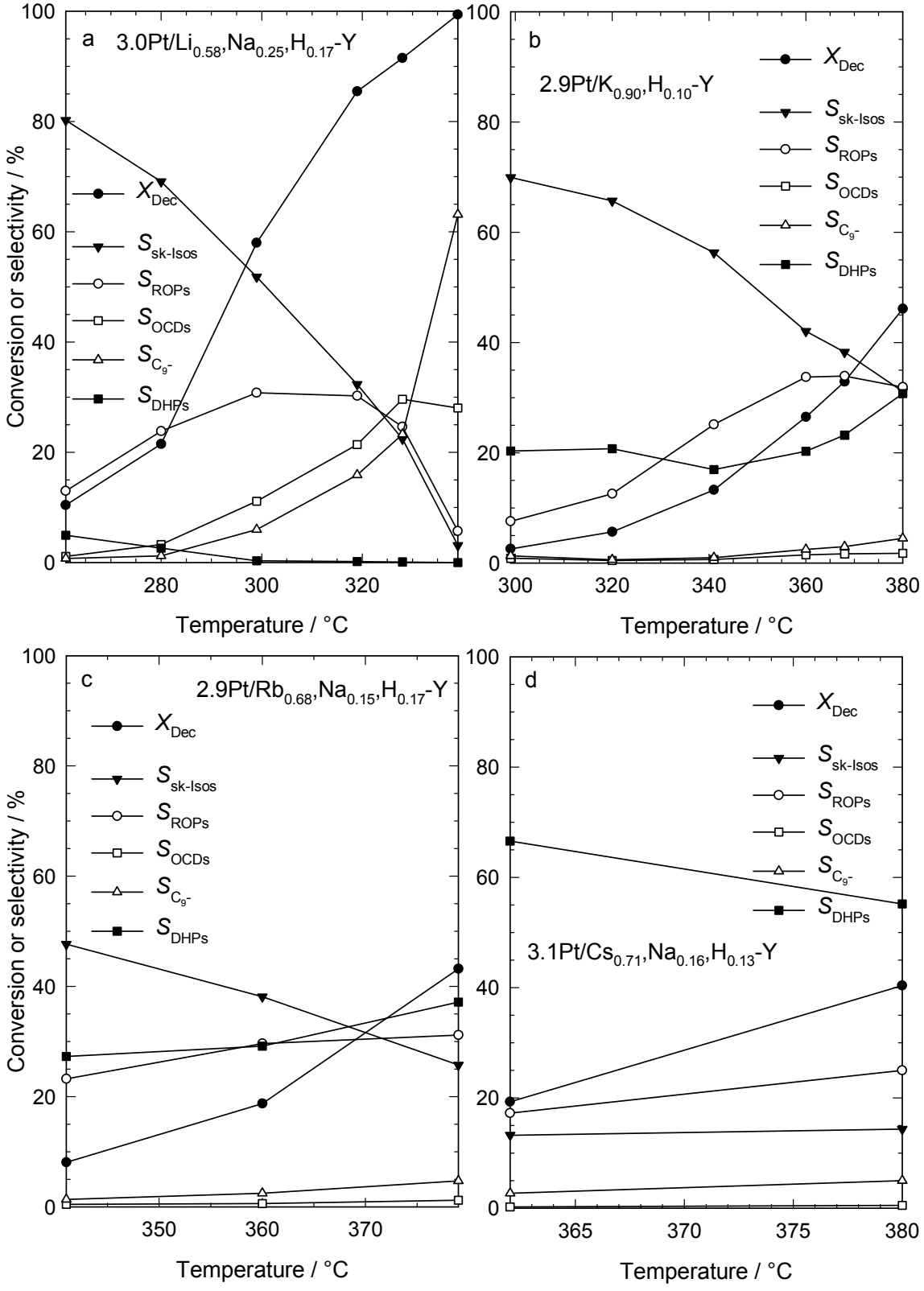

Figure 8.19: Conversion of decalin and selectivities of different groups of products in dependence of the reaction temperature for platinum-containing zeolite Y catalysts with different alkali cations.

The highest selectivity of OCDs is observed on catalyst 3.0Pt/$Li_{0.58}$,$Na_{0.25}$,$H_{0.17}$-Y, namely 30 %. Nevertheless, the performance of the sodium-exchanged catalyst 3.0Pt/$Na_{0.88}$,$H_{0.12}$-Y (Section 8.1.2) is significantly better with a selectivity and yield of OCDs of 41 and 39 %, respectively. An overview of the maximal selectivities of OCDs on all catalysts of this series is given in Table 8.4.

Table 8.4: Maximum yields of open-chain decanes obtained on the platinum-containing alkali-Y catalysts.

Catalyst	T_r / °C	X_{Dec} / %	S_{OCDs} / %	$Y_{OCDs, max.}$ / %	Y_{OCNs} / %	Y_{C_9-} / %
3.0Pt/$Li_{0.58}$,$Na_{0.25}$,$H_{0.17}$-Y	328	91.5	29.6	27.1	1.1	21.3
3.0Pt/$Na_{0.88}$,$H_{0.12}$-Y	361	96.3	40.7	39.1	3.9	32.8
2.9Pt/$K_{0.90}$,$H_{0.10}$-Y	380	46.1	1.8	0.8	-	2.1
2.9Pt/$Rb_{0.68}$,$Na_{0.15}$,$H_{0.17}$-Y	379	43.2	1.2	0.5	-	2.0
3.1Pt/$Cs_{0.71}$,$Na_{0.16}$,$H_{0.13}$-Y	380	40.4	0.5	0.2	-	2.0

On the alkaline-exchanged Y zeolites loaded with iridium no spiro[4.5]decane is formed on the potassium, rubidium and cesium catalysts. In case of platinum all catalysts do form the spiro compound. Only on 3.1Pt/$Cs_{0.71}$,$Na_{0.16}$,$H_{0.13}$-Y much less spiro[4.5]decane is formed. This difference to the iridium-containing catalysts could perhaps be a hint that platinum is able to isomerize decalin in small quantities into the spiro compound.

The carbon number distributions of the hydrocracked products are depicted in Figure 8.20. The distribution of catalyst 3.0Pt/$Li_{0.58}$,$Na_{0.25}$,$H_{0.17}$-Y resembles the one of 3.0Pt/$Na_{0.88}$,$H_{0.12}$-Y even though the M-shape is more pronounced on catalyst 3.0Pt/$Li_{0.58}$,$Na_{0.25}$,$H_{0.17}$-Y. The other three catalysts with a lower activity show pronounced secondary hydrocracking leading to large amounts of methane and unsymmetrical curves indicated also by $\sum S_j^*$ of nearly 300 %.

The distribution of the selectivities of the decane isomers on 3.0Pt/$Li_{0.58}$,$Na_{0.25}$,$H_{0.17}$-Y resembles that of 3.7Pt/$Na_{0.86}$,$H_{0.14}$-Y given in Figure 8.10 (Section 8.1.2).

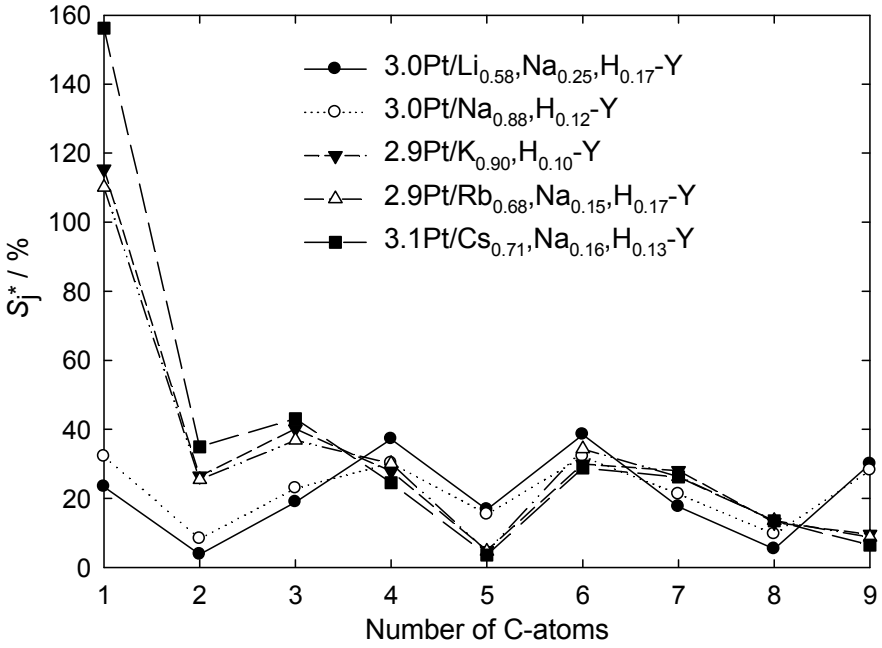

Figure 8.20: Modified hydrocracking selectivities S_j^* on the platinum-containing alkali-Y catalysts:

3.0Pt/$Li_{0.58}$,$Na_{0.25}$,$H_{0.17}$-Y: T_r =328 °C; X_{Dec} =92 %; $Y_{C_{9^-}}$ = 21 %; $\sum S_j^*$ = 191 %.

3.0Pt/$Na_{0.88}$,$H_{0.12}$-Y: T_r =361 °C; X_{Dec} =96 %; $Y_{C_{9^-}}$ = 33 %; $\sum S_j^*$ = 200 %.

2.9Pt/$K_{0.90}$,$H_{0.10}$-Y: T_r =380 °C; X_{Dec} =46 %; $Y_{C_{9^-}}$ = 2 %; $\sum S_j^*$ = 295 %.

2.9Pt/$Rb_{0.68}$,$Na_{0.15}$,$H_{0.17}$-Y: T_r =379 °C; X_{Dec} =43 %; $Y_{C_{9^-}}$ = 2 %; $\sum S_j^*$ = 290 %.

3.1Pt/$Cs_{0.71}$,$Na_{0.16}$,$H_{0.13}$-Y: T_r =380 °C; X_{Dec} =40 %; $Y_{C_{9^-}}$ = 2 %; $\sum S_j^*$ = 337 %.

8.3 Influence of the n_{Si} / n_{Al} Ratio

In the preceding section, the strength of the Brønsted acid sites was varied by using different charge-compensating cations. In addition, the n_{Si} / n_{Al} ratio of zeolites has an impact on the strength of Brønsted acid sites. Based on the next nearest neighbor theory (see Section 4.1), the strength of Brønsted acid sites should increase from LSX over X to Y and should be even higher in the dealuminated Y zeolites. FAU zeolites with different n_{Si} / n_{Al} ratios and a metal loading of 3 wt.-% iridium or platinum and sodium as charge-compensating cation were prepared and tested in the hydroconversion of decalin.

8.3.1 Iridium-Containing FAU Catalysts

As shown in the previous Section 8.2 for alkali-Y zeolites the strength of Brønsted acid sites has an influence on the activity of the catalysts in the hydroconversion of decalin. With increasing n_{Si} / n_{Al} ratio and hence increasing strength of the Brønsted acid sites the activity of the catalysts increases, only catalyst 3.1Ir/$Na_{0.77}$,$H_{0.23}$-Y-5.49 has a lower activity as expected (Figure 8.21). The large difference in the activity between the LSX (n_{Si} / n_{Al} = 1.01) and X (n_{Si} / n_{Al} = 1.21) catalysts on the one hand and the catalysts with an n_{Si} / n_{Al} ratio between 2.41 and 5.49 could demonstrate that the Brønsted acid sites play a minor role in the former catalysts.

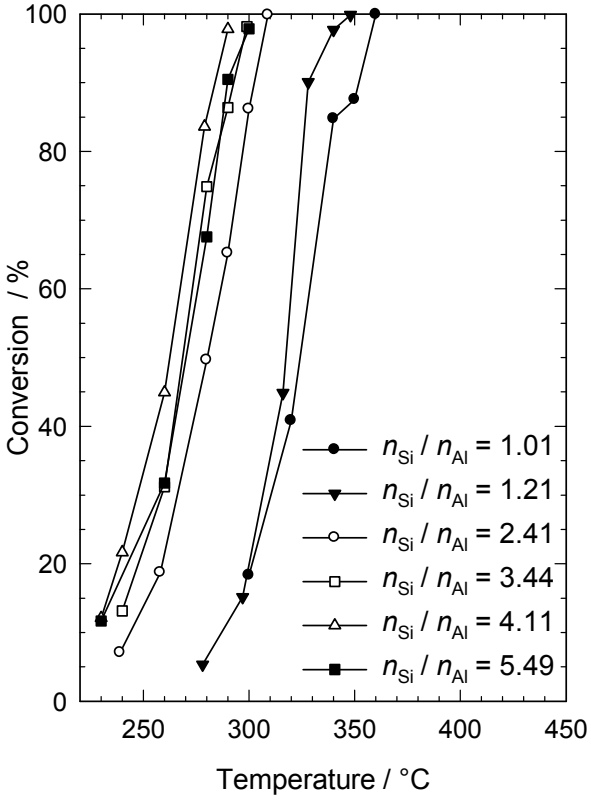

Figure 8.21: Dependence of the decalin conversion on the reaction temperature for iridium-containing faujasite-type catalysts with different n_{Si} / n_{Al} ratios.

In Figure 8.22 the selectivities obtained in the hydroconversion of cis-decalin are depicted for two catalysts from this series. At low conversions the formation of ring opening products is prevailing on all catalysts, as it seems to be typical for iridium-containing catalysts. The selectivity of skeletal isomers at low conversions increases with increasing n_{Si} / n_{Al} ratio indicating a higher isomerization tendency on catalysts with stronger Brønsted acid sites. The performance of the catalyst 2.9Ir/$Na_{0.90}$,$H_{0.10}$-Y could be improved by enhancing the strength of Brønsted acid sites. The highest yield of open-chain decanes is observed on

catalyst 3.2Ir/$Na_{0.81}$,$H_{0.19}$-Y-4.11 with 39.1 % and, in addition, a yield of open-chain nonanes of 10.5 %. With even stronger Brønsted acid sites the yield of OCDs decreases again (Table 8.5).

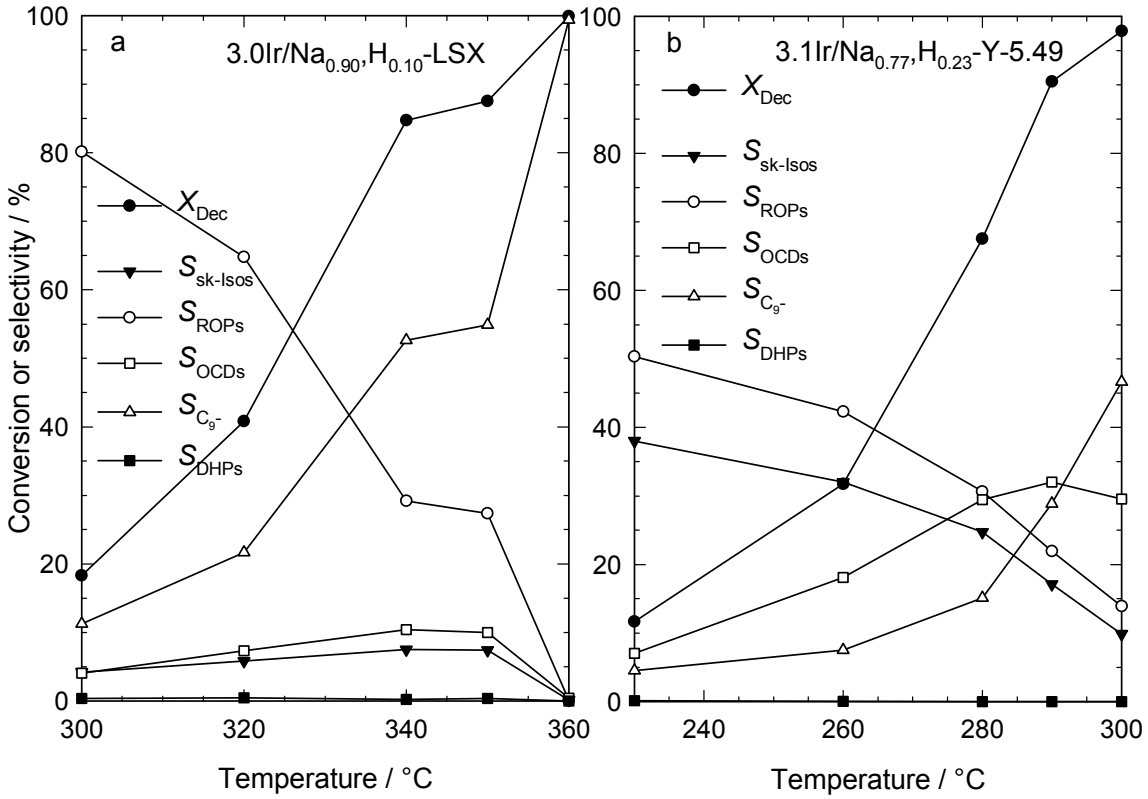

Figure 8.22: Conversion of decalin and selectivities of different groups of products in dependence of the reaction temperature for iridium-containing FAU catalysts with an n_{Si} / n_{Al} ratio of 1.01 (LSX) and 5.49.

Table 8.5: Maximum yields of open-chain decanes obtained on FAU catalysts with different n_{Si} / n_{Al} ratios and 3 wt.-% iridium.

Catalyst	T_r / °C	X_{Dec} / %	S_{OCDs} / %	$Y_{OCDs, max.}$ / %	Y_{OCNs} / %	Y_{C_9-} / %
3.0Ir/$Na_{0.90}$,$H_{0.10}$-LSX	340	84.7	10.4	8.8	10.2	44.6
2.5Ir/$Na_{0.91}$,$H_{0.09}$-X	328	90.1	22.4	20.2	12.3	44.5
2.9Ir/$Na_{0.90}$,$H_{0.10}$-Y	300	86.2	35.7	30.7	7.2	24.6
3.3Ir/$Na_{0.88}$,$H_{0.12}$-Y-3.44	299	98.2	38.6	37.9	13.0	43.6
3.2Ir/$Na_{0.81}$,$H_{0.19}$-Y-4.11	290	97.8	40.0	39.1	10.5	39.3
3.1Ir/$Na_{0.77}$,$H_{0.23}$-Y-5.49	290	90.5	32.0	29.0	3.7	26.1

On catalyst 3.0Ir/$Na_{0.90}$,$H_{0.10}$-LSX the signal of the skeletal isomer spiro[4.5]decane could not be observed over the whole temperature range. Again, as described for the potassium-,

rubidium- and cesium-containing Ir/Y catalysts (Section 8.2.1) the first products observed are the products of direct ring opening of decalin, namely cis-/trans-1-methyl-2-propylcylohexane, cis-/trans-1,2-diethylcyclohexane and butylcyclohexane. All catalysts on which the absence of the spiro compound was observed have a low strength of Brønsted acid sites in common. A deeper discussion about the envisaged mechanism on this kind of catalysts is presented in Section 8.6.

On catalysts with a higher n_{Si} / n_{Al} ratio than 1.01 the selectivity of spiro[4.5]decane at conversions between 12 and 19 % increases with increasing n_{Si} / n_{Al} ratio (Table 8.6). In the same order the maximum selectivity of open-chain decanes increases as well. In Figure 8.23, the maximum achieved selectivities of OCDs are plotted against the selectivity of spiro[4.5]decane at low conversion. The higher the selectivity of spiro[4.5]decane (up to 10 %) the higher the selectivity of OCDs at high conversions. After a strong increase of the curve a plateau is reached around 40 % selectivity and at even higher selectivities of spiro[4.5]decane the selectivity of OCDs is decreasing.

Table 8.6: Comparison of the selectivity of spiro[4.5]decane S_{spiro} on the iridium-containing FAU catalysts at low conversion.

Catalyst	T_r / °C	X_{Dec} / %	S_{spiro} / %
3.0Ir/$Na_{0.90}$,$H_{0.10}$-LSX	300	18.3	0.0
2.5Ir/$Na_{0.91}$,$H_{0.09}$-X	297	15.2	0.7
2.9Ir/$Na_{0.90}$,$H_{0.10}$-Y	258	18.7	4.6
3.3Ir/$Na_{0.88}$,$H_{0.12}$-Y-3.44	240	13.2	7.5
3.2Ir/$Na_{0.81}$,$H_{0.19}$-Y-4.11	230	12.1	9.8
3.1Ir/$Na_{0.77}$,$H_{0.23}$-Y-5.49	230	11.7	17.4

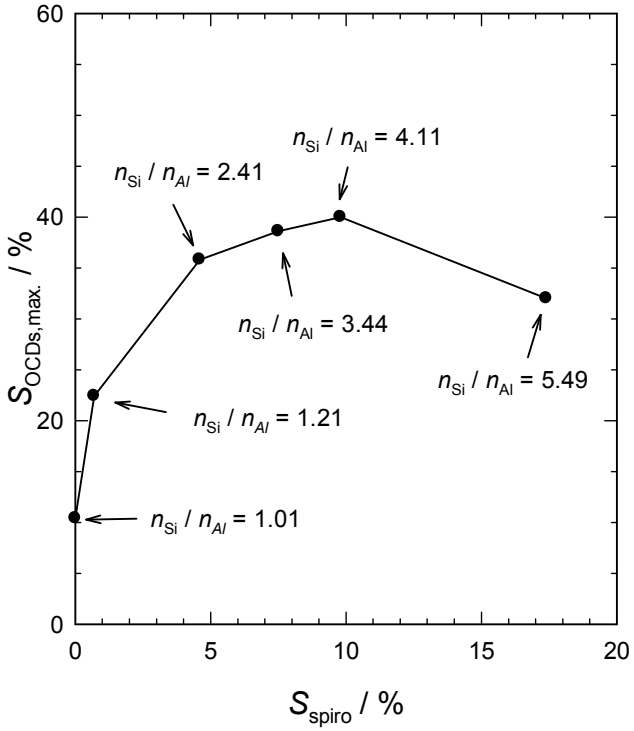

Figure 8.23: Maximum selectivities of open-chain decanes versus selectivity of spiro[4.5]decane at X_{Dec} = 12 to 19 % on the iridium-containing FAU catalysts. The n_{Si} / n_{Al} ratios of the different faujasite catalysts are also given.

In Figure 8.24, the carbon number distributions of the hydrocracked products are given. The distributions for catalysts with an n_{Si} / n_{Al} ratio of 1.01 to 2.41 consist of hammock-shaped curves typical for hydrogenolysis. With higher n_{Si} / n_{Al} ratios the selectivities of C_4, C_5 and C_6 are increasing leading to a nearly equal distribution of C_2 to C_8. C_1 and C_9 are formed with the highest selectivities. On catalyst 3.1Ir/$Na_{0.77}$,$H_{0.23}$-Y-5.49 the strength of the Brønsted acid sites seems to be so high that bifunctional catalysis takes place leading to high selectivities of C_4 and C_6 overlapped by hydrogenolysis leading to C_1 and C_9.

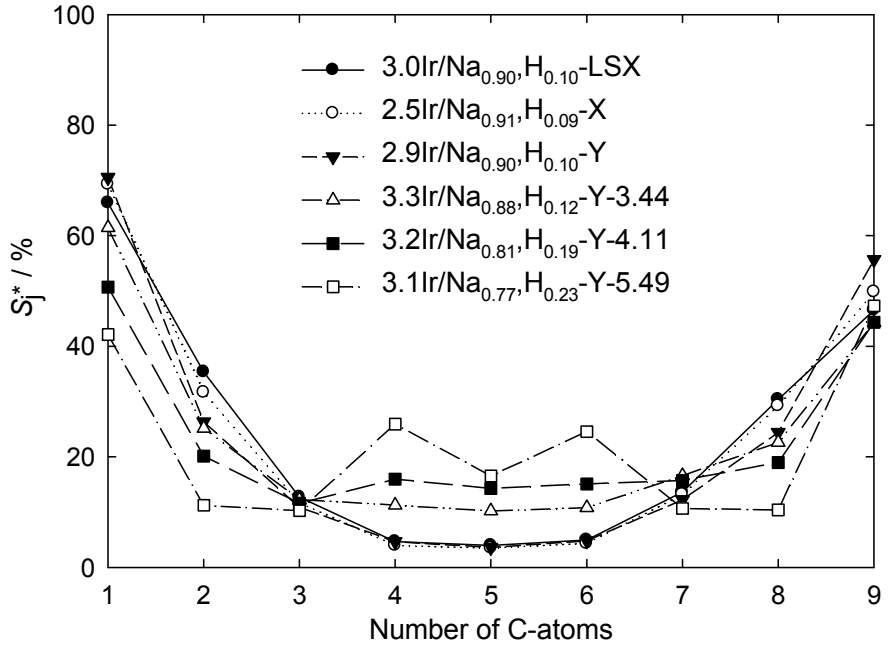

Figure 8.24: Modified hydrocracking selectivities S_j^* on the iridium-containing FAU catalysts with different n_{Si} / n_{Al} ratios:

3.0Ir/$Na_{0.90}$,$H_{0.10}$-LSX: T_r = 340 °C; X_{Dec} = 85 %; $Y_{C_{9^-}}$ = 42 %; $\sum S_j^*$ = 222 %.

2.5Ir/$Na_{0.91}$,$H_{0.09}$-X: T_r = 328 °C; X_{Dec} = 90 %; $Y_{C_{9^-}}$ = 43 %; $\sum S_j^*$ = 219 %.

2.9Ir/$Na_{0.90}$,$H_{0.10}$-Y: T_r = 300 °C; X_{Dec} = 86 %; $Y_{C_{9^-}}$ = 24 %; $\sum S_j^*$ = 217 %.

3.3Ir/$Na_{0.88}$,$H_{0.12}$-Y-3.44: T_r = 299 °C; X_{Dec} = 98 %; $Y_{C_{9^-}}$ = 44 %; $\sum S_j^*$ = 212 %.

3.2Ir/$Na_{0.81}$,$H_{0.19}$-Y-4.11: T_r = 290 °C; X_{Dec} = 98 %; $Y_{C_{9^-}}$ = 39 %; $\sum S_j^*$ = 204 %.

3.1Ir/$Na_{0.77}$,$H_{0.23}$-Y-5.49: T_r = 290 °C; X_{Dec} = 91 %; $Y_{C_{9^-}}$ = 25 %; $\sum S_j^*$ = 198 %.

8.3.2 Platinum-Containing FAU Catalysts

As with the iridium-containing FAU catalysts with different n_{Si} / n_{Al} ratios the activity of the platinum-containing FAU catalysts increases with increasing n_{Si} / n_{Al} ratio and hence increasing strength of the Brønsted acid sites (Figure 8.25). Again the catalysts with an n_{Si} / n_{Al} ratio of 1.01 and 1.21 are much less active than the catalysts with a higher ratio. On these catalysts mainly dehydrogenated products are formed as also observed on the low-activity potassium-, rubidium- or cesium-containing Pt/Y catalysts (Section 8.2.2). A few skeletal isomers are formed but much less than typically observed on Pt/Na-Y catalysts (Section 8.1.2). The selectivities of the catalysts with a higher n_{Si} / n_{Al} ratio than 1.21 in the hydroconversion of decalin are depicted in Figure 8.26 on the representative 3.0Pt/$Na_{0.89}$,$H_{0.11}$-Y-3.44.

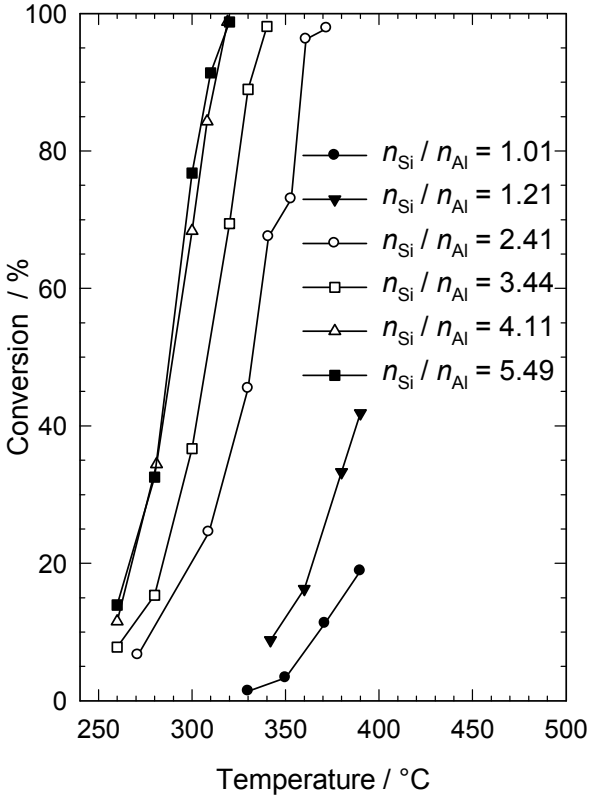

Figure 8.25: Dependence of the decalin conversion on the reaction temperature for platinum-containing faujasite-type catalysts with different n_{Si} / n_{Al} ratios.

The three dealuminated Y catalysts with stronger Brønsted acid sites than in 3.0Pt/$Na_{0.88}$,$H_{0.12}$-Y show similar behaviors as the latter one (see Section 8.1.2), *i. e*. skeletal isomers are prevailing at low conversion. As the conversion increases, the selectivity of skeletal isomers decreases and the selectivities of ROPs and OCDs increase. An overview of the maximal OCDs yields reached on the catalysts is given in Table 8.7. At variance to the iridium-containing faujasites, the variation of the n_{Si} / n_{Al} ratio does not improve the performance of catalyst 3.0Pt/$Na_{0.88}$,$H_{0.12}$-Y. On all catalysts spiro[4.5]decane is observed but there is no obvious correlation between the selectivity of spiro[4.5]decane and the selectivity of open-chain decanes. Nevertheless, the selectivity of the spiro compound in all cases is significantly higher than on their iridium-containing counterparts.

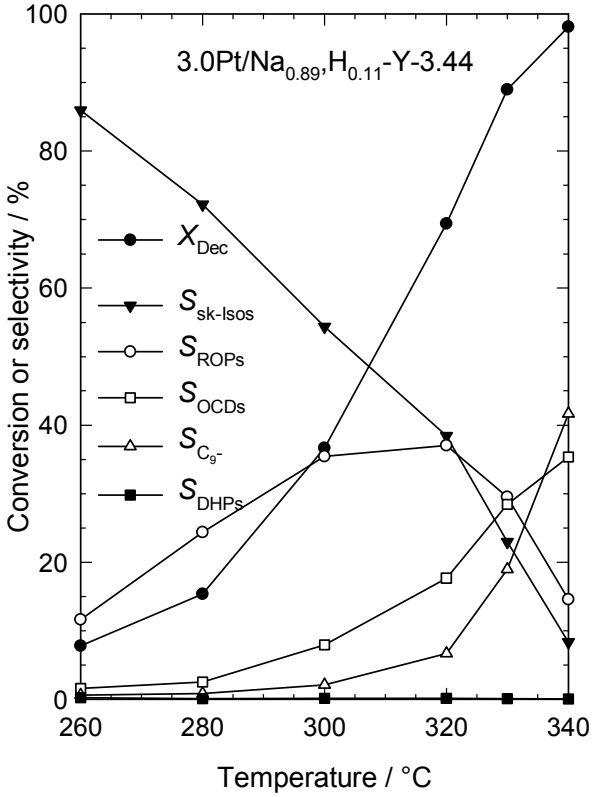

Figure 8.26: Conversion of decalin and selectivities of different groups of products on 3.0Pt/$Na_{0.89}$,$H_{0.11}$-Y-3.44 at different temperatures.

Table 8.7: Maximum yields of open-chain decanes obtained on FAU catalysts with different n_{Si} / n_{Al} ratios and 3 wt.-% platinum.

Catalyst	T_r / °C	X_{Dec} / %	S_{OCDs} / %	$Y_{OCDs, max.}$ / %	Y_{OCNs} / %	Y_{C_9-} / %
3.0Pt/$Na_{0.88}$,$H_{0.12}$-Y	361	96.3	40.7	39.1	3.9	32.8
3.0Pt/$Na_{0.89}$,$H_{0.11}$-Y-3.44	340	98.1	35.4	34.7	3.7	40.9
2.8Pt/$Na_{0.80}$,$H_{0.20}$-Y-4.11	319	98.8	35.2	34.8	3.1	42.6
2.9Pt/$Na_{0.75}$,$H_{0.25}$-Y-5.49	320	98.8	26.6	26.3	3.4	59.7

In Figure 8.27, the carbon number distributions of the hydrocracked products are presented for the catalysts with a higher n_{Si} / n_{Al} ratio than 1.21. The distributions for the other catalysts from this series are not shown because of the very low yields of hydrocracked products. The distributions consist of M-shaped curves, typical for bifunctional catalysis, to which hydrogenolysis curves are superimposed which lead to C_1 and C_9. The tendency can be observed that the higher the n_{Si} / n_{Al} ratio the higher the contribution of bifunctional catalysis.

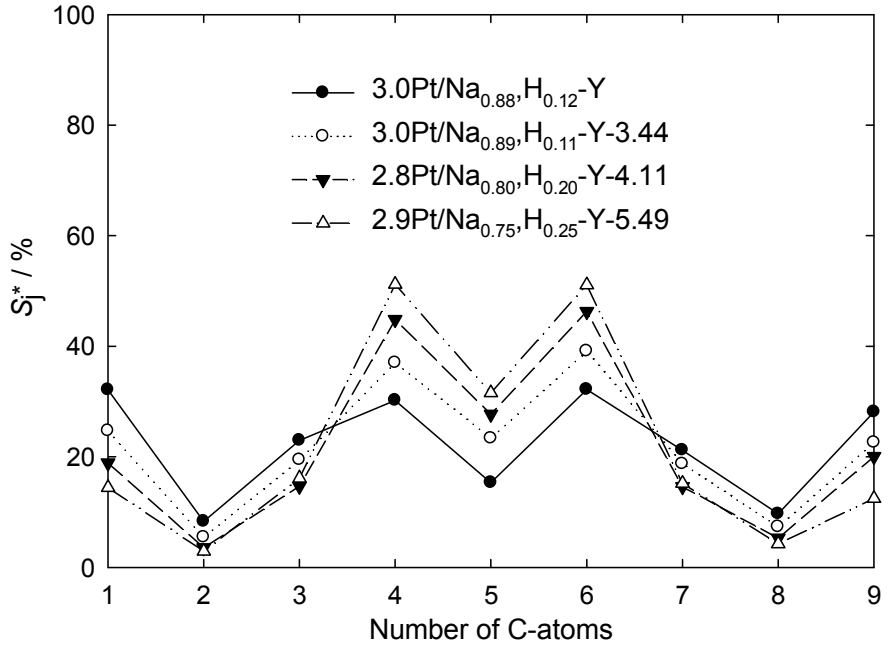

Figure 8.27: Modified hydrocracking selectivities S_j^* on the platinum-containing FAU catalysts with different n_{Si} / n_{Al} ratios:

3.0Pt/$Na_{0.88}$,$H_{0.12}$-Y: T_r = 361 °C; X_{Dec} = 96 %; $Y_{C_{9^-}}$ = 33 %; $\sum S_j^*$ = 200 %.

3.0Pt/$Na_{0.89}$,$H_{0.11}$-Y-3.44: T_r = 340 °C; X_{Dec} = 98 %; $Y_{C_{9^-}}$ = 41 %; $\sum S_j^*$ = 197 %.

2.8Pt/$Na_{0.80}$,$H_{0.20}$-Y-4.11: T_r = 319 °C; X_{Dec} = 99 %; $Y_{C_{9^-}}$ = 42 %; $\sum S_j^*$ = 196 %.

2.9Pt/$Na_{0.75}$,$H_{0.25}$-Y-5.49: T_r = 320 °C; X_{Dec} = 99 %; $Y_{C_{9^-}}$ = 60 %; $\sum S_j^*$ = 199 %.

8.4 Influence of the La^{3+} Concentration

Not only the strength of Brønsted acid sites is an important key factor in hydrocracking reactions of hydrocarbons but also the concentration of these. The effect of the strength of Brønsted acid sites was discussed in Sections 8.2 and 8.3. Now the concentration of Brønsted acid sites in FAU catalysts containing platinum or iridium as a metal is varied. Since H-Y zeolites and especially H-X zeolites are not very stable, the concentration of Brønsted acid sites was varied by different exchange degrees of lanthanum ions which stabilize the acidic zeolite on the one hand and on the other hand generate Brønsted acid sites via the Hirschler-Plank mechanism as described in Section 4.2. In order to have the possibility to reach a very high exchange degree with lanthanum ions the metal content was reduced to 1 wt.-% because the metal as well as lanthanum were introduced via ion exchange and thus competed with each other for the cation sites in the zeolites. As metals again iridium and platinum were chosen. As acidic supports zeolites X and Y, two which possess Brønsted acid sites of different strength, were ion-exchanged with different

concentrations of lanthanum nitrate and investigated as catalysts for the hydroconversion of decalin.

8.4.1 Iridium-Containing Catalysts

8.4.1.1 La-Y Catalysts

Three iridium-containing La-Y catalysts with different lanthanum exchange degrees of 18, 33 and 45 % were prepared and tested in the hydroconversion of decalin. The results were compared with those obtained on 1.0Ir/$Na_{0.93}$,$H_{0.07}$-Y (Section 8.1.1) containing only the Brønsted acid sites generated by the reduction of the iridium cations. The changes in the activity of the catalysts upon incorporation of lanthanum ions and thus additional Brønsted acid sites are shown in Figure 8.28a.

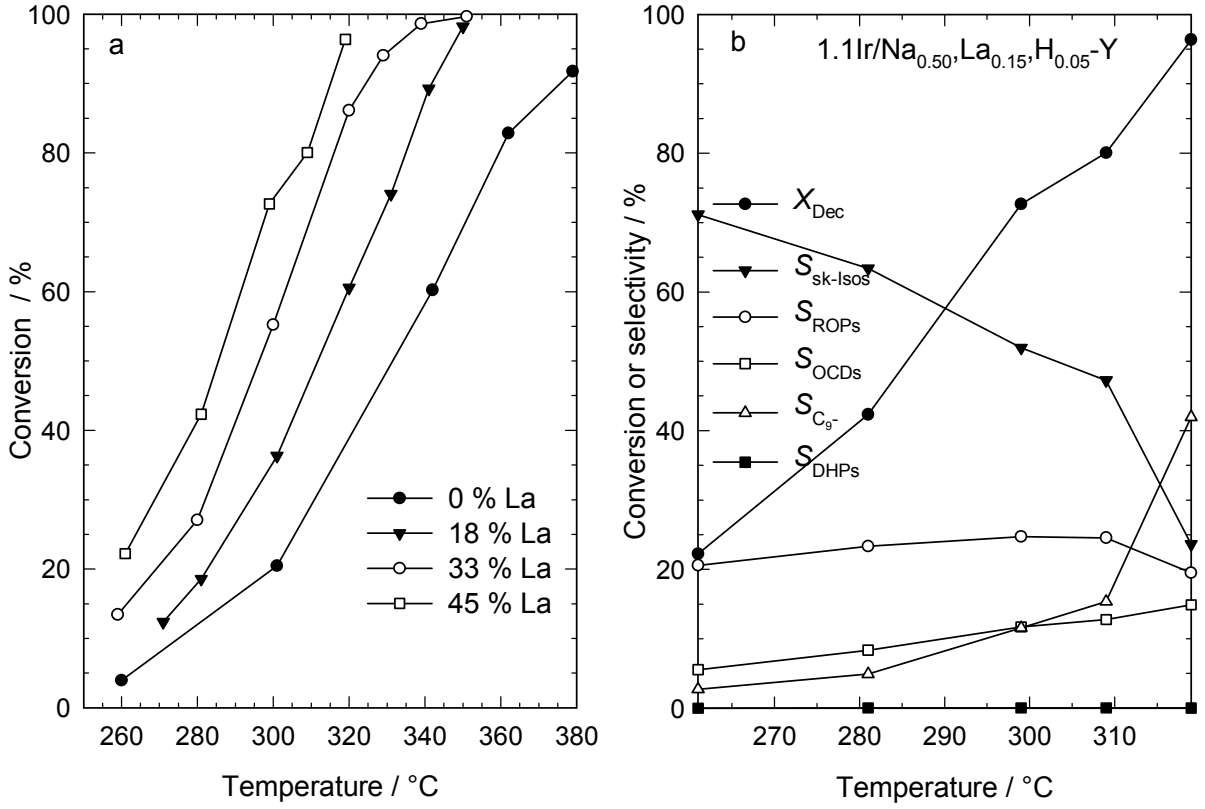

Figure 8.28: Conversion of decalin in dependence of the reaction temperature for 1 wt.-% iridium-containing La-Y catalysts with different degrees of lanthanum exchange (a) and selectivities of different groups of products on the catalyst 1.1Ir/$Na_{0.50}$,$La_{0.15}$,$H_{0.05}$-Y with a lanthanum exchange degree of 45 % (b).

Due to the incorporation of additional active sites the activity of the catalysts increases with higher exchange degrees of lanthanum. At around 20 % conversion on catalyst

1.0Ir/$Na_{0.93}$,$H_{0.07}$-Y the selectivities of skeletal isomers of decalin and ring opening products are approximately the same (Section 8.1.1, Figure 8.2). By incorporation of a higher concentration of Brønsted acid sites much more skeletal isomers of decalin are formed as primary products as can be seen in Figure 8.28b for catalyst 1.1Ir/$Na_{0.50}$,$La_{0.15}$,$H_{0.05}$-Y, the catalyst with the highest exchange degree of lanthanum ions of 45 %.

The incorporation of lanthanum ions with an exchange degree of 18 % in catalyst 1.2Ir/$Na_{0.77}$,$La_{0.06}$,$H_{0.05}$-Y improved the performance of catalyst 1.0Ir/$Na_{0.93}$,$H_{0.07}$-Y (Table 8.8). The highest selectivity and yield of OCDs are 27 and 26 % at 350 °C, respectively. In addition a yield of 7 % of open-chain nonanes is achieved. Nevertheless, the result of this catalyst is much lower than the yield of 39 % on catalyst 3.3Ir/$Na_{0.90}$,$H_{0.10}$-Y-4.11 (Section 8.3.1). A higher concentration of Brønsted acid sites leads to worse results concerning the formation of open-chain decanes.

Table 8.8: Maximum yields of open-chain decanes obtained on iridium-containing La-Y catalysts with different lanthanum exchange degrees.

Catalyst	T_r / °C	X_{Dec} / %	S_{OCDs} / %	$Y_{OCDs,\ max.}$ / %	Y_{OCNs} / %	Y_{C_9-} / %
1.0Ir/$Na_{0.93}$,$H_{0.07}$-Y	379	91.8	23.8	21.9	4.3	27.5
1.2Ir/$Na_{0.77}$,$La_{0.06}$,$H_{0.05}$-Y	350	98.2	26.7	26.2	7.0	47.3
1.2Ir/$Na_{0.63}$,$La_{0.11}$,$H_{0.04}$-Y	329	94.0	22.3	21.0	2.0	29.9
1.1Ir/$Na_{0.50}$,$La_{0.15}$,$H_{0.05}$-Y	319	96.4	14.9	14.4	1.3	40.4

The carbon number distributions of the hydrocracked products obtained on the iridium-containing La-Y catalysts at temperatures where the highest yield of OCDs is observed, are depicted in Figure 8.29. The distributions obtained on the catalysts with 0 and 18 % lanthanum exchange degree consist of non-ideal hammock-shaped curves which indicate mainly carbon-carbon bond cleavage by hydrogenolysis. The catalysts with a higher lanthanum exchange degree of 18 % show more and more the M-shaped distribution curves typical for bifunctional catalysts. These two catalysts show in addition a worse performance concerning the formation of OCDs indicating that a high contribution of C-C bond rupture via carbocations seems to be unfavorable for the formation of open-chain decanes. An optimal balance between the metal and the acid function is thus needed.

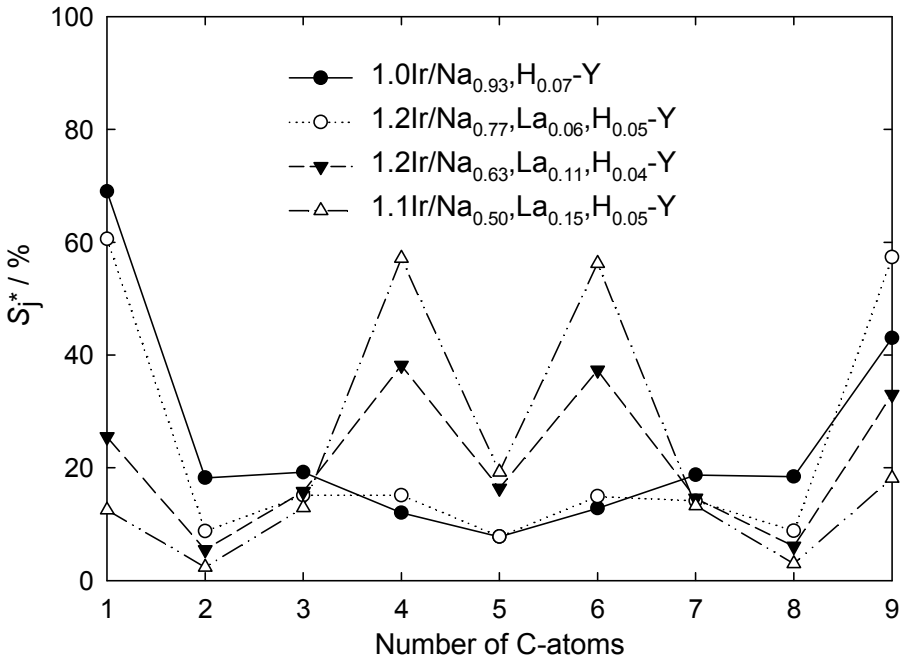

Figure 8.29: Modified hydrocracking selectivities S_j^* on the iridium-containing La-Y catalysts with different lanthanum exchange degrees:

1.0Ir/$Na_{0.93}$,$H_{0.07}$-Y: T_r = 379 °C; X_{Dec} = 92 %; $Y_{C_{9^-}}$ = 28 %; $\sum S_j^*$ = 219 %.

1.2Ir/$Na_{0.77}$,$La_{0.06}$,$H_{0.05}$-Y: T_r = 350 °C; X_{Dec} = 98 %; $Y_{C_{9^-}}$ = 47 %; $\sum S_j^*$ = 207 %.

1.2Ir/$Na_{0.63}$,$La_{0.11}$,$H_{0.04}$-Y: T_r = 329 °C; X_{Dec} = 94 %; $Y_{C_{9^-}}$ = 30 %; $\sum S_j^*$ = 192 %.

1.1Ir/$Na_{0.50}$,$La_{0.15}$,$H_{0.05}$-Y: T_r = 319 °C; X_{Dec} = 96 %; $Y_{C_{9^-}}$ = 40 %; $\sum S_j^*$ = 195 %.

The multibranched decanes are prevailing on all catalysts, but the fraction of methylnonanes is increasing with increasing concentration of Brønsted acid sites. No deactivation could be observed on the catalyst with the highest lanthanum exchange degree up to a time-on-stream of 35 h.

8.4.1.2 La-X Catalysts

On the iridium-containing La-Y catalysts discussed in Section 8.4.1.1, a lanthanum exchange degree of 33 % was sufficient to get a catalyst with a prevailing contribution of C-C bond rupture via carbocations leading to low amounts of the desired open-chain decanes and high contributions of the paring reaction with its products iso-butane and methylcyclopentane. In order to avoid the paring reaction or at least to enlarge the range of possible lanthanum exchange degrees without causing mainly C-C bond rupture via carbocations, La-X was used as a support since its Brønsted acid sites should have a lower strength. As observed

already on Ir/La-Y catalysts the activity of the catalysts increased with increasing lanthanum exchange degree and thus increasing concentration of Brønsted acid sites (Figure 8.30). Between the catalyst without lanthanum ions 0.94Ir/$Na_{0.90}$,$H_{0.10}$-X and catalyst 0.85Ir/$La_{0.30}$,$H_{0.07}$,$Na_{0.03}$-X with an exchange degree of 90 % a temperature difference of around 120 °C in order to reach the same conversion is visible.

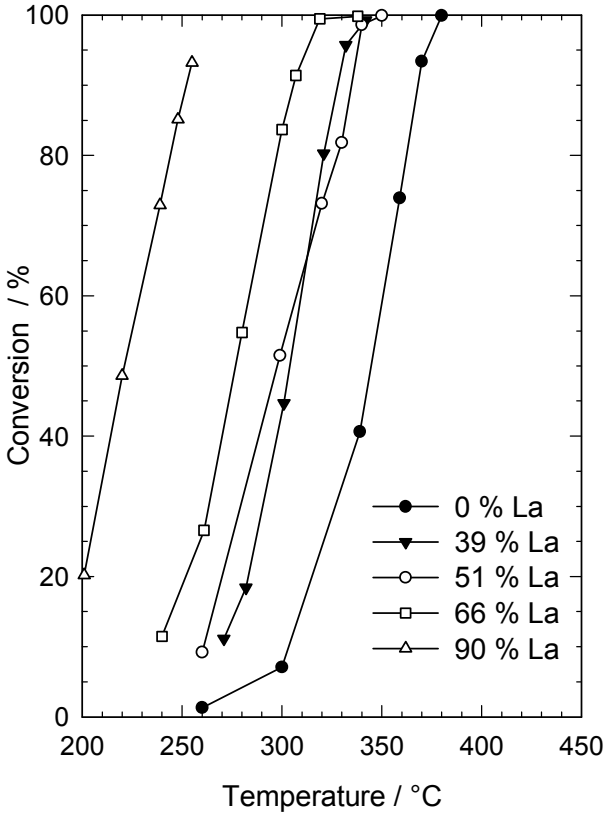

Figure 8.30: Dependence of the decalin conversion on the reaction temperature for 1 wt.-% iridium-containing La-X catalysts with different degrees of lanthanum exchange.

The selectivities obtained on the iridium-containing La-X catalysts in the hydroconversion of cis-decalin are depicted in Figure 8.31. At low conversion the prevailing products on catalyst 0.94Ir/$Na_{0.90}$,$H_{0.10}$-X (Figure 8.31a), which has only the Brønsted acid sites generated during the reduction of the noble metal, are ring opening products. With increasing concentration of Brønsted acid sites (Figure 8.31b) the fraction of skeletal isomers is increasing. On catalyst 0.85Ir/$La_{0.30}$,$H_{0.07}$,$Na_{0.03}$-X (Figure 8.31c), which has nearly the maximal possible concentration of lanthanum ions, skeletal isomers are strongly prevailing at low conversion indicating that now mainly the Brønsted acid sites are involved in the hydroconversion of decalin.

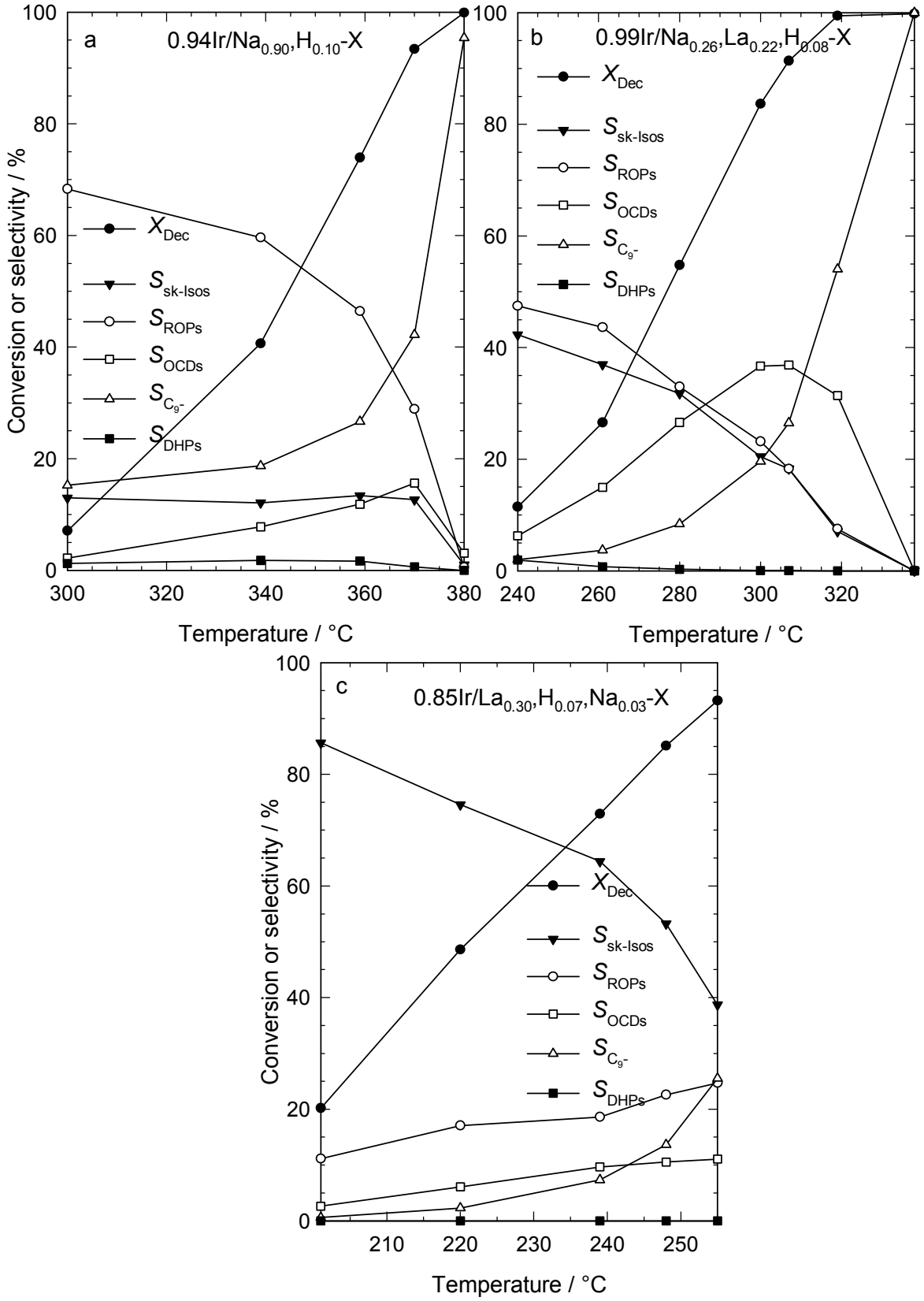

Figure 8.31: Conversion of decalin and selectivities of different groups of products in dependence of the reaction temperature for 1 wt.-% iridium-containing zeolites X with different lanthanum exchange degrees at different temperatures.

The best performance concerning the formation of OCDs is achieved on catalyst 0.99Ir/$Na_{0.26}$,$La_{0.22}$,$H_{0.08}$-X (Table 8.9). The maximal yield of open-chain decanes is 34 % at 307 °C. Due to the incorporation of Brønsted acid sites not only the activity of catalyst 0.94Ir/$Na_{0.90}$,$H_{0.10}$-X can be enhanced but also significantly the yield of open-chain decanes. These values are slightly lower than those obtained on catalyst 3.3Ir/$Na_{0.90}$,$H_{0.10}$-Y-4.11 with a maximum selectivity and yield of 40 and 39 %, respectively, but one should bear in mind that the metal loading was reduced from 3.3 wt.-% to 0.99 wt.-%. This reduced metal loading will possibly lead to high savings of expenses on an industrial scale. A higher exchange degree of lanthanum than 66 % leads to a very sharp decrease of the yield of OCDs.

Table 8.9: Maximum yields of open-chain decanes obtained on iridium-containing La-X catalysts with different lanthanum exchange degrees.

Catalyst	T_r / °C	X_{Dec} / %	S_{OCDs} / %	$Y_{OCDs, max.}$ / %	Y_{OCNs} / %	Y_{C_9-} / %
0.94Ir/$Na_{0.90}$,$H_{0.10}$-X	370	93.4	15.6	14.6	10.0	39.4
1.1Ir/$Na_{0.52}$,$La_{0.13}$,$H_{0.09}$-X	332	95.7	31.1	29.8	12.0	46.0
0.94Ir/$Na_{0.41}$,$La_{0.16}$,$H_{0.11}$-X	340	98.6	34.0	33.6	9.5	47.5
0.99Ir/$Na_{0.26}$,$La_{0.22}$,$H_{0.08}$-X	307	91.4	36.9	33.7	3.5	24.2
0.85Ir/$La_{0.30}$,$H_{0.07}$,$Na_{0.03}$-X	255	93.2	11.1	10.3	0.1	23.8

In Figure 8.32, the carbon number distributions of the hydrocracked products are presented. Clearly, the carbon number distribution on 0.94Ir/$Na_{0.90}$,$H_{0.10}$-X consists of a hammock-shaped curve which is indicative of hydrogenolysis and was already observed on the Ir/Na,H-Y catalysts (Section 8.1.1). For 0.85Ir/$La_{0.30}$,$H_{0.07}$,$Na_{0.03}$-X the distribution consists of a superposition of the M-shaped curves typical for bifunctional catalysts and a small contribution of hydrogenolysis leading to C_1 and C_9. The M-shape originates from the paring reaction leading to equal amounts of iso-butane and methylcyclopentane. 0.94Ir/$Na_{0.41}$,$La_{0.16}$,$H_{0.11}$-X shows an almost equal amount of all carbon numbers from C_2 to C_8 but the fractions of C_1 and C_9 are dominating. The best catalyst 0.99Ir/$Na_{0.26}$,$La_{0.22}$,$H_{0.08}$-X shows slightly enlarged fractions of C_4 and C_6 indicating a higher contribution of carbocation chemistry. These results emphasize the role of Brønsted acid sites. On catalyst 0.94Ir/$Na_{0.90}$,$H_{0.10}$-X with the lowest concentration of acid sites the dominating mechanism of carbon-carbon bond cleavage seems to be hydrogenolysis, as indicated by the hammock-shaped distribution curve of the hydrocracked products. On catalyst 0.85Ir/$La_{0.30}$,$H_{0.07}$,$Na_{0.03}$-X with the highest concentration of Brønsted acid sites the acid-catalyzed mechanism is dominating. The best yield of open-chain decanes is obtained on a

catalyst showing an intermediate behavior. Thus, the concentration of Brønsted acid sites can clearly influence the mechanism of decalin hydroconversion.

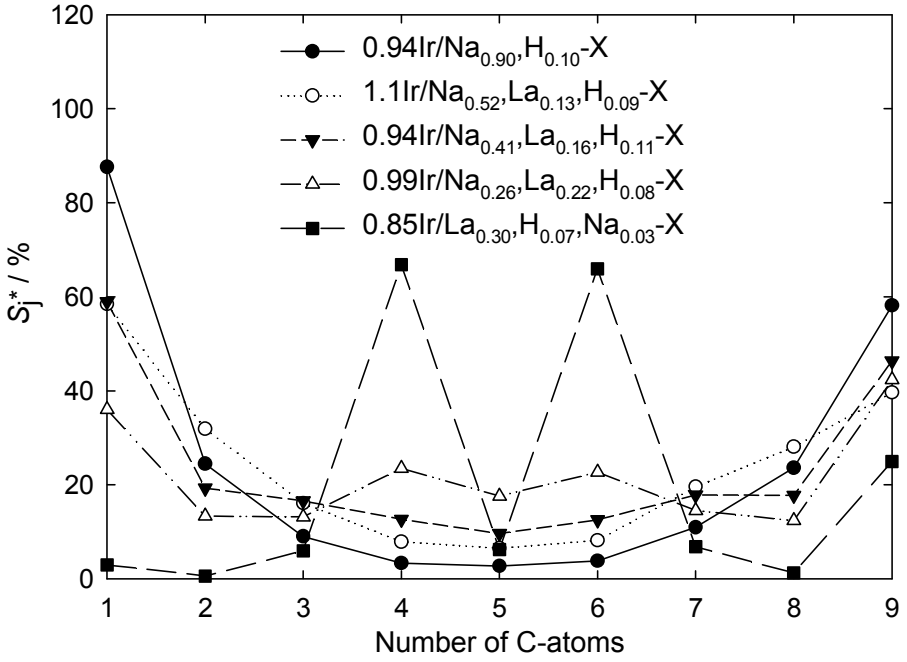

Figure 8.32: Modified hydrocracking selectivities S_j* on the iridium-containing La-X catalysts with different lanthanum exchange degrees:

0.94Ir/$Na_{0.90}$,$H_{0.10}$-X: T_r = 370 °C; X_{Dec} = 93 %; $Y_{C_{9-}}$ = 37 %; ∑ S_j* = 232 %.

1.1Ir/$Na_{0.52}$,$La_{0.13}$,$H_{0.09}$-X: T_r = 332 °C; X_{Dec} = 96 %; $Y_{C_{9-}}$ = 46 %; ∑ S_j* = 216 %.

0.94Ir/$Na_{0.41}$,$La_{0.16}$,$H_{0.11}$-X: T_r = 340 °C; X_{Dec} = 99 %; $Y_{C_{9-}}$ = 47 %; ∑ S_j* = 213 %

0.99Ir/$Na_{0.26}$,$La_{0.22}$,$H_{0.08}$-X: T_r = 307 °C; X_{Dec} = 91 %; $Y_{C_{9-}}$ = 24 %; ∑ S_j* = 195 %.

0.85Ir/$La_{0.30}$,$H_{0.07}$,$Na_{0.03}$-X: T_r = 255 °C; X_{Dec} = 93 %; $Y_{C_{9-}}$ = 22 %; ∑ S_j* = 186 %.

The results in this section also show that the hydroconversion of decalin on a bifunctional Ir/La-X catalyst starts at 120 °C lower temperatures than the hydrogenolysis on iridium (Figure 8.30). In the carbon number distribution found on catalyst 0.85Ir/$La_{0.30}$,$H_{0.07}$,$Na_{0.03}$-X a higher amount of C_9 than methane is obtained. Hydrogenolysis on a metal should normally lead to the same molar amounts of methane and C_9 or, if severe secondary hydrocracking takes place, to higher amounts of methane than C_9. Perhaps the detection of methane or the assignment of C_9 compounds is not accurate. The C_9 fraction consists of 60 % cis- and trans-1-ethyl-2-methylcyclohexane, the remaining 40 % are composed of about 20 different compounds. Hence, the C_9 fraction does not only consist of one or two compounds which would lead to a stronger influence of one erroneously assigned signal. Another possible origin of the large amounts of C_9 could be the disproportionation of two cyclic C_{10} molecules to C_9 and C_{11} as observed on a bifunctional Pt/Ca-Y catalyst [106]. However, no C_{11} compounds could be detected by on-line gas chromatography.

As already observed on the iridium-containing La-Y catalysts the multibranched decanes are prevailing on the catalysts with a low concentration of Brønsted acid sites. The fraction of the methylnonanes increases with increasing concentration of Brønsted acid sites. On catalyst 0.85Ir/$La_{0.30}$,$H_{0.07}$,$Na_{0.03}$-X nearly the same amount of methylnonanes and multibranched decanes is formed.

8.4.2 Platinum-Containing Catalysts

8.4.2.1 La-Y Catalysts

Three platinum-containing La-Y catalysts with different lanthanum exchange degrees of 21, 33 and 48 % were prepared and tested in the hydroconversion of cis-decalin. The results were compared with those obtained with 0.94Pt/$Na_{0.94}$,$H_{0.06}$-Y (Section 8.1.2) containing only the Brønsted acid sites generated by the reduction of the platinum cations.

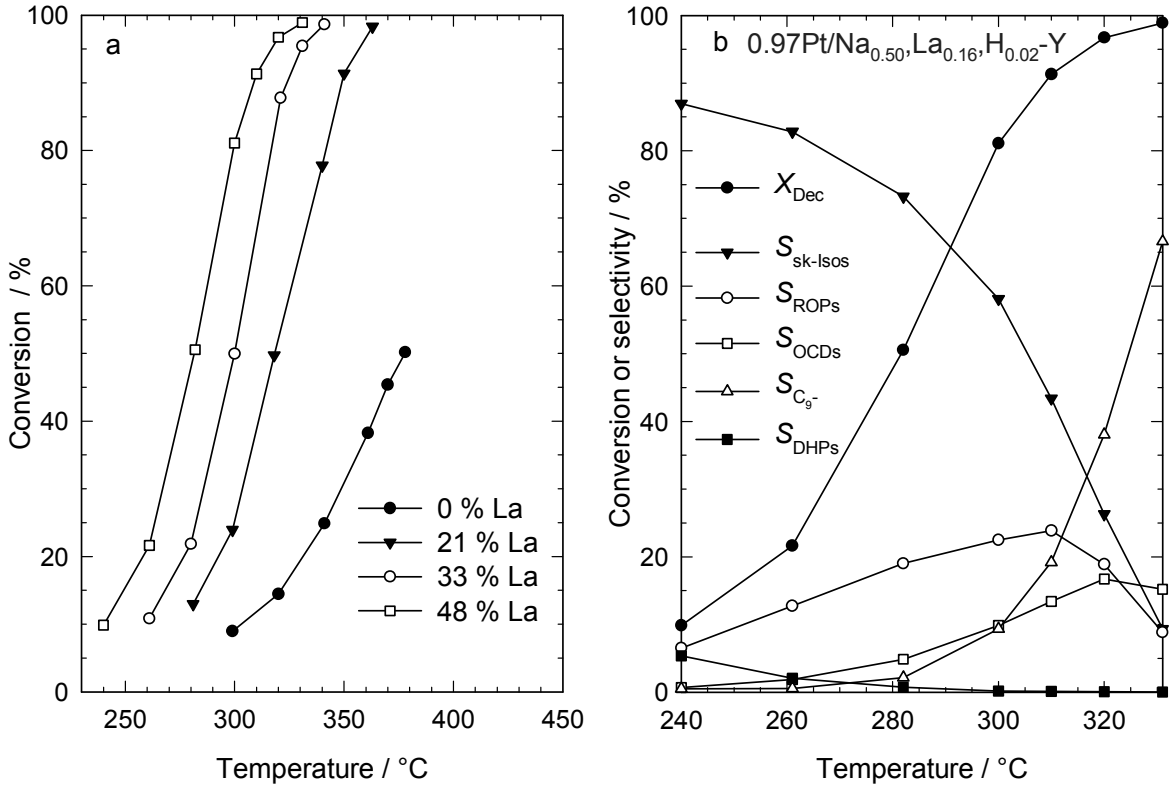

Figure 8.33: Conversion of decalin in dependence of the reaction temperature for 1 wt.-% platinum-containing La-Y catalysts with different degrees of lanthanum exchange (a) and selectivities of different groups of products on the catalyst 0.97Pt/$Na_{0.50}$,$La_{0.16}$,$H_{0.02}$-Y with a lanthanum exchange degree of 48 % (b).

Upon increasing the lanthanum exchange degree and thus the concentration of Brønsted acid sites the activity of the catalysts increases (Figure 8.33a) as observed on iridium-containing La-X and La-Y catalysts (Section 8.4.1). The selectivities obtained on the platinum-containing La-Y catalyst with the highest exchange degree of lanthanum in the hydroconversion of cis-decalin are depicted in Figure 8.33b. On all catalysts the skeletal isomers of decalin are prevailing at low conversions like in case of 0.94Pt/$Na_{0.94}$,$H_{0.06}$-Y (Section 8.1.2). In contrast to the latter catalyst the activity of all lanthanum-containing catalysts is higher leading to negligible amounts of dehydrogenated products. In addition, higher yields of open-chain decanes are achieved on the lanthanum-containing catalysts. An overview of the maximal yields of OCDs is given in Table 8.10. The highest selectivity and yield of open-chain decanes are achieved on catalyst 0.95Pt/$Na_{0.76}$,$La_{0.07}$,$H_{0.03}$-Y with 31 % and 30 %, respectively, at 363 °C. The higher concentration of Brønsted acid sites in catalyst 0.95Pt/$Na_{0.76}$,$La_{0.07}$,$H_{0.03}$-Y than in 0.94Pt/$Na_{0.94}$,$H_{0.06}$-Y can strongly improve the performance of the latter catalyst in the hydroconversion of decalin concerning the formation of open-chain decanes. Nevertheless, the yield of OCDs obtained on the best Pt/La-Y catalyst is much lower compared to catalyst 3.7Pt/$Na_{0.86}$,$H_{0.14}$-Y with a yield of 41 %.

Table 8.10: Maximum yields of open-chain decanes obtained on platinum-containing La-Y catalysts with different lanthanum exchange degrees.

Catalyst	T_r / °C	X_{Dec} / %	S_{OCDs} / %	$Y_{OCDs,\ max.}$ / %	Y_{OCNs} / %	Y_{C_9-} / %
0.95Pt/$Na_{0.76}$,$La_{0.07}$,$H_{0.03}$-Y	363	98.3	30.9	30.3	2.9	43.8
1.2Pt/$Na_{0.62}$,$La_{0.11}$,$H_{0.05}$-Y	331	95.4	28.8	27.5	1.2	28.7
0.97Pt/$Na_{0.50}$,$La_{0.16}$,$H_{0.02}$-Y	320	96.7	16.7	16.2	0.4	36.8

The carbon number distributions of the hydrocracked products obtained on the platinum-containing La-Y catalysts, at temperatures at which the highest yields of OCDs are observed, are depicted in Figure 8.34. Catalyst 0.94Pt/$Na_{0.94}$,$H_{0.06}$-Y shows an unsymmetrical curve which is believed to be a typical curve for hydrogenolysis on platinum (see Section 8.1.2) with a large amount of methane. Secondary hydrocracking is responsible for the unsymmetrical curve and the large value of $\sum S_j^*$ = 264 %. All other carbon number distributions show an M-shaped curve with a superposition of hydrogenolysis leading to methane and C_9. The M-shaped curve is pronounced for high lanthanum exchange degrees.

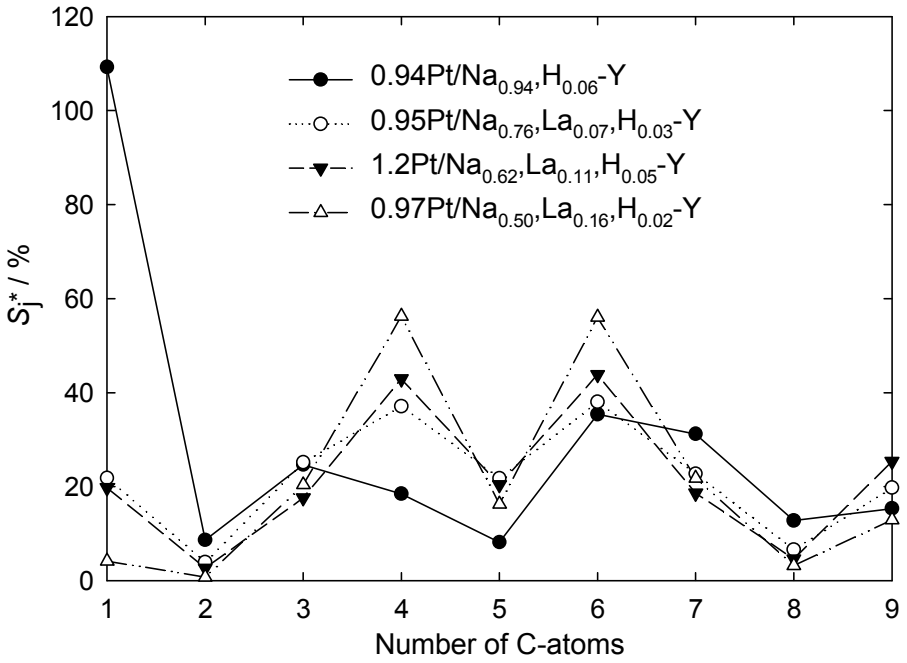

Figure 8.34: Modified hydrocracking selectivities S_j* on the platinum-containing La-Y catalysts with different lanthanum exchange degrees:

0.94Pt/$Na_{0.94}$,$H_{0.06}$-Y: T_r =378 °C; X_{Dec} = 50 %; $Y_{C_{9^-}}$ = 2 %; $\sum S_j$* = 264 %.

0.95Pt/$Na_{0.76}$,$La_{0.07}$,$H_{0.03}$-Y: T_r = 363 °C; X_{Dec} = 98 %; $Y_{C_{9^-}}$ = 44 %; $\sum S_j$* = 197 %.

1.2Pt/$Na_{0.62}$,$La_{0.11}$,$H_{0.05}$-Y: T_r = 331 °C; X_{Dec} = 95 %; $Y_{C_{9^-}}$ = 29 %; $\sum S_j$* = 196 %.

0.97Pt/$Na_{0.50}$,$La_{0.16}$,$H_{0.02}$-Y: T_r = 320 °C; X_{Dec} = 97 %; $Y_{C_{9^-}}$ = 37 %; $\sum S_j$* = 192 %.

In contrast to the selectivities of OCDs on Pt/Na,H-Y catalysts (Section 8.1.2), on which the sum of the selectivities of n-decane and all monobranched decanes were higher than or at least equal to the selectivity of multibranched decanes, the introduction of Brønsted acid sites generates more highly branched decane isomers.

8.4.2.2 La-X Catalysts

On the platinum-containing La-Y catalysts of Section 8.4.2.1, a lanthanum exchange degree of 21 % was sufficient to obtain a catalyst with a prevailing contribution of C-C bond rupture via carbocations leading to low amounts of the desired open-chain decanes and high amounts of the paring reaction products iso-butane and methylcyclopentane. In order to avoid this paring reaction or at least to enlarge the range of possible lanthanum exchange degrees without causing mainly C-C bond rupture via carbocations, La-X was used as a support since its Brønsted acid sites should have a lower strength. As observed already on all other La-X and La-Y catalysts the activity of the catalysts increases with increasing

lanthanum exchange degree and thus increasing concentration of Brønsted acid sites (Figure 8.35). Between the catalyst without lanthanum ions 0.96Pt/$Na_{0.88}$,$H_{0.12}$-X and catalyst 1.0Pt/$La_{0.30}$,$H_{0.06}$,$Na_{0.04}$-X with an exchange degree of 90 % a temperature difference of around 180 °C in order to reach the same conversion is visible which is even more than observed on the iridium-containing counterparts in Section 8.4.1.2.

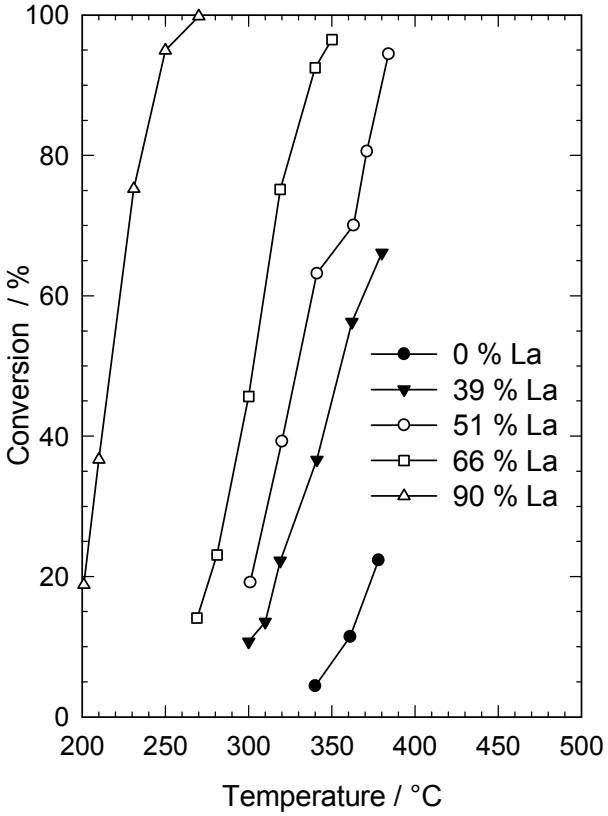

Figure 8.35: Dependence of the decalin conversion on the reaction temperature for 1 wt.-% platinum-containing La-X catalysts with different degrees of lanthanum exchange.

Catalyst 0.96Pt/$Na_{0.88}$,$H_{0.12}$-X shows a low activity in the hydroconversion of decalin. At 380 °C, which is the maximal possible temperature of the catalytic equipment, a conversion of only 22 % is reached. The primary products are skeletal isomers of decalin, but also significant amounts of dehydrogenated products (S_{DHPs} = 45 %) are formed (Figure 8.36). Much more tetralin than naphthalene is formed, and the obtained values fit well with the values calculated for thermodynamic equilibrium between cis-decalin, trans-decalin, tetralin and naphthalene at 380 °C and 50 bar [92]. Increasing the concentration of Brønsted acid sites via a lanthanum exchange of 39 % increases the activity of the catalysts and a conversion of 66 % is reached at 380 °C. The highest selectivity of dehydrogenated products is 16 %. Nevertheless, both catalysts show a nonsatisfying result concerning the formation of open-chain decanes.

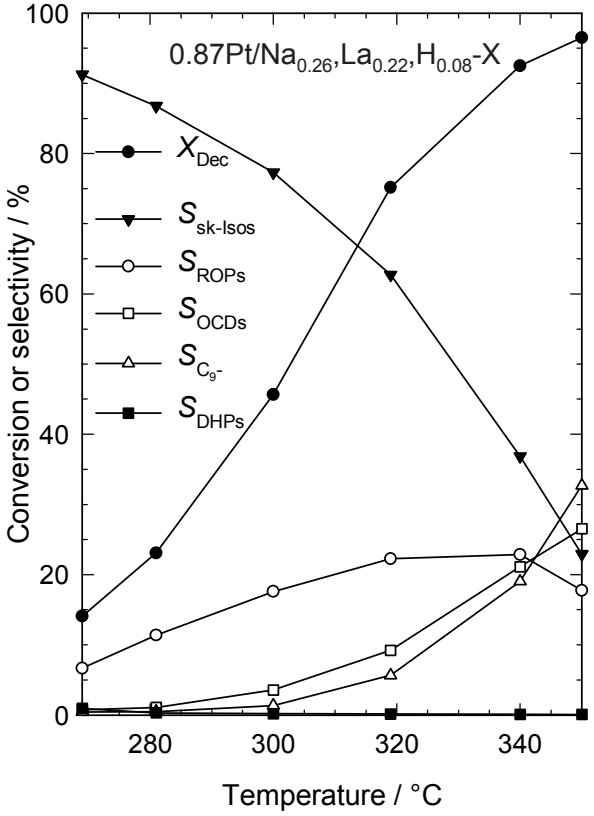

Figure 8.36: Conversion of decalin and selectivities of different groups of products in dependence of the reaction temperature for catalyst 0.87Pt/$Na_{0.26}$,$La_{0.22}$,$H_{0.08}$-X.

On all catalysts, as shown for catalyst 0.87Pt/$Na_{0.26}$,$La_{0.22}$,$H_{0.08}$-X (Figure 8.36), the prevailing products at low conversions are skeletal isomers. At higher temperatures the selectivity of skeletal isomers is decreasing, and ROPs, OCDs and C_9- are formed. The highest selectivity of OCDs is achieved, as in the case of iridium, on the support with 66 % exchange degree of lanthanum. On catalyst 0.87Pt/$Na_{0.26}$,$La_{0.22}$,$H_{0.08}$-X a selectivity of OCDs of 27 % and a yield of 26 % is achieved at 350 °C. These values are much lower than those observed on the best catalyst 3.7Pt/$Na_{0.86}$,$H_{0.14}$-Y with S_{OCDs} = 42 % and Y_{OCDs} = 41 % and even lower than those on the best Pt/La-Y catalyst, 0.95Pt/$Na_{0.76}$,$La_{0.07}$,$H_{0.03}$-Y with S_{OCDs} = 31 % and Y_{OCDs} = 30 %. An overview of the maximal OCDs yields reached on the platinum-containing La-X catalysts is given in Table 8.11. Unlike in the case of iridium, it is not possible to reduce the platinum loading without a significant loss in the formation of OCDs.

Table 8.11: Maximum yields of open-chain decanes obtained on platinum-containing La-X catalysts with different lanthanum exchange degrees.

Catalyst	T_r / °C	X_{Dec} / %	S_{OCDs} / %	$Y_{OCDs, max.}$ / %	Y_{OCNs} / %	Y_{C_9-} / %
0.99Pt/$Na_{0.43}$,$La_{0.17}$,$H_{0.06}$-X	384	94.5	23.0	21.8	0.8	22.7
0.87Pt/$Na_{0.26}$,$La_{0.22}$,$H_{0.08}$-X	350	96.5	26.5	25.6	0.7	31.6
1.0Pt/$La_{0.30}$,$H_{0.06}$,$Na_{0.04}$-X	250	95.0	12.7	12.1	0.1	28.0

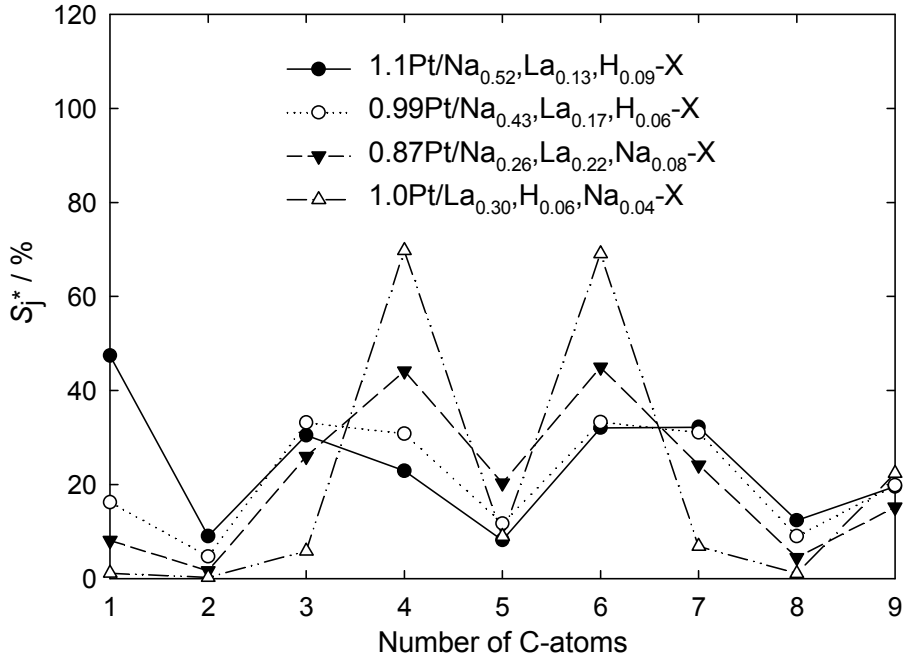

Figure 8.37: Modified hydrocracking selectivities S_j* on the platinum-containing La-X catalysts with different lanthanum exchange degrees:

1.1Pt/$Na_{0.52}$,$La_{0.13}$,$H_{0.09}$-X: T_r = 380 °C; X_{Dec} = 66 %; Y_{C_9-} = 3 %; $\sum S_j$* = 214 %.

0.99Pt/$Na_{0.43}$,$La_{0.17}$,$H_{0.06}$-X: T_r = 384 °C; X_{Dec} = 95 %; Y_{C_9-} = 23 %; $\sum S_j$* = 189 %.

0.87Pt/$Na_{0.26}$,$La_{0.22}$,$H_{0.08}$-X: T_r = 350 °C; X_{Dec} = 97 %; Y_{C_9-} = 32 %; $\sum S_j$* = 189 %.

1.0Pt/$La_{0.30}$,$H_{0.06}$,$Na_{0.04}$-X: T_r = 250 °C; X_{Dec} = 95 %; Y_{C_9-} = 28 %; $\sum S_j$* = 185 %.

In Figure 8.37, the carbon number distributions of the hydrocracked products are presented for the platinum-containing La-X catalysts at conditions of the maximal yields of OCDs. The results of catalyst 0.96Pt/$Na_{0.88}$,$H_{0.12}$-X are not shown because of the very low yield of hydrocracked products of 0.2 %. The catalysts with 39 and 51 % lanthanum exchange degree possess the typical distribution of Pt/Na,H-Y catalysts (Section 8.1.2) with nearly the same amounts of C_3, C_4, C_6, and C_7 and only small amounts of C_2, C_5 and C_8. But this time

also very small amounts of methane and C_9 are formed. The distribution curve for the highly exchanged lanthanum catalyst 1.0Pt/$La_{0.30}$,$H_{0.06}$,$Na_{0.04}$-X consists of a superposition of the M-shaped curve typical for bifunctional catalysts and a small contribution of hydrogenolysis leading to C_1 and C_9. Catalyst 0.87Pt/$Na_{0.26}$,$La_{0.22}$,$H_{0.08}$-X shows a distribution curve which is a mixture of the above-mentioned two distributions.

As already observed on the platinum-containing La-Y catalysts (Section 8.4.2.1) the higher concentration of Brønsted acid sites leads to more branched decane isomers than observed on Pt/Na,H-Y catalysts (Section 8.1.2).

8.5 Influence of the n_{Ir} / n_{Pt} Ratio in Bimetallic Catalysts

Alloys of two metals can have completely different properties than both metals alone. Therefore, three Y catalysts with a total metal content of 3 wt.-% and different n_{Ir} / (n_{Ir} + n_{Pt}) ratios of 0.76, 0.50 and 0.25 were prepared and tested in the hydroconversion of decalin. The obtained results were compared to those on the monometallic catalysts 2.9Ir/$Na_{0.90}$,$H_{0.10}$-Y (Section 8.1.1) and 3.0Pt/$Na_{0.88}$,$H_{0.12}$-Y (Section 8.1.2). The activity of the catalysts is presented in Figure 8.38. The monometallic iridium-containing catalyst is much more active than the monometallic platinum-containing catalyst. The three bimetallic catalysts behave as one would expect from physical mixtures of both metals: the higher the iridium content and thus the n_{Ir} / (n_{Ir} + n_{Pt}) ratio the higher the activity of the catalyst.

In Figure 8.39 the selectivities of the hydroconversion of cis-decalin on the bimetallic Ir,Pt catalysts are depicted. At low conversions, catalyst 2.3Ir,0.73Pt/$Na_{0.90}$,$H_{0.10}$-Y (Figure 8.39a) shows, as expected, the typical behavior of catalyst 2.9Ir/$Na_{0.90}$,$H_{0.10}$-Y with the prevailing formation of ring opening products. Nevertheless, there is a higher fraction of skeletal isomers than in the monometallic 2.9Ir/$Na_{0.90}$,$H_{0.10}$-Y catalyst. The higher the fraction of platinum in the bimetallic catalysts the higher is the selectivity of skeletal isomers at low conversion. At higher conversion the selectivities of skeletal isomers and ring opening products decrease, and the selectivity of open-chain decanes goes through a maximum. The temperature of this maximum shifts to higher values the higher the fraction of platinum in the catalyst.

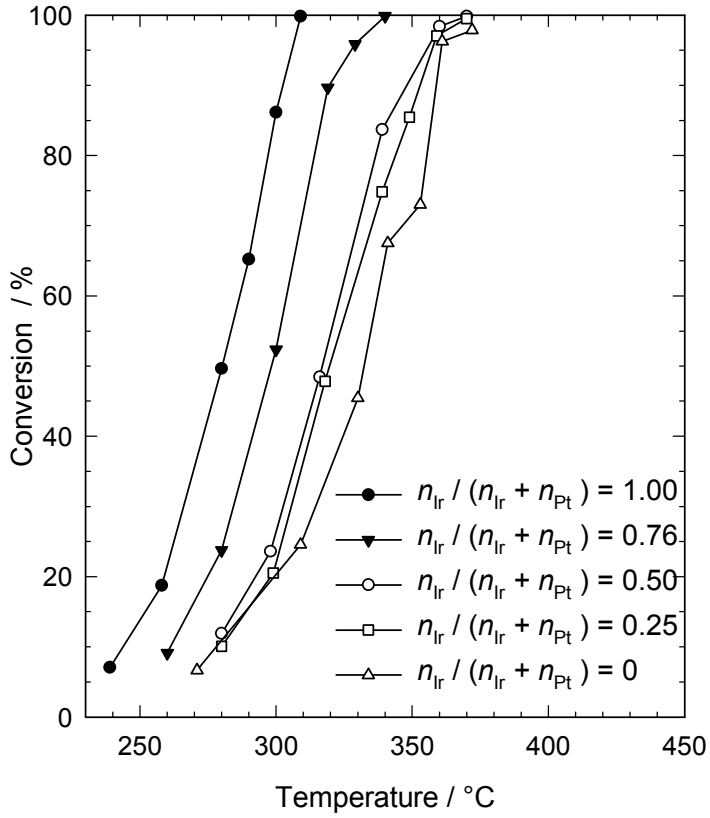

Figure 8.38: Dependence of the decalin conversion on the reaction temperature for bimetallic Ir,Pt/Na,H-Y catalysts with different n_{Ir} / (n_{Ir} + n_{Pt}) ratios.

An overview of the maximal selectivities of open-chain decanes obtained on the three bimetallic catalysts in comparison to the monometallic Y catalysts is shown in Table 8.12. The results demonstrate that small amounts of platinum can improve the performance of the monometallic 2.9Ir/$Na_{0.90}$,$H_{0.10}$-Y catalyst concerning the formation of open-chain decanes, perhaps due to enhanced isomerization properties. Higher fractions of platinum do not lead to higher selectivities of OCDs. None of the bimetallic catalysts shows higher selectivities and yields of OCDs than the monometallic 3.0Pt/$Na_{0.88}$,$H_{0.12}$-Y catalyst.

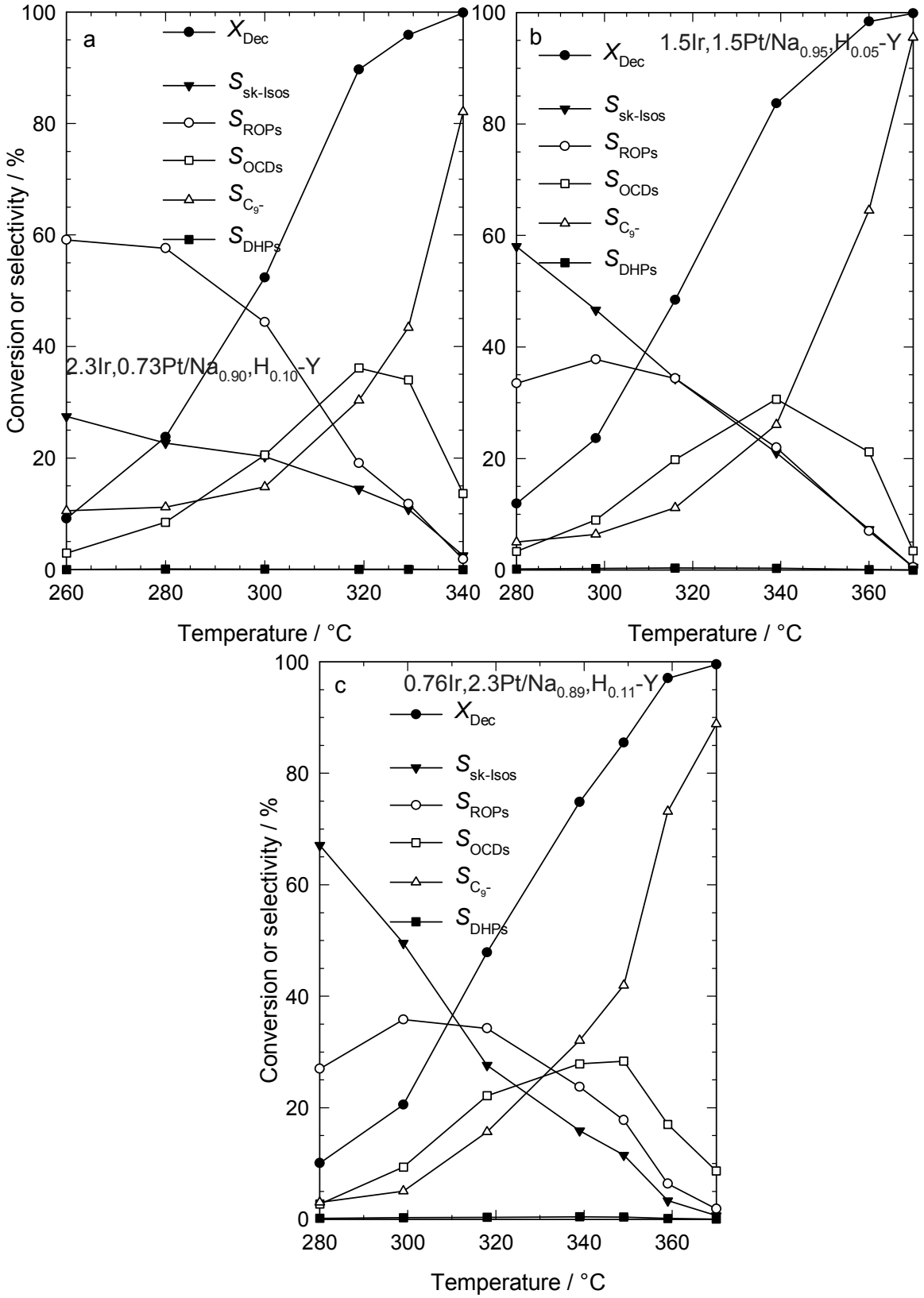

Figure 8.39: Conversion of decalin and selectivities of different groups of products in dependence of the reaction temperature for three bimetallic Ir,Pt/Na,H-Y catalysts with different n_{Ir} / (n_{Ir} + n_{Pt}) ratios.

Table 8.12: Maximum yields of open-chain decanes obtained on bimetallic Ir,Pt/Na,H-Y catalysts.

Catalyst	T_r / °C	X_{Dec} / %	S_{OCDs} / %	$Y_{OCDs, max.}$ / %	Y_{OCNs} / %	$Y_{C_{9^-}}$ / %
2.9Ir/$Na_{0.90}$,$H_{0.10}$-Y	300	86.2	35.7	30.7	7.2	24.6
2.3Ir,0.73Pt/$Na_{0.90}$,$H_{0.10}$-Y	319	89.7	36.2	32.4	8.7	27.2
1.5Ir,1.5Pt/$Na_{0.95}$,$H_{0.05}$-Y	339	83.7	30.6	25.6	3.6	21.8
0.76Ir,2.3Pt/$Na_{0.89}$,$H_{0.11}$-Y	349	85.5	28.4	24.2	5.6	35.9
3.0Pt/$Na_{0.88}$,$H_{0.12}$-Y	361	96.3	40.7	39.1	3.9	32.8

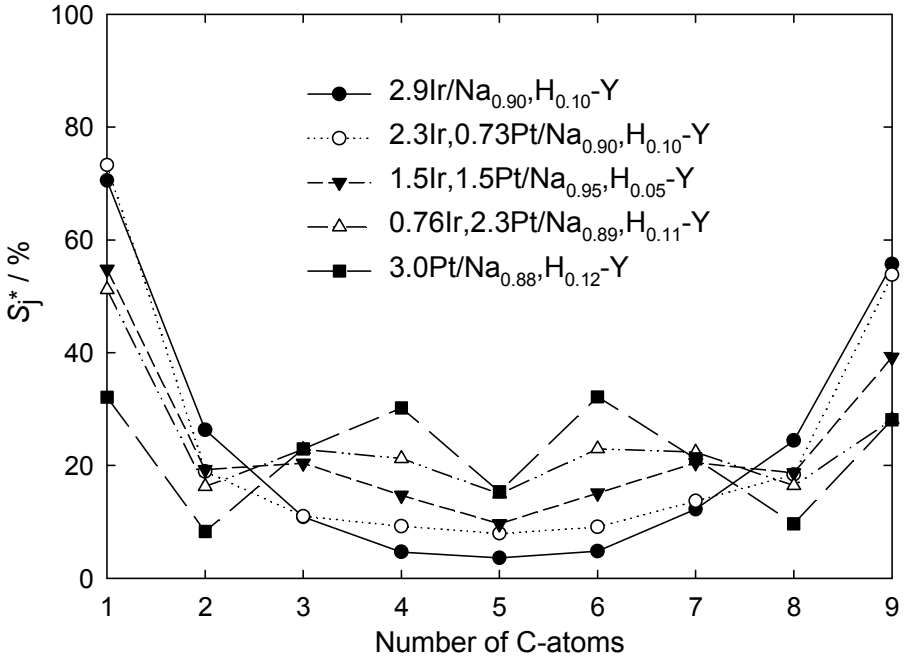

Figure 8.40: Modified hydrocracking selectivities S_j^* on mono- and bimetallic Ir,Pt/Na,H-Y catalysts:

2.9Ir/$Na_{0.90}$,$H_{0.10}$-Y: T_r = 300 °C; X_{Dec} = 86 %; $Y_{C_{9^-}}$ = 24 %; $\sum S_j^*$ = 217 %.

2.3Ir,0.73Pt/$Na_{0.90}$,$H_{0.10}$-Y: T_r = 319 °C; X_{Dec} = 90 %; $Y_{C_{9^-}}$ = 27 %; $\sum S_j^*$ = 215 %.

1.5Ir,1.5Pt/$Na_{0.95}$,$H_{0.05}$-Y: T_r = 339 °C; X_{Dec} = 84 %; $Y_{C_{9^-}}$ = 22 %; $\sum S_j^*$ = 210 %.

0.76Ir,2.3Pt/$Na_{0.89}$,$H_{0.11}$-Y: T_r = 349 °C; X_{Dec} = 85 %; $Y_{C_{9^-}}$ = 36 %; $\sum S_j^*$ = 216 %.

3.0Pt/$Na_{0.88}$,$H_{0.12}$-Y: T_r = 361 °C; X_{Dec} = 96 %; $Y_{C_{9^-}}$ = 33 %; $\sum S_j^*$ = 200 %.

In Figure 8.40, the carbon number distributions of the hydrocracked products on the three bimetallic catalysts in comparison to the monometallic catalysts are given. Catalyst 2.3Ir,0.73Pt/$Na_{0.90}$,$H_{0.10}$-Y with an $n_{Ir} / (n_{Ir} + n_{Pt})$ ratio of 0.76 shows a hammock-shaped curve, as does the monometallic catalyst 2.9Ir/$Na_{0.90}$,$H_{0.10}$-Y, which is indicative of

hydrogenolysis. Catalyst 0.76Ir,2.3Pt/$Na_{0.89}$,$H_{0.11}$-Y with an n_{Ir} / (n_{Ir} + n_{Pt}) ratio of 0.25 shows a similar distribution as catalyst 3.0Pt/$Na_{0.88}$,$H_{0.12}$-Y with high amounts of C_3, C_4, C_6 and C_7. The distribution curve for catalyst 1.5Ir,1.5Pt/$Na_{0.95}$,$H_{0.05}$-Y with an n_{Ir} / (n_{Ir} + n_{Pt}) ratio of 0.50 is nicely located between those for the other two bimetallic catalysts.

All results suggest that the bimetallic catalysts probably do not form alloys. The catalytic performances of the catalysts are conform with the results one would suggest for physical mixtures of Ir/Na,H-Y and Pt/Na,H-Y catalysts.

8.6 Different Mechanisms Occurring During the Ring Opening of Decalin on Faujasite Catalysts

As discussed in Section 4.3.1 there exist four pure hydrocracking and cracking mechanisms for C-C bond rupture of hydrocarbons. Contributions of thermal hydrocracking can be excluded as proven in Section 7.2. Since all investigated catalysts are metal-containing ones the possible hydrocracking mechanisms occurring in the hydroconversion of decalin are expected to be hydrogenolysis on the metal or hydrocracking on bifunctional catalysts.

The catalytic results of the hydroconversion of decalin presented in Sections 8.1 to 8.5 suggest that the main catalysts investigated do not show a pure hydrocracking mechanism, instead one of both above-mentioned mechanisms are prevailing and the other one is superimposed. Nevertheless, on some catalysts an almost pure mechanism can be obtained. On non- or very weakly acidic metal catalysts hydrogenolysis on the respective metal is observed. On these samples there is a large difference in the catalytic behavior of iridium- and platinum-containing catalysts. By introducing more and more acidity to the samples the differences between platinum- and iridium-containing catalysts diminish (Figure 8.41) until the zeolite behaves as a hydrocracking catalyst where the metal has only a hydrogenation and dehydrogenation function and hence the nature of the metal has hardly any influence on the hydroconversion of decalin. It must be borne in mind that the term “acidity” does not stand for a clearly defined physico-chemical quantity, but it rather embraces a variety of properties, such as the concentration and strength or strength distribution of the acid sites, without indicating which of these properties is precisely meant.

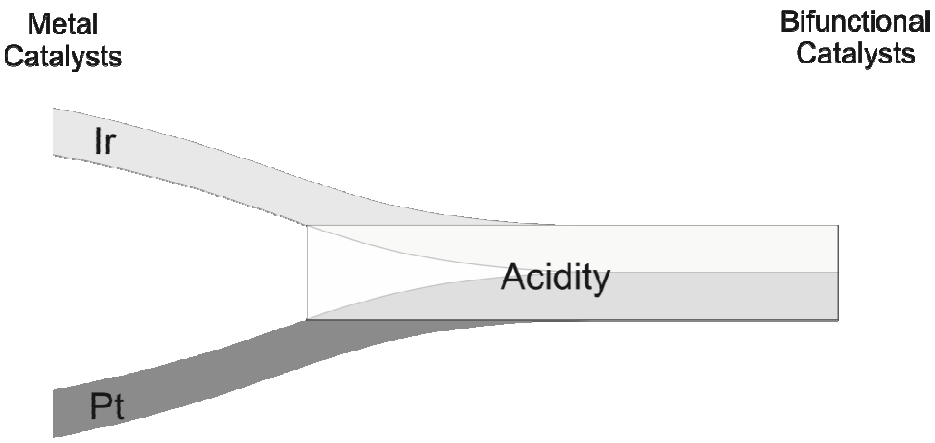

Figure 8.41: Schematic representation of the mechanistic situation of hydrocracking decalin on non-acidic noble-metal catalysts (hydrogenolysis) and the shift on the mechanism towards bifunctional hydrocracking upon incorporating acidity.

In the following sections, our mechanistic views concerning hydrocracking of decalin on bifunctional catalysts (Section 8.6.1), hydrogenolysis on iridium (Section 8.6.2) and hydrogenolysis on platinum (Section 8.6.3) are presented.

8.6.1 Hydrocracking on Bifunctional Catalysts

On two out of all catalysts investigated a nearly ideal bifunctional hydrocracking was observed, as concluded from the carbon number distribution of the hydrocracked products (Figure 8.42). On the two highly lanthanum-exchanged iridium and platinum catalysts, very similar M-shaped carbon number distributions were obtained with pronounced maxima at C_4 and C_6. Possible origins for the too large C_9 fractions were discussed in Section 8.4.1.2. The C_4 fractions consist mainly of iso-butane (Pt/La-X: 96 mol-%, Ir/La-X: 96 mol-%), and the C_6 fractions contain large amounts of methylcyclopentane (Pt/La-X: 81 mol-%, Ir/La-X: 77 mol-%). Presumably, a portion of the methylcyclopentane originally formed on the two catalysts is ring-opened to 2-methylpentane (Pt/La-X: 7 mol-%, Ir/La-X: 10 mol-%), 3-methylpentane (Pt/La-X: 4 mol-%, Ir/La-X: 6 mol-%) and n-hexane (Pt/La-X: 2 mol-%, Ir/La-X: 1 mol-%). These large amounts of iso-butane and methylcyclopentane can be explained by the paring reaction (see also Section 4.3.1.4). In this very selective reaction the C_{10} one-ring naphthenes undergo skeletal isomerizations in the alkyl side chains instead of endocyclic carbon-carbon bond rupture until a possible isomer for the type A β-scission is reached, leading to iso-butane and methylcyclopentane. The three possible isomers for the type A β-scissions were already shown in Figure 4.13 in Section 4.3.1.4.

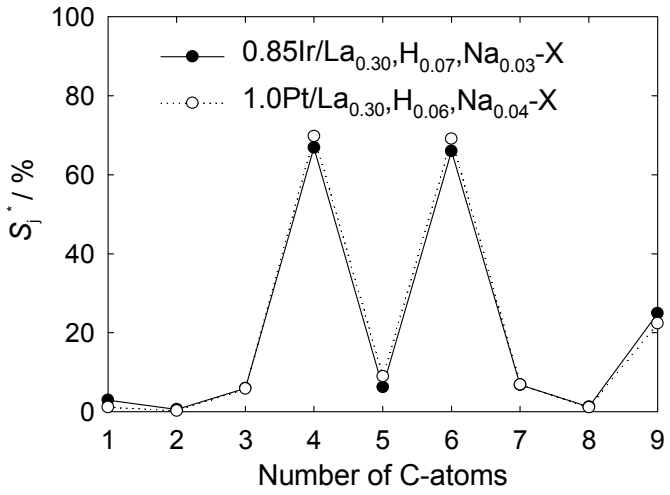

Figure 8.42: Modified hydrocracking selectivities S_j^* on bifunctional catalysts:
0.85Ir/$La_{0.30}$,$H_{0.07}$,$Na_{0.03}$-X: T_r = 255 °C; X_{Dec} = 93 %; $Y_{C_{9^-}}$ = 22 %; $\sum S_j^*$ = 186 %.
1.0Pt/$La_{0.30}$,$H_{0.06}$,$Na_{0.04}$-X: T_r = 250 °C; X_{Dec} = 95 %; $Y_{C_{9^-}}$ = 28 %; $\sum S_j^*$ = 185 %.

The hydroconversion of decalin on the two bifunctional catalysts starts with the skeletal isomerization of decalin. A large number of skeletal isomers are obtained at low conversion which are mainly identified by the molar mass of 138 g·mol^{-1} determined by GC/MS. The highest selectivity has an isomer directly neighbored to trans-decalin as shown in a gas chromatogram (Section 8.2.1, Figure 8.16). The assignment of the GC/MS with the highest probability is spiro[4.5]decane. This assignment is not safe since this compound is also assigned to two other skeletal isomers in the chromatogram. This skeletal isomer of decalin seems to be the very first product formed during the hydroconversion of decalin, and this signal can be observed on nearly all investigated catalysts (except the catalysts discussed in Section 8.6.2), even if they have low isomerization tendencies like Ir/Na,H-Y catalysts. This signal is directly neighbored to the signal of trans-decalin as shown in the gas chromatogram of 2.9Ir/$Na_{0.90}$,$H_{0.10}$-Y in Figure 8.16, Section 8.2.1. The separation of the column used in the gas chromatograph is nearly identical to the order of the boiling points of the compounds. The boiling points of trans- and cis-decalin are 187.95 °C (102 KPa, [107]) and 195.7 °C (101 KPa, [108]), respectively. Spiro[4.5]decane has a boiling point of 185 °C at 101 KPa [109] and should therefore occur next to trans-decalin in the gas chromatogram.

The mechanistic views of skeletal isomerization of aliphatic hydrocarbons on bifunctional catalysts are applied for the isomerization of decalin in order to identify which isomers would be expected [42]. Type A isomerizations in which the number of branchings remains constant are considered to be faster than type B isomerizations in which the number of branchings increases or decreases. Type A rearrangements of carbenium ions proceed via classical 1,2-alkyl and hydride shifts. Products predicted by the type A mechanism are spiro[4.5]decane,

bicyclo[4.3.1]decane and bicyclo[5.3.0]decane, as illustrated in Figure 8.43. Thus, the mechanistic view would support the idea of spiro[4.5]decane as a first isomerization product. The other two isomers could not be found under the reaction products of the decalin hydroconversion on these two bifunctional catalysts, although the retention time of bicyclo[5.3.0]decane is well-known from other catalysts where traces of this compound are found. This could presumably be due to a higher cyclic stress of seven-membered rings in contrast to six-membered rings and to the lower stability of the secondary carbenium ions (Figure 8.43 middle and right) in comparison to tertiary ones (Figure 8.43 left).

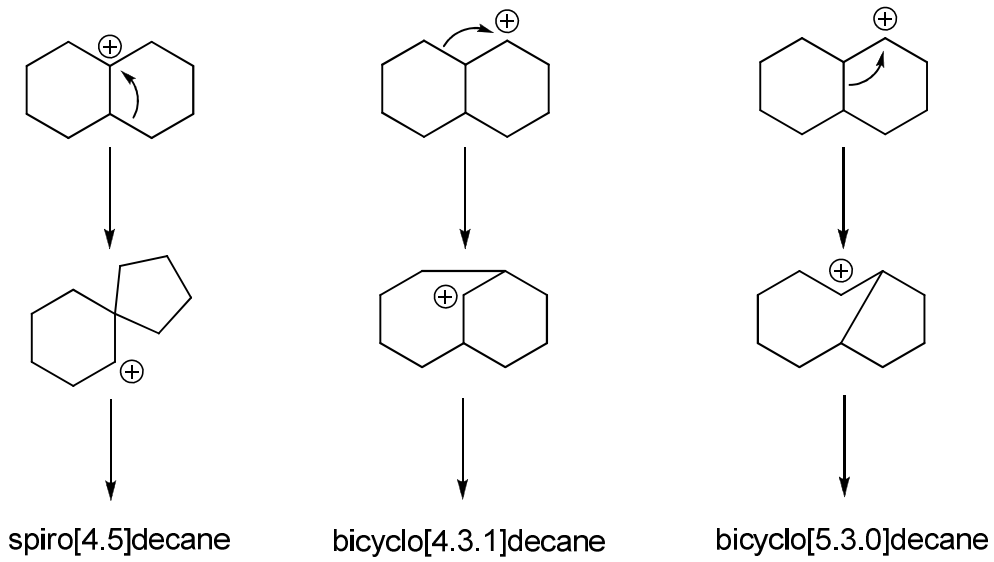

Figure 8.43: Type A isomerization of the tertiary and secondary carbenium ions derived from decalin.

Skeletal isomerization of decalin occurring as a first step on bifunctional catalysts is in accordance with a mechanism proposed by Kubička *et al.* [54] for the decalin transformation on Pt/H-Beta which is depicted in Figure 4.16 in Section 4.3.2. Suggestions, which kind of isomers are likely to be formed were made in Ref. [55] and illustrated in Figure 4.17 in Section 4.3.2. Only one group reported about the observation of spiro[4.5]decane as a product of the decalin hydroconversion on bifunctional catalysts [71], other groups consider only products of type B skeletal isomerization as products like methylbicyclo[4.3.0]nonane [51, 52].

All the numerous skeletal isomers of decalin can undergo ring opening and hydrocracking leading to very complex product mixtures. Hence, tracing back the precise pathway of formation of each of these product hydrocarbons is too complicate. The carbon number distribution of the hydrocracked products gives hints to what happens next. After ring opening of one naphthenic ring of the skeletal isomers of decalin into ring opening products,

these products mainly undergo skeletal isomerization in the alkyl side chain as described above, and the paring reaction occurs leading very selectively to iso-butane and methylcyclopentane.

While invoking the occurrence of the paring reaction satisfactorily explains the large amounts of hydrocracked products with 4 and 6 carbon atoms on the two bifunctional catalysts, it does not account for small amounts of hydrocarbons with other carbon numbers and the formation of open-chain decanes. It cannot be ruled out that a small contribution of hydrogenolysis on the noble metals plays a role in the formation of C_1 and C_9 hydrocarbons and perhaps also in the formation of open-chain decanes. The identical gas chromatograms, activities, selectivities and even the branchings of the decane isomers on the iridium- and the platinum-containing La-X catalysts are rather an indication that the metal has only a dehydrogenation / hydrogenation function which is typical for bifunctional catalysts, otherwise it would be expected that the different kind of metals should generate different products as seen in the following sections.

8.6.2 Hydrogenolysis on Iridium

On many investigated iridium-containing catalysts carbon number distribution curves with a hammock shape are observed, as summarized in Figure 8.44, which are assigned to hydrogenolysis on iridium leading to large amounts of methane and C_9. Nevertheless, not on all catalysts showing such a hammock-shaped curve pure hydrogenolysis on iridium is taking place. During the variation of the strength of Brønsted acid sites on some catalysts with a very low strength of these sites the absence of the skeletal isomer spiro[4.5]decane is observed, and then a gas chromatogram with less product hydrocarbons is obtained which can be easily distinguished from gas chromatograms obtained from the products generated on Ir/Na,H-Y catalysts which possess also a hammock-shaped distribution curve. In Figure 8.44, the carbon number distributions of the hydrocracked products obtained on three iridium-containing catalysts are shown. For all catalysts the hammock-shaped curves are nearly identical, nevertheless, on catalyst 2.9Ir/$Na_{0.90}$,$H_{0.10}$-Y spiro[4.5]decane is formed indicating that the catalyst has an isomerization function, presumably strong enough Brønsted acid sites. On the two other catalysts with nearly the same amount of iridium and thus the same concentration of Brønsted acid sites, the strength seems to be too low to allow isomerization, and accordingly no spiro[4.5]decane is observed, not even in traces. In addition to catalysts 2.6Ir/$Cs_{0.71}$,$Na_{0.16}$,$H_{0.13}$-Y and 3.0Ir/$Na_{0.90}$,$H_{0.10}$-LSX, also 2.7Ir/$K_{0.88}$,$H_{0.12}$-Y and 2.6Ir/$Rb_{0.70}$,$Na_{0.15}$,$H_{0.15}$-Y belong to this category of catalysts.

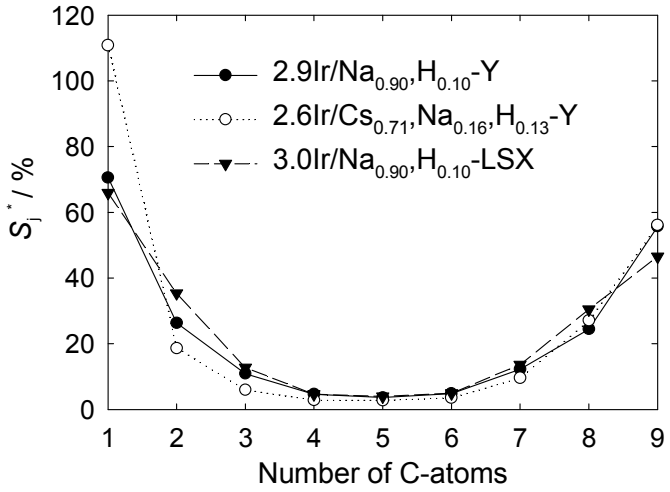

Figure 8.44: Modified hydrocracking selectivities S_j* on iridium-containing catalysts with mainly hydrogenolysis activity:

2.9Ir/$Na_{0.90}$,$H_{0.10}$-Y: T_r = 300 °C; X_{Dec} = 86 %; $Y_{C_{9^-}}$ = 24 %; $\sum S_j$* = 217 %.

2.6Ir/$Cs_{0.71}$,$Na_{0.16}$,$H_{0.13}$-Y: T_r = 319 °C; X_{Dec} = 85 %; $Y_{C_{9^-}}$ = 51 %; $\sum S_j$* = 243 %.

3.0Ir/$Na_{0.90}$,$H_{0.10}$-LSX: T_r = 340 °C; X_{Dec} = 85 %; $Y_{C_{9^-}}$ = 42 %; $\sum S_j$* = 222 %.

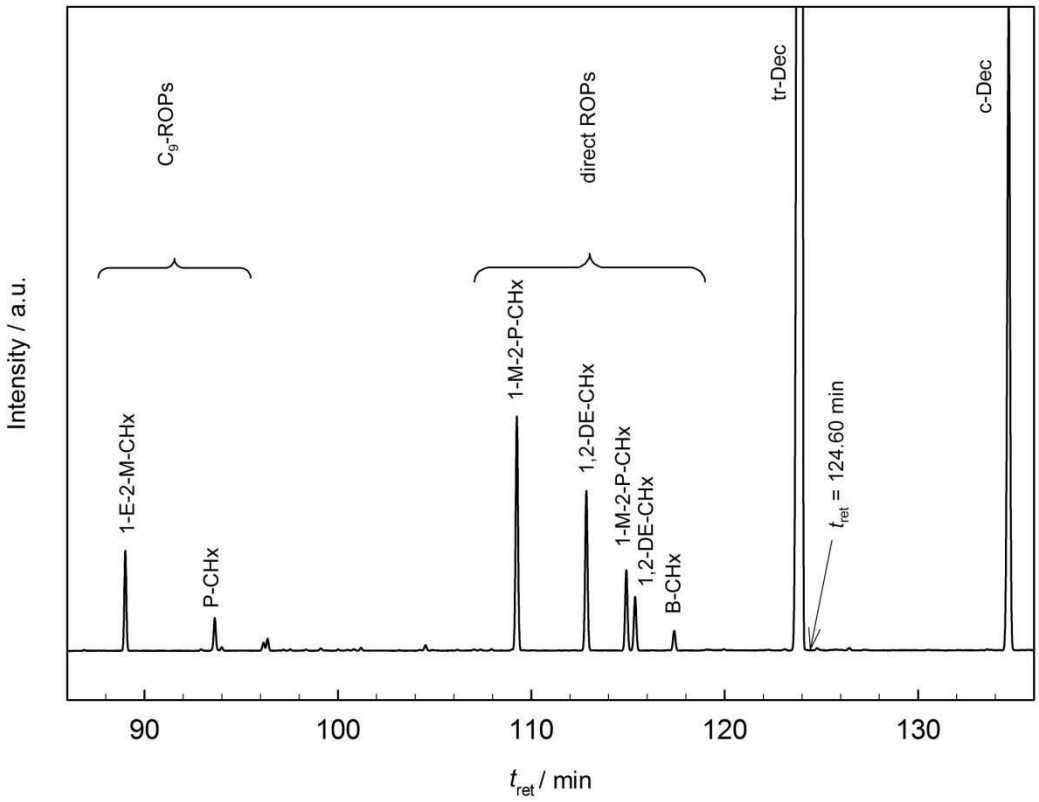

Figure 8.45: Extraction of the gas chromatogram of the product of cis-decalin hydroconversion on 2.6Ir/$Cs_{0.71}$,$Na_{0.16}$,$H_{0.13}$-Y at T_r = 262 °C and X_{Dec} = 8.9 %.

In Figure 8.45, a section of the gas chromatogram of the product obtained in the hydroconversion of cis-decalin on catalyst 2.6Ir/$Cs_{0.71}$,$Na_{0.16}$,$H_{0.13}$-Y at a low conversion of X_{Dec} = 8.9 % is depicted as an example. The signal at t_{ret} = 124.60 min, which is assigned to spiro[4.5]decane, is absent. The product group of ring opening products consists mainly of butylcyclohexane (B-CHx), cis- and trans-1-methyl-2-propylcyclohexane (1-M-2-P-CHx) and cis- and trans-1,2-diethylcyclohexane (1,2-DE-CHx) which are directly formed by ring opening of decalin (direct ROPs). Furthermore, the chromatogram is dominated by two more peaks assigned to 1-ethyl-2-methylcyclohexane (1-E-2-M-CHx) and propylcyclohexane (P-CHx). 1-Ethyl-2-methylcyclohexane would be expected to occur as a cis- and a trans-isomer. From the hydroconversion experiments of perhydroindan it can be expected that a small signal next to propylcyclohexane is the second isomer.

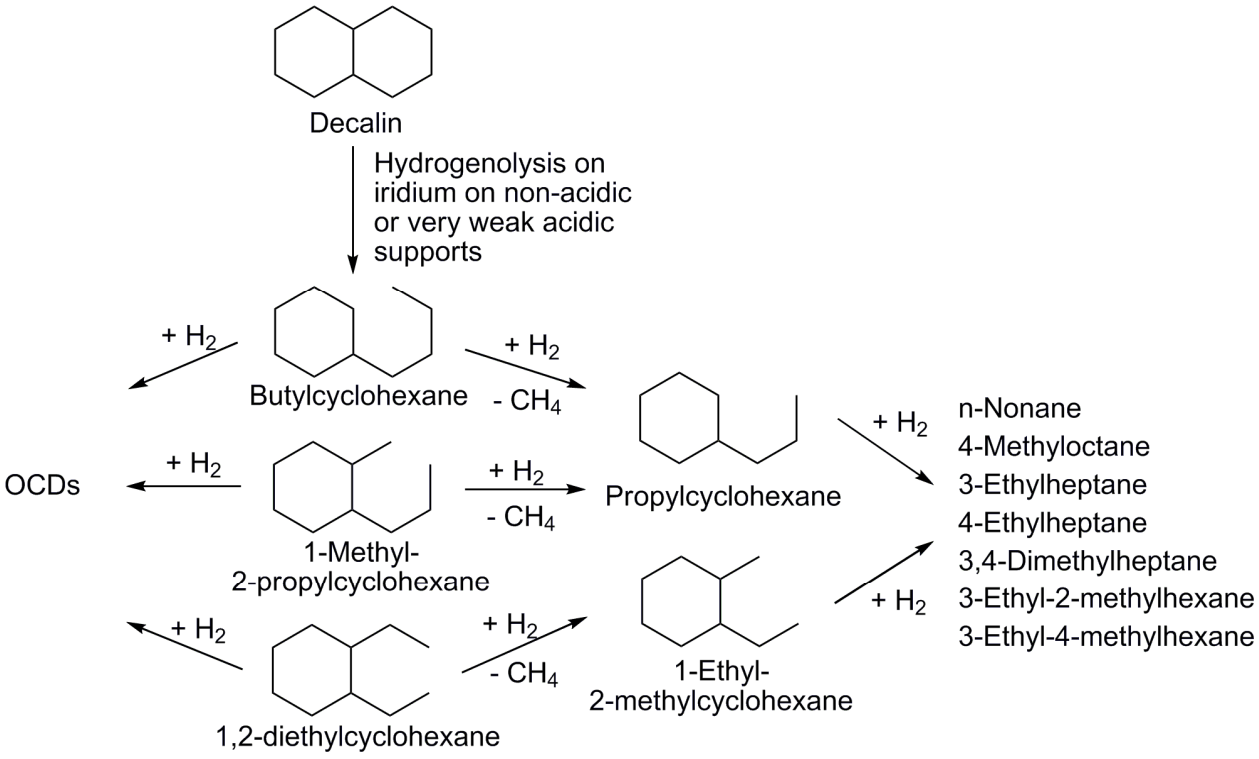

Figure 8.46: Pathways for the hydrogenolytic steps on iridium on non-acidic or very mildly acidic supports.

On the basis of the results obtained on the catalysts with a very low strength of Brønsted acid sites, it can be concluded that, on such catalysts, hydrogenolysis of one endocyclic carbon-carbon bond of decalin is the first main catalytic step leading to five direct ROPs (two have cis / trans isomers) as depicted in Figure 8.46. This step is very selective as shown by the data in Table 8.13. On all four catalysts 95 - 96 % of all ring opening products are the five

direct ROPs. About 60 % of the direct ROPs consist of 1-methyl-2-propylcyclohexane, 35 % of 1,2-diethylcyclohexane and only 5 % of butylcyclohexane. As mentioned in Section 4.3.1.2, depending on the dispersion and kind of noble metal, the C-C bond rupture of endocyclic bonds can happen selectively between secondary carbon atoms or statistically (non-selectively). The expected selectivities for both mechanisms are also depicted in Table 8.13. The experimental data suggest that the hydrogenolysis on iridium proceeds mainly through the selective mechanism.

Table 8.13: Details on the formation of direct ROPs at low conversion.

Catalyst	T_r / °C	X_{Dec} / %	$\frac{S_{direct\ ROPs}}{S_{ROPs}}$	$\frac{S_{B\text{-}CHx}}{S_{direct\ ROPs}}$	$\frac{S_{1\text{-}M\text{-}2\text{-}P\text{-}CHx}}{S_{direct\ ROPs}}$	$\frac{S_{1,2\text{-}DE\text{-}CHx}}{S_{direct\ ROPs}}$
3.0Ir/$Na_{0.90}$,$H_{0.10}$-LSX	320	40.8	0.95	0.09	0.57	0.34
2.7Ir/$K_{0.88}$,$H_{0.12}$-Y	281	28.4	0.96	0.05	0.60	0.35
2.6Ir/$Rb_{0.70}$,$Na_{0.15}$,$H_{0.15}$-Y	280	36.3	0.96	0.04	0.59	0.37
2.6Ir/$Cs_{0.71}$,$Na_{0.16}$,$H_{0.13}$-Y	282	26.2	0.96	0.04	0.59	0.37
predicted for non-selective ring opening of decalin	-	-	1.00	0.40	0.40	0.20
predicted for selective ring opening of decalin	-	-	1.00	0.00	0.67	0.33

In a next step these direct ROPs can undergo either endocyclic hydrogenolysis leading to open-chain decanes or exocyclic abstraction of methane leading to the direct C_9-ROPs propylcyclohexane (P-CHx) or 1-ethyl-2-methylcyclohexane (1-E-2M-CHx). An additional support for these reaction pathways is given in Figure 8.47. The direct ROPs are indeed primary products, and with increasing conversion they are converted into direct C_9-ROPs. In further consecutive reactions OCDs and direct OCNs are formed.

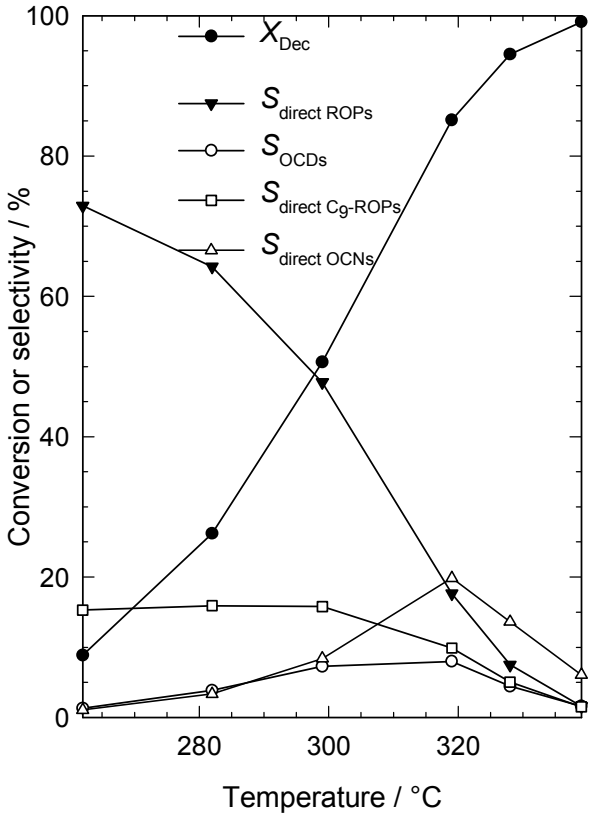

Figure 8.47: Temperature dependence of decalin conversion and selectivities of direct ROPs, OCDs, direct C_9-ROPs and direct OCNs on catalyst 2.6Ir/$Cs_{0.71}$,$Na_{0.16}$,$H_{0.13}$-Y.

The important role of exocyclic methane abstraction is reflected in the carbon number distribution of the hydrocracked products (Figure 8.44). The hammock-shaped curve originates mainly from the preferred formation of C_1 and C_9 fragments. 31 % of the C_9 fraction on catalyst 2.6Ir/$Cs_{0.71}$,$Na_{0.16}$,$H_{0.13}$-Y consist of the direct C_9-ROPs 1-ethyl-2-methylcyclohexane and propylcyclohexane. Almost the entire remaining C_9 hydrocarbons (67 %) are open-chain nonanes formed by hydrogenolytic ring opening of the direct C_9-ROPs. Again this step proceeds in a very selective manner. On catalyst 2.6Ir/$Cs_{0.71}$,$Na_{0.16}$,$H_{0.13}$-Y even at 85 % conversion 93% of all observed OCNs are products of the ring opening of the direct C_9-ROPs. A gas chromatogram of the corresponding section is given in Figure 8.48.

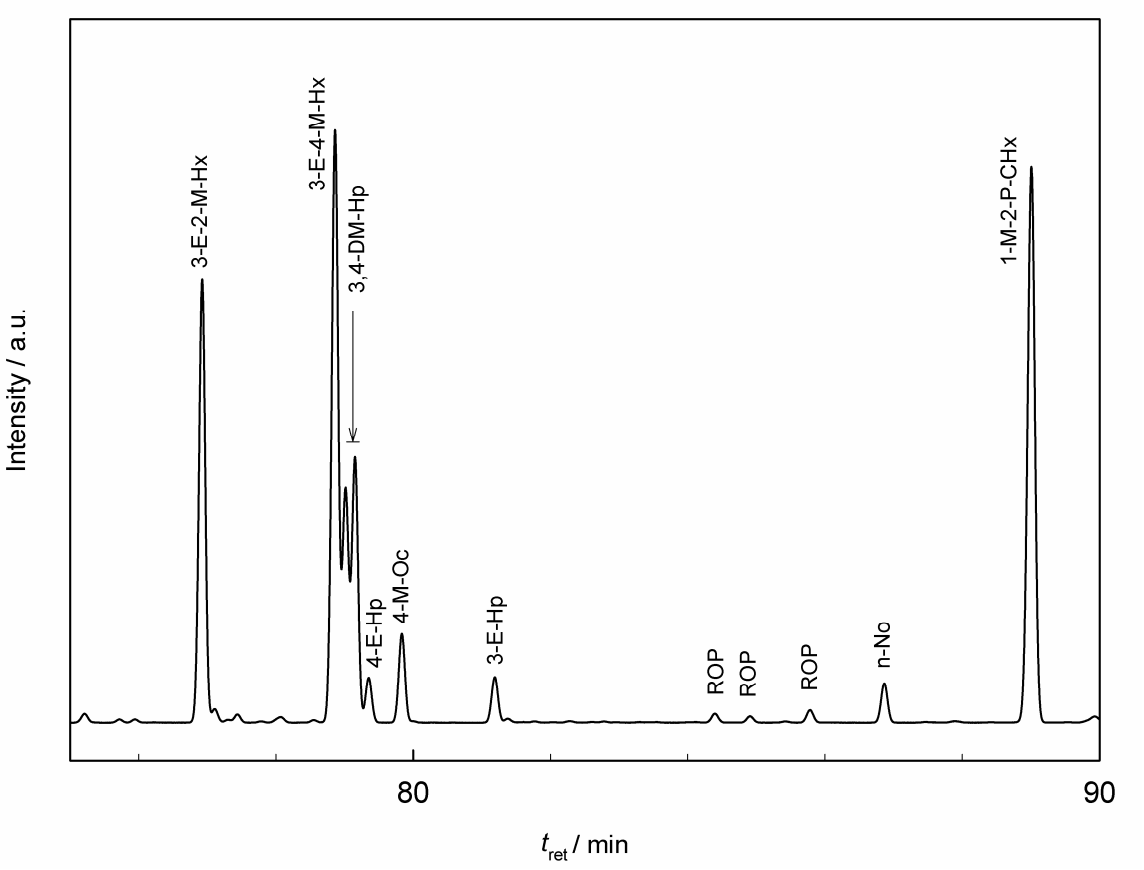

Figure 8.48: Extraction of the gas chromatogram of the product of cis-decalin hydroconversion on 2.6Ir/$Cs_{0.71}$,$Na_{0.16}$,$H_{0.13}$-Y at T_r = 319 °C and X_{Dec} = 85.1 %.

Table 8.14: Selectivities of open-chain nonanes obtained on catalyst 2.6Ir/$Cs_{0.71}$,$Na_{0.16}$,$H_{0.13}$-Y at X_{Dec} = 85 % by ring opening of the direct C_9-ROPs P-CHx (27 %) and 1-E-2-M-CHx (73 %) in comparison to the expected values of non-selective and selective ring opening.

	experimental	**predicted for non-selective ring opening**	**predicted for selective ring opening**
$S_{n\text{-}No}$ / $S_{direct\ OCNs}$	0.02	0.21	0.00
$S_{4\text{-}M\text{-}Oc}$ / $S_{direct\ OCNs}$	0.05	0.21	0.14
$S_{3\text{-}E\text{-}Hp}$ / $S_{direct\ OCNs}$	0.03	0.12	0.00
$S_{4\text{-}E\text{-}Hp}$ / $S_{direct\ OCNs}$	0.03	0.10	0.14
$S_{3,4\text{-}DM\text{-}Hp}$ / $S_{direct\ OCNs}$	0.27	0.12	0.24
$S_{3\text{-}E\text{-}2\text{-}M\text{-}Hx}$ / $S_{direct\ OCNs}$	0.25	0.12	0.24
$S_{3\text{-}E\text{-}4\text{-}M\text{-}Hx}$ / $S_{direct\ OCNs}$	0.35	0.12	0.24

The selectivities of the individual direct OCNs are listed in Table 8.14, again in comparison to the expected values for selective and non-selective ring opening. The selectivities resemble those predicted for selective ring opening, but the selectivities of 4-methyloctane and 4-ethylheptane are lower than expected. Some deviations could originate from the competitive formation of OCNs through methane abstraction of OCDs.

Selectivities of the open-chain decanes are not listed individually, because some OCDs to be expected by endocyclic hydrogenolysis of the direct ROPs could not be safely identified in the chromatograms. This is mainly due to the fact that some OCDs formed by hydrogenolysis like 4-isopropylheptane are not preferentially formed as isomerization products of n-decane on bifunctional catalysts which are mainly used for peak assignment (Section 7.1).

8.6.3 Hydrogenolysis on Platinum

The same four supports on which nearly pure hydrogenolysis on iridium was observed show a different catalytic behavior when loaded with platinum. These catalysts are very little active and form tetralin and naphthalene with high selectivities. As depicted in Figure 8.20 in Section 8.2.2, the carbon number distributions of the hydrocracked products obtained on these catalysts are similar to the curves obtained on Pt/Na,H-Y catalysts except for the higher $\sum S_j^*$ of approximately 300 % due to higher modified selectivities of C_2, C_3 and especially C_1. In contrast to the iridium-containing catalysts the signal of spiro[4.5]decane was still observed on all catalysts (Table 8.15). On the potassium- and rubidium-containing Y catalysts the selectivity of spiro[4.5]decane at low conversion is in the same range as on Pt/Na,H-Y catalysts but on the cesium-containing Y catalyst and on LSX the selectivity is much lower. Possibly, on the latter two catalysts a purer hydrogenolysis on the metal is taking place indicated also by higher selectivities of dehydrogenated products. The observation of spiro[4.5]decane on the platinum-containing catalysts in contrast to the iridium-containing catalysts can be due to either the lower hydrogenolysis activity of platinum and thus a higher influence of the Brønsted acid sites with low strength or to an isomerization activity of the metal platinum (see also Section 4.3.1.2).

Table 8.15: Comparison of the selectivities of spiro[4.5]decane S_{spiro}.

Catalyst	T_r / °C	X_{Dec} / %	S_{spiro} / %
2.9Pt/$K_{0.90}$,$H_{0.10}$-Y	360	26.5	23.7
2.9Pt/$Rb_{0.68}$,$Na_{0.15}$,$H_{0.17}$-Y	360	18.7	23.6
3.1Pt/$Cs_{0.71}$,$Na_{0.16}$,$H_{0.13}$-Y	362	19.2	6.3
2.9Pt/$Na_{0.89}$,$H_{0.11}$-LSX	390	18.9	1.5

In Figure 8.49, a section of the gas chromatogram of the product of the cis-decalin hydroconversion on catalyst 3.1Pt/$Cs_{0.71}$,$Na_{0.16}$,$H_{0.13}$-Y at a low conversion of X_{Dec} = 19.3 % is depicted as an example. The large peaks of tetralin and naphthalene are not shown. As obvious, besides spiro[4.5]decane several skeletal isomers of decalin are formed. Isomers from type A isomerization of decalin as bicyclo[5.3.0]decane (see Figure 8.43, Section 8.6.1) and from consecutive type A isomerization of spiro[4.5]decane, namely bicyclopentyl could be identified. In addition, also isomers of type B isomerization like methylbicyclo[3.3.1]nonane and methylbicyclo[4.3.0]nonane are formed. In a next step the direct ROPs butylcyclohexane, 1-methyl-2-propylcyclohexane and 1,2-diethylcyclohexane with a relative distribution of 64, 27 and 9 % are formed. This distribution matches neither a selective nor a non-selective mechanism of hydrogenolysis (see Table 8.13, Section 8.6.2). A closer look at the hydrocracked products, which are formed in very low yields, reveals that cyclic C_6 to C_8 hydrocarbons are mainly formed, namely 1,2-dimethylcyclohexane, ethylcyclohexane, methylcyclohexane and cyclohexane. In addition, the associated light hydrocarbons methane, ethane, propane and only n-butane are observed.

All in all, the platinum-containing catalysts are very little active in the hydrogenolysis of carbon-carbon bonds, leading mainly to dehydrogenated products of decalin due to the thermodynamic equilibrium. In addition, the first necessary step for the formation of open-chain decanes or nonanes, the opening of one ring of decalin occurs but then mainly hydrogenolysis of exocyclic C-C bonds leading to hydrocracked products takes place. On these catalysts only traces of open-chain decanes are observed. Pure hydrogenolysis on platinum does not seem to be the ideal mechanism for enhancing the cetane number of diesel fuels.

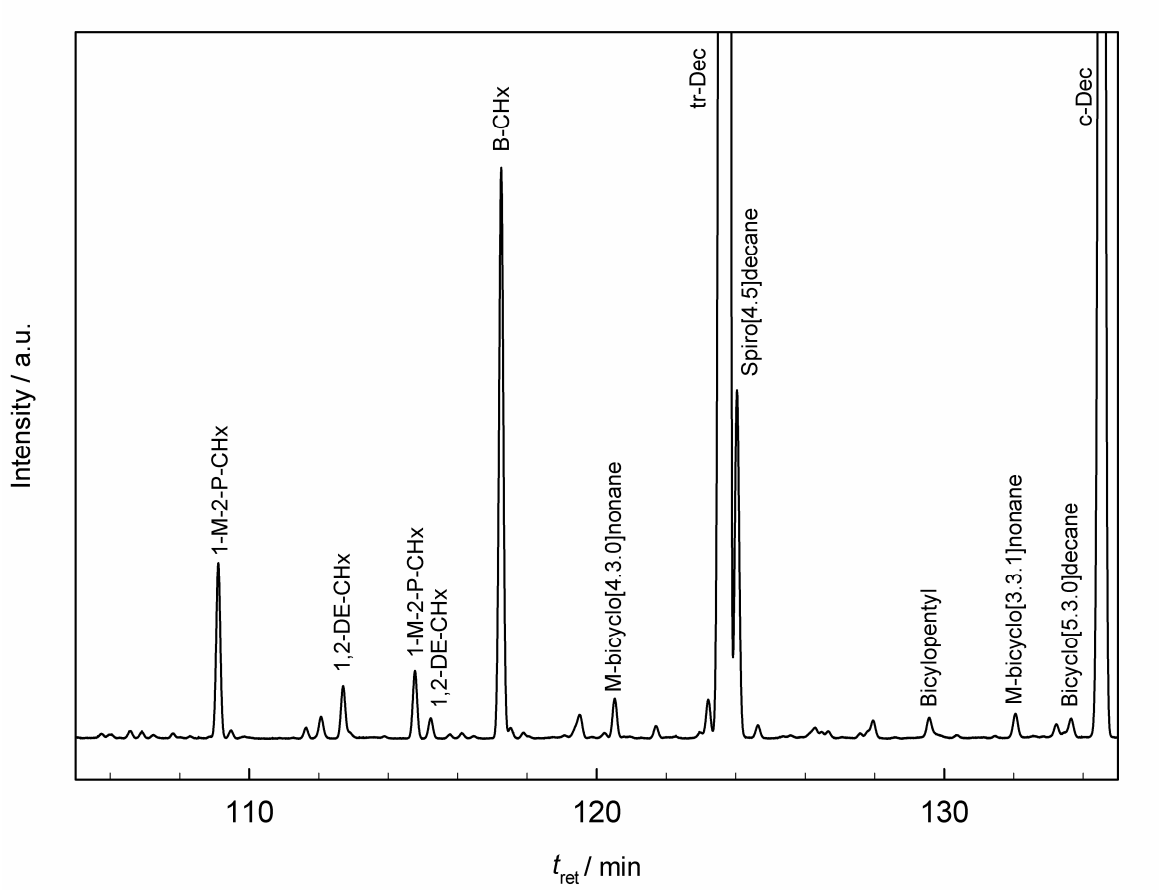

Figure 8.49: Extraction of the gas chromatogram of the product of cis-decalin hydroconversion on 3.1Pt/$Cs_{0.71}$,$Na_{0.16}$,$H_{0.13}$-Y at T_r = 362 °C and X_{Dec} = 19.3 %.

8.7 Properties of High-Performance Ir or Pt/FAU Catalysts

In Table 8.16, the top three FAU catalysts containing iridium or platinum are listed. The best iridium-containing catalysts are obtained by varying the strength and the concentration of the Brønsted acid sites. It looks as if the carbon number distribution of the hydrocracked products is a useful tool to evaluate if a catalyst under investigation needs a higher or lower concentration or a higher or lower strength of Brønsted acid sites in order to achieve high yields of open-chain decanes. A pure hydrogenolysis on iridium generates a hammock-shaped distribution curve (Figure 8.50 left). By increasing the strength of the acid sites slightly the curves remain unchanged, but then in case of the two best catalysts the curves are lifted slightly in the range of C_4 to C_6. An even higher strength leads to weak maxima at C_4 and C_6 indicating a superimposition of bifunctional catalysis. In the latter case the yield of OCDs decreases. By varying the concentration of Brønsted acid sites the same observations can be made. A catalyst with a very low concentration of Brønsted acid sites possesses a hammock-shaped curve. Upon increasing the concentration of the acid sites the curves are

lifted between C_3 and C_7 until they show pronounced maxima at C_4 and C_6. The best catalyst shows a lifted curve with very local maxima at C_4 and C_6.

Table 8.16: Overview of the best three iridium- and platinum-containing FAU catalysts concerning the formation of OCDs.

Catalyst	T_r / °C	X_{Dec} / %	S_{OCDs} / %	$Y_{OCDs,\ max.}$ / %	Y_{OCNs} / %
3.2Ir/$Na_{0.81}$,$H_{0.19}$-Y-4.11	290	97.8	40.0	39.1	10.5
3.3Ir/$Na_{0.88}$,$H_{0.12}$-Y-3.44	299	98.2	38.6	37.9	13.0
0.99Ir/$Na_{0.26}$,$La_{0.22}$,$H_{0.08}$-X	307	91.4	36.9	33.7	3.5
3.7Pt/$Na_{0.86}$,$H_{0.14}$-Y	360	98.3	41.8	41.1	5.6
3.0Pt/$Na_{0.88}$,$H_{0.12}$-Y	361	96.3	40.7	39.1	3.9
2.7Pt/$Na_{0.88}$,$H_{0.12}$-Y	373	98.8	37.4	36.9	5.7

The results on the iridium-containing catalysts demonstrate that a balance between the concentration and strength of Brønsted acid sites as well as the metal loading is needed. The carbon number distribution curve of the hydrocracked products can be a good tool for the optimization of future catalysts.

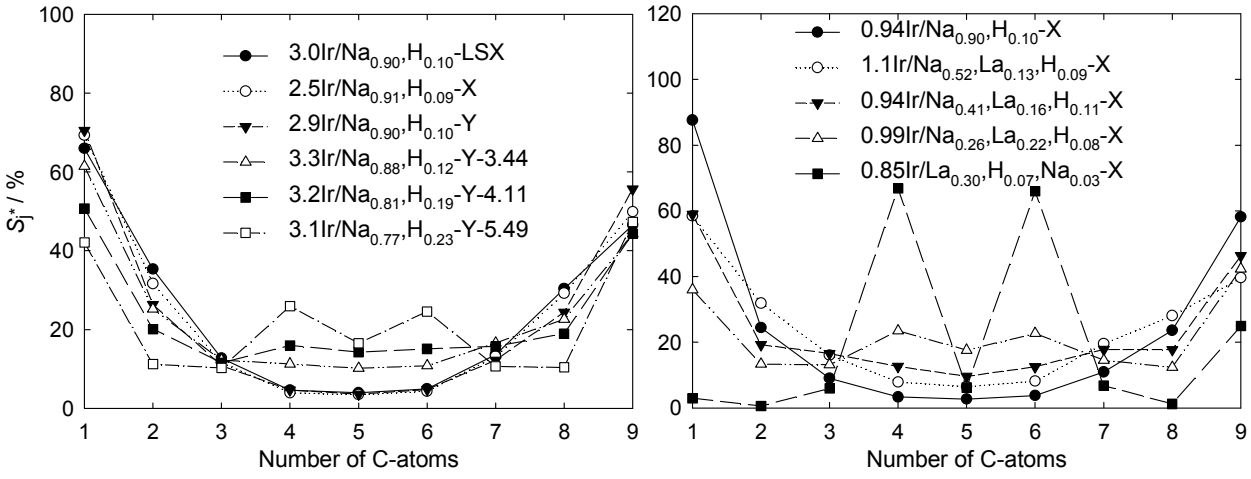

Figure 8.50: Changes in the modified hydrocracking selectivities S_j^* upon varying the strength (left) and concentration (right) of Brønsted acid sites. Details see Figure 8.24 and Figure 8.32 in Sections 8.3.1 and 8.4.1.2.

The platinum-containing catalysts show slightly better performances concerning the yield of open-chain decanes. In addition, the OCDs formed are less branched than the decane isomers obtained on iridium-containing catalysts, which is preferred in view of the enhancement of the cetane number in diesel fuels. The best platinum-containing catalyst is a

Na,H-Y catalyst with approximately 3 wt.-% platinum. The acid strength and concentration seem to be in an optimal balance in this system. Every effort to vary the strength or concentration of Brønsted acid sites so far led to lower yields of OCDs. The Pt/Na,H-Y system appears to be very sensitive towards every change in the concentration or strength of Brønsted acid sites. A lower strength of Brønsted acid sites than in the above-mentioned systems leads to a strong decrease of the activity and the formation of dehydrogenated products of decalin. A higher strength or a higher concentration of Brønsted acid sites leads to a strong contribution of bifunctional catalysis with large amounts of iso-butane and methylcyclopentane. Unfortunately, without being able to determine the concentration and strength of Brønsted acid sites, it is not possible to predict which property has to be changed to enhance the performance of an investigated platinum-containing FAU catalyst. The carbon number distribution can only give a hint if the concentration or strength of the Brønsted acid sites in the system is too high when a pronounced M-shape is visible. Possibly, the carbon number distribution of the hydrocracked products is not as sensitive as in case of iridium because hydrogenolysis on platinum alone leads to the formation of C_3, C_4, C_6 and C_7 hydrocarbons which makes it difficult to differentiate if bifunctional catalysis (C_4 and C_6) is superimposed to a small extent.

The best platinum- or iridium-containing catalysts are mainly ones on which the hydrogenolysis on the metal is dominating, but Brønsted acid sites are needed to improve the performance. In the platinum-containing catalysts the contribution of bifunctional catalysis improves at least the activity of the system, and in the iridium-containing catalysts this contribution leads to an isomerization function which allows better performances. These catalysts are denoted in Figure 8.51 as trifunctional catalysts in order to emphasize that in contrast to the bifunctional catalysts the metal is not only responsible for the dehydrogenation / hydrogenation but also for the hydrogenolysis. This figure is similar to Figure 8.41, but supplemented with the results obtained in this work especially with hints to identify the different groups of catalysts.

The changes in the strength and concentration of Brønsted acid sites occurring upon chemically modifying the catalysts are based on the knowledge of the current literature. For a validation of the mechanistic views advanced here appropriate methods for reliably measuring both the strength and the concentration of Brønsted acid sites in metal-containing zeolites of the type used in this work remain to be developed.

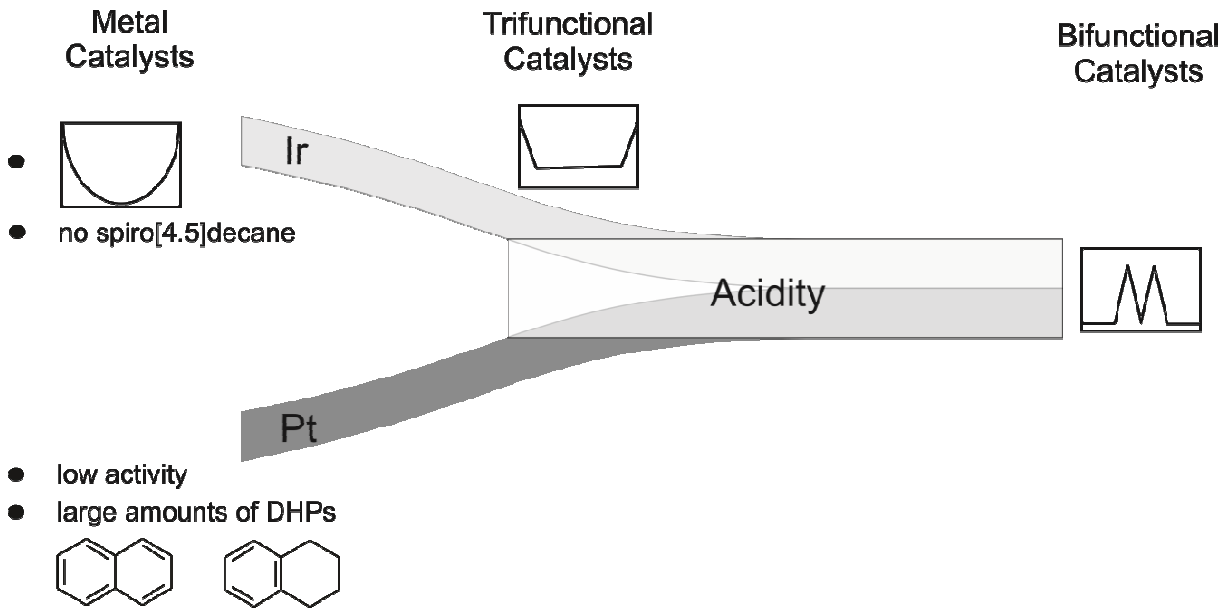

Figure 8.51: Overview of the different mechanisms occurring in the ring opening of decalin and some significant hints for each mechanism.

9 Ring Opening of Decalin on Catalysts Based on Zeolite ZSM-12 (MTW)

Zeolite ZSM-12 possesses the narrowest pore system of all 12-membered ring zeolites as also indicated by a very low Spaciousness Index (see Section 4.3.1.4, Figure 4.14). This zeolite was used as a catalyst in the hydroconversion of decalin in order to check for shape-selective effects as observed, for example, in the hydroconversion of methylcyclohexane with ZSM-5. On the H-ZSM-5 catalyst the shape selectivity lead to a contribution of Haag-Dessau hydrocracking in addition to the commonly observed bimolecular cracking [110]. Furthermore, only negligible deactivation of the catalyst was observed, which is usually a great problem of monofunctional acidic catalysts in the hydroconversion of hydrocarbons (see Section 4.3.2).

9.1 Noble-Metal Containing ZSM-12 Catalysts

Two pairs of catalysts were prepared for the hydroconversion of decalin. One set was a Na-ZSM-12 zeolite loaded with 3 wt.-% of platinum or iridium and only those Brønsted acid sites which are generated by the reduction of the noble metal. The resulting catalysts are 2.9Pt/$H_{0.95}$,$Na_{0.05}$-ZSM-12-39 and 1.7Ir/$H_{0.65}$,$Na_{0.35}$-ZSM-12-39. Unfortunately, a metal loading of only 1.7 wt.-% was achieved on the iridium-containing catalyst. A successful exchange with 2.9 wt.-% platinum suggests that there are enough exchangeable cation sites in the zeolite, but perhaps due to steric effects it is not possible for the iridium complex to reach all exchangeable sites. The other set of catalysts was based on a partially ammonium-exchanged Na-ZSM-12 zeolite loaded with approximately 1 wt.-% of iridium (0.94Ir/$H_{0.66}$,$Na_{0.34}$-ZSM-12-42) or platinum (1.3Pt/$H_{0.76}$,$Na_{0.24}$-ZSM-12-42). Due to the prior ammonium exchange additional Brønsted acid sites were generated in the catalysts. The metal content of these two catalysts was lowered due to the problems encountered with the first two catalysts what hampers a direct comparison of all four catalysts.

The results of the hydroconversion of decalin on all four catalysts are depicted in Figure 9.1. At low conversion skeletal isomers are prevailing on all four catalysts even on the iridium-containing catalysts. This indicates a strong contribution of the Brønsted acid sites in the hydroconversion of decalin since iridium alone has no or very low isomerization properties, as the results obtained on the FAU catalysts show. At higher conversions the selectivities of the skeletal isomers of decalin decrease, and ring opening products, open-chain decanes

and hydrocracked products are formed. The selectivity of dehydrogenated products is negligible, and no hydrocarbons with more than ten carbon atoms are detected.

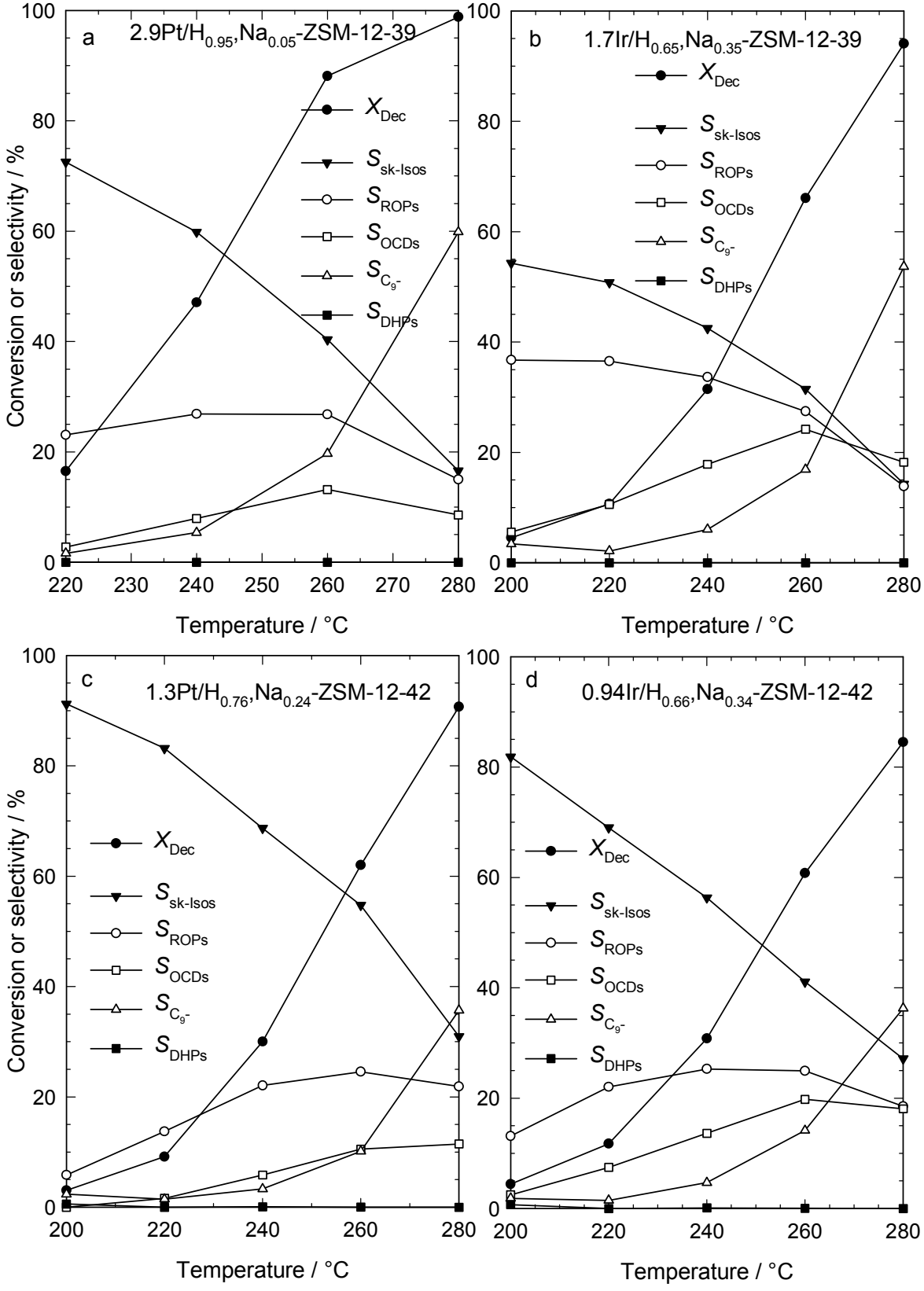

Figure 9.1: Conversion of decalin and selectivities of different groups of products in dependence of the reaction temperature for metal-containing ZSM-12 catalysts.

Since monofunctional iridium-containing FAU catalysts are usually more active than monofunctional platinum-containing FAU catalysts, the similar activities of all four ZSM-12 catalysts could stem from a large contribution of Brønsted acid sites. Both iridium-containing catalysts show the best performances concerning the formation of open-chain decanes. The yields of open-chain nonanes are negligible. In Table 9.1, the maximum yields of OCDs of all four catalysts are listed. The values are much lower than those obtained on the best faujasite catalysts.

Table 9.1: Maximum yields of open-chain decanes obtained on metal-containing ZSM-12 catalysts.

Catalyst	T_r / °C	X_{Dec} / %	S_{OCDs} / %	$Y_{OCDs,\ max.}$ / %	Y_{OCNs} / %
2.9Pt/$H_{0.95}$,$Na_{0.05}$-ZSM-12-39	260	88.1	13.2	11.6	0.2
1.7Ir/$H_{0.65}$,$Na_{0.35}$-ZSM-12-39	280	94.1	18.2	17.1	3.2
1.3Pt/$H_{0.76}$,$Na_{0.24}$-ZSM-12-42	280	90.7	11.5	10.4	0.2
0.94Ir/$H_{0.66}$,$Na_{0.34}$-ZSM-12-42	280	84.5	18.1	15.3	1.0

In Figure 9.2, the carbon number distributions of the hydrocracked products are presented for the four metal-containing ZSM-12 catalysts. Clearly, they consist of a superposition of the M-shaped curves typical for bifunctional catalysts and a large contribution of hydrogenolysis leading to C_1 and C_9. The contribution of hydrogenolysis is more pronounced for the iridium catalysts than for the platinum catalysts. The pronounced M-shaped curve even on the first two catalysts in which only the Brønsted acid sites generated by the reduction of the metal exist, indicates that the Brønsted acid sites in ZSM-12 zeolites with an n_{Si} / n_{Al} ratio of approximately 40 are very strong.

A better performance of ZSM-12 catalysts can presumably be obtained by reducing the strength of the Brønsted acid sites. This can be achieved by decreasing the n_{Si} / n_{Al} ratio, but the lowest possible value is *ca*. 20, which is possibly not enough to reduce significantly the strength of the acid sites. Otherwise, the strength could be lowered by exchanging the charge-compensating sodium ions with potassium ions or by isomorphous substitution of the aluminum in the lattice with boron [111]. No indications were obtained for shape selectivity occurring.

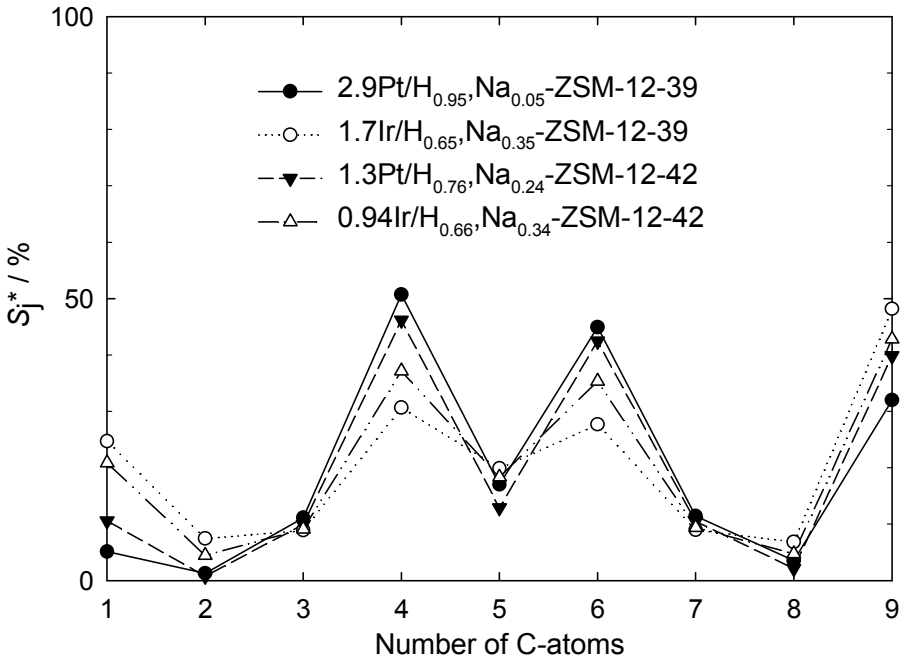

Figure 9.2: Modified hydrocracking selectivities S_j^* on the metal-containing ZSM-12 catalysts:

2.9Pt/$H_{0.95}$,$Na_{0.05}$-ZSM-12-39: T_r = 260 °C; X_{Dec} = 88 %; $Y_{C_{9^-}}$ = 17 %; $\sum S_j^*$ = 177 %.

1.7Ir/$H_{0.65}$,$Na_{0.35}$-ZSM-12-39: T_r = 260 °C; X_{Dec} = 66 %; $Y_{C_{9^-}}$ = 11 %; $\sum S_j^*$ = 183 %.

1.3Pt/$H_{0.76}$,$Na_{0.24}$-ZSM-12-42: T_r = 260 °C; X_{Dec} = 62 %; $Y_{C_{9^-}}$ = 6 %; $\sum S_j^*$ = 175 %.

0.94Ir/$H_{0.66}$,$Na_{0.34}$-ZSM-12-42: T_r = 260 °C; X_{Dec} = 61 %; $Y_{C_{9^-}}$ = 9 %; $\sum S_j^*$ = 182 %.

9.2 Monofunctional Acidic ZSM-12 Catalysts

Two H-ZSM-12 zeolites were prepared with the largest possible differences in the n_{Si} / n_{Al} ratios of 24 and 125 in order to investigate their behavior in the hydroconversion of decalin. The performance of the monofunctional acidic catalysts is shown in Figure 9.3. For each temperature a new batch of catalyst was used because of the fast deactivation of the acidic catalysts (Figure 9.4). Figure 9.3 shows data obtained after 45 min time-on-stream. Comparison of both catalysts with different n_{Si} / n_{Al} ratios reveals a higher activity of catalyst H-ZSM-12-125 with a lower concentration but higher strength of acid sites at comparable temperatures.

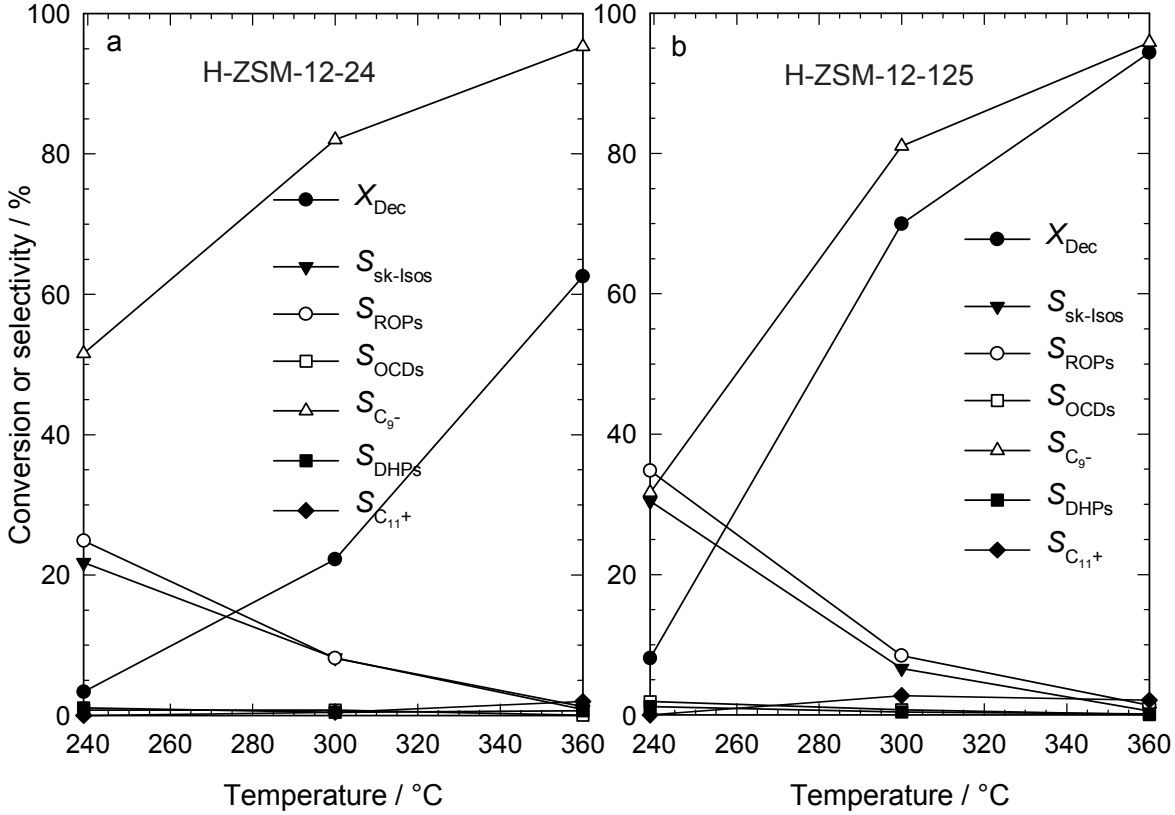

Figure 9.3: Conversion of decalin and selectivities of different groups of products in dependence of the reaction temperature for monofunctional H-ZSM-12 catalysts after 45 min time-on-stream.

In contrast to the metal-containing ZSM-12 zeolites discussed in Section 9.1, on the H-ZSM-12 catalysts the selectivity of hydrocracked products is dominating over the whole temperature range which is very pronounced on zeolite H-ZSM-12-24. A higher concentration of Brønsted acid sites seems to favor the formation of cracked products. The selectivities of skeletal isomers and ring opening products are nearly equal for both catalysts. At temperatures above 300 °C small amounts of products with more than ten carbon atoms are formed, and their selectivity slightly increases with increasing temperature. The formation of these hydrocarbons is probably due to the disproportionation of two cyclic C_{10} molecules to C_9 and C_{11}, as observed with methylcyclopentane and cyclohexane on a bifunctional Pt/Ca-Y catalyst [106]. In the chromatogram of H-ZSM-12 hydrocarbons with up to 13 carbon atoms are obtained. Only very small amounts of OCDs were observed, especially at lower temperatures. The maximum selectivities of OCDs at 239 °C were 0.95 % for catalyst H-ZSM-12-24 and 1.9 % for catalyst H-ZSM-12-125.

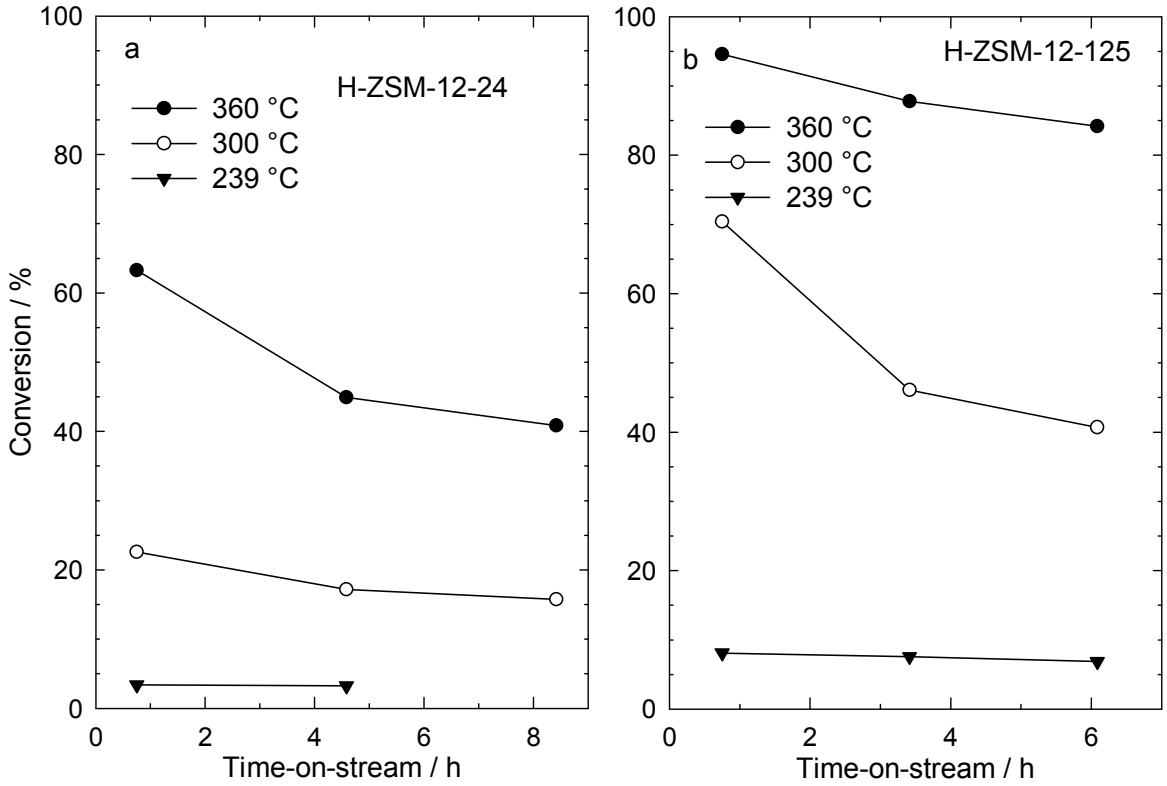

Figure 9.4: Conversion of decalin on the monofunctional H-ZSM-12 catalysts in dependence of time-on-stream.

Catalyst deactivation occurs during hydroconversion of decalin on both H-ZSM-12 catalysts. The dependence of the decalin conversion on time-on-stream is depicted in Figure 9.4. As a general trend, deactivation tends to be more severe, as the reaction temperature is raised. It is found in these experiments that, in spite of the deactivation, product selectivities are not significantly affected within the time-on-streams covered with the two catalysts.

Elemental analyses for carbon of the fresh and spent H-ZSM-12 catalysts are given in Table 9.2. The measured carbon contents do not significantly depend on the reaction temperature of the catalytic experiment, but the n_{Si} / n_{Al} ratio seems to have a strong influence on the amount of coke deposited on the spent catalyst. The catalyst with the higher n_{Si} / n_{Al} ratio shows a higher initial activity but also a higher rate of deactivation. Similar observations were reported by Gopal and Smirniotis [112]. These authors studied the hydroconversion of cyclopentane on 0.5Pt/H-ZSM-12 catalysts with different n_{Si} / n_{Al} ratios. They observed a strong influence of the n_{Si} / n_{Al} ratio of their catalysts on the time-on-stream stabilities: Their samples with the lowest n_{Si} / n_{Al} ratios gave the best time-on-stream behavior, and with increasing n_{Si} / n_{Al} ratio, the ZSM-12 catalysts underwent a more severe deactivation. Interestingly enough, this deactivation behavior of ZSM-12 was at complete variance to the

one shown by other zeolite catalysts based, for example, on zeolites Beta, mordenite or Y [112].

Table 9.2: Carbon content of different H-ZSM-12 samples before and after hydroconversion of cis-decalin at different temperatures.

Catalyst	**Temperature / °C**	**Time-on-stream / h**	**Carbon content / wt.-%**
H-ZSM-12-24	-	0	0.05
H-ZSM-12-24	300	16	0.55
H-ZSM-12-24	360	15.5	0.45
H-ZSM-12-125	-	0	0.08
H-ZSM-12-125	239	15	4.72
H-ZSM-12-125	300	6.5	4.76
H-ZSM-12-125	360	14.5	4.26

No n_H / n_C ratios of the carbonaceous deposits on the spent catalysts were measured, but a visual inspection of the H-ZSM-12-125 catalysts revealed large differences in their colors. The color of H-ZSM-12-125 used as a catalyst at 239 °C hardly differed from that of the fresh zeolite, and the higher the reaction temperature, the darker were the used catalysts. This suggests that, upon increasing the temperature of the catalytic reaction, the coke deposits on the catalysts are getting poorer and poorer in hydrogen.

Another experiment, this time undertaken with the H-ZSM-12-24 zeolite, may also be worth being mentioned: After the catalyst had been on-stream with cis-decalin for 15 h at 300 °C, it was flushed with hydrogen (without decalin) for 3 h at 5.2 MPa and 350 °C at a flow rate of 130 $cm^3 \cdot min^{-1}$. Afterwards, the catalyst was again tested in the hydroconversion of cis-decalin at 300 °C. The activity of the catalyst turned out to be significantly lower than that of the original H-ZSM-12 zeolite. This illustrates that monofunctional H-ZSM-12 catalysts used in the hydroconversion of decalin cannot be satisfactorily regenerated in a hydrogen flow at 350 °C.

In Figure 9.5, the modified cracking selectivities S_j^* are plotted versus the carbon number of the cracked products for the experiment on H-ZSM-12-24 at T_r = 360 °C. The carbon number distribution on H-ZSM-12-125 at T_r = 360 °C is similar and therefore not shown. There are various noteworthy features in this product distribution. Firstly, secondary cracking occurred to a significant extent, as indicated by the lack of symmetry in the molar product distribution and a $\sum S_j^*$ far above 200 %. Secondly, while the light products up to C_6 are fully saturated,

unsaturated hydrocarbons occur in the C_7 to C_9 fractions. The unsaturated hydrocarbons consist mainly of aromatics like toluene, xylenes and ethylbenzene but also cyclohexene derivates are present. Thirdly, there is no M-shaped distribution curve as in hydrocracking of C_{10} naphthenes on bifunctional catalysts. Finally, while C_4 and C_3 products are clearly dominating, there are noticeable amounts of methane and ethane as well. Since there is no metal component on the catalyst and the occurrence of hydrogenolysis can hence be ruled out, the most likely pathway for the formation of methane and ethane is Haag/Dessau cracking on the Brønsted acid sites [42, 113]. It can be speculated that not only the formation of methane and ethane, but also the hydrogenation of the C_3 to C_6 products happens on the Brønsted acid sites according to a Haag/Dessau-like mechanism. The results of cracking decalin under elevated hydrogen pressure on H-ZSM-12-24 lacking a noble metal has several features in common with cracking of mono-ring naphthenes like methylcyclohexane in H-ZSM-5 [114, 115]: At 400 °C, the naphthene was completely converted into light alkanes, mainly ethane, propane and n-butane. There was, however, no catalyst deactivation during the conversion of methylcyclohexane in the acidic H-ZSM-5 catalyst at 400 °C, whereas conversion of the bicyclic decalin in H-ZSM-12 at 360 °C is accompanied by coking and deactivation (*vide supra*). A *CMR* between 0.05 and 0.15 indicates a prevailing of the bimolecular mechanism (see Section 4.3.1.3).

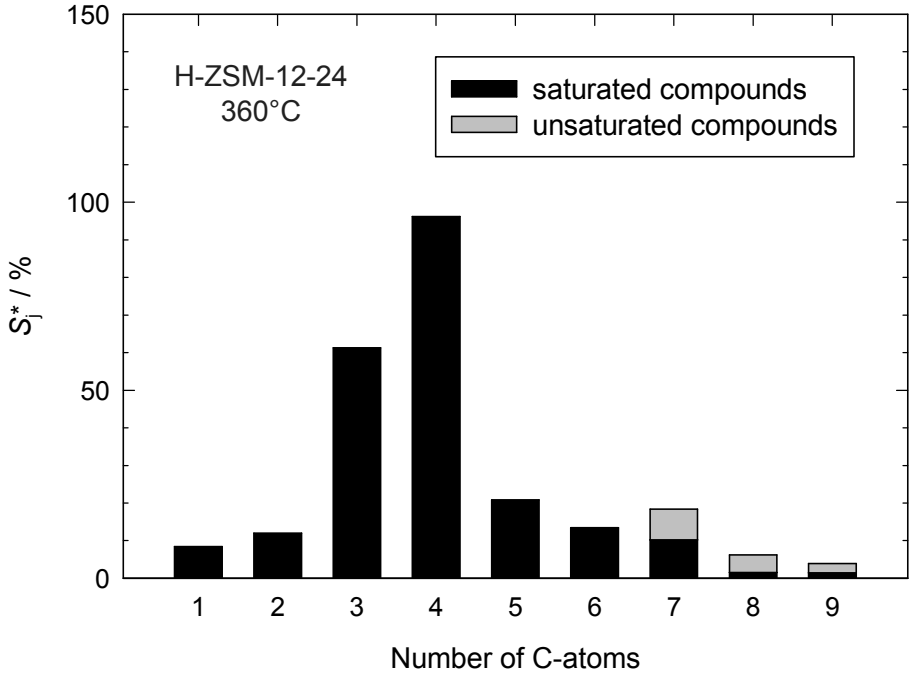

Figure 9.5: Modified cracking selectivities S_j^* on catalyst H-ZSM-12-24:
T_r = 360 °C; X_{Dec} = 63 %; $Y_{C_{9^-}}$ = 60 %; $\sum S_j^*$ = 241 %.

Among the skeletal isomers and ring opening products, unsaturated hydrocarbons are found as well. Via GC/MS analysis cyclohexene (M = 138 g·mol^{-1}) and benzene (M = 134 g·mol^{-1}) derivatives could be identified and are classified as ROPs, and components with a molar mass of 132 g·mol^{-1} are classified as sk-Isos. Generally, the degree of unsaturation in the sk-Isos and ROPs increases with increasing reaction temperature. On H-ZSM-12-24, for instance, 0 %, 7 % and 38 % of the sk-Isos are unsaturated in the products obtained at 239 °C, 300 °C and 360 °C, respectively. Both, on H-ZSM-12-24 and H-ZSM-12-125, about 50 % of the ROPs are unsaturated at 239 °C and 300 °C, and about 78 % at 360 °C.

Perhaps there is a contribution of the Haag-Dessau mechanism on these H-ZSM-12 zeolites, nevertheless the contribution is too small to obtain profitably catalysts for the ring opening of decalin into open-chain decanes. The two catalysts suffer from fast deactivation, very large amounts of cracking and significant amounts of unsaturated products. These problems are in accordance with the results observed on other monofunctional acidic catalysts in the hydroconversion of decalin or tetralin as summarized in Section 4.3.2.

9.3 Isomerization of cis-Decalin

Even though the results obtained on the ZSM-12 catalysts in the hydroconversion of decalin are not very promising some interesting observations concerning the stereoisomerization of cis- and trans-decalin could be made. On all metal-containing ZSM-12, MCM-22 and FAU catalysts investigated in this work, except 3.1Pt/$Cs_{0.71}$,$Na_{0.16}$,$H_{0.13}$-Y (Pt/Cs-Y), the $n_{tr\text{-}Dec}$ / ($n_{tr\text{-}Dec}$ + $n_{c\text{-}Dec}$) ratio was approximately 0.90. In contrast, on the H-ZSM-12 catalysts only values of 0.04 for H-ZSM-12-24 and 0.07 for H-ZSM-12-125 were observed. In Figure 9.6, the molar fractions of trans-decalin obtained on different catalysts in the hydroconversion of cis-decalin are illustrated.

In all experiments cis-decalin with an $n_{tr\text{-}Dec}$ / ($n_{tr\text{-}Dec}$ + $n_{c\text{-}Dec}$) ratio of 0.01 was used. Tests without a catalyst showed a temperature dependence of this ratio between 0.05 at 210 °C and 0.15 at 390 °C. The thermodynamic equilibrium values are between 0.75 (400 °C) and 0.87 (225 °C) [92]. The $n_{tr\text{-}Dec}$ / ($n_{tr\text{-}Dec}$ + $n_{c\text{-}Dec}$) ratios measured on all metal-containing catalysts of this work vary between 0.93 at low temperatures and 0.87 at higher temperatures. On these catalysts more trans-decalin is formed than expected from the thermodynamic equilibrium values. Exceptions are catalyst Pt/Cs-Y with values between 0.79 and 0.83 and catalyst Pt/Rb-Y with values between 0.82 and 0.85. On the H-ZSM-12 catalysts hardly any isomerization from cis- to trans-decalin can be observed.

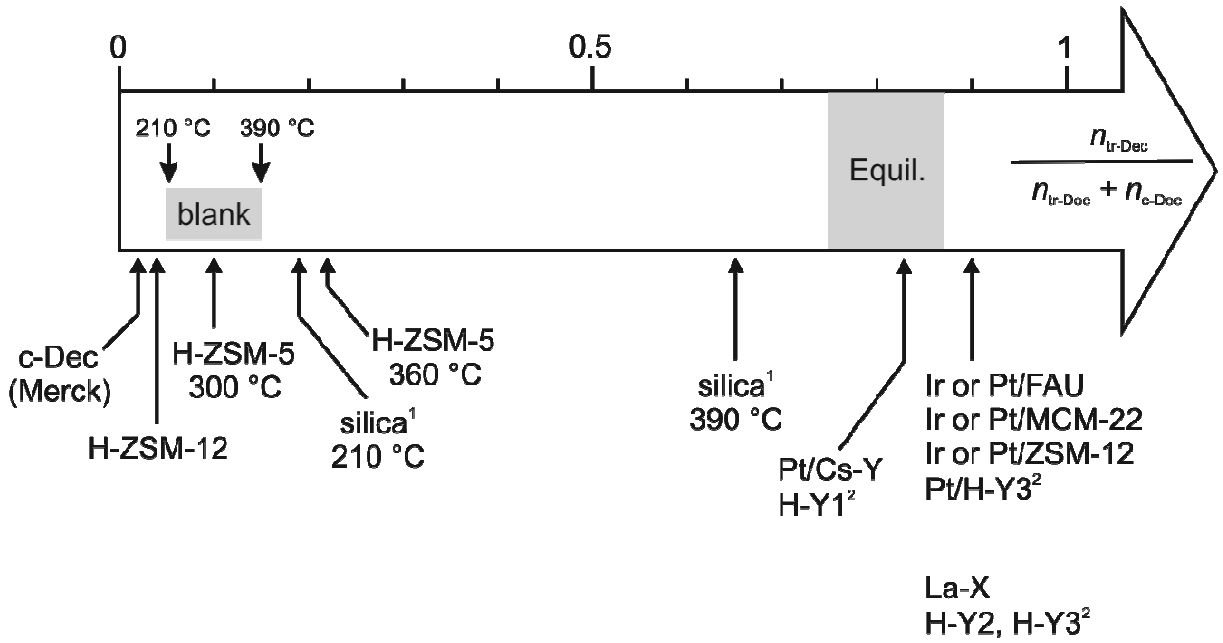

Figure 9.6: Molar fractions of trans-decalin observed on different catalysts during the hydroconversion of cis-decalin. The catalysts indicated with [1] and [2] are taken from Ref. [103] and [52].

In Figure 9.7, three possible mechanisms for the isomerization of cis-decalin to trans-decalin are shown. Weitkamp [116] proposed a dehydrogenation / hydrogenation mechanism on metal-containing catalysts leading to 1,9- or 9,10-octalin as intermediates as shown in Figure 9.7a. These observations are in agreement with experimental results of Lai and Song [117] on metal-containing H-mordenites starting from a decalin mixture with an $n_{tr\text{-}Dec}$ / ($n_{tr\text{-}Dec}$ + $n_{c\text{-}Dec}$) ratio of 0.49 at atmospheric pressure. The catalysts were very active in the isomerization of cis- to trans-decalin under H_2 atmosphere and gave an $n_{tr\text{-}Dec}$ / ($n_{tr\text{-}Dec}$ + $n_{c\text{-}Dec}$) ratio of 0.93. Under a nitrogen atmosphere these catalysts were much less effective for the isomerization of cis- to trans-decalin and reached only molar fractions of trans-decalin of 0.60. In contrast, on monofunctional acidic catalysts (H-Y, La,H-Y, H-mordenite) the gas environment (nitrogen or hydrogen) had no effect on the isomerization performance. All catalysts were able to isomerize cis- to trans-decalin, but H-mordenite was less effective which was explained with a lower acidity of this catalyst. Unfortunately, the authors did not differentiate whether they meant with the term acidity the concentration or strength of Brønsted acid sites. With increasing temperature the $n_{tr\text{-}Dec}$ / ($n_{tr\text{-}Dec}$ + $n_{c\text{-}Dec}$) ratio obtained on H-Y and La,H-Y increased and reached values around 0.92 at 300 °C. The authors considered the same mechanism as proposed for the metal-containing catalysts (Figure 9.7a), but it seems to be more reasonable to assume carbonium (Figure 9.7b) or carbenium ions (Figure 9.7c) as intermediates [50] since dehydrogenation / hydrogenation reactions are not common for Brønsted or Lewis acid sites .

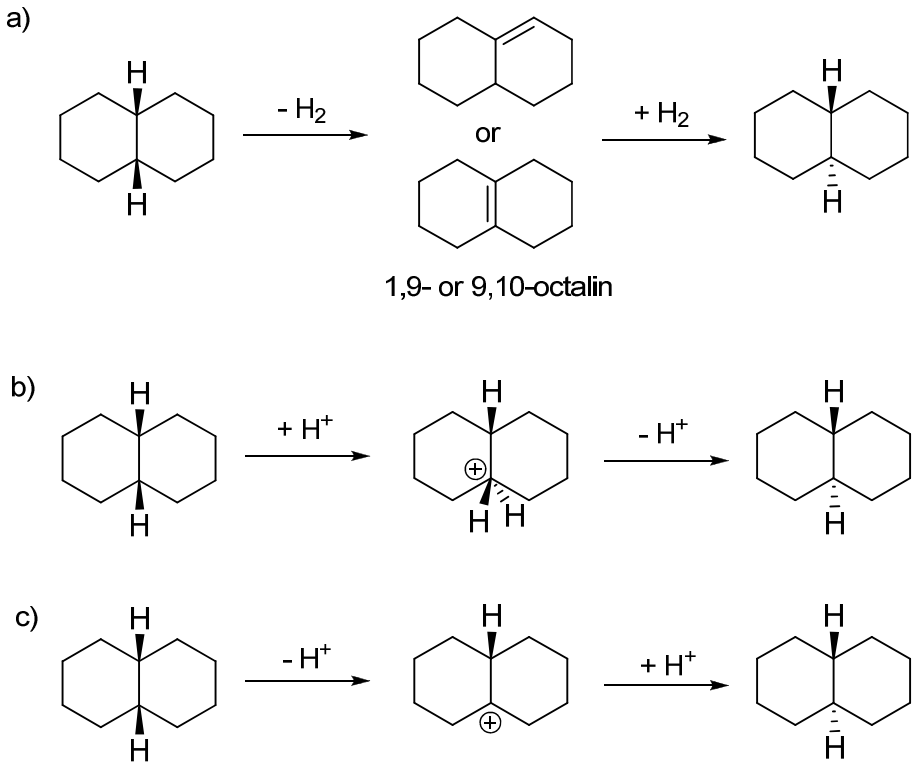

Figure 9.7: Isomerization of cis-decalin to trans-decalin: a) Dehydrogenation / hydrogenation mechanism, b) carbonium ion mechanism c) carbenium ion mechanism, after Ref. [50].

The $n_{tr\text{-}Dec}$ / ($n_{tr\text{-}Dec}$ + $n_{c\text{-}Dec}$) ratios of the metal-containing catalysts investigated in this work are above the equilibrium values. Mostad *et al.* [118] observed also trans-decalin values above the equilibrium on H-Y catalysts and explained it by shape-selective effects on Y zeolites. The pore discrimination of trans-decalin and consequently the selective conversion of cis-decalin was explained by the slightly smaller molecular dimension and more flexible conformation of the latter isomer. Other authors explained the high amounts of trans-decalin with a much higher reactivity of cis-decalin than trans-decalin [52].

The very low isomerization tendency of H-ZSM-12 is perhaps a hint that the cis-decalin molecule (0.56 x 0.67 x 0.88 nm, [118]) cannot penetrate the relatively narrow 12-membered ring pores of ZSM-12 (0.56 x 0.59 x 0.60 nm, [119]). Accordingly, the isomerization of cis-decalin is taking place on the Brønsted acid sites on the outer surface of the zeolite. The same zeolite loaded with iridium or platinum results in $n_{tr\text{-}Dec}$ / ($n_{tr\text{-}Dec}$ + $n_{c\text{-}Dec}$) ratios of approximately 0.9 which is perhaps due to metal sites on the outer surface.

Further experiments with monofunctional acidic catalysts were done to assure the influence of the outer surface of the zeolites. Zeolite $La_{0.30}H_{0.06}Na_{0.04}$-X with large 12-membered ring pores and zeolite H-ZSM-5 with 10-membered ring pores were used for a comparison. The

channels of ZSM-5 should be too small to give access to cis-decalin [120]. On La-X again an $n_{tr\text{-}Dec} / (n_{tr\text{-}Dec} + n_{c\text{-}Dec})$ ratio of 0.92 is observed at all temperatures while on H-ZSM-5 significantly lower ratios are obtained. Depending on the temperature the ratios vary between 0.10 and 0.22. Since cis-decalin cannot enter the pores the isomerization has to occur on the Brønsted acid sites on the outer surface. The difference in the isomerization between H-ZSM-12 and H-ZSM-5 is perhaps due to the area of the outer surface. The crystal size of ZSM-5 is less than 0.5 µm whereas the crystal sizes of H-ZSM-12-24 and H-ZSM-12-125 are between 3 and 1 µm, respectively, resulting in lower outer surface areas on the latter zeolites. Similar observations can be made on silica catalysts on which the $n_{tr\text{-}Dec} / (n_{tr\text{-}Dec} + n_{c\text{-}Dec})$ ratio varies between 0.20 and 0.65. The temperature dependence of the ratio is in line with results of Lai and Song [117].

On catalyst La-X, cis-decalin can enter the pore system and has access to a larger number of Brønsted acid sites than located on the outer surface. This results in $n_{tr\text{-}Dec} / (n_{tr\text{-}Dec} + n_{c\text{-}Dec})$ ratios of 0.92 even at lower temperatures. This is in line with results of Santikunaporn *et al.* [52]. They investigated three H-Y zeolites with different concentrations of Brønsted acid sites (H-Y1 < H-Y2 < H-Y3) in the hydroconversion of decalin at 260 °C. The two catalysts with a higher concentration of Brønsted acid sites showed $n_{tr\text{-}Dec} / (n_{tr\text{-}Dec} + n_{c\text{-}Dec})$ ratios of 0.95 and 0.92. On catalyst H-Y1 a ratio of only 0.83 was observed indicating a lower concentration of the Brønsted acid sites but nevertheless a significant isomerization to trans-decalin took place.

The results suggest that the isomerization of cis-decalin to trans-decalin occurs on metal-containing as well as on monofunctional acidic catalysts. The isomerization on metal sites with presumably 1,9- and 9,10-octalin as intermediates (Figure 9.7a) seems to be faster than on Brønsted acid sites. Catalysts with a low concentration of Brønsted acid sites like H-Y1 need higher temperatures to reach the thermodynamic equilibrium composition or even higher molar fractions of trans-decalin as shown in [117]. These dependences of the $n_{tr\text{-}Dec} / (n_{tr\text{-}Dec} + n_{c\text{-}Dec})$ ratio on the zeolite type could help to decide whether the cis-decalin can penetrate the pores of a zeolite or not. On monofunctional acidic catalysts on which cis-decalin has access to the pores (La-X) and thus to a large number of Brønsted acid sites, an $n_{tr\text{-}Dec} / (n_{tr\text{-}Dec} + n_{c\text{-}Dec})$ ratio of approximately 0.90 is reached. On H-ZSM-5 and H-ZSM-12 the ratios are significantly below 0.30, indicating a very low concentration of Brønsted acid sites presumably located on the outer surface of these catalysts.

10 Ring Opening of Decalin on MCM-22 (MWW)

The framework of MCM-22 contains two non-intersecting 10-membered ring pore systems (Section 4.1) which the decalin molecules should not be able to penetrate. The decalin molecules are expected to have only access to the 12-membered ring pockets on the outer surface of MCM-22. The idea is that decalin adsorbs on the active sites inside these pockets and undergoes ring opening there. The diffusion of the primary products out of the pockets is expected to be faster than out of the channels of zeolites, and in that way the readsorption on further active sites and consecutive cracking of ROPs and OCDs can perhaps be avoided.

Two catalysts loaded with approximately 3 wt.-% iridium or platinum were prepared. As observed on the ZSM-12 catalysts the iridium complex was not able to exchange quantitatively. After the first ion exchange only an iridium loading of 0.77 wt.-% was achieved. After a second ion exchange for 95 h the final iridium loading of 1.4 wt.-% was reached (Section 5.1.2.3). Possibly, the iridium complex is bulkier than the platinum complex and has diffusion limitations.

In Figure 10.1, the results obtained in the hydroconversion of cis-decalin on the two MCM-22 catalysts are depicted. As usual on catalysts with a low concentration of Brønsted acid sites, ring opening products are prevailing on the iridium-containing catalyst at low conversion, whereas skeletal isomers dominate on the platinum-containing catalyst. At higher temperatures the platinum-containing catalyst shows very low selectivities towards ROPs and OCDs. The hydrocracking activity is very high on this catalyst, so that the ring opening products and maybe open-chain decanes that may have formed are directly transferred into hydrocarbons with less than 10 carbon atoms. An overview of the maximal yields of OCDs reached on the two catalysts is given in Table 10.1.

Table 10.1: Maximum yields of open-chain decanes obtained on the MCM-22 catalysts.

Catalyst	T_r / °C	X_{Dec} / %	S_{OCDs} / %	$Y_{OCDs,\ max.}$ / %	Y_{OCNs} / %
1.4Ir/$H_{0.54}$,$Na_{0.46}$-MCM-22	282	88.6	21.5	19.1	2.8
2.9Pt/$H_{0.76}$,$Na_{0.24}$-MCM-22	310	97.8	3.3	3.3	0.1

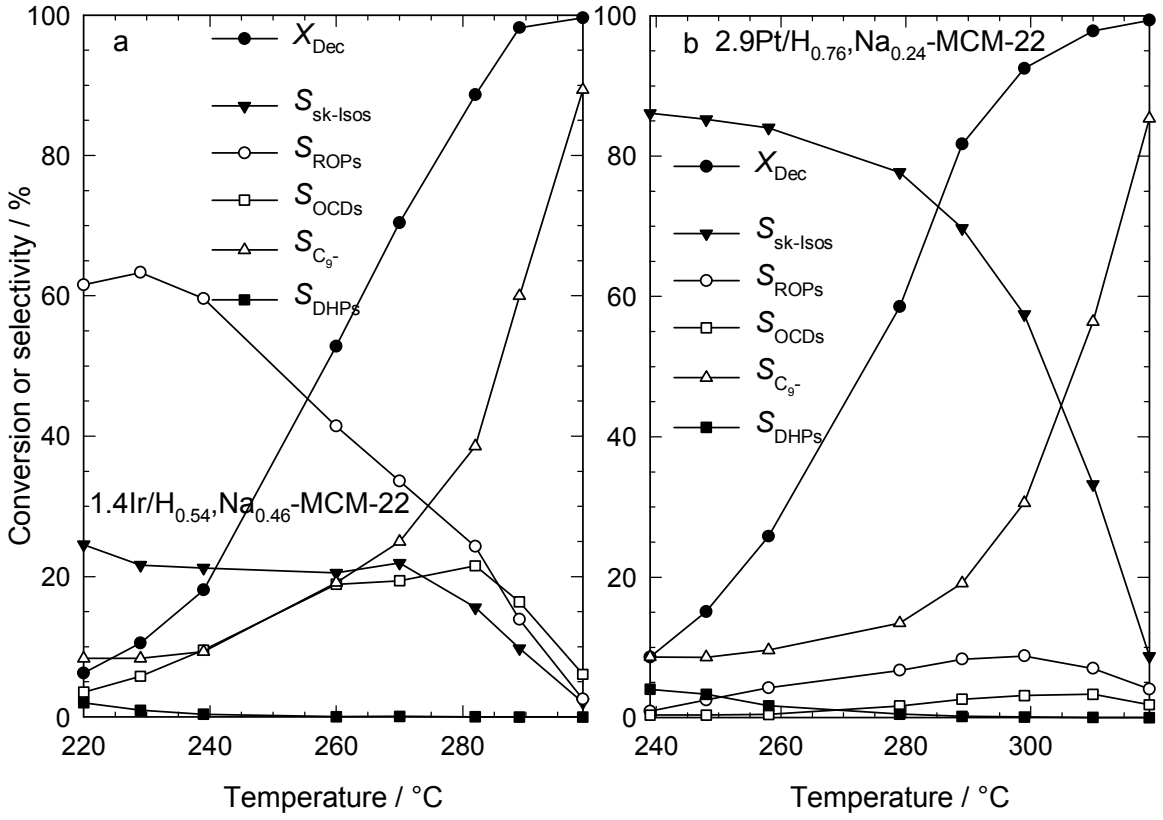

Figure 10.1: Conversion of decalin and selectivities of different groups of products in dependence of the reaction temperature for MCM-22 catalysts.

In Figure 10.2, the carbon number distributions of the hydrocracked products obtained on the two catalysts are given. On the iridium-containing catalyst relatively large amounts of C_4 and C_6 are formed. 80 % of the C_4 fraction consists of iso-butane. The $n_{M\text{-}CPn}$ / $n_{i\text{-}Bu}$ ratio is only 0.12, but large amounts of n-hexane, 2-M-Pn and 3-M-Pn are also present. These products could have formed via ring opening of methylcyclopentane. By adding these three products to the molar amount of methylcyclopentane the ratio $n_{M\text{-}CPn}$ / $n_{i\text{-}Bu}$ is 1.00. In addition to the large C_4 and C_6 fractions also C_1 and C_9 obtained via hydrogenolysis and a relatively large amount of C_5 are observed. On the platinum-containing catalyst secondary cracking is taking place indicated by $\sum S_j^*$ = 269 %. This secondary cracking can be observed over the whole temperature range leading to nearly negligible amounts of C_7 to C_9. The dominating products are propane and the C_4 fraction which consists to 62 % of iso-butane. The distribution curve looks similar to the one obtained on H-ZSM-12-24 (Section 9.2) except for the absence of unsaturated compounds. The unusual distribution of the hydrocracked products cannot be explained by hydrocracking via hydrogenolysis or bifunctional hydrocracking. Perhaps, this is a hint for a shape-selectivity effect.

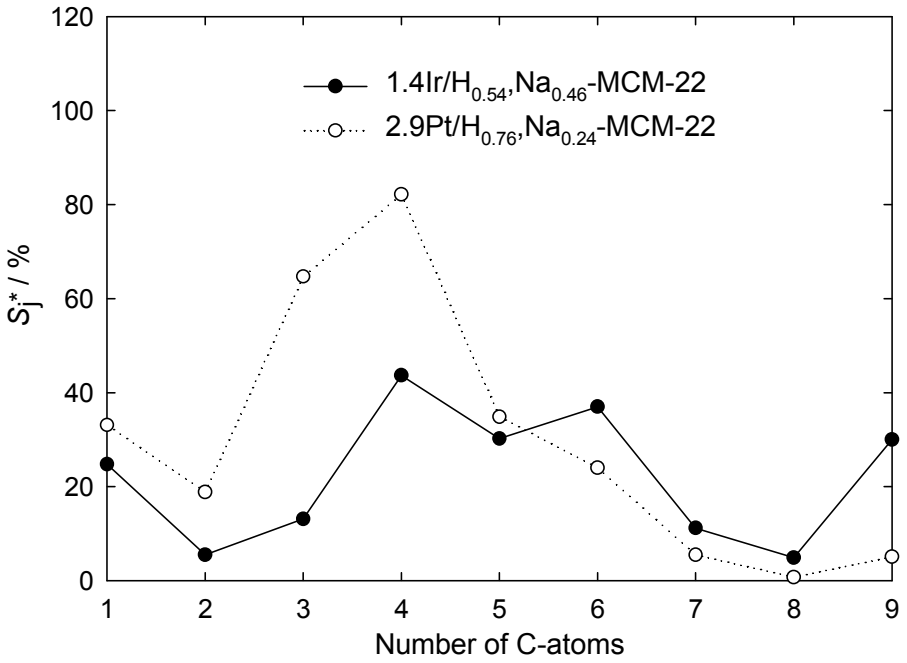

Figure 10.2: Modified hydrocracking selectivities S_j^* on the MCM-22 catalysts:
1.4Ir/$H_{0.54}$,$Na_{0.46}$-MCM-22: T_r = 282 °C; X_{Dec} =89 %; $Y_{C_{9^-}}$ = 34 %; $\sum S_j^*$ = 200 %.
2.9Pt/$H_{0.76}$,$Na_{0.24}$-MCM-22: T_r = 310 °C; X_{Dec} = 98 %; $Y_{C_{9^-}}$ = 55 %; $\sum S_j^*$ = 269 %.

The breakdown of the selectivities of OCDs into differently branched decanes on both catalysts reveal no surprises. On the iridium-containing catalyst the multibranched decanes are prevailing, while on the platinum-containing catalyst the combined selectivities of n-decane and the monobranched decanes exceed that of the multibranched decanes. Only negligible deactivation and no changes in the selectivities are observed upon 60 h time-on-stream.

The idea of reducing the probability of readsorption by using only the pockets on the surface of the MCM-22 catalyst for the hydroconversion of decalin and thus reducing the consecutive hydrocracking to hydrocarbons with less than ten carbon atoms could not be supported by the catalytic results. On the platinum-containing catalysts the skeletal isomers are almost completely converted to hydrocracked products. On the iridium-containing catalyst a yield of 19 % of open-chain decanes but also large amounts of hydrocracked products are observed. Probably this is due to the relatively high strength of Brønsted acid sites as visible in the carbon number distribution of this catalyst. Experiments with MCM-22 of lower acid strength like boron-containing MCM-22 could help to understand the catalytic results.

11 References

[1] Regulation (EC) No. 715/2007 of the European Parliament and of the Council.

[2] E. Brevoord, in: “Catalysts Courier“, S. Docter (Ed.), Vol. 59, Albemarle Catalysts, 2005, p. 10-11.

[3] K. Nakakita, K. Akihama, W. Weissman, J.T. Farrell, Int. J. Engine Res. 6 (2005) 187-205.

[4] DIN EN 590:2009+A1:2010, “Kraftstoffe für Kraftfahrzeuge – Dieselkraftstoff – Anforderung und Prüfverfahren“.

[5] J. Weitkamp, in: “Handbook of Heterogeneous Catalysis”, 2nd Edn., G. Ertl, H. Knözinger, F. Schüth, J. Weitkamp (Eds.), Vol. 7, Wiley-VCH, Weinheim, 2008, p. 3133-3152.

[6] W. Löwenstein, Am. Mineralogist 39 (1954) 92-96.

[7] H. van Koningsveld, Schemes for Building Zeolite Framework Models: http://www.iza-structure.org/databases/ (Access on 30.08.2010).

[8] S.L. Lawton, M.E. Leonowicz, R.D. Partridge, P. Chu, M.K. Rubin, Microporous Mesoporous Mater. 23 (1998) 109-117.

[9] H.K. Beyer, in: “Molecular Sieves - Science and Technology”, H.G. Karge, J. Weitkamp (Eds.), Vol. 3, Springer-Verlag, Berlin, Heidelberg, 2002, p. 203-255.

[10] M. Feuerstein, M. Hunger, G. Engelhardt, J.P. Amoureux, Solid State Nucl. Magn. Reson. 7 (1996) 95-103.

[11] D.H. Olson, Zeolites 15 (1995) 439-443.

[12] G.H. Kühl, J. Phys. Chem. Solids 38 (1977) 1259-1263.

[13] J. Weitkamp, Solid State Ionics 131 (2000) 175-188.

[14] H. Klein, H. Fuess, M. Hunger, J. Chem. Soc., Faraday Trans. 91 (1995) 1813-1824.

[15] G.H. Kühl, in: “Catalysis and Zeolites-Fundamentals and Applications”, J. Weitkamp, L. Puppe (Eds.), Springer-Verlag, Berlin, Heidelberg, New York, 1999, p. 81-197.

[16] L.A. Pine, P.J. Maher, W.A. Wachter, J. Catal. 85 (1984) 466-476.

[17] E. O´Donoghue, D. Barthomeuf, Zeolites 6 (1986) 267-270.

[18] Y.S. Chen, M. Guisnet, M. Kern, J.L. Lemberton, New J. Chem. 11 (1987) 623-626.

[19] J.-C. Lavelley, R. Anquetil, J. Czyzniewska, M. Ziolek, J. Chem. Soc., Faraday Trans. 92 (1996) 1263-1266.

[20] R.T. Sanderson, in: “Chemical Bonds and Bond Energy”, 2nd Edn, E.M. Loebl (Ed.), Physical Chemistry, Vol. 21, Academic Press, New York, 1976, 218 pp.

[21] P.E. Pickert, J.A. Rabo, E. Dempsey, V. Schomaker, in “Proceedings of the Third International Congress on Catalysis”, W.M.H. Sachtler, G.C.A. Schuit, P. Zwietering (Eds.), Vol. 1, North-Holland Publishing Company, Amsterdam, 1965, p. 714-728.

[22] A.E. Hirschler, J. Catal. 2 (1963) 428-439.

[23] J.W. Ward, J. Catal. 13 (1969) 321-327.

[24] L. Moscou, M. Lakeman, J. Catal. 16 (1970) 173-180.

[25] E.F.T. Lee, L.V.C. Rees, Zeolites 7 (1987) 143-147.

[26] E.F.T. Lee, L.V.C. Rees, Zeolites 7 (1987) 545-548.

[27] J. Huang, Y. Jiang, V.R.R. Marthala, Y.S. Ooi, J. Weitkamp, M. Hunger, Microporous Mesoporous Mater. 104 (2007) 129-136.

[28] P.E. Eberly, Jr., C.N. Kimberlin, in: “Molecular Sieve Zeolites – II”, E.M. Flanigen, L.B. Sand (Eds.), Advances in Chemistry Series, Vol. 102, American Chemical Society, Washington, D.C., 1971, p. 374-388.

[29] H.G. Karge, L.C. Jozefowicz, in: “Zeolites and Related Microporous Materials: State of the Art 1994”, J. Weitkamp, H.G. Karge, H. Pfeifer, W. Hölderich (Eds.), Studies in Surface Science and Catalysis, Vol. 84, Part A, Elsevier, Amsterdam, 1994, p. 685-692.

[30] J. Huang, Y. Jiang, M. Hunger, in: “From Zeolites to Porous MOF Materials - the 40th Anniversary of International Zeolite Conference”, R. Xu, Z. Gao, J. Chen, W. Yan (Eds.), Studies in Surface Science and Catalysis, Vol. 170, Part A, Elsevier, Amsterdam, 2007, p. 622-628.

[31] M. Weihe, M. Hunger, M. Breuninger, H.G. Karge, J. Weitkamp, J. Catal. 198 (2001) 256-265.

[32] M. Hunger, G. Engelhardt, J. Weitkamp, Microporous Mater. 3 (1995) 497-510.

[33] J.M. Bennett, J.V. Smith, Mat. Res. Bull. 3 (1968) 865-875.

[34] D.-S. Shy, S.-H. Chen, J. Lievens, S.-B. Liu, K.-J. Chao, J. Chem. Soc., Faraday Trans. 87 (1991) 2855-2859.

[35] V.P. Shiralkar, S.B. Kulkarni, J. Therm. Anal. 25 (1982) 399-407.

[36] K. Hedden, J. Weitkamp, Chem. Ing. Tech. 55 (1983) 907-914.

[37] J.H. Sinfelt, “Bimetallic Catalysts”, John Wiley & Sons, New York, 1983, p. 9-31.

[38] G.C. Bond, in: “Metal-Catalysed Reactions of Hydrocarbons”, M.V. Twigg, M.S. Spencer (Eds.), Fundamental and Applied Catalysis, Springer, New York, 2005, 666 pp.

[39] F.G. Gault, in: “Advances in Catalysis”, D.D. Eley, H. Pines, P.B. Weisz (Eds.), Vol. 30, Academic Press, New York, 1981, p. 1-95.

[40] G. Maire, G. Plouidy, J.C. Prudhomme, F.G. Gault, J. Catal. 4 (1965) 556-569.

[41] J. Weitkamp, P.A. Jacobs, J.A. Martens, Appl. Catal. 8 (1983) 123-141.

[42] J. Weitkamp, M. Hunger, in: “Introduction to Zeolite Science and Practice”, J. Čejka, H. van Bekkum, A. Corma, F. Schüth (Eds.), Studies in Surface Science and Catalysis, Vol. 168, Elsevier, Amsterdam, 2007, p. 787-835.

[43] W.O. Haag, R.M. Dessau, in: “Proceedings of the 8th International Congress on Catalysis“, Vol. 2, Verlag Chemie, Weinheim, DECHEMA, Frankfurt am Main, 1984, p. 305-316.

[44] A.F.H. Wielers, M. Vaarkamp, M.F.M. Post, J. Catal. 127 (1991) 51-66.

[45] J. Weitkamp, A. Raichle, Y. Traa, M. Rupp, F. Fuder, Chem. Commun. (2000) 403-404.

[46] C.J. Egan, G.E. Langlois, R.J. White, J. Am. Chem. Soc. 84 (1962) 1204-1212.

[47] R.F. Sullivan, C.J. Egan, G.E. Langlois, R.P. Sieg, J. Am. Chem. Soc. 83 (1961) 1156-1160.

[48] J. Weitkamp, S. Ernst, R. Kumar, Appl. Catal. 27 (1986) 207-210.

[49] Y. Traa, S. Sealy, J. Weitkamp, in: “Molecular Sieves-Science and Technology”, H.G. Karge, J. Weitkamp (Eds.), Vol. 5, Springer-Verlag, Berlin, Heidelberg, 2007, p. 103-154.

[50] D. Kubička, N. Kumar, P. Mäki-Arvela, M. Tiitta, V. Niemi, T. Salmi, D.Y. Murzin, J. Catal. 222 (2004) 65-79.

[51] D. Kubička, N. Kumar, P. Mäki-Arvela, M. Tiitta, V. Niemi, H. Karhu, T. Salmi, D.Y. Murzin, J. Catal. 227 (2004) 313-327.

[52] M. Santikunaporn, J.E. Herrera, S. Jongpatiwut, D.E. Resasco, W.E. Alvarez, E.L. Sughrue, J. Catal. 228 (2004) 100-113.

[53] M.A. Arribas, A. Martínez, Appl. Catal., A 230 (2002) 203-217.

[54] D. Kubička, T. Salmi, M. Tiitta, D.Y. Murzin, Fuel 88 (2009) 366-373.

[55] D. Kubička, M. Rönnholm, S.-P. Reinikainen, T. Salmi, D.Y. Murzin, Anal. Chim. Acta 537 (2005) 339-348.

[56] M.A. Arribas, P. Concepción, A. Martínez, Appl. Catal., A 267 (2004) 111-119.

[57] M.A. Arribas, A. Corma, M.J. Díaz-Cabañas, A. Martínez, Appl. Catal., A 273 (2004) 277-286.

[58] H. Ma, X. Yang, G. Wen, G. Tian, L. Wang, Y. Xu, B. Wang, Z. Tian, L. Lin, Catal. Lett. 116 (2007) 149-154.

[59] M.A. Arribas, J.J. Mahiques, A. Martínez, in: “Zeolites and Mesoporous Materials at the Dawn of the 21st Century”, A. Galarneau, F. Di Renzo, F. Fajula, J. Vedrine (Eds.), Studies in Surface Science and Catalysis, Vol. 135, Elsevier, Amsterdam, 2001, p. 303.

[60] M.A. Arribas, A. Martínez, G. Sastre, in: “Impact of Zeolites and Other Porous Materials on the New Technologies at the Beginning of the New Millennium”, R. Aiello, G. Giordano, F. Testa (Eds.), Studies in Surface Science and Catalysis, Vol. 142, Part B, Elsevier, Amsterdam, 2002, p. 1015-1022.

[61] H. Liu, X. Meng, D. Zhao, Y. Li, Chem. Eng. J. 140 (2008) 424-431.

[62] K.C. Mouli, V. Sundaramurthy, A.K. Dalai, Z. Ring, Appl. Catal., A 321 (2007) 17-26.

[63] N. Kumar, A. Lazuen, D. Kubička, T. Heikkilä, V.-P. Lehto, H. Karhu, T. Salmi, D.Y. Murzin, in: "Scientific Bases for the Preparation of Heterogeneous Catalysts", E.M. Gaigneaux, M. Devillers, D.E. De Vos, S. Hermans, P.A. Jacobs, J.A. Mertens, P. Ruiz (Eds.), Studies in Surface Science and Catalysis, Vol. 162, Elsevier, Amsterdam, 2006, p. 401-408.

[64] N. Kumar, D. Kubička, A.L. Garay, P. Mäki-Arvela, T. Heikkilä, T. Salmi, D.Y. Murzin, Top. Catal. 52 (2009) 380-386.

[65] H. Vuori, R.J. Silvennoinen, M. Lindblad, H. Österholm, A.O.I. Krause, Catal. Lett. 131 (2009) 7-15.

[66] S.J. Ardakani, X. Liu, K.J. Smith, Appl. Catal., A 324 (2007) 9-19.

[67] X. Liu, K.J. Smith, Appl. Catal., A 335 (2008) 230-240.

[68] S.G.A. Ferraz, F.M.Z. Zotin, L.R.R. Araujo, J.L. Zotin, Appl. Catal., A 384 (2010) 51-57.

[69] E. Morgado, Jr., J.L. Zotin, M.A.S. de Abreu, D. de Oliveira Rosas, P.M. Jardim, B.A. Marinkovic, Appl. Catal., A 357 (2009) 142-149.

[70] K.C. Mouli, V. Sundaramurthy, A.K. Dalai, J. Mol. Catal., A 304 (2009) 77-84.

[71] R. Contreras, J. Ramírez, R. Cuevas-García, A. Gutiérrez-Alejandre, P. Castillo-Villalón, G. Macías, I. Puente-Lee, Catal. Today 148 (2009) 49-54.

[72] M. Daage, G.B. McVicker, M.S. Touvelle, C.W. Hudson, D.P. Klein, B.R. Cook, J.G. Chen, S. Hantzer, D.E.W. Vaughan, E.S. Ellis, Prepr. – Am. Chem. Soc., Div. Pet. Chem. 47 (2002) 38-40.

[73] M. Daage, G.B. McVicker, M.S. Touvelle, C.W. Hudson, D.P. Klein, B.R. Cook, J.G. Chen, S. Hantzer, D.E.W. Vaughan, E.S. Ellis, in: "Zeolites and Mesoporous Materials at the Dawn of the 21st Century", A. Galarneau, F. Di Renzo, F. Fajula, J. Vedrine (Eds.), Studies in Surface Science and Catalysis, Vol. 135, Elsevier, Amsterdam, 2001, p. 159.

[74] US Patent 5 763 731, April 12, 1996, Exxon Research and Engineering Company (Inv.: G.B. McVicker, M.S. Touvelle, C.W. Hudson, D.E.W. Vaughan, M. Daage, S. Hantzer, D.P. Klein, E.S. Ellis, B.R. Cook, O.C. Feeley, J.E. Baumgartner).

[75] WO 97/09288, March 13, 1997, Exxon Research and Engineering Company (Inv.: G.B. McVicker, M.S. Touvelle, C.W. Hudson, D.E.W. Vaughan, M. Daage, S. Hantzer, D.P. Klein, E.S. Ellis, B.R. Cook, O.C. Feeley, J.E. Baumgartner).

[76] A. Infantes-Molina, J. Mérida-Robles, E. Rodríguez-Catellón, J.L.G. Fierro, A. Jiménez-López, Appl. Catal., A 341 (2008) 35-42.

[77] S. Albertazzi, E. Rodríguez-Castellón, M. Livi, A. Jiménez-López, A. Vaccari, J. Catal. 228 (2004) 218-224.

[78] M. Jacquin, D.J. Jones, J. Rozière, A. Jiménez-López, E. Rodríguez-Castellón, J.M.T. Menayo, M. Lenarda, L. Storaro, A. Vaccari, S. Albertazzi, J. Catal. 228 (2004) 447-459.

[79] U. Nylén, J.F. Delgado, S. Järås, M. Boutonnet, Appl. Catal., A 262 (2004) 189-200.

[80] U. Nylén, L. Sassu, S. Melis, S. Järås, M. Boutonnet, Appl. Catal., A 299 (2006) 1-13.

[81] U. Nylén, J.M. Arechederra, B. Pawelec, J.F. Delgado, M.P. Pascual, J.L.G. Fierro, Energy Fuels 22 (2008) 2138-2148.

[82] G.B. McVicker, M. Daage, M.S. Touvelle, C.W. Hudson, D.P. Klein, W.C. Baird, Jr., B.R. Cook, J.G. Chen, S. Hantzer, D.E.W. Vaughan, E.S. Ellis, O.C. Feeley, J. Catal. 210 (2002) 137-148.

[83] S. Ernst, P.A. Jacobs, J.A. Martens, J. Weitkamp, Zeolites 7 (1987) 458-462.

[84] K. Yoo, R. Kashfi, S. Gopal, P.G. Smirniotis, M. Gangoda, R.N. Bose, Microporous Mesoporous Mater. 60 (2003) 57-68.

[85] H. Koller, B. Burger, A.M. Schneider, G. Engelhardt, J. Weitkamp, Microporous Mater. 5 (1995) 219-232.

[86] R.A. Dalla Batta, M. Boudart, in: “Proceedings of the 5th International Congress on Catalysis”, J.W. Hightower (Ed.), Vol. 2, North-Holland Publishing Company, Amsterdam, 1973, p. 1329-1341.

[87] G. Engelhardt, U. Lohse, E. Lippmaa, M. Tarmak, M. Mägi, Z. Anorg. Allg. Chem. 482 (1981) 49-64.

[88] D. Santi, personal communication, 2010.

[89] J. Weitkamp, R. Gläser, in: “Handbook of Heterogeneous Catalysis“, 2nd Edn., G. Ertl, H. Knözinger, F. Schüth, J. Weitkamp (Eds.), Vol. 4, Wiley-VCH, Weinheim, 2008, p. 2045-2053.

[90] R. Beaumont, D. Barthomeuf, J. Catal. 27 (1972) 45-51.

[91] B. Weinberger, F.D. Lamari, S.B. Kayiran, A. Gicquel, D. Levesque, AIChE J. 51 (2005) 142-148.

[92] A. Haas, Diploma Thesis, University of Stuttgart, 2008.

[93] S. Xiao, R.L.V. Mao, G. Denes, J. Mater. Chem. 5 (1995) 1251-1255.

[94] S. Yang, A. Novrotsky, Microporous Mesoporous Mater. 37 (2000) 175-186.

[95] Q.L. Wang, G. Giannetto, M. Guisnet, Zeolites 10 (1990) 301-303.

[96] M.M.J. Treacy, J.B. Higgins, in: “Collection of Simulated XRD Powder Patterns for Zeolites”, 5th Edn., Elsevier, Amsterdam, 2007, p. 301.

[97] J. Čejka, G. Košová, N. Žilková, I. Hrubá, in: “Impact of Zeolites and Other Porous Materials on the New Technologies at the Beginning of the New Millennium”, R. Aiello, G. Giordano, F. Testa (Eds.), Studies in Surface Science and Catalysis, Vol. 142, Part A, Elsevier, Amsterdam, 2002, p. 247-254.

[98] US Patent 4 954 325, October 6, 1988, Mobil Oil Corp. (Inv.: M.K. Rubin, P. Chu).

[99] M. Hunger, S. Ernst, J. Weitkamp, Zeolites 15 (1995) 188-192.

[100] C. Delitala, M.D. Alba, A.I. Becerro, D. Delpiano, D. Meloni, E. Musu, I. Ferino, Microporous Mesoporous Mater. 118 (2009) 1-10.

[101] J. Weitkamp, Ind. Eng. Chem. Prod. Res. Dev., 21 (1982) 550-558

[102] J. Weitkamp, in: “Hydrocracking and Hydrotreating”, J.W. Ward, S.A. Qader (Eds.), ACS Symposium Series, Vol. 20, American Chemical Society, 1975, p. 1-27.

[103] A. Haas, personal communication, 2010.

[104] J. Weitkamp, S. Ernst, in: “Catalysis 1987“, J. Ward (Ed.), Studies in Surface Science and Catalysis, Vol. 38, Elsevier, Amsterdam, 1988, p. 367-382.

[105] J. Weitkamp, P.A. Jacobs, J.A. Martens, Appl. Catal. 8 (1983) 123-141.

[106] H. Schulz, J. Weitkamp, H. Eberth, in: “Proceedings of the 5th International Congress on Catalysis”, J.W. Hightower (Ed.), Vol. 2, North-Holland Pub. Co., Amsterdam, 1973, p. 1229-1239.

[107] L.H. Bird, E.F. Daly, Trans. Faraday Soc. 35 (1939) 588-592.

[108] D.L. Camin, F.D. Rossini, J. Phys. Chem. 59 (1955) 1172-1179.

[109] C.S. Marvel, L.A. Brooks, J. Am. Chem. Soc. 63 (1941) 2630-2632.

[110] A. Raichle, PhD Thesis, University of Stuttgart, 2002.

[111] C.T.-W. Chu, C.D. Chang, J. Phys. Chem. 89 (1985) 1569-1571.

[112] S. Gopal, P.G. Smirniotis, J. Catal. 205 (2002) 231-243.

[113] W.O. Haag, R.M. Dessau, in: “Proceedings of the 8th International Congress on Catalysis”, Vol. 2, Verlag Chemie, Weinheim, 1984, p. II305-II316.

[114] J. Weitkamp, A. Raichle, Y. Traa, Appl. Catal. A 222 (2001) 277-297.

[115] A. Raichle, Y. Traa, F. Fuder, M. Rupp, J. Weitkamp, Angew. Chem. Intern. Ed. Engl. 40 (2001) 1243-1246.

[116] A.W. Weitkamp, Adv. Catal. 18 (1968) 1-110.

[117] W.-C. Lai, C. Song, Catal. Today 31 (1996) 171-181.

[118] H.B. Mostad, T.U. Riis, O.H. Ellestad, Appl. Catal. 58 (1990) 105-117.

[119] http://www.iza-structure.org/databases/ (Access on 30.08.2010).

[120] F. Hernandez, L. Moudafi, F. Fajula, F. Figueras, in: “Proceedings of the 8th International Congress on Catalysis“, Vol. 2, Verlag Chemie, Weinheim, DECHEMA, Frankfurt am Main, 1984, p. 447-457.

12 Appendices

12.1 Retention Times

Table 12.1: Retention times (t_{ret}) and products of the hydroconversion of perhydroindan, as of September 07, 2010. For the conditions of the gas chromatographic analyses see Section 5.4, Table 5.5.

t_{ret} / min	Product	t_{ret} / min	Product
12.20	methane	56.41	2,4-dimethylhexane
12.59	ethane	56.57	C_8
13.50	propane	57.79	1,2,4-trimethylcyclopentane
14.88	iso-butane	57.89	3,3-dimethylhexane
16.05	n-butane	59.17	1,2,3-trimethylcyclopentane
16.58	propene	59.63	1,3,4-trimethylcyclopentane
20.05	2-methylbutane	60.59	trimethylpentane
22.03	n-pentane	61.43	2,3-dimethylhexane
25.45	2,2-dimethylbutane	61.80	3-ethyl-2-methylpentane
28.91	2,3-dimethylbutane	62.11	C_8
29.35	2-methylpentane	62.34	2-methylheptane
31.23	3-methylpentane	62.63	4-methylheptane
33.52	n-hexane	63.23	3,4-dimethylhexane
37.18	2,2-dimethylpentane	63.54	C_8
37.75	methylcyclopentane	63.80	3-methylheptane
38.13	2,4-dimethylpentane	64.07	3-ethylhexane
39.19	C_7	64.54	ROP
41.63	benzene	64.85	1,3-dimethylcyclohexane
42.37	3,3-dimethylpentane	65.21	1,4-dimethylcyclohexane
43.27	cyclohexane	65.88	trimethylhexane
44.28	2-methylhexane	66.45	1,1-dimethylcyclohexane
44.75	2,3-dimethylpentane	66.73	1-ethyl-3-methylcyclopentane
45.49	1,3-dimethylcyclopentane	67.14	1-ethyl-3-methylcyclopentane
45.81	3-methylhexane	67.41	1-ethyl-2-methylcyclopentane
47.22	1,3-dimethylcyclopentane	67.98	1-ethyl-1-methylcyclopentane
47.67	3-ethylpentane	68.68	n-octane
48.20	1,2-dimethylcyclopentane	69.41	ROP
48.29	C_7	69.76	1,2,3-trimethylcyclopentane
50.04	n-heptane	69.94	dimethylcyclohexane
54.08	dimethylcyclopentane	70.60	C_8
54.34	methylcyclohexane	71.18	(1-ethylmethyl)cyclopentane
54.73	1,1,3-trimethylcyclopentane	71.45	C_8
55.94	2,5-dimethylhexane	71.84	C_8
56.30	ethylcyclopentane	72.04	2,3,5-trimethylhexane

t_{ret} / min	Product	t_{ret} / min	Product
72.30	OCN	83.52	ROP
72.53	2,2-dimethylheptane	83.88	ROP
72.76	C_8	84.03	ROP
73.09	1-ethyl-2-methylcyclopentane	84.22	ROP
73.27	2,4-dimethylheptane	84.55	1-methyl-2-propylcyclopentane
73.56	OCN	84.71	ROP
73.90	4,4-dimethylheptane	84.84	ROP
74.16	ROP	85.30	trimethylcyclopentane
74.51	2,6-dimethylheptane	85.41	ROP
74.62	C_8	85.65	1-methyl-2-propylcyclopentane
74.86	propylcyclopentane	85.89	ROP
75.10	1,3,5-trimethylcyclopentane	86.18	ethyl-methylcyclohexane
75.30	ethylcyclohexane	86.71	ethyl-methylcyclohexane
75.70	2,5-dimethylheptane	87.06	diethylcyclopentane
75.87	3,5-dimethylheptane	87.26	(2-methylpropyl)cyclopentane
76.02	3,5-dimethylheptane	87.43	sk-Iso
76.31	3,3-dimethylheptane	88.13	n-nonane
76.52	trimethylcyclohexane	88.46	ROP
76.88	ROP	88.74	ROP
77.11	ROP	88.99	ROP
77.39	ROP	89.17	ROP
78.07	3-ethyl-2-methylhexane	89.58	sk-Iso
78.28	ROP	89.77	1,2,3-trimethylcyclohexane
78.48	ROP	90.09	ROP
78.62	ROP	90.37	1-ethyl-2-methylcyclohexane
78.98	ROP	90.72	ROP
79.23	3-ethyl-3-methylhexane	90.89	1-ethyl-4-methylcyclohexane
79.74	2,3-dimethylheptane	91.19	1-ethyl-1-methylcyclohexane
80.05	3-ethyl-4methylhexane	91.43	ROP
80.19	3,4-dimethylheptane	91.60	ROP
80.33	3,4-dimethylheptane	92.03	1-methyl-2-propylcyclohexane
80.53	4-ethylheptane	92.27	2,4,6-trimethylheptane
81.03	4-methyloctane	92.58	2,3,5-trimethylheptane
81.19	2-methyloctane	92.78	diethylcyclopentane
81.51	ROP	92.95	sk-Iso
81.62	C_8	93.08	(1-methylethyl)cyclohexane
81.80	ROP	93.39	ROP
82.00	C_8	93.64	2,5-dimethyloctane
82.08	C_8	93.74	3,5-dimethyloctane
82.39	3-ethylheptane	94.06	3,5-dimethyloctane
82.57	3-methyloctane	94.29	2,7-dimethyloctane
82.87	ROP	94.35	sk-Iso
83.02	ROP	94.60	ROP
83.28	ROP	95.01	1-ethyl-2-methylcyclohexane

t_{ret} / min	Product	t_{ret} / min	Product
95.21	propylcyclohexane	108.11	C_{10}
95.65	butylcyclopentane	108.67	cis-perhydroindan
95.89	sk-Iso	108.85	C_{10}
96.20	sk-Iso	109.42	C_{10}
96.30	sk-Iso	109.92	C_{10}
96.64	sk-Iso	110.23	1,4-diethylcyclohexane
97.02	OCD	110.40	C_{10}
97.15	OCD	110.75	C_{10}
97.47	ethyl-dimethylcyclohexane	111.43	C_{10}
97.63	sk-Iso	111.53	C_{10}
97.90	sk-Iso	111.75	C_{10}
98.17	sk-Iso	112.49	C_{10}
98.54	sk-Iso	113.12	bicyclo[3.3.1]nonane
98.74	2-methylbicyclo[3.3.0]octane	113.32	decalin
99.05	2-ethylbicyclo[2.2.1]heptane	113.78	C_{10}
99.58	sk-Iso	114.38	C_{10}
99.61	sk-Iso	114.50	C_{10}
99.82	C_{10}	114.86	C_{10}
100.13	sk-Iso	115.56	C_{10}
100.47	OCD	116.45	methyl-propylcyclohexane
100.98	trans-perhydroindan	116.65	C_{10}
101.36	5-methylnonane	116.87	indan
101.50	sk-Iso	117.43	C_{10}
101.77	4-methylnonane	118.93	butylcyclohexane
101.93	C_{10}	119.22	C_{10}
102.21	2-methylnonane	121.26	octahydro-5-methyl-1H-inden
102.63	C_{10}	121.58	C_{10}
103.00	C_{10}	121.95	C_{10}
103.30	ethyl-methylcyclohexane	122.65	C_{10}
103.46	sk-Iso	124.74	C_{10}
103.71	DHP	125.32	undecane
103.87	3-methylnonane	125.85	C_{10}
104.06	C_{10}	126.28	C_{10}
105.13	C_{10}	127.95	C_{10}
105.70	C_{10}	129.29	C_{10}
105.86	C_{10}	133.30	C_{11}
106.35	C_{10}	135.11	methyldecalin
106.57	C_{10}	139.80	C_{11}
106.70	C_{10}	141.75	C_{11}
107.18	C_{10}	144.07	C_{11}
107.35	1-methyl-2-propylcyclohexane	144.88	C_{11}

Table 12.2: Retention times (t_{ret}) and products of the hydroconversion of cis-decalin, as of September 07, 2010. For the conditions of the gas chromatographic analyses see Section 5.4, Table 5.5.

t_{ret} / min	Product	t_{ret} / min	Product
11.95	methane	58.80	1,3,4-trimethylcyclopentane
12.30	ethane	59.80	toluene[a]
13.20	propane	60.60	2,3-dimethylhexane
14.55	iso-butane	60.95	3-ethyl-2-methylpentane
15.70	n-butane	61.30	C_8
16.25	propene	61.55	2-methylheptane
19.60	2-methylbutane	61.85	4-methylheptane
21.55	n-pentane	62.40	3,4-dimethylhexane
24.95	2,2-dimethylbutane	62.70	C_8
28.30	2,3-dimethylbutane	63.00	3-methylheptane
28.75	2-methylpentane	63.25	3-ethylhexane
30.60	3-methylpentane	63.70	C_8
32.90	n-hexane	64.00	1,3-dimethylcyclohexane
36.55	2,2-dimethylpentane	64.35	1,4-dimethylcyclohexane
37.10	methylcyclopentane	65.10	C_8
37.45	2,4-dimethylpentane	65.60	1,1-dimethylcyclohexane
38.50	C_7	65.90	1-ethyl-3-methylcyclopentane
40.95	C_7	66.30	1-ethyl-3-methylcyclopentane
41.65	C_7	66.55	1-ethyl-2-methylcyclopentane
42.50	cyclohexane	67.15	1-ethyl-1-methylcyclopentane
43.55	2-methylhexane	67.65	n-octane
44.00	2,3-dimethylpentane	67.80	1,2-dimethylcyclohexane
44.70	1,1-dimethylcyclopentane	68.60	1,2,3,4-tetramethylcyclopentane
45.10	3-methylhexane	68.85	C_8
46.45	1,3-dimethylcyclopentane	69.05	1,4-dimethylcyclohexane
46.90	1,3-dimethylcyclopentane	69.75	C_8
47.45	1,2-dimethylcyclopentane	70.35	propylcyclopentane
47.60	C_7	70.95	C_8
49.25	n-heptane	71.20	2,3,5-trimethylhexane
53.30	1,2-dimethylcyclopentane	71.40	C_8
53.50	methylcyclohexane	71.65	2,2-dimethylheptane
53.90	1,1,3-trimethylcyclopentane	72.20	C_9
55.15	2,5-dimethylhexane	72.40	2,4-dimethylheptane
55.45	C_8	72.80	C_9
55.60	ethylcyclopentane	73.05	4,4-dimethylheptane
55.80	C_8	73.30	C_9
56.95	1,2,4-trimethylcyclopentane	73.50	4-ethyl-2-methylhexane
57.10	3,3-dimethylhexane	73.60	2,6-dimethylheptane
58.35	1,2,3-trimethylcyclopentane	73.75	C_9

t_{ret} / min	Product	t_{ret} / min	Product
74.00	C_9	85.00	1,1,3,5-tetramethylcyclohexane
74.25	1,3,5-trimethylcyclopentane	85.25	1-ethyl-4-methylcyclohexane
74.45	ethylcyclohexane	85.75	ROP
74.85	2,5-dimethylheptane	86.15	C_9
75.05	3,5-dimethylheptane	86.25	1,1,4,4-tetramethylcyclohexane
75.20	C_9	86.40	C_9
76.00	1,1,4-trimethylcyclohexane	86.65	1,1,3-trimethylcyclohexane
76.25	C_9	87.20	n-nonane
76.55	1,3-diethylcyclopentane	87.45	3,3,5-trimethylheptane
77.20	3-ethyl-2-methylhexane	87.75	3-ethyl-2-methylheptane
77.40	C_9	87.90	C_9
77.55	ethylbenzene[a]	88.20	sk-Iso
77.60	C_9	88.55	C_9
77.75	C_9	88.75	sk-Iso
78.10	C_9	89.15	C_9
78.40	3-ethyl-3-methylhexane	89.35	1-ethyl-2-methylcyclohexane
78.85	2,3-dimethylheptane	89.80	sk-Iso
79.15	3-ethyl-4methylhexane / dimethylbenzene[a]	89.90	C_9
79.30	3,4-dimethylheptane / dimethylbenzene[a]	90.15	OCD
79.45	3,4-dimethylheptane	90.25	OCD
79.65	4-ethylheptane	90.60	ROP
80.15	4-methyloctane	90.85	sk-Iso
80.30	2-methyloctane	91.00	OCD
80.60	C_9	91.30	2,4-dimethyloctane
80.85	C_9	91.40	sk-Iso
81.05	C_9	91.60	2,3-dimethyloctane
81.50	3-ethylheptane	91.80	ROP
81.70	3-methyloctane	91.95	sk-Iso
81.80	C_9	92.10	4,4-dimethyloctane
81.95	C_9	92.25	sk-Iso
82.10	C_9	92.40	sk-Iso
82.35	C_9	92.65	3,5-dimethyloctane
82.60	2,4,6-trimethylheptane	92.80	2,5-dimethyloctane
82.95	C_9	93.10	3,5-dimethyloctane
83.05	1,1,3,5-tetramethylcyclohexane	93.30	1,2,4,5-tetramethylcyclohexane
83.30	C_9	93.40	1,5-dimethylbicyclo[3.2.1]octane
83.55	C_9	93.65	2,7-dimethyloctane
83.70	C_9	93.85	1-ethyl-2-methylcyclohexane
83.85	C_9 / dimethylbenzene[a]	94.00	propylcyclohexane
84.30	C_9	94.15	OCD
84.50	C_9	94.25	OCD
84.75	1,2,3-trimethylcyclohexane	94.40	sk-Iso

t_{ret} / min	Product	t_{ret} / min	Product
94.75	2,6-dimethyloctane	102.45	sk-Iso
95.00	OCD	102.60	sk-Iso / unsaturated C_9[a]
95.40	3,3-dimethyloctane	102.70	sk-Iso
95.50	sk-Iso	102.85	3-methylnonane
95.65	sk-Iso	103.00	sk-Iso
95.80	sk-Iso	103.15	sk-Iso
96.00	3,6-dimethyloctane	103.45	sk-Iso
96.25	3,6-dimethyloctane	103.70	sk-Iso
96.40	ROP	104.15	ROP
96.55	sk-Iso	104.50	3,7,7-trimethylbicyclo[4.1.0]heptane
96.65	sk-Iso	104.70	sk-Iso
96.75	3-ethyl-2-methylheptane	104.95	sk-Iso
96.95	sk-Iso	105.25	sk-Iso
97.15	sk-Iso	105.45	sk-Iso
97.25	OCD	105.55	sk-Iso
97.35	sk-Iso	105.85	sk-Iso
97.55	OCD	106.05	unsaturated C_9[a]
97.60	sk-Iso	106.30	1-methyl-3-propylcyclohexane
97.75	sk-Iso	106.50	sk-Iso
97.95	4,5-dimethyloctane	106.75	sk-Iso
98.25	sk-Iso	107.00	ROP
98.50	ethylmethylbenzene[a]	107.15	tert-butylcyclohexane
98.55	1,1,4,4-tetramethylcyclohexane	107.45	sk-Iso
98.75	1,2,3,5-tetramethylcyclohexane	107.85	sk-Iso
98.85	sk-Iso	108.30	sk-Iso
99.00	ethylmethylbenzene[a]	108.60	sk-Iso
99.15	sk-Iso	108.90	sk-Iso
99.30	sk-Iso	109.05	1-methyl-3(methylethyl)cyclohexane
99.50	4-ethyloctane	109.15	sk-Iso
99.65	sk-Iso	109.35	n-decane
99.90	ROP	109.65	1-methyl-2-propylcyclohexane
100.10	sk-Iso	110.05	ROP
100.20	trimethylbenzene[a]	110.35	ROP
100.45	5-methylnonane	110.55	sk-Iso
100.75	4-methylnonane	110.60	sk-Iso
100.90	ROP	110.75	ROP
101.15	2-methylnonane	111.00	sk-Iso
101.30	1,4-diethylcyclohexane	111.35	ROP
101.55	1,4-diethylcyclohexane	111.50	sk-Iso
101.65	sk-Iso	111.80	sk-Iso
101.90	1-ethyl-2,4-dimethylcyclohexane	112.05	1,4-diethylcyclohexane
102.20	3-ethyloctane	112.20	sk-Iso

t_{ret} / min	Product	t_{ret} / min	Product
112.40	sk-Iso	123.00	sk-Iso
112.55	sk-Iso	123.70	sk-Iso
112.75	sk-Iso / unsaturated C_9[a]	124.20	trans-decalin
112.90	sk-Iso	124.60	spiro[4.5]decane
113.15	1,2-diethylcyclohexane	124.90	sk-Iso
113.25	1-ethyl-1,4-dimethylcyclohexane	125.25	sk-Iso
113.30	sk-Iso	125.50	sk-Iso
113.40	sk-Iso	126.10	sk-Iso, unsaturated ROP[a]
113.60	sk-Iso	126.60	sk-Iso, unsaturated ROP[a]
113.90	sk-Iso	126.80	sk-Iso
114.40	sk-Iso	127.05	sk-Iso
114.65	sk-Iso	127.20	sk-Iso / unsaturated sk-Iso[a]
114.85	sk-Iso	127.85	sk-Iso
115.35	1-methyl-2-propylcyclohexane	128.10	sk-Iso / unsaturated ROP[a]
115.60	sk-Iso	128.40	sk-Iso / unsaturated sk-Iso[a]
115.70	unsaturated C_9[a]	128.65	sk-Iso
115.80	1,2-diethylcyclohexane	129.60	sk-Iso
116.35	1-(methylpropyl)cyclohexane	129.75	sk-Iso
116.70	ROP	130.15	bicyclopentyl
117.00	sk-Iso	130.95	sk-Iso
117.20	sk-Iso	131.45	sk-Iso
117.80	butylcyclohexane	132.10	sk-Iso
117.95	sk-Iso	132.65	endo-2-methylbicyclo[3.3.1]nonane
118.05	unsaturated ROP[a]	133.40	sk-Iso
118.10	sk-Iso	133.85	bicyclo[5.3.0]decane
118.45	pentylcyclopentane	134.30	sk-Iso
118.60	sk-Iso	134.70	sk-Iso
118.85	sk-Iso	135.30	cis-decalin
119.05	sk-Iso, unsaturated ROP[a]	136.10	sk-Iso
119.30	sk-Iso	136.60	sk-Iso / tetramethylbenzene[a]
119.70	sk-Iso	137.25	sk-Iso
120.05	octahydro-5-methyl-1H-indene	137.35	sk-Iso / tetramethylbenzene[a]
120.40	unsaturated ROP[a]	138.65	decahydro-2-methylnaphthalene
120.50	sk-Iso	141.20	sk-Iso
120.75	unsaturated ROP[a]	142.00	sk-Iso / unsaturated sk-Iso[a]
120.80	sk-Iso	142.80	sk-Iso
121.25	sk-Iso, unsaturated ROP[a]	143.35	sk-Iso
121.50	sk-Iso	144.70	cyclodecane / unsaturated sk-Iso[a]
121.90	sk-Iso	145.00	sk-Iso
122.20	sk-Iso	145.20	sk-Iso
122.70	sk-Iso	145.50	unsaturated sk-Iso[a]

t_{ret} / min	Product	t_{ret} / min	Product
147.00	sk-Iso[a]	152.60	naphthalene
147.50	tetralin	153-181	C_{11}[a]
148.90	sk-Iso[a]	182-215	C_{12}[a]
151.00	sk-Iso[a]	216-222	C_{13}[a]

[a] these signals occurred only in the chromatograms of products obtained on monofunctional acidic catalysts

12.2 Evaluation of Conversion, Yields and Selectivities in the Catalytic Conversion of cis-Decalin with Hydrogen

12.2.1 Nomenclature

12.2.1.1 Symbols

Symbol	Unit	Designation
A	– (or counts)	dimensionless peak area in the chromatogram
$\bar{A}$	– (or counts)	arithmetic mean of peak areas from various chromatograms
f	–	compound-specific FID correction factor
m	kg	mass
$\dot{m}$	$kg \cdot s^{-1}$	mass flux
M	$kg \cdot mol^{-1}$	molar mass
Δm	–	relative mass gain that accompanies the conversion of cis-decalin into its products
n	mol	molar amount
$\dot{n}$	$mol \cdot s^{-1}$	molar flux
p, q	–	carbon number of hydrocracked products
s	kg (or $kg \cdot counts^{-1}$)	reciprocal sensitivity of the FID
S	–	selectivity

Symbol	Unit	Designation
S^*	–	modified selectivity defined in Eq. (12.33)
x	–	stoichiometric factor of hydrogen, see Eq. (12.1)
X	–	conversion
Y	–	yield
ν	–	stoichiometric factor

12.2.1.2 Indices

Bz	benzene
c-Dec	cis-decalin
conv	converted
GSL	in the gas sampling loop
i	a reactant in the stoichiometric equation
in	entering the reactor
j	a product or group of products in the stoichiometric equation
out	leaving the reactor

12.2.1.3 Abbreviations

Bz	benzene
C_9-	hydrocarbons with less than 10 carbon atoms (hydrocracked products)
C_{11}^+	hydrocarbons with more than 10 carbon atoms
c-Dec	cis-decalin
Eq(s).	equation(s)
FID	flame ionization detector
GC	gas chromatograph(y)
GSL	gas sampling loop
M-CPn	methylcyclopentane
2-M-Pr	2-methylpropane (isobutane)
Nap	naphthalene
n-Pn	n-pentane
OCD(s)	open-chain decane(s)
ROP(s)	ring opening product(s)
sk-Iso(s)	skeletal isomer(s)
tr-Dec	trans-decalin
Ttr	tetralin

12.2.2 Conversion $X_{c\text{-}Dec}$

12.2.2.1 Fundamentals

In this work cis-decalin was used as a model hydrocarbon (i = c-Dec). This hydrocarbon was converted in a flow reactor in the presence of a large excess of hydrogen at elevated pressure. A simplified stoichiometry is given in Eq. (12.1):

$$\text{c-Dec} + x\,H_2 \rightarrow \quad \text{Products j} \tag{12.1}$$

Under these conditions, the following products are formed: trans-decalin (x = 0; j = tr-Dec), skeletal isomers with two naphthenic rings (x = 0; j = sk-Isos), ring opening products with one naphthenic ring left (x = 1; j = ROPs), open-chain decanes (x = 2; j = OCDs) and hydrocracked products with less than 10 carbon atoms ($x \geq 2$; j = C_9-). In exceptional cases, tetralin (x = -3; j = Ttr), naphthalene (x = -5; j = Nap) and hydrocarbons with more than 10 carbon atoms ($x < 0$; j = C_{11}^+) are also formed but, for the sake of simplicity, these are not included in the subsequent considerations.

The conversion is conveniently defined by one of the following equations:

$$X_{c-Dec} = \frac{(\dot{n}_{c-Dec})_{in} - (\dot{n}_{c-Dec})_{out}}{(\dot{n}_{c-Dec})_{in}} \tag{12.2}$$

or

$$X_{c-Dec} = \frac{(\dot{m}_{c-Dec})_{in} - (\dot{m}_{c-Dec})_{out}}{(\dot{m}_{c-Dec})_{in}} \tag{12.3}$$

where $\dot{n}$ and $\dot{m}$ are the molar flux and the mass flux, respectively.

For product analysis, an on-line gas chromatograph (GC) with a gas sampling loop (GSL) was employed, and Eq. (12.4) applies which is a modified version of Eq. (12.3) with absolute masses of the compounds inside the GSL:

$$X_{c-Dec} = \frac{(m_{c-Dec})_{GSL\ at\ X=0} - (m_{c-Dec})_{GSL}}{(m_{c-Dec})_{GSL\ at\ X=0}} \tag{12.4}$$

Here, $(m_{\text{c-Dec}})_{\text{GSL}}$ is the mass of unconverted cis-decalin captured in the gas sampling loop, whereas $(m_{\text{c-Dec}})_{\text{GSL at } X = 0}$ is a fictitious mass of cis-decalin that would have been entrapped in the gas sampling loop, if no chemical transformation of cis-decalin had occurred in the flow reactor, *i. e.*, at $X_{\text{c-Dec}} = 0$. While $(m_{\text{c-Dec}})_{\text{GSL}}$ can be directly obtained from the area of the cis-decalin peak in the chromatogram (see Section 12.2.2.2), there are three options for evaluating $(m_{\text{c-Dec}})_{\text{GSL at } X = 0}$ (see Section 12.2.2.3).

12.2.2.2 Calculating $(m_{\text{c-Dec}})_{\text{GSL}}$ from the Area of the cis-Decalin Peak

As long as the flame ionization detector is operated in its linear range, the mass of cis-decalin detected is proportional to the dimensionless peak area times the compound-specific FID correction factor $f_{\text{c-Dec}}$:

$$\left(m_{\text{c-Dec}}\right)_{\text{GSL}} \sim f_{\text{c-Dec}} \cdot A_{\text{c-Dec}} \tag{12.5}$$

The factor of proportionality s in Eq. (12.6)

$$\left(m_{\text{c-Dec}}\right)_{\text{GSL}} = s \cdot f_{\text{c-Dec}} \cdot A_{\text{c-Dec}} \tag{12.6}$$

may be understood in terms of a reciprocal sensitivity of the flame ionization detector employed, *i. e.*, the lower the value of s, the higher is the peak area per unit mass of a compound to be detected:

$$\frac{1}{s} = \frac{f_{\text{c-Dec}} \cdot A_{\text{c-Dec}}}{\left(m_{\text{c-Dec}}\right)_{\text{GSL}}} \tag{12.7}$$

The numerical value of s is, in principle, accessible by separate calibration experiments, *i. e.*, by injecting known masses of cis-decalin and measuring the respective values of $A_{\text{c-Dec}}$. However, as will be shown below, the value of s is not really needed for calculating the conversion of cis-decalin.

The compound-specific FID correction factor f_{i} or f_{j} is approximately unity for all hydrocarbons. Usually, its value for a given hydrocarbon is referenced to benzene, *i. e.*, f_{Bz} is set equal to 1.000. The compound-specific FID correction factor for cis-decalin is

$$f_{c-Dec} = \frac{m_{c-Dec} \cdot A_{Bz}}{m_{Bz} \cdot A_{c\text{-}Dec}} \tag{12.8}$$

A comparison of Eqs. (12.7) and (12.8) shows that $1/s = A_{Bz} / m_{Bz}$.

According to Eq. (12.8), the compound-specific correction factors for cis-decalin ($f_{c\text{-}Dec}$) or for any product (f_j) can, in principle, be obtained by injecting known masses of cis-decalin or product j and benzene into the GC and measuring the resulting peak areas. Apart from the fact that this is a cumbersome procedure, it implies that (i) every peak in the chromatogram can be unambiguously assigned and (ii) each product j is available as a pure compound. These preconditions will not be fulfilled in our experiments.

To get access to the compound-specific FID factors needed in this work, another approach will therefore be chosen: It appears that the ions generated in the flame of an FID mostly result from the element carbon in the hydrocarbon to be detected (whereas the element hydrogen is essentially "FID-silent"). In other words, the FID correction factors for hydrocarbons, that are richer in hydrogen than benzene, will be larger than unity and *vice versa*. In quantitative terms, this can be accounted for in the following manner for cis-decalin

$$f_{c-Dec} = \frac{\frac{M_{c-Dec}}{M_{C,c-Dec}}}{\frac{M_{Bz}}{M_{C,Bz}}} = \frac{\frac{138\ \text{g}\cdot\text{mol}^{-1}}{120\ \text{g}\cdot\text{mol}^{-1}}}{\frac{78\ \text{g}\cdot\text{mol}^{-1}}{72\ \text{g}\cdot\text{mol}^{-1}}} = 1.062 \tag{12.9}$$

or for any product hydrocarbon j

$$f_j = \frac{\frac{M_j}{M_{C,j}}}{\frac{M_{Bz}}{M_{C,Bz}}} = \frac{\frac{M_j}{M_{C,j}}}{1.083} \tag{12.10}$$

where $M_{c\text{-}Dec}$, M_{Bz} and M_j are, respectively, the molar masses of cis-decalin, benzene and product j and $M_{C,c\text{-}Dec}$, $M_{C,Bz}$ and $M_{C,j}$ the molar masses of carbon in the respective hydrocarbon. FID correction factors calculated in this manner for some selected hydrocarbons relevant to this project are listed in Table 12.3.

It follows that Eq. (12.6) can be re-written as

$$(m_{\mathrm{c-Dec}})_{\mathrm{GSL}} = s \cdot 1.062 \cdot A_{\mathrm{c-Dec}} \tag{12.11}$$

Table 12.3: Compound-specific FID correction factors *f* of some hydrocarbons relevant to this project calculated by Eqs. (12.9) and (12.10).

Hydrocarbon	**Formula**	***f***
Methane	CH_4	1.231
Ethane	C_2H_6	1.154
Propane	C_3H_8	1.129
Butanes	C_4H_{10}	1.116
Pentanes	C_5H_{12}	1.108
Hexanes	C_6H_{14}	1.103
Methylcyclopentane (M-CPn)	C_6H_{12}	1.077
Open-chain decanes (OCDs)	$C_{10}H_{22}$	1.093
Ring opening products (ROPs)	$C_{10}H_{20}$	1.077
Skeletal isomers of c-Dec (sk-Isos)	$C_{10}H_{18}$	1.062
trans-Decalin (tr-Dec)	$C_{10}H_{18}$	1.062
cis-Decalin (c-Dec)	$C_{10}H_{18}$	1.062
Tetralin	$C_{10}H_{12}$	1.016
Naphthalene	$C_{10}H_8$	0.985

12.2.2.3 Calculating $(m_{\mathrm{c\text{-}Dec}})_{\mathrm{GSL\ at}\ X=0}$ in Eq. (12.4)

a) Method 1

Prior to and, desirably, after a catalytic experiment, the feed mixture consisting of hydrogen and vapors of cis-decalin is sent to the GC for analysis. In these auxiliary measurements, the reactor is by-passed, *i. e.*, no conversion of cis-decalin occurs. It is advisable to activate the sampling valve several times and to use the arithmetic mean of the cis-decalin peak areas $\bar{A}_{\mathrm{c\text{-}Dec\ at}\ X\,=\,0}$. Inserting into Eq. (12.6) and using the appropriate compound-specific FID correction factor gives

$$(m_{\mathrm{c-Dec}})_{\mathrm{GSL\ at}\ X=0} = s \cdot 1.062 \cdot \overline{A}_{\mathrm{c-Dec\ at}\ X=0} \tag{12.12}$$

b) Method 2

This is an approximation which relies on the fact that, in the hydroconversion of cis-decalin, the sum of the masses of all product hydrocarbons is not too different from the mass of cis-decalin converted, the ultimate reason being the very low molar mass of the reactant hydrogen. This is exemplified in Figure 12.1 which is a reasonable reaction network of cis-decalin and which starts from n_i = 1 kmol of the reactant corresponding to a mass of m_i = 138 kg.

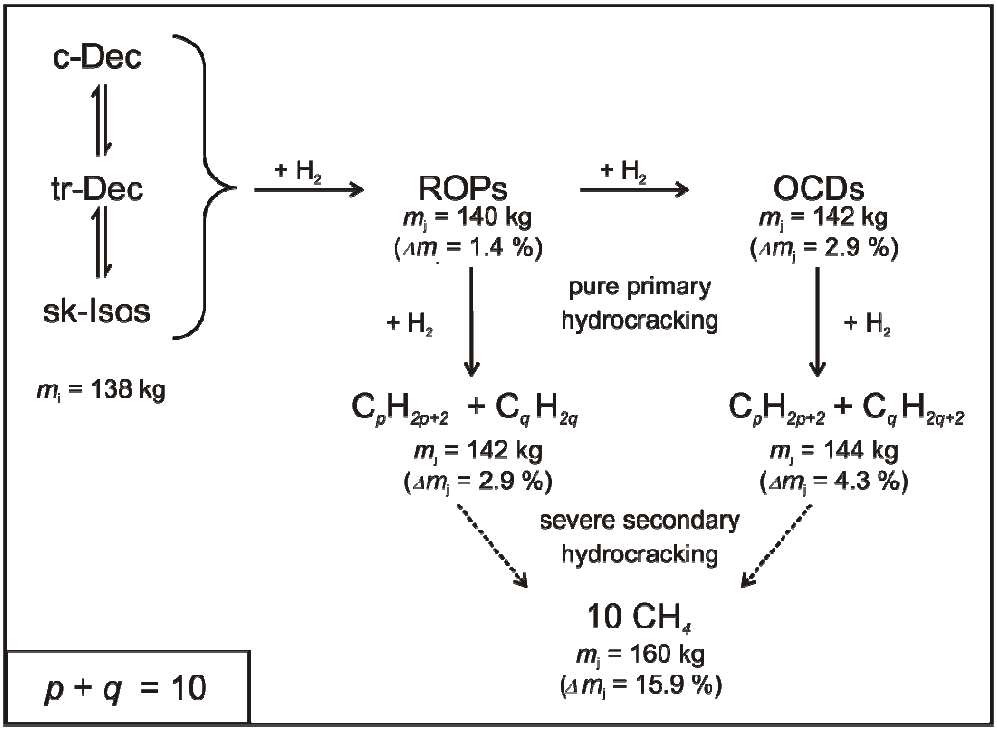

Figure 12.1: Reaction network for the hydroconversion of 1 kmol of cis-decalin and mass gain at total conversion into the respective products.

No mass gain at all occurs, as long as cis-decalin is converted into trans-decalin or skeletal isomers. Upon a total conversion into ring opening products or open-chain decanes, the mass gain [$\Delta m_j = (m_j - m_i) / m_i$] is as low as 1.4 % and 2.9 %, respectively. A complete primary hydrocracking of ROPs or OCDs would still be accompanied by a low mass gain amounting to 2.9 % and 4.3 %, respectively. Even after the most severe hydrocracking all the way down to methane, the mass gain would still be moderate, *viz.* 15.9 %.

Method 2 is then based on the assumption that the mass of cis-decalin converted is approximated by

$$\left(m_{\text{c-Dec}}\right)_{\text{conv}} \approx \sum_{\text{j}} \left(m_{\text{j}}\right)_{\text{GSL}} \tag{12.13}$$

with j = tr-Dec, sk-Isos, ROPs, OCDs and C_9-. Expressing the product masses m_{j} by equations analogous to Eq. (12.6)

$$\left(m_{\text{j}}\right)_{\text{GSL}} = s \cdot f_{\text{j}} \cdot A_{\text{j}} \tag{12.14}$$

and substituting Eq. (12.14) into Eq. (12.13) gives

$$\left(m_{\text{c-Dec}}\right)_{\text{conv}} \approx \sum_{\text{j}} s \cdot f_{\text{j}} \cdot A_{\text{j}} = s \cdot \sum_{\text{j}} f_{\text{j}} \cdot A_{\text{j}} \tag{12.15}$$

Finally, $(m_{\text{c-Dec}})_{\text{GSL at } X = 0}$ is obtained by

$$\left(m_{\text{c-Dec}}\right)_{\text{GSL at } X=0} = \left(m_{\text{c-Dec}}\right)_{\text{conv}} + \left(m_{\text{c-Dec}}\right)_{\text{GSL}} \tag{12.16}$$

Substituting Eqs. (12.6) and (12.16) into Eq. (12.4) gives the conversion of c-Dec. Note that *s*, the reciprocal sensitivity of the FID, appears as a factor in both the nominator and denominator of Eq. (12.4) and cancels upon inserting Eqs. (12.6) and (12.16).

c) Method 3

Method 3 is based on a more rigorous mass balance in the calculation of $(m_{\text{c-Dec}})_{\text{conv}}$ from the product masses $\left(m_{\text{j}}\right)_{\text{GSL}} = s \cdot f_{\text{j}} \cdot A_{\text{j}}$. Following are the masses of cis-decalin converted to generate the respective masses of products found in the gas sampling loop:

- tr-Dec: $$\left(m_{\text{c-Dec}}\right)_{\text{conv}} = s \cdot f_{\text{tr-Dec}} \cdot A_{\text{tr-Dec}} \tag{12.17}$$

- sk-Isos: $$\left(m_{\text{c-Dec}}\right)_{\text{conv}} = s \cdot f_{\text{sk-Isos}} \cdot \sum_{\text{sk-Isos}} A_{\text{sk-Isos}} \tag{12.18}$$

- ROPs: $$\left(m_{\text{c-Dec}}\right)_{\text{conv}} = \frac{M_{\text{c-Dec}}}{M_{\text{ROPs}}} \cdot s \cdot f_{\text{ROPs}} \cdot \sum_{\text{ROPs}} A_{\text{ROPs}} \tag{12.19}$$

- OCDs: $$\left(m_{\text{c-Dec}}\right)_{\text{conv}} = \frac{M_{\text{c-Dec}}}{M_{\text{OCDs}}} \cdot s \cdot f_{\text{OCDs}} \cdot \sum_{\text{OCDs}} A_{\text{OCDs}} \qquad (12.20)$$

- C_9-: $$\left(m_{\text{c-Dec}}\right)_{\text{conv}} = s \cdot \sum_{C_9-} \frac{|\nu_{\text{c-Dec}}|}{\nu_{C_9-}} \cdot \frac{M_{\text{c-Dec}}}{M_{C_9-}} \cdot f_{C_9-} \cdot A_{C_9-} \qquad (12.21)$$

$\nu_{\text{c-Dec}}$ and ν_{C_9-} are the stoichiometric factors in the equation leading from cis-decalin to the respective hydrocracked products, e.g.,

– 3 cis-decalin + 3 H_2 → 5 methylcyclopentane

$\nu_{\text{c-Dec}}$ = - 3; $\nu_{\text{M-CPn}}$ = + 5; $\frac{|\nu_{\text{c-Dec}}|}{\nu_{\text{M-CPn}}} = +\frac{3}{5}$

– cis-decalin + 3 H_2 → 2 n-pentane

$\nu_{\text{c-Dec}}$ = - 1; $\nu_{\text{n-Pn}}$ = + 2; $\frac{|\nu_{\text{c-Dec}}|}{\nu_{\text{n-Pn}}} = +\frac{1}{2}$

– 2 cis-decalin + 7 H_2 → 5 2-methylpropane

$\nu_{\text{c-Dec}}$ = - 2; $\nu_{\text{2-M-Pr}}$ = + 5; $\frac{|\nu_{\text{c-Dec}}|}{\nu_{\text{2-M-Pr}}} = +\frac{2}{5}$

Note that the stoichiometric factors are negative for all reactants i and positive for all products j.

From Eqs. (12.17) to (12.21), the most generally applicable one is Eq. (12.21). If j is a hydrocarbon with 10 carbon atoms, the correction factor $|\nu_{\text{c-Dec}}| / \nu_{\text{j}}$ is unity, and Eqs. (12.19) or (12.20) result. If j is an isomer of cis-decalin, the correction factor $M_{\text{c-Dec}} / M_{\text{j}}$ is unity as well, and Eqs. (12.17) or (12.18) result.

The mass of cis-decalin converted is

$$\left(m_{\text{c-Dec}}\right)_{\text{conv}} = s \cdot \sum_{\text{j}} \frac{|\nu_{\text{c-Dec}}|}{\nu_{\text{j}}} \cdot \frac{M_{\text{c-Dec}}}{M_{\text{j}}} \cdot f_{\text{j}} \cdot A_{\text{j}} \qquad (12.22)$$

Substituting Eqs. (12.6) and (12.22) into Eq. (12.16) and Eqs. (12.6) and (12.16) into Eq. (12.4) gives the conversion of c-Dec according to method 3.

In cases, where tetralin, naphthalene and/or hydrocarbons with more than 10 carbon atoms are formed, these can easily be included into the formalisms developed above.

In case of lumping cis- and trans-decalin into a single pseudo-compound Dec, all the above formalisms can still be applied, the only difference being that the conversion is referenced to Dec, *i. e*., both stereoisomers are treated as reactants i, and trans-decalin does not appear among the products j.

12.2.3 Yield Y_j

The yield of a product or groups of products j in a flow reactor is defined as

$$Y_j = \frac{(\dot{n}_j)_{out} - (\dot{n}_j)_{in}}{(\dot{n}_i)_{in}} \cdot \frac{|\nu_i|}{\nu_j} \tag{12.23}$$

in this work, $(\dot{n}_j)_{in}$ will generally be 0. For the reasons discussed in Section 12.2.2.1, the remaining Eq. (12.23) can be re-written as

$$Y_j = \frac{(n_j)_{GSL}}{(n_{c\text{-}Dec})_{GSL\ at\ X=0}} \cdot \frac{|\nu_{c\text{-}Dec}|}{\nu_j} \tag{12.24}$$

or

$$Y_j = \frac{\frac{1}{M_j} \cdot (m_j)_{GSL}}{\frac{1}{M_{c-Dec}} \cdot (m_{c\text{-}Dec})_{GSL\ at\ X=0}} \cdot \frac{|\nu_{c\text{-}Dec}|}{\nu_j} \tag{12.25}$$

or

$$Y_j = \frac{(m_j)_{GSL}}{(m_{c\text{-}Dec})_{GSL\ at\ X=0}} \cdot \frac{|\nu_{c\text{-}Dec}|}{\nu_j} \cdot \frac{M_{c-Dec}}{M_j} \tag{12.26}$$

The designation of $(m_{c\text{-}Dec})_{GSL\ at\ X\ =\ 0}$ has been discussed in the context of Eq. (12.4). Here again, methods 1, 2 and 3 (see Section 12.2.2.3) can be employed for its evaluation:

– Method 1:

$$\left(m_{\text{c-Dec}}\right)_{\text{GSL at } X=0} = s \cdot 1.062 \cdot \overline{A}_{\text{c-Dec at } X=0} \tag{12.12}$$

– Method 2:

$$\left(m_{\text{c-Dec}}\right)_{\text{GSL at } X=0} = \left(m_{\text{c-Dec}}\right)_{\text{conv}} + \left(m_{\text{c-Dec}}\right)_{\text{GSL}} \tag{12.16}$$

with

$$\left(m_{\text{c-Dec}}\right)_{\text{conv}} = s \cdot \sum_{\text{j}} f_{\text{j}} \cdot A_{\text{j}} \tag{12.15}$$

and

$$\left(m_{\text{c-Dec}}\right)_{\text{GSL}} = s \cdot f_{\text{c-Dec}} \cdot A_{\text{c-Dec}} \tag{12.6}$$

– Method 3:

$$\left(m_{\text{c-Dec}}\right)_{\text{GSL at } X=0} = \left(m_{\text{c-Dec}}\right)_{\text{conv}} + \left(m_{\text{c-Dec}}\right)_{\text{GSL}} \tag{12.16}$$

with

$$\left(m_{\text{c-Dec}}\right)_{\text{conv}} = s \cdot \sum_{\text{j}} \frac{\left|\nu_{\text{c-Dec}}\right|}{\nu_{\text{j}}} \cdot \frac{M_{\text{c-Dec}}}{M_{\text{j}}} \cdot f_{\text{j}} \cdot A_{\text{j}} \tag{12.22}$$

and

$$\left(m_{\text{c-Dec}}\right)_{\text{GSL}} = s \cdot f_{\text{c-Dec}} \cdot A_{\text{c-Dec}} \tag{12.6}$$

Using, e.g., method 3 and substituting

$$\left(m_{\text{j}}\right)_{\text{GSL}} = s \cdot f_{\text{j}} \cdot A_{\text{j}} \tag{12.14}$$

in Eq. (12.26) results in

$$Y_j = \frac{s \cdot f_j \cdot A_j}{s \cdot \sum_j \frac{|\nu_{c-Dec}|}{\nu_j} \cdot \frac{M_{c-Dec}}{M_j} \cdot f_j \cdot A_j + s \cdot f_{c-Dec} \cdot A_{c-Dec}} \cdot \frac{|\nu_{c-Dec}|}{\nu_j} \cdot \frac{M_{c-Dec}}{M_j}$$

or

$$Y_j = \frac{f_j \cdot A_j}{\sum_j \frac{|\nu_{c-Dec}|}{\nu_j} \cdot \frac{M_{c-Dec}}{M_j} \cdot f_j \cdot A_j + f_{c-Dec} \cdot A_{c-Dec}} \cdot \frac{|\nu_{c-Dec}|}{\nu_j} \cdot \frac{M_{c-Dec}}{M_j} \quad (12.27)$$

12.2.4 Selectivity S_j

The selectivity of a product or group of products j in a flow reactor is defined as

$$S_j = \frac{(\dot{n}_j)_{out} - (\dot{n}_j)_{in}}{(\dot{n}_i)_{in} - (\dot{n}_i)_{out}} \cdot \frac{|\nu_i|}{\nu_j} \quad (12.28)$$

In this work, $(\dot{n}_j)_{in}$ will generally be 0. For the reasons discussed in Section 12.2.2.1, the remaining Eq. (12.28) can be re-written as

$$S_j = \frac{(n_j)_{GSL}}{(n_{c\text{-}Dec})_{conv}} \cdot \frac{|\nu_{c\text{-}Dec}|}{\nu_j} \quad (12.29)$$

or

$$S_j = \frac{\frac{1}{M_j} \cdot (m_j)_{GSL}}{\frac{1}{M_{c-Dec}} \cdot (m_{c\text{-}Dec})_{conv}} \cdot \frac{|\nu_{c\text{-}Dec}|}{\nu_j} \quad (12.30)$$

or

$$S_j = \frac{(m_j)_{GSL}}{(m_{c\text{-}Dec})_{conv}} \cdot \frac{|\nu_{c\text{-}Dec}|}{\nu_j} \cdot \frac{M_{c-Dec}}{M_j} \quad (12.31)$$

Substituting Eqs. (12.14) and (12.22) into Eq. (12.31) gives

$$S_j = \frac{s \cdot f_j \cdot A_j}{s \cdot \sum_j \frac{|\nu_{c-Dec}|}{\nu_j} \cdot \frac{M_{c-Dec}}{M_j} \cdot f_j \cdot A_j} \cdot \frac{|\nu_{c\text{-}Dec}|}{\nu_j} \cdot \frac{M_{c-Dec}}{M_j}$$

or

$$S_j = \frac{f_j \cdot A_j}{\sum_j \frac{|\nu_{c\text{-}Dec}|}{\nu_j} \cdot \frac{M_{c-Dec}}{M_j} \cdot f_j \cdot A_j} \cdot \frac{|\nu_{c\text{-}Dec}|}{\nu_j} \cdot \frac{M_{c-Dec}}{M_j} \tag{12.32}$$

Where the summation must include all products (j = tr-Dec, sk-Isos, ROPs, OCDs and C_9-). A summation over the selectivities of all products as defined by Eq. (12.32) will give 1.00 or 100 %.

12.2.5 Modified Selectivity S_j^*

In experiments with a significant amount of hydrocracking it was informative to evaluate a modified selectivity S_j^*

$$S_j^* = \frac{(\dot{n}_j)_{out}}{(\dot{n}_i)_{converted\ to\ C_{9^-}}} \tag{12.33}$$

where j is a hydrocracked product. With

$$S_j^* = \frac{(n_j)_{GSL}}{(n_{c\text{-}Dec})_{converted\ to\ C_{9^-}}} \tag{12.34}$$

or

$$S_j^* = \frac{\frac{1}{M_j} \cdot (m_j)_{GSL}}{\frac{1}{M_{c-Dec}} \cdot (m_{c\text{-}Dec})_{converted\ to\ C_{9^-}}} \tag{12.35}$$

and substituting Eqs. (12.14) and (12.21) for the nominator and denominator, respectively, gives

$$S_j^* = \frac{\frac{1}{M_j} \cdot s \cdot f_j \cdot A_j}{\frac{1}{M_{c-Dec}} \cdot s \cdot \sum_j f_j \cdot A_j \cdot \frac{|\nu_{c-Dec}|}{\nu_j} \cdot \frac{M_{c-Dec}}{M_j}} \tag{12.36}$$

or

$$S_j^* = \frac{\frac{1}{M_j} \cdot f_j \cdot A_j}{\frac{1}{M_{c-Dec}} \cdot \sum_j f_j \cdot A_j \cdot \frac{|\nu_{c-Dec}|}{\nu_j} \cdot \frac{M_{c-Dec}}{M_j}} \qquad (12.37)$$

where j = C_9-.

For a pure primary hydrocracking, $\sum_j S_j^*$ = 2.00 or 200 %, whereas for the extreme case of a severe hydrocracking all the way down to methane

$$\text{c-Dec} + 11\ H_2 \rightarrow 10\ CH_4 \qquad (12.38)$$

$\sum_j S_j^* = S_{CH_4}^*$ = 10.00 or 1 000 %. Note that the modified selectivity thus defined has been occasionally used in the pertinent literature under the designation "moles per 100 moles hydrocracked".